

[Home](#) » [SOFIA Observer's Handbook for Cycle 6](#)

SOFIA Observer's Handbook for Cycle 6

Changelog

Changelog

The following log includes the dates of publication and lists sections containing major updates for all current and past versions of the handbook. The current version is listed at the top in **bold** font.

v6.2.2	Oct. 11, 2018	DCS link URLs updated
v6.2.1	June 15, 2018	Section 8.1: Table 8.1 sensitivity values updated.
v6.2.0	Nov. 15, 2017	Sections 1.1–1.3, 5.2, 7.2, & 8.2.
v6.1.1	June 5, 2017	No major updates.
v6.1.0	May 1, 2017	Observer's Handbook for Cycle 6 released.

New versions of the Observer's Handbook from Cycle 6 onward will follow the following schedule of releases:

Observer's Handbook Versions

Version	Coincides with	Approx. Annual Publish Date
6.1.0	Call for Proposals	end of April
6.1.1	Update to Call for Proposals	June
6.2.0	Phase II begins	October
6.2.x	Phase II Concludes	January

Versions have the format (Observing Cycle).(Phase).(Revision). Intermediate revisions may be released until the conclusion of Phase II.

i. Table of Contents

Table of Contents

Jump To Instrument:

[EXES](#) | [FIFLI-LS](#) | [FLITECAM](#) | [FORCAST](#) | [FPI+](#) | [GREAT](#) | [HAWC+](#) | [HIPO](#)

- Changelog
- i. Table of Contents
- ii. Preface
- 1. Introduction
 - 1.1 SOFIA and Its Instruments
 - 1.2 Observing on an Aircraft
 - 1.2.1 Scheduling and Flight Planning
 - 1.2.2 Acquisition and Guiding
 - 1.2.3 Observing Moving Targets
 - 1.2.4 Line-of-Sight (LOS) Rewinds
 - 1.3 Performing Background Limited Observations
 - 1.3.1 Chopping and Nodding
 - 1.3.1.1 Symmetric and Asymmetric Chopping Techniques
 - 1.3.1.1a Symmetric Chopping Variations
 - 1.3.1.1b Asymmetric Chopping Variations
 - 1.3.1.2 Alternatives to Chop-Nod Cycles
- 2. EXES
 - 2.1 Specifications
 - 2.1.1 Instrument Overview
 - 2.1.1.1 Design
 - 2.1.2 Performance
 - 2.1.2.1 Optics
 - 2.1.2.2 Detector
 - 2.2 Planning Observations
 - 2.2.1 Wavelength Calibration
 - 2.2.2 Flux Calibration and Atmospheric Line Correction
 - 2.2.3 Overheads
 - 2.2.4 As a Principle Investigator Instrument
- 3. FIFI-LS
 - 3.1 Specifications
 - 3.1.1 Instrument Overview
 - 3.1.1.1 Integral Field Concept
 - 3.1.1.2 Selection of the Dichroic
 - 3.1.1.3 Beam Rotator
 - 3.1.2 Performance
 - 3.1.2.1 Comparison with the PACS Spectrometer
 - 3.1.2.2 Spectral Resolution
 - 3.1.2.3 Integration Time Estimates
 - 3.2 Planning Observations
 - 3.2.1 Observing Modes
 - 3.2.1.1 Symmetric Chop
 - 3.2.1.2 Asymmetric Chop
 - 3.2.1.3 Bright Object
 - 3.2.1.4 Spectral Scan
 - 3.2.2 Integration Time Estimates
 - 3.2.3 Spectral Dithering
 - 3.2.4 Mapping
- 4. FLITECAM
 - 4.1 Specifications

- 4.1.1 Instrument Overview
 - 4.1.1.1 Design
- 4.1.2 Performance
 - 4.1.2.1 Camera Performance
 - 4.1.2.2 Filter Suite
 - 4.1.2.3 Imaging Sensitivities
 - 4.1.2.4 Grisms
 - 4.1.2.5 Spectroscopic Sensitivities
- 4.2 Planning Observations
 - 4.2.1 Imaging Observations
 - 4.2.1.1 Estimation of Exposure Times
 - 4.2.2 Spectroscopic Observations
 - 4.2.2.1 Estimation of Exposure Times
- 5. FORCAST
 - 5.1 Specifications
 - 5.1.1 Instrument Overview
 - 5.1.1.1 Design
 - 5.1.2 Performance
 - 5.1.2.1 Camera Performance
 - 5.1.2.2 Filter Suite
 - 5.1.2.3 Imaging Sensitivity
 - 5.1.2.4 Grisms
 - 5.1.2.5 Spectroscopic Sensitivity
 - 5.2 Planning Observations
 - 5.2.1 Imaging Observations
 - 5.2.1.1 Estimation of Exposure Times
 - 5.2.2 Spectroscopic Observations
 - 5.2.2.1 Estimation of Exposure Times
- 6. FPI+
 - 6.1 Specifications
 - 6.1.1 Instrument Overview
 - 6.1.1.1 Design
 - 6.1.1.2 Angular Resolution
 - 6.1.2 Performance
 - 6.1.2.1 Filter Suite
 - 6.1.2.2 Imaging Sensitivities
 - 6.1.2.3 Camera Performance
 - 6.2 Planning Observations
 - 6.2.1 Observing Modes
 - 6.2.2 Estimation of Exposure Times
 - 6.2.3 Overheads
- 7. GREAT
 - 7.1 Specifications
 - 7.1.1 Instrument Overview
 - 7.1.1.1 Design
 - 7.1.1.2 Configurations
 - 7.1.2 Performance
 - 7.1.2.1 Imaging Sensitivities
 - 7.2 Planning Observations

- 7.2.1 Observing Modes Overview
 - 7.2.1.1 AOTs
 - 7.2.1.2 Spectroscopic Stability Limitations
- 7.2.2 Estimation of Exposure Times
- 7.2.3 OTF Technical Details
 - 7.2.3.1 Coordinates and Array Geometry
 - 7.2.3.2 OTF Mapping
 - 7.2.3.2a upGREAT LFA Channel
 - 7.2.3.2.b 4GREAT L1 Channel
 - 7.2.3.3 OTF Array Mapping
 - 7.2.3.3a upGREAT LFA Channel
- 8. HAWC+
 - 8.1 Specifications
 - 8.1.1 Instrument Overview
 - 8.1.1.1 Design
 - 8.1.2 Performance
 - 8.1.2.1 Filters
 - 8.1.2.2 Total Intensity Imaging Sensitivities
 - 8.1.2.3 Polarimetry Imaging Sensitivities
 - 8.2 Planning Observations
 - 8.2.1 Total Intensity Observations
 - 8.2.1.1 On the Fly Mapping
 - 8.2.1.1a Lissajous
 - 8.2.1.1b Box
 - 8.2.1.2 Nod Match Chop
 - 8.2.2 Polarimetry Observations
 - 8.2.2.1 Nod Match Chop
- 9. HIPO
 - 9.1 Specifications
 - 9.1.1 Instrument Overview
 - 9.1.1.1 Design
 - 9.1.1.2 Angular Resolution
 - 9.1.1.3 Filter Suites
 - 9.1.2 Performance
 - 9.1.2.1 Imaging Sensitivities
 - 9.1.2.2 Sensitivity Spreadsheet
 - 9.2 Planning Observations
- 10. The Data Cycle System
 - 10.1 Data Rights and Availability

Users may also navigate through the entire Observer's Handbook by using the complete Table of Contents menu to the right.

[Return to Top of Page](#)

ii. Preface

Table of Contents

- ii. Preface

Return to the Table of Contents for this section at any time by selecting [Return to Table](#)

of [Contents](#). Users may also navigate through the entire Observer's Handbook by using the complete Table of Contents menu to the right.

ii. [Preface](#)

The SOFIA Observer's Handbook for Cycle 6 (hereafter referred to as the Observer's Handbook), provides detailed information about SOFIA operations and the instruments that will be available for observations during Cycle 6, nominally scheduled for 1 February, 2018–31 January, 2019. This document is the primary technical reference for astronomers who wish to submit a proposal in response to the SOFIA Cycle 6 [Call for Proposals](#) (CfP). The CfP document and the Observer's Handbook (along with the documents and websites explicitly referred to within) contain information sufficient for planning viable SOFIA observations.

SOFIA is a joint project of NASA and the Deutsches Zentrum für Luft und Raumfahrt (DLR). The SOFIA Science Center (SSC), responsible for overseeing the scientific aspects of the mission, is located at the NASA Ames Research Center in Moffett Field, CA. Flight operations are conducted out of the NASA Armstrong Flight Research Center (AFRC) in Palmdale, CA. The Science Mission Operations are jointly managed by the Universities Space Research Association (USRA) for NASA and by the Deutsches SOFIA Institut (DSI), in Stuttgart, for DLR. Aircraft operations are managed by NASA AFRC.

This version of the handbook is applicable to for Cycle 6. Between the time of writing and the start of Cycle 6 observations, the analysis of data obtained as part of ongoing Instrument Commissioning work for HAWC+ are likely to provide more empirical information regarding instrument performance. The Observer's Handbook will be updated as necessary and the list of changes will be included at the beginning of the document. Critical updates will also be published on the Cycle 6 web page. Any information that supersedes what is given in this document will be explicitly indicated.

The following additional documents are available on the [SOFIA Information for Researchers web pages](#).

- The [SOFIA Cycle 6 Call for Proposals](#) describes how to prepare and submit proposals. It includes details on how proposals will be evaluated. It formally establishes the policies for all matters concerned with the rules governing SOFIA Cycle 6 for guest observers.
- The [FORCAST Observation Modes](#) document provides an explanation of the basic FORCAST observing modes for imaging observations.
- The [HIPO Throughput/Sensitivity Spreadsheet](#) provides tools to estimate the signal-to-noise for HIPO observations.
- The [Science Instrument Suite web pages](#) provide a brief overview of the suite of instruments that will be available on SOFIA once it reaches full operational capability.
- [The Science Vision for the Stratospheric Observatory for Infrared Astronomy](#) presents many compelling science questions that SOFIA is uniquely positioned to address. The complementarity among several astronomical facilities (current and future, particularly in the IR/mm wavelength regime) are discussed where relevant. *Please note, that any information regarding the performance of the telescope and instruments contained within the "Science Vision" is superseded by this document and the SOFIA web sites.*

1. Introduction

- 1. Introduction
 - 1.1 [SOFIA and Its Instruments](#)
 - 1.2 [Observing on an Aircraft](#)
 - 1.2.1 [Scheduling and Flight Planning](#)
 - 1.2.2 [Acquisition and Guiding](#)
 - 1.2.3 [Observing Moving Targets](#)
 - 1.2.4 [Line-of-Sight \(LOS\) Rewinds](#)
 - 1.3 [Performing Background Limited Observations](#)
 - 1.3.1 [Chopping and Nodding](#)
 - 1.3.1.1 [Symmetric and Asymmetric Chopping Techniques](#)
 - 1.3.1.1a [Symmetric Chopping Variations](#)
 - 1.3.1.1b [Asymmetric Chopping Variations](#)
 - 1.3.1.2 [Alternatives to Chop-Nod Cycles](#)
 - 1.3.2 [Alternatives to Chop-Nod Cycles](#)

1.1 SOFIA and Its Instruments

1.1 [SOFIA and Its Instruments](#)

The Stratospheric Observatory for Infrared Astronomy (SOFIA) is a telescope with an effective diameter of 2.5 meters, carried aboard a Boeing 747-SP aircraft. It is the successor to the smaller Kuiper Airborne Observatory, which was operated by NASA from 1974 to 1996. The observing altitudes for SOFIA are between 37,000 and 45,000 feet, above 99% of the water vapor in the Earth's atmosphere. The telescope was designed to allow imaging and spectroscopic observations from 0.3 to 1600 μm , with specific capabilities dependent on an evolving science instrument suite, making it one of the premier facilities for astronomical observations at infrared and sub-millimeter wavelengths. The present instrument suite provides coverage from 0.3–612 μm with additional capabilities currently in development.

The telescope for SOFIA was supplied by the DLR as the major part of the German contribution to the observatory. It is a bent Cassegrain with 2.7 m parabolic primary mirror (2.5 m effective aperture) and a 0.35 m diameter hyperbolic chopping secondary mirror. The telescope is mounted in an open cavity in the aft section of the aircraft and views the sky through a port-side door. The telescope is articulated by magnetic torque motors around a spherical bearing through which the Nasmyth beam passes. The unvignetted elevation range of the telescope is 20°–60°. The cross-elevation travel is only $\pm 3^\circ$ and, therefore, most of the azimuthal telescope movement required for tracking is provided by steering the airplane. Thus, the flight plan is determined by the list of targets to be observed during each flight.

The telescope feeds two f/19.6 Nasmyth foci, an IR focus for the science instruments and a visible light focus for guiding, using a dichroic and an aluminum flat. The secondary mirror is designed to chop at amplitudes of up to ± 5 arcmin at a frequency ≤ 10 Hz and up to ± 10 arcmin at a rate of ≤ 2 Hz. The visible beam is fed into the Focal Plane Imager (FPI+), which is an optical focal plane guiding camera. Independent of the FPI are two other optical imaging and guiding cameras, the Wide Field Imager (WFI) and the Fine Field Imager (FFI), both of which are installed on the front ring of the telescope.

Eight instruments, covering a wide range of wavelengths and resolving powers as shown in [Figure 1.1-1](#), are available for use on SOFIA. Three of the instruments are Facility-class Science Instruments (FSIs), which will be maintained and operated by the Science Mission Operations (SMO) staff.

FIFI-LS: Far Infrared Field-Imaging Line Spectrometer

An integral-field far-infrared spectrometer

FLITECAM: First Light Infrared Test Experiment Camera

A near-IR camera (including its grism modes) (FSI)

FORCAST: Faint Object InfraRed Camera for the SOFIA Telescope

A focal plane CCD imagerd-IR camera (including its grism modes) (FSI)

FPI+: Focal Plane Imager

A focal plane CCD imager

HAWC+: High-resolution Airborne Wideband Camera + Polarimeter

A far-IR camera and polarimeter (FSI)

Two instruments are Principal Investigator-class Science Instruments (PSIs), which will be maintained and operated by the Instrument Principal Investigator (PI) teams.

EXES: Echelon-Cross-Echelle Spectrograph

A mid-infrared high-resolution spectrograph (PSI)

GREAT: German Receiver for Astronomy at Terahertz Frequencies

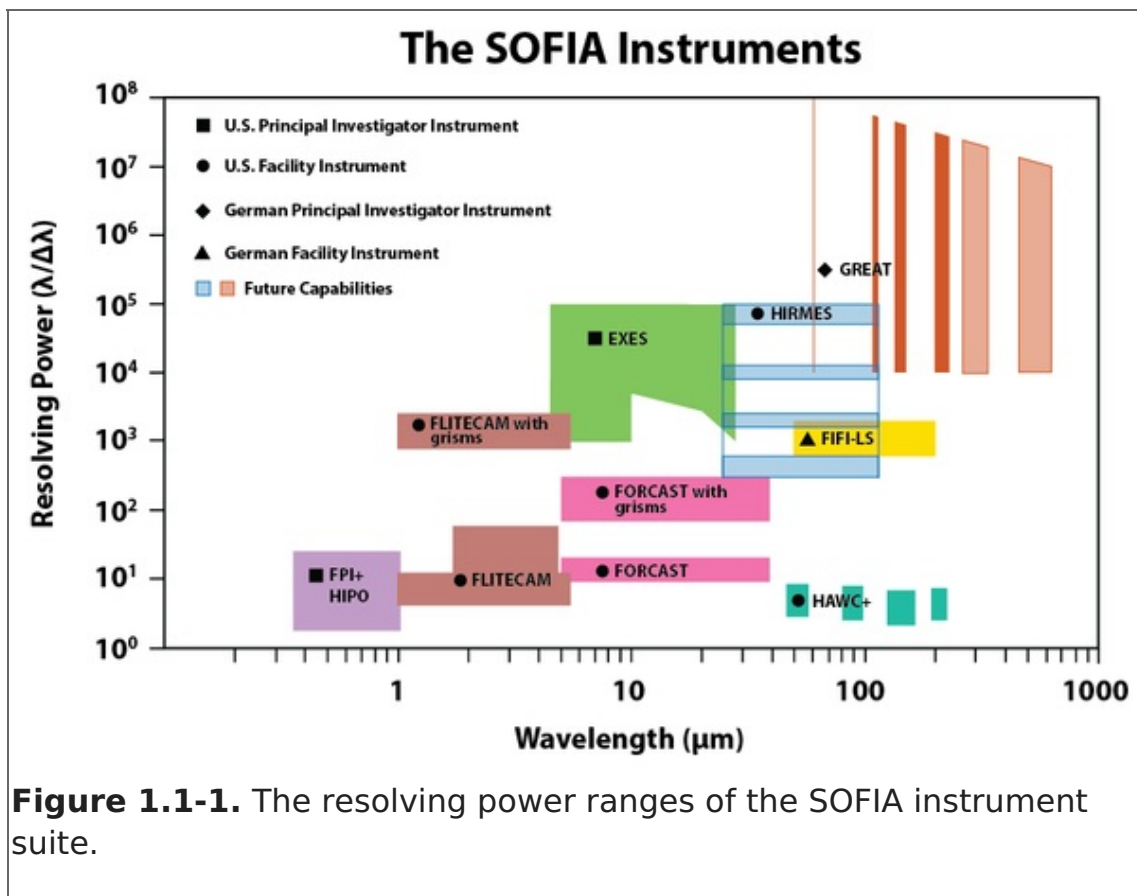
A heterodyne spectrometer, including the seven-beam receiver array upGREAT (PSI)

One instrument is a Special Purpose, Principal Investigator-class Science Instrument (SSI).

HIPO: High-speed Imaging Photometer for Occultations

A high-speed optical photometer

Figure 1.1-1.



The instrument capabilities, the available modes, and the resulting performance specifications of the telescope are described in later sections. For the purpose of this document, *configuration* refers to the setup of the telescope and instrument whereas *mode* refers to observational techniques employed during operations. Common combinations of configurations and modes are represented as selectable options within the Unified SOFIA Proposal and observation Tool (USPOT) via individual Astronomical Observation Templates (AOTs). Please note that this naming convention may not necessarily be employed uniformly in external resources for the instruments, i.e. in websites or documentation not managed by the SOFIA team.

Most of the observing time on SOFIA is open to the international astronomical community via Guest Observer (GO) proposal calls, which are issued on a yearly basis. The first of these proposal calls was for Early Science, for which observations were obtained in a series of flights from May–July, September, and November 2011. The first open call for proposals, Cycle 1, covered the period from late 2012 to the end of 2013. The current proposal call is for Cycle 6 observations, which will take place between 1 February, 2018 and 31 January, 2019. Proposals are being solicited for the Cycle 6 SOFIA flights by USRA on behalf of NASA. The observations will take place during a series of Science Flight Campaigns, each of which will focus on a single instrument configuration, over the duration of the cycle. The campaigns will be interspersed with aircraft maintenance and instrument commissioning. A single Southern Hemisphere observing series with up to two instruments is under consideration for the Cycle 6 time period, nominally in the months of July and August, during the southern winter.

[Return to Top of Page](#)

[1.2 Observing on an Aircraft](#)

[Table of Contents](#)

- 1.2 Observing on an Aircraft
 - 1.2.1 Scheduling and Flight Planning
 - 1.2.2 Acquisition and Guiding
 - 1.2.3 Observing Moving Targets
 - 1.2.4 Line-of-Sight (LOS) Rewinds

Return to the Table of Contents for this section at any time by selecting [Return to Table of Contents](#). Users may also navigate through the entire Observer's Handbook by using the complete Table of Contents menu to the right.

1.2 Observing on an Aircraft

The duration of each SOFIA flight is expected to be between 9–10 hours, 7–8 hours of which will be available for observing at altitudes of 37,000–45,000 feet. FPI+ is always available. Among the other instruments, only one will be installed on the telescope at any time, with the exception of the FLIPO configuration (FLITECAM + HIPO). The SMO director will determine the total number of flights dedicated to each instrument, after consideration of the number of TAC (Time Allocation Committee) approved proposals for each.

Proposals should request observing time in units of hours. Once a proposal has been approved, the first stage is complete and the proposer is then expected to carry out the detailed planning of their observations in consultation with a support scientist or, for PI instruments, with the instrument team. This second stage of observation planning is known as Phase II. Proposers of successful proposals will be informed who their SMO support scientists are and how to contact them.

On each SOFIA flight, there will be one or more seats available for PIs or designated Co-Investigators (Cols) of the proposals scheduled for that flight. Since there are a limited number of seats available on each flight, the choice of proposers given the opportunity to fly on SOFIA will be made by the SMO director according to a number of considerations, including the complexity of the observations to be performed, the duration of science observations for each program on the flight, and the proposal rank.

The observations will be carried out either by members of the instrument team along with SOFIA personnel, or solely by SOFIA personnel. The proposers on board SOFIA will participate in the observing, and monitor the data as it is received, but will have limited decision making abilities. For example, the proposer will be allowed to make real-time changes to exposure times for different filters or channels. However, changing targets or any modifications that alter the durations of flight-legs will not be allowed.

Those PIs or Cols chosen to fly aboard SOFIA will be required to complete a flight participation form, a medical release form, and documentation related to badging. In addition, they will be required to participate in an Egress Training course prior to being allowed on board the aircraft. Full details will be provided to proposers of approved proposals during the Phase II process.

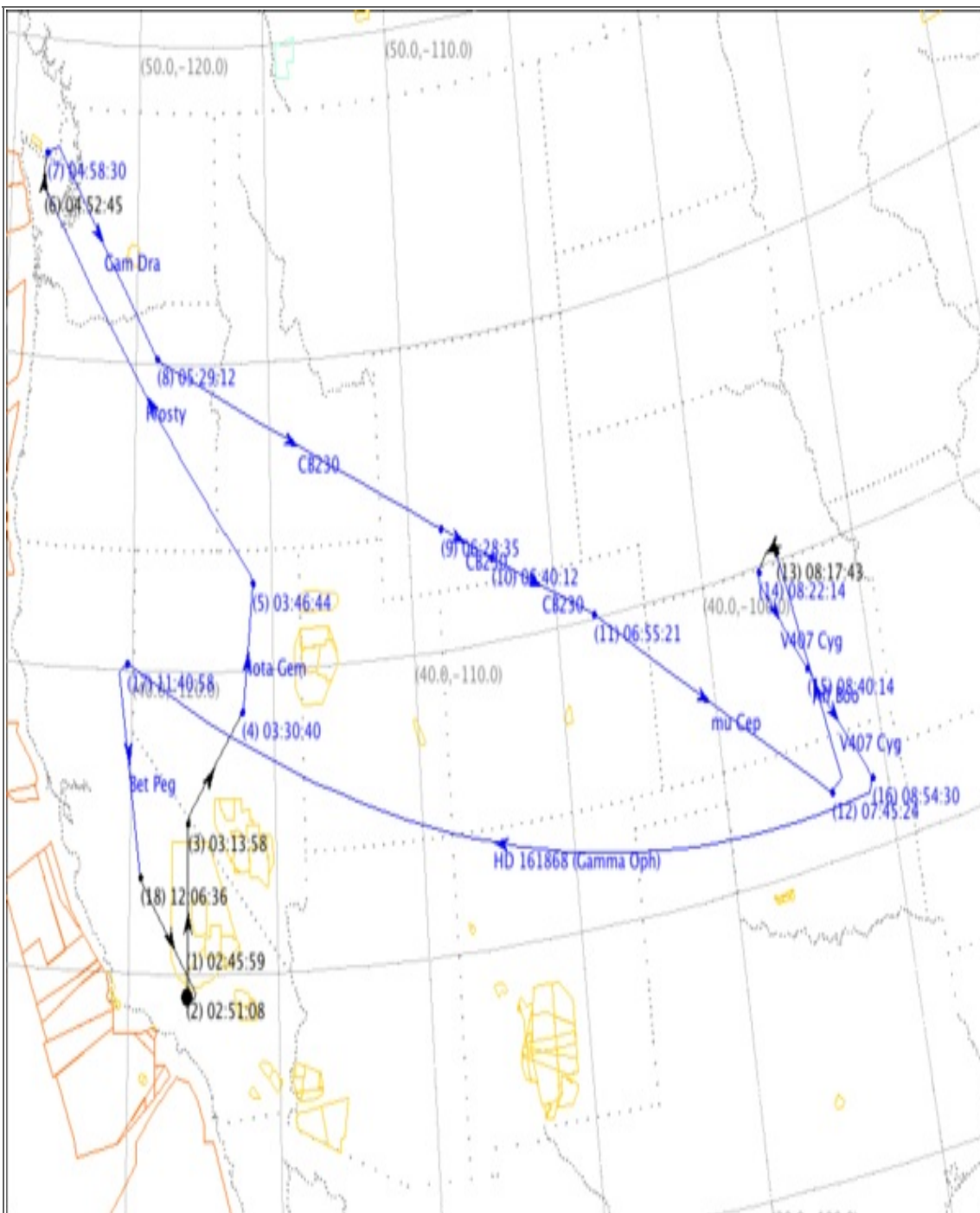
[Return to Table of Contents](#)

1.2.1 Scheduling and Flight Planning

Scheduling and flight planning will be handled by the SMO staff and is not the responsibility of the proposer. However, an understanding of the flight planning process and the restrictions inherent to airborne astronomy may be useful in preparing a successful proposal.

The most distinctive aspect of SOFIA flight planning is the interdependency of the targets observed in a flight. Because the azimuthal pointing is controlled primarily by the aircraft heading and because, in normal operations, the take-off and landing air fields are the same, efficient flight plans must generally balance eastbound with westbound flight legs and southbound with northbound legs. This also means that for any flight only a limited fraction of the observing can be performed in a given region of the sky. An example of a flight plan flown during Basic Science in May 2011 is shown in [Figure 1.2-1](#) below. More examples of flight plans can be found on the webpages for earlier cycles.

Figure 1.2-1.



Flight Plan Name: File: BS1_01_Wx12_Fallon.fp
 Flight ID: 2011/05/06
 Est. Takeoff Time: 2011-May-06 02:45 UTC
 Est. Landing Time: 2011-May-06 12:29 UTC
 Flight Duration: 09:44
 Weather Forecast : 0000 Mon May 16 2011 - 1200 Wed May 18 2011 UTC
 Saved: 2011-May-16 22:37 UTC User: kbower

Figure 1-1. This is a sample flight plan flown in May 2011 during Basic Science. The take-off and landing were both from Palmdale, CA. Each leg is labeled with a time stamp and observing target when appropriate. Flight legs shown in black were "dead legs" during which no target was observed. The orange and yellow outlines indicate airspace with varying degree of restrictions which add to the complexity of designing efficient flight plans.

For the proposer this leads to several considerations:

- A strong scientific case must be made for observations with rigid time constraints or strict cadences in order to justify the restrictions they will impose on flight planning.
- Because the sky distribution of targets typically proposed for SOFIA observations (centered on the Galactic plane and certain regions of star formation, including Orion) is highly inhomogeneous, targets in areas that complement these high-target-density regions will allow more efficient flight planning and will likely have a higher chance – for a given scientific rating – to be scheduled. Consequently, it may be advantageous for those who can choose between targets from a large source pool for their SOFIA proposals and for those who plan to submit survey proposals to emphasize sources from complementary regions.
- For example, objects that complement the potentially popular Orion molecular clouds include circumpolar targets or targets north of about 40° with a right ascension in a roughly 6 to 8 hour wide window centered about 6 hours before or after the right ascension of Orion.
- The maximum length of flight legs will be determined by the need for efficient flight plans as well as the typical requirement that SOFIA take-off and land in Palmdale, California. In most cases, the longest possible observing leg on a given target is ~ 4 hours. Therefore, observations of targets requiring long integrations may have to be done over multiple flights and flight legs.
- Proposals may be submitted for observations for which the flight does not originate or end in Palmdale, CA, for example, in order to conduct observations under time constraints that require a specific flight path or that require a single flight leg in excess of ~ 4 hours. Such proposals would be equivalent to a deployment and due to resource requirements and the impact that this would have on flight planning, the scientific justification must be strong. The final decision on whether to allow programs with such a high impact on scheduling and flight planning will be made at the Director's discretion.

Proposers are encouraged to review the Flight Planning presentation delivered by Dr. Randolph Klein at the SOFIA User's Workshop in November, 2011. The full list of presentations can be found on the SOFIA web site. In addition, a much more detailed discussion of target scheduling and flight planning can be found in the [Observation Scheduling and Flight Planning White Paper](#).

[Return to Table of Contents](#)

1.2.2 Acquisition and Guiding

SOFIA has three optical cameras for acquisition, guiding, and tracking. The Wide Field Imager (WFI) and Fine Field Imager (FFI) are mounted on the telescope head ring. The upgraded Focal Plane Imager (FPI+) images the focal plane of the telescope via a dichroic and a tertiary mirror. All three imagers use 1024x1024 pixel, frame-transfer CCD cameras.

The WFI has a $6^\circ \times 6^\circ$ field of view, and is expected to achieve a centroid precision of $\sim 8''$ for stars brighter than $R = 9$. The field of view of the FFI is 70×70 arcmin². It is expected to achieve a centroid precision of ~ 1 arcsec for $R = 11$ or brighter stars. The FPI+ has an ~ 8 arcmin diameter field of view and is expected to provide a centroid precision of 0.05 arcsec for $R = 16$ (no chopping) and $R = 14$ (chopping) or brighter stars.

Most observers do not need to select guide stars as they will be chosen by the SMO staff.

However proposers should be aware that the guiding cannot be done on IR sources unless they are optically bright.

[Return to Table of Contents](#)

1.2.3 Observing Moving Targets

Once SOFIA achieves its nominal operating capabilities, it will be able to observe solar system targets by (i) guiding on the object itself, (ii) offset guiding from field stars, or (iii) predictive tracking based on accurate ephemerides.

Successful guiding on a moving target requires it to be bright at visible wavelengths, where the guider cameras operate. We are typically able to guide on solar system targets with $R \leq 10$ and that have a non-sidereal angular speed of 1 arcsec/s or less. The minimum acceptable solar elongation for a target is limited by the lower elevation limit of the telescope and the rule that no observations can be acquired before sunset or after sunrise. The minimum solar elongation is roughly 24 degrees.

Identification of solar system targets will be done manually by the Telescope Operator by inspecting images obtained with the FPI. The ephemerides of the proposed target must be accurate enough to allow for unambiguous identification. While the required accuracy could vary somewhat based on the complexity of the background star field, it should in general be better than about 30/arcsec.

[Return to Table of Contents](#)

1.2.4 Line-of-Sight (LOS) Rewinds

The SOFIA telescope mounting is similar to that of a typical altitude-azimuth telescope. One such similarity is that while tracking a target, the image rotates within the field of view. However, the SOFIA telescope is also similar to an on-orbit gyro-stabilized telescope, with a third control axis along the line of sight (LOS). So the sky image in the focal plane does not change orientation until the telescope approaches an LOS limit. Then the telescope must be slewed about the LOS axis to at least mid-range, or more typically to near the opposite limit. Each of these "LOS rewinds" interrupts observing for ~10 to 15 seconds and may have to occur several times during an observing leg. The range of LOS rotation is limited to only $\pm \sim 3^\circ$, and the frequency of LOS rewinds depends on the rate of field rotation. This in turn depends on the target's current azimuth and elevation, and weakly on the aircraft latitude. This is similar to the field rotation that occurs at ground-based altazimuth telescopes, but the rate differs due to the aircraft ground speed. Each target's azimuth and elevation are unknown until the observation is scheduled into a flight plan, and therefore the field rotation angles and rotation rate are not available until then. The overall character of the airborne field rotation rate in the observable sky above the aircraft is shown in [Figure 1.2-2](#). The corresponding maximum time between LOS rewinds is shown in [Figure 1.2-3](#).

Figure 1.2-1.

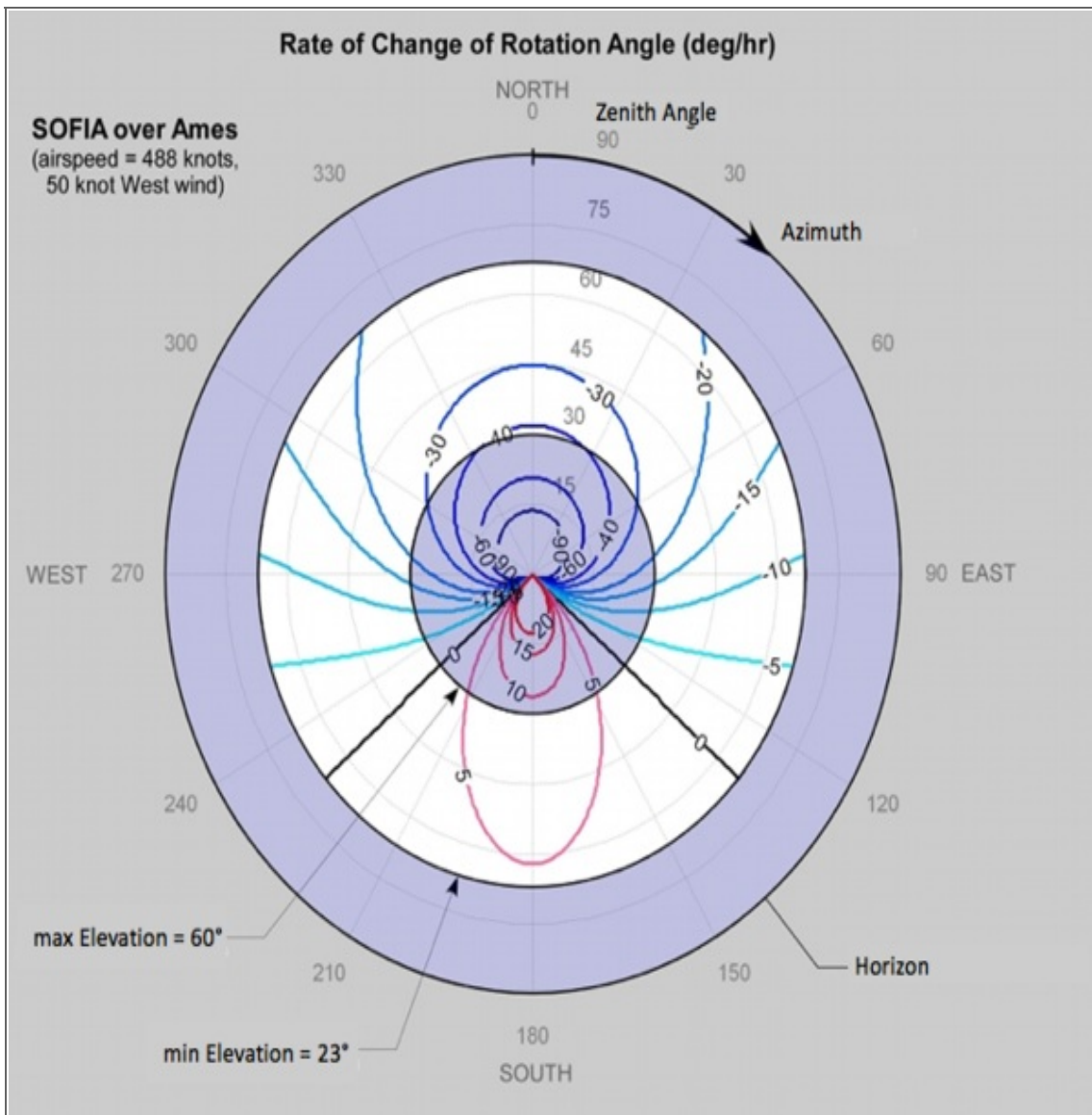


Figure 1-2. This plot shows the rate of change in the rotation angle (degrees/hour) as a function of target elevation and azimuth. The rates are calculated assuming an aircraft latitude of 37° N. The observable range of elevation angles is shown in white.

Figure 1.2-3.

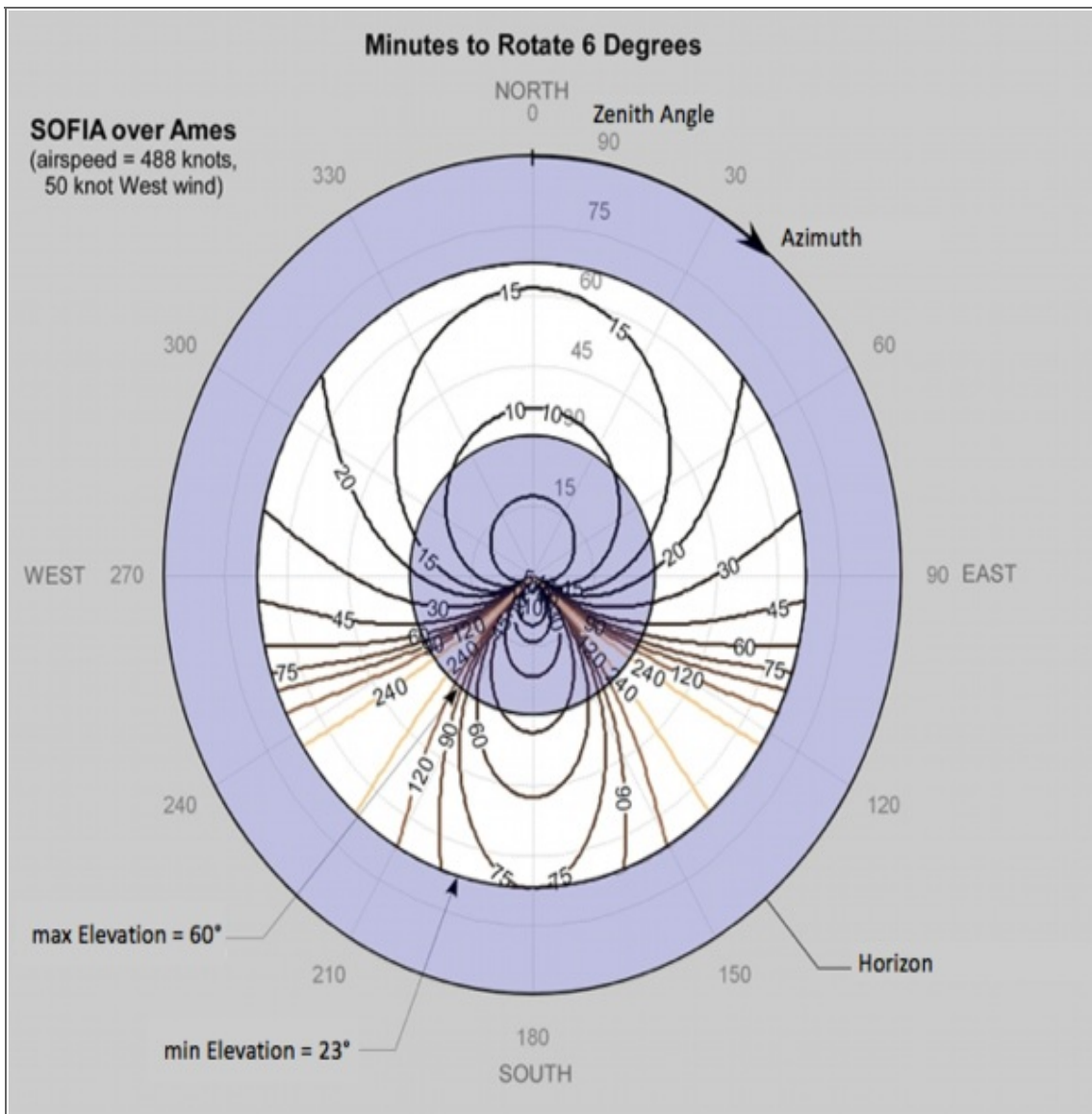


Figure 1-3. This plot shows the time it takes for the field of view to rotate by 6 degrees as a function of target elevation and azimuth. The times are calculated assuming an aircraft latitude of 37° N. The observable range of elevation angles is shown in white.

For the majority of SOFIA flights that originate in Palmdale, Figures 1.2-2 or 1.2-3 can be used to anticipate what may occur in this regard. Targets at high northern declinations require eastward headings, and may require quite frequent LOS rewinds. Targets near the celestial equator are likely to have very little or no field rotation and may not need any LOS rewind, even during a long observing leg.

For example, during the summer months the W3 star forming region rises in the northeast while it is in the observable elevation range (20° to 60°). On Figure 1.2-2, this indicates field rotation rates of about -25° to -35° per hour, or roughly 6 degrees every 15 minutes as indicated on Figure 1.2-3.

When using Figures 1.2-2 and 1.2-3 to estimate the rotation of field, it is important to bear in mind some associated caveats. In practice the time between LOS rewinds is often a little shorter due to the need for some margin near the limits, especially if there is any turbulence. The plotted rates were calculated for latitude North 37° and the rates are weakly dependent on latitude. Even on local flights from Palmdale, SOFIA may make

observations in the latitude range North 20° to North 55°.

Special care must be taken when designing spectroscopic observations of extended regions. Proposers should bear in mind that the orientation of the slit on their targets will change with each LOS rewind. For point sources this should not cause problems—but for extended sources this means that after each rewind the slit will be sampling a slightly different region of the source. In addition, there is no way to choose the orientation of the slit on the target. However, once the likely range of rotation angle values is known, the orientation of a spectrograph slit (e.g. in EXES) on a region can be anticipated.

Two of the Science Instruments, FIFI-LS and GREAT, use a K-mirror to rotate the telescope FIR image before it arrives at the detectors. This is slaved to the onboard real-time rotation angle, so that during an observing leg the observed orientation of the FIR image is held constant.

[Return to Table of Contents](#)

1.3 Performing Background Limited Observations

Table of Contents

- [1.3 Performing Background Limited Observations](#)
 - [1.3.1 Chopping and Nodding](#)
 - [1.3.1.1 Symmetric and Asymmetric Chopping Techniques](#)
 - [1.3.1.1a Symmetric Chopping Variations](#)
 - [1.3.1.1b Asymmetric Chopping Variations](#)
 - [1.3.2 Alternatives to Chop-Nod Cycles](#)

Return to the Table of Contents for this section at any time by selecting [Return to Table of Contents](#). Users may also navigate through the Handbook using the Table of Contents menu to the right.

1.3 Performing Background Limited Observations

Because the sky is so bright in the infrared (IR) relative to astronomical sources, the way in which observations are made in the IR is considerably different from the (more familiar) way they are made in the optical. Any raw image or spectrum of a region in the IR is overwhelmed by this sky background emission. The situation is similar to trying to observe in the optical during the day. The bright daylight sky swamps the detector and makes it impossible to see astronomical sources in the raw images.

SOFIA operates at altitudes above 99% of the water vapor in the atmosphere. The average atmospheric transmission across the SOFIA bandpasses is about 80% at these altitudes. There are however a number of strong absorption features which, even at these altitudes, can make the atmosphere opaque. Broad band filters, such as those on FORCAST, account for the presence of such features. However, when using high-resolution tunable instruments such as EXES, FIFI-LS, and GREAT, it is necessary to examine the atmospheric transmission at the wavelengths of interest in detail. This may be done using the more general web interface to the [ATRAN](#) program that was developed and provided to the SOFIA program by Steve Lord, or through the more instrument specific SOFIA Instrument Time Calculator ([SITE](#)). A plot of the atmospheric transmission seen by SOFIA in comparison to that achieved at Mauna Kea is shown in [Figure 1.3-1](#) below.

Figure 1.3-1.

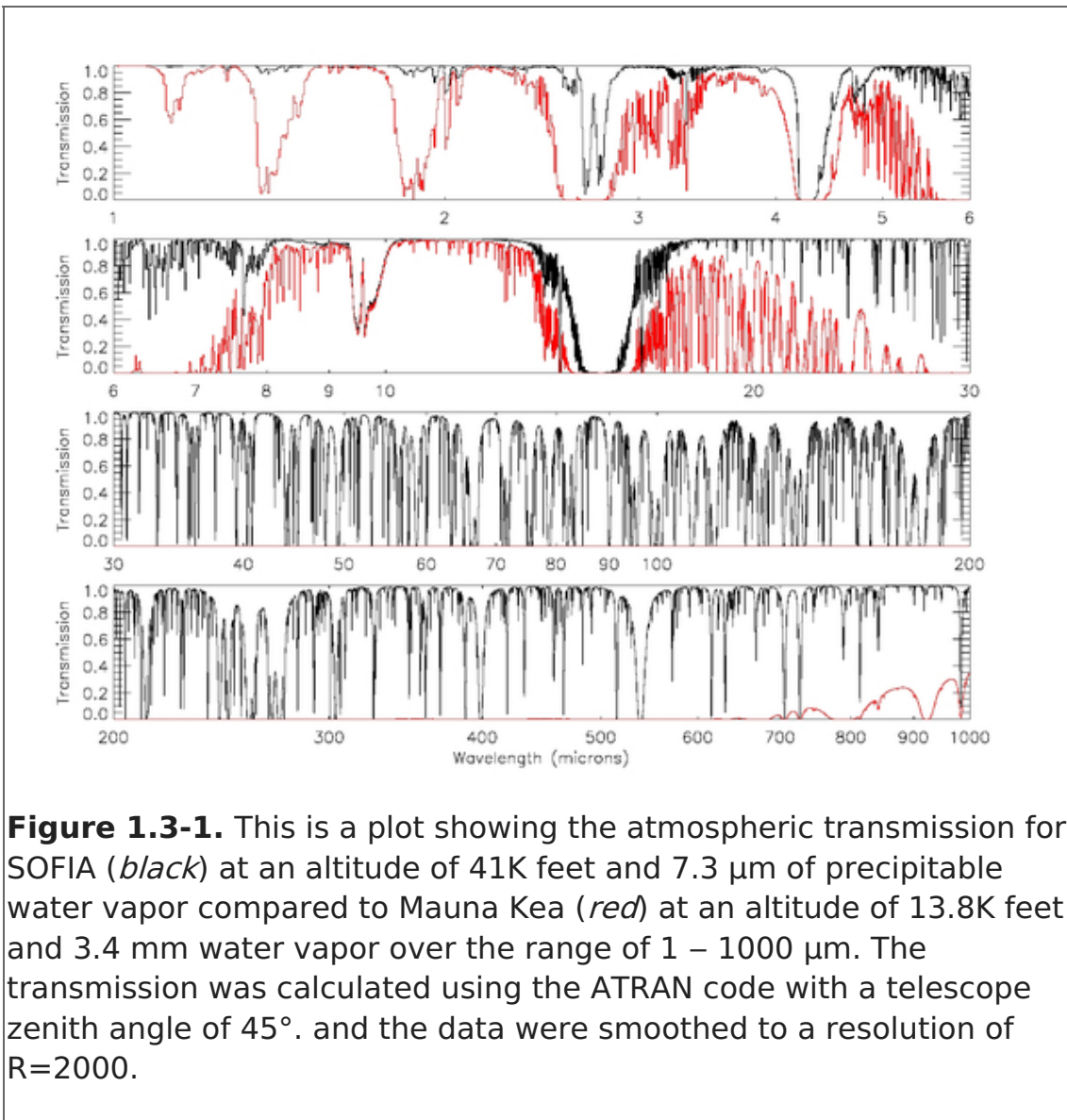


Figure 1.3-1. This is a plot showing the atmospheric transmission for SOFIA (*black*) at an altitude of 41K feet and 7.3 μm of precipitable water vapor compared to Mauna Kea (*red*) at an altitude of 13.8K feet and 3.4 mm water vapor over the range of 1 – 1000 μm. The transmission was calculated using the ATRAN code with a telescope zenith angle of 45°. and the data were smoothed to a resolution of R=2000.

In addition to its dependence on wavelength due to the presence of absorption features, the atmospheric transmission varies with latitude and with time of year, primarily due to differences in the amount of water vapor. It also exhibits variations on smaller time scales due to changes in the location of the tropopause. Full discussions of these issues may be found in Haas & Phister 1998 (PASP, 110, 339) and Horn & Becklin 2001 (PASP, 113, 997).

The variations in atmospheric water vapor could have a significant impact on some observations, particularly when using EXES, FIFI-LS, and GREAT or grism modes with FLITECAM and FORCAST. For example, GREAT observations of a line situated on the shoulder of an atmospheric water feature could be strongly affected by water vapor variability. [SITE](#) allows the user to specify the water vapor overburden and adjusts the time estimates appropriately. The water vapor monitor has been installed and is currently undergoing testing, but may not be fully functional during Cycle 6.

[Return to Table of Contents](#)

1.3.1 Chopping and Nodding

In order to remove the background from the IR image and detect the faint astronomical

sources, observations of another region (free of sources) are made and the two images are subtracted. However, the IR is highly variable, both spatially and—more importantly—temporally. It would take far too long (on the order of seconds) to reposition a large telescope to observe this sky background region: by the time the telescope had moved and settled at the new location, the sky background level would have changed so much that the subtraction of the two images would be useless. In order to avoid this problem, the secondary mirror (which is considerably smaller than the primary mirror) of the telescope is tilted, rather than moving the entire telescope. This allows observers to look at two different sky positions very quickly (on the order of a few to 10 times per second) by tilting the secondary. Tilting the secondary between two positions is known as **chopping**.

Unfortunately, moving the secondary mirror causes the telescope to be slightly misaligned, which introduces optical distortions in the images—notably, the optical aberration known as coma and additional background emission from the telescope that is considerably smaller than the sky emission but present nonetheless. The additional telescopic background mentioned can be removed by moving the entire telescope to a new position and then chopping the secondary again between two positions. (Subtracting the two chop images at this new telescope position will remove the sky emission but leave the additional telescopic background due to the misalignment; subtracting the result from the chop-subtracted image at the first telescope position will then remove the background.)

Since the process of moving to a new position is needed to remove the additional background from the telescope, not the sky, it can be done on a much longer timescale. (The variation in the telescopic backgrounds occurs on timescales on the order of tens of sec to minutes, much slower than that the variation in the sky emission.) This movement of the entire telescope, on a much longer timescale than chopping, is known as **nodding**. The two nod positions are usually referred to as nod A and nod B. The distance between the two nod positions is known as the **nod throw**.

The chop-subtracted images at nod position B are then subtracted from the chop--subtracted images at nod position A. The result will be an image of the region, without the sky background emission or the additional emission resulting from tilting the secondary during the chopping process. The sequence of chopping in one telescope position, nodding, and chopping again in a second position is known as a **chop/nod cycle**.

Again, because the IR sky is so bright, deep images of a region cannot be obtained (as they are in the optical) by simply observing the region for a long time with the detector collecting photons (integrating) continuously. As stated above, the observations require chopping and nodding at fairly frequent intervals. Hence deep observations are made by effectively stacking a series of chop/nod images. Furthermore, IR detectors are not perfect, and often have bad pixels or flaws. In order to avoid these defects on the arrays, and prevent them from marring the final images, observers employ a technique known as dithering. **Dithering** entails moving the position of the telescope slightly with respect to the center of the region observed each time a new chop/nod cycle is begun, or after several chop/nod cycles. When the images are processed, the observed region will appear in a slightly different place on the detector. This means that the bad pixels do not appear in the same place relative to the observed region. The individual images can then

be registered and averaged or medianed, a process that will eliminate (in theory) the bad pixels from the final image.

Many of the instruments onboard SOFIA implement chopping and/or nodding techniques in order to minimize the contribution of background noise in observations; [Table 1.3-1](#) provides the nomenclature between some of the SOFIA instruments with similar chopping and nodding techniques. Depending on the instrument and the required exposure time and resolution for the object being observed, other methods of optimization may be more beneficial to the observation ([Section 1.3.2](#)).

Table 1.3-1.

Inter-Instrumentation Mode Translations

Technique	EXES	FIFI-LS	FLITECAM	FORCAST	GREAT ³	HAWC+
Symmetric Chopping¹		Symmetric Chop		NMC	Beam Switching	NMC
				NPC		
Asymmetric Chopping¹		Bright Object				
		Asymmetric Chop		C2NC2		
				NXCAC		
Nodding Only	Nod On Slit		Nod Along Slit		Total Power	
	Nod Off Slit		Nod Off Slit			
Dithering Only	Map		Stare	Slitscan		
Continuous²						OTFMAP

¹Modes listed under Chopping may or may not also nod and/or dither.

²Modes listed under Continuous are non-discrete methods of observation for eliminating background noise and are discussed in [Section 1.3.2](#).

³GREAT implements chopping and nodding techniques, but is also limited by the temperature of the receiver. See [Section 7.1.2.1](#) for calculations.

1.3.1.1 Symmetric and Asymmetric Chopping Techniques

Chopping can be done either symmetrically or asymmetrically. The distance between the two chop positions is known as the **chop throw**.

Symmetric chopping means that the secondary mirror is tilted symmetrically about the telescope optical axis (also known as the **boresight**) in the two chop positions. Variations of symmetric chopping techniques include the general C2 and C2N techniques, with variations known as NMC (Nod Match Chop) and NPC (Nod Perp Chop). Symmetric chopping modes use the standard ABBA nod cadence, as described in Section 1.3.1.1.

Asymmetric chopping means that the secondary is aligned with the telescope boresight in one position, but is tilted away from the boresight in the chop position. A variation of the basic asymmetric chop mode is C2NC2. Asymmetric chopping modes use an ABA nod cadence, as described in [Section 1.3.1.1b](#).

Figure 1.3-2.

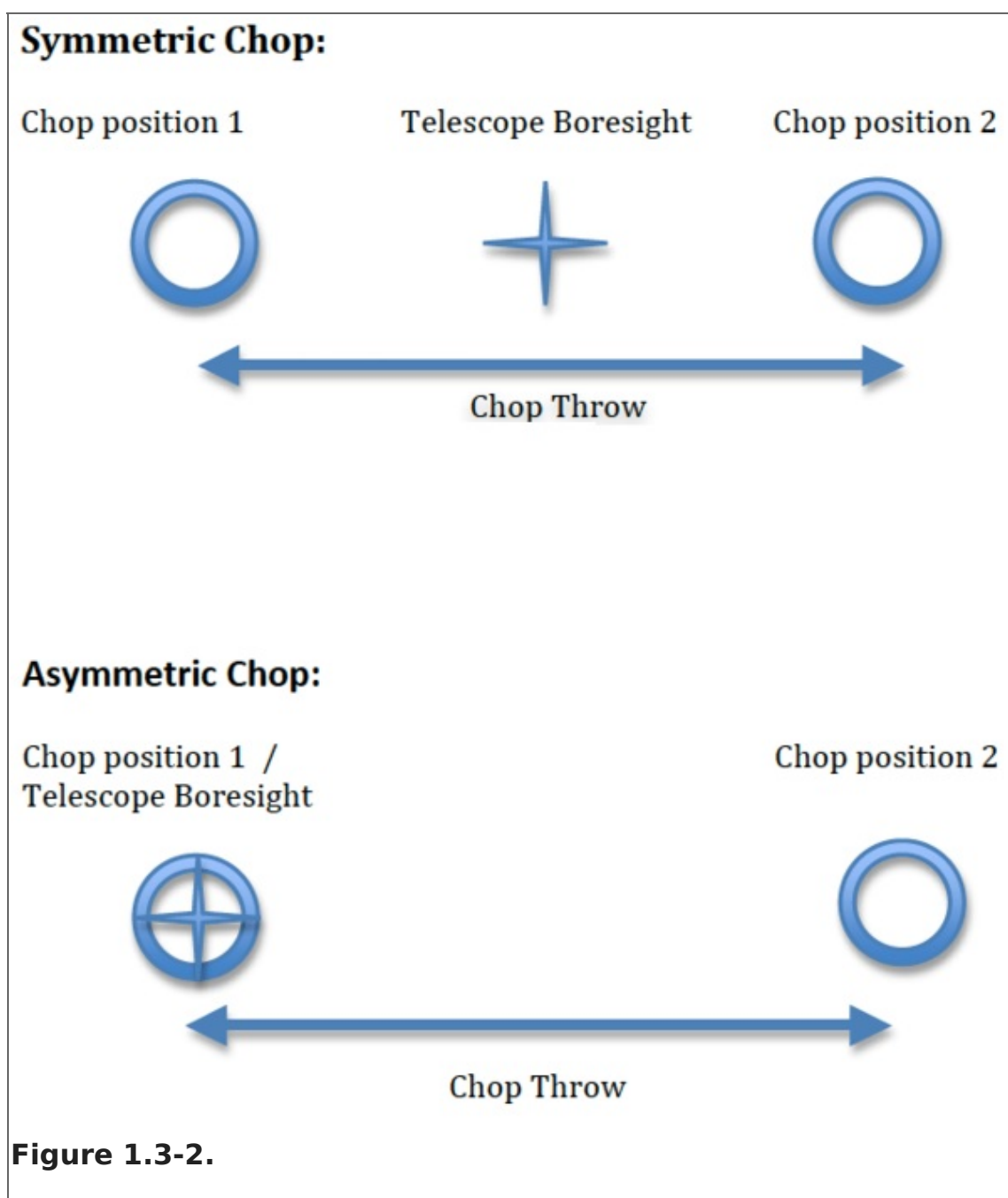


Figure 1.3-2.

Figure 1.3-3.

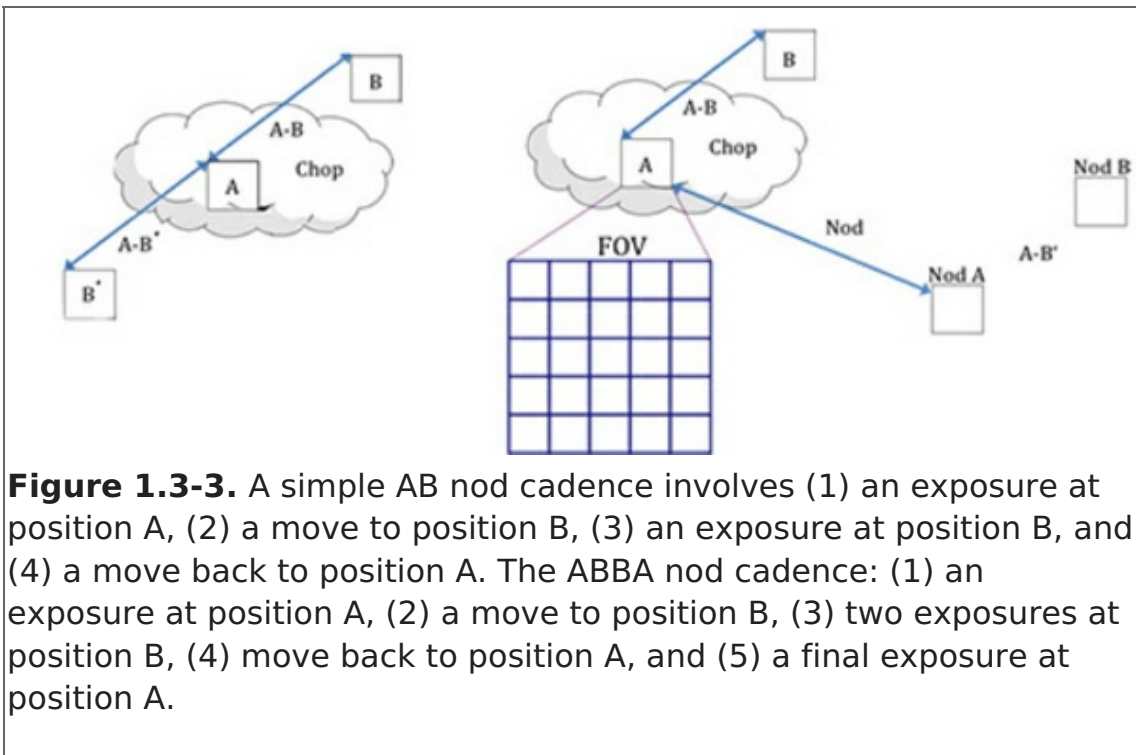


Figure 1.3-3. A simple AB nod cadence involves (1) an exposure at position A, (2) a move to position B, (3) an exposure at position B, and (4) a move back to position A. The ABBA nod cadence: (1) an exposure at position A, (2) a move to position B, (3) two exposures at position B, (4) move back to position A, and (5) a final exposure at position A.

[Return to Table of Contents](#)

1.3.1.1a Symmetric Chopping Variations

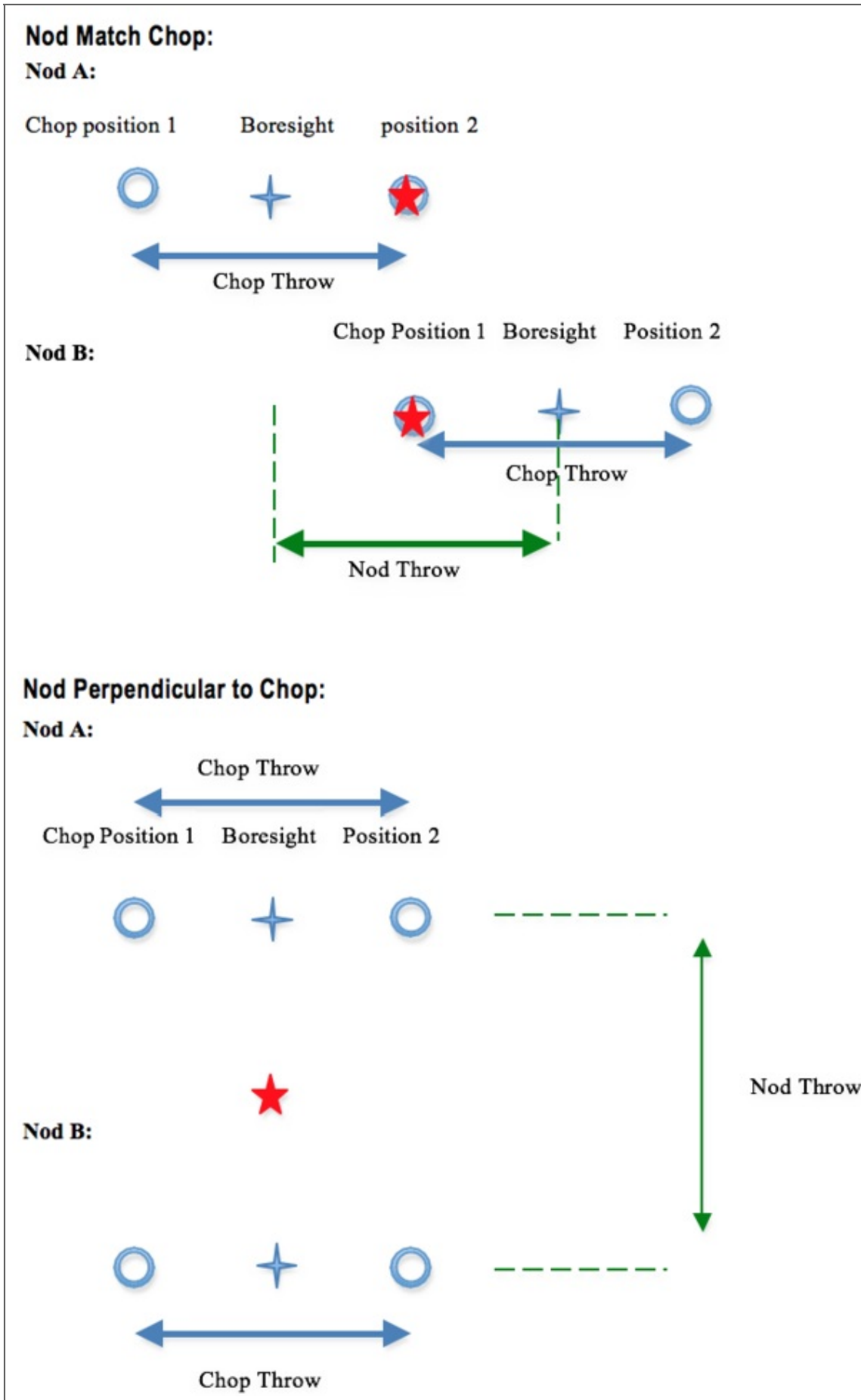
The shared characteristic of symmetric chopping methods is the symmetric chop about the optical axis of the telescope. NMC and NPC differ in their nodding techniques. Note from Table 1.3-1 that NMC is referred to as Asymmetric Chop for FIFI-LS, Beam Switching for GREAT, and NMC for both HAWC+ and FORCAST.

In NMC, the telescope is pointed at a position half of the chop throw distance away from the object to be observed, and the secondary chops between two positions, one of which is centered on the object. The nod throw has the same magnitude as the chop throw (hence the name Nod_Match_Chop), and is in a direction exactly 180 degrees from that of the chop direction i.e. anti-parallel, such that when the telescope nods, the source is located in the opposite chop position. This mode uses the standard ABBA nod cadence. The final image generated by subtracting the images obtained for the two chop positions at nod A and those at nod B and then subtracting the results will produce three images of the star, one positive and two negative, with the positive being twice as bright as the negatives.

In the case of NPC, the nod is perpendicular to the chop. The telescope is offset by half the nod throw from the target in a direction perpendicular to the chop direction, and the secondary chops between two positions. The nod throw usually (but not necessarily) has the same magnitude as the chop but is in a direction perpendicular to the chop direction. This mode also uses the standard ABBA nod cadence. The final image is generated by subtracting the images obtained for the two chop positions at nod A and those at nod B

and then subtracting the results; it will therefore have four images of the star in a rectangular pattern, with the image values alternating positive and negative. Unlike NMC, each beam in NPC has the same relative intensity.

Figure 1.3-4.



[Return to Table of Contents](#)

1.3.1.1b Asymmetric Chopping Variations

In C2NC2 (known as Asymmetric Chop in FIFI-LS observations), the telescope is first pointed at the target (position A). In this first position, the secondary is aligned with the optical axis (or boresight) for one observation and then is tilted some amount (often 180–480 arcseconds) for the second (asymmetrically chopped) observation. This is an asymmetric C2 mode observation. The telescope is then slewed some (usually large) amount away from the target to a sky region without sources (position B), and the asymmetric chop pattern is repeated. C2NC2 observations are taken as a series of 8 (C2) files in the sequence A B A A B A A B, i.e. an ABA nod cadence with dithering to remove correlated noise. Again, the time between slews is typically 30 sec. This mode is particularly useful for large extended objects, smaller objects that are situated within crowded fields, or regions of diffuse emission with only limited sky positions suitable for background removal.

Figure 1.3-5.

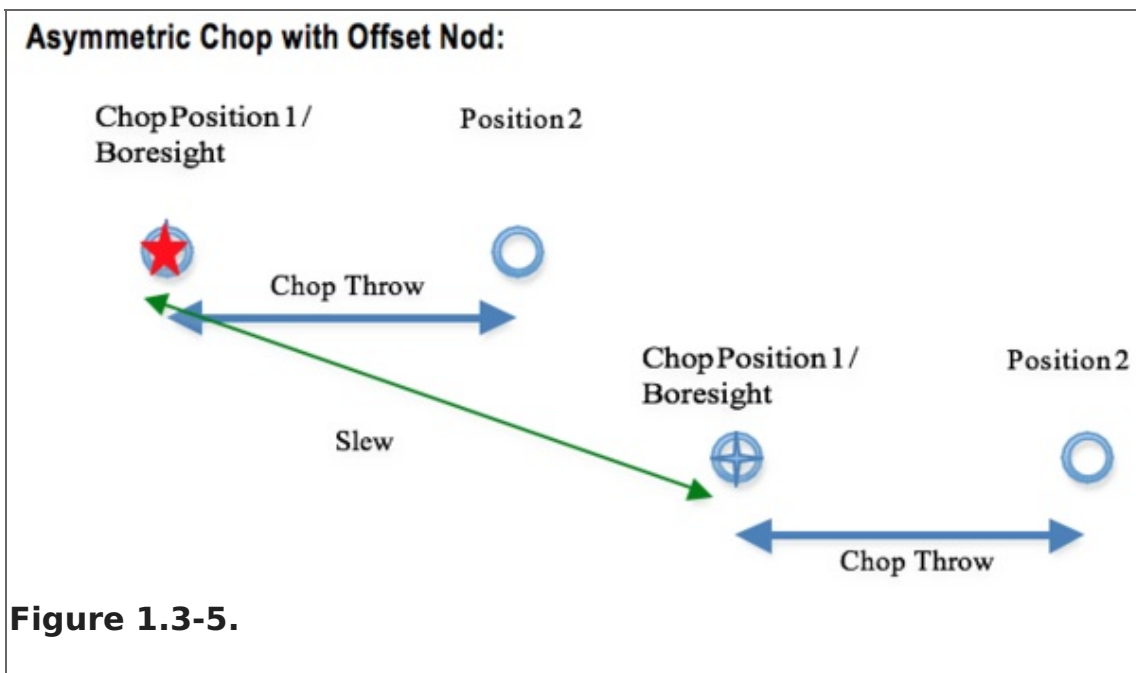


Figure 1.3-5.

Figure 1.3-6 demonstrates how a C2NC2 observation might be designed for a large, extended object. It is immediately apparent from the figure, that C2NC2 has an efficiency of only ~20%. This is a much lower efficiency than either symmetric chopping variations since only a single chop position out of a full chop/nod cycle is on source. This should be taken into consideration when designing science proposals.

Figure 1.3-6.

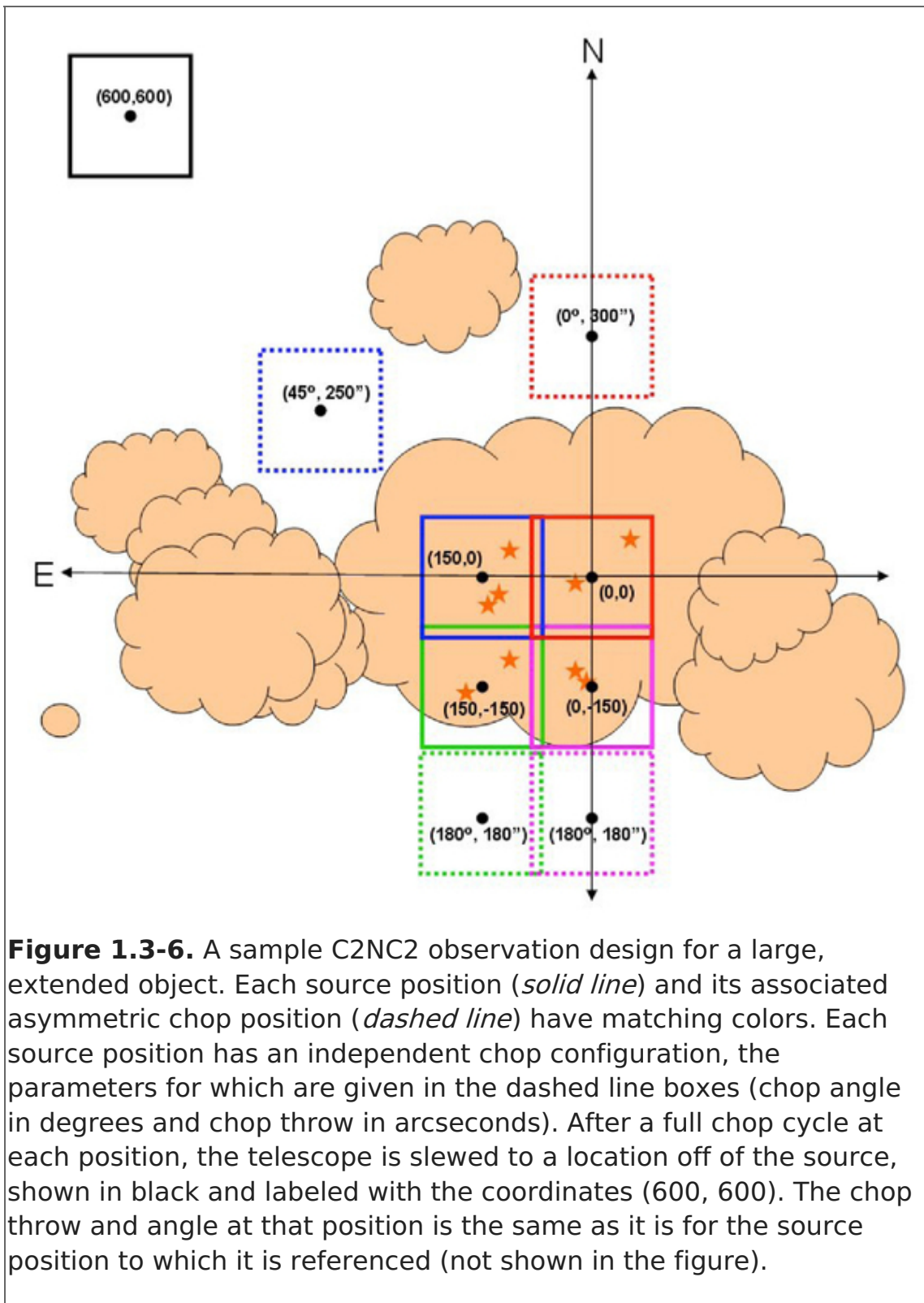


Figure 1.3-6. A sample C2NC2 observation design for a large, extended object. Each source position (*solid line*) and its associated asymmetric chop position (*dashed line*) have matching colors. Each source position has an independent chop configuration, the parameters for which are given in the dashed line boxes (chop angle in degrees and chop throw in arcseconds). After a full chop cycle at each position, the telescope is slewed to a location off of the source, shown in black and labeled with the coordinates (600, 600). The chop throw and angle at that position is the same as it is for the source position to which it is referenced (not shown in the figure).

The Asymmetric Chop mode of FIFI-LS typically implements an ABBA nod sequence, but is otherwise equivalent to C2NC2. NXCAC (Nod not related to Chop with Asymmetric Chop) mode is the FORCAST grism version of C2NC2.

Bright Object mode for FIFI-LS is also an asymmetric chopping mode, using observations of two map positions and one off-position per nod-cycle through an asymmetric chop. This technique is utilized to improve the efficiency of mapping bright objects, where the total observing time is dominated by telescope movements.

[Return to Table of Contents](#)

1.3.2 Alternatives to Chop-Nod Cycles

As chopping and nodding require a considerable amount of an observation's awarded time spent off-source, the amount of exposure time observing on the target is limited and subject to large observational overheads waiting for the telescope and/or secondary mirror assembly to complete chop/nod/dither movements. An alternative is to implement continuous scanning techniques. Of the instruments currently offered on SOFIA, only GREAT, HAWC+, and FPI+ offer continuous scanning methods of observation.

Nodding Only Modes

GREAT

Total Power - The telescope alternates between the target and a nearby reference position that is free of emission, using ON-OFF source cycles (typically spending ≤ 30 seconds on source). This mode is used when observing an extended source or a crowded region.

EXES

Nod On Slit - The telescope is nodded along the slit at distances that keep the target within the slit length. The nod throw is half the slit length. This is the most efficient EXES mode for point sources.

Nod Off Slit - The telescope is nodded such as that the object is not on the slit. This is used for extended sources or when the PSF is larger than four times the slit length.

Dithering Only Modes

EXES

Map - The telescope is moved perpendicular to the slit while EXES takes spectra on a grid of telescope positions, which are always one dimensional stripes.

FLITECAM

Stare - STARE mode observations involve a single telescope pointing centered on the source with dither pattern relative to it to facilitate background subtraction and image calibration. Dithering can be performed by selecting from pre-programmed dither patterns, or by defining a custom pattern. Observational experience has shown that STARE observations without dithers are particularly challenging with FLITECAM due to thermal background issues. Therefore, we recommend using dithers with at least 9 points, particularly longward of $2.2 \mu\text{m}$.

FORCAST

Slitscan - In Slitscan mode, the slit is moved across a target in discrete steps using dithers perpendicular to the slit axis to yield a spectroscopic map of an entire area of sky.

Continuous Scans

HAWC+

On The Fly Mapping (OTFMAP) - In this case, scan rates must reach (~ 2 Hz) x

(HAWC+ beam width) in order to remove the source from the atmospheric background—implying rates of $\sim 10\text{--}80$ arcseconds per second depending on the bandpass. HAWC+ offers two scan types for OTFMAP scan patterns: Lissajous and Box. In Lissajous observations, the telescope follows a parametric curvature at a non-repeating period to eventually cover the scan amplitude. In contrast, Box scans drive the telescope in a linear fashion at a specified rate in one direction for a given length and then moved perpendicularly before scanning in the reverse direction—similar to how one would mow a very large lawn. Lissajous scans are recommended for sources smaller than the HAWC+ FOV at a given bandpass, while Box scans are more efficient at mapping large areas several times the FOV.

Note: GREAT also has an On the Fly Astronomical Observation Template (AOT), but is not included in this section because GREAT observations are performed in either Total Power or Beam Switching modes.

Other Scans

FIFI-LS

Spectral Scan - This mode is implemented to target spectral features much wider than the bandwidth like solid state features. The problem is a good atmospheric calibration over the whole observed wavelength range. The spectrum has to be pieced together from many different exposures. The best way to take such data and how to reduce it is still being investigated. If this observing mode is considered, please contact the instrument scientist via the SOFIA Help-Desk.

[Return to Table of Contents](#)

2. EXES

- 2. EXES
 - 2.1 [Specifications](#)
 - 2.1.1 [Instrument Overview](#)
 - 2.1.1.1 [Design](#)
 - 2.1.2 [Performance](#)
 - 2.1.2.1 [Optics](#)
 - 2.1.2.2 [Detector](#)
 - 2.2 [Planning Observations](#)
 - 2.2.1 [Wavelength Calibration](#)
 - 2.2.2 [Flux Calibration and Atmospheric Line Correction](#)
 - 2.2.3 [Overheads](#)
 - 2.2.4 [As a Principle Investigator Instrument](#)

2.1 Specifications

Table of Contents

- 2.1 [Specifications](#)
 - 2.1.1 [Instrument Overview](#)
 - 2.1.1.1 [Design](#)
 - 2.1.2 [Performance](#)
 - 2.1.2.1 [Optics](#)
 - 2.1.2.2 [Detector](#)

Return to the Table of Contents for this section at any time by selecting [Return to Table of Contents](#). Users may also navigate through the entire Observer's Handbook by using the complete Table of Contents menu to the right.

2.1 Specifications

2.1.1 Instrument Overview

The **Echelon-cross-Echelle Spectrograph (EXES)** operates in the 4.5–28.3 μm wavelength region, at high ($R \approx 50,000$ – $100,000$), medium ($R \approx 5000$ – $20,000$) and low ($R \approx 1000$ – 3000) spectral resolution. The instrument uses a 1024×1024 Si:As detector array. High resolution is provided by an echelon—a coarsely-ruled, steeply-blazed aluminum reflection grating—along with an echelle grating to cross-disperse the spectrum. The echelon can be bypassed so that the echelle acts as the sole dispersive element. This results in single order spectra at medium- or low-resolution depending on the incident angle.

[Return to Table of Contents](#)

2.1.1.1 Design

EXES is a liquid helium cooled instrument. The cryostat is approximately 24 inches in diameter and 72 inches long. There are two cryogen reservoirs: one for liquid nitrogen and one for liquid helium. These are at the forward end, as mounted on SOFIA, with the entrance window on the aft end toward the telescope. There are three layers of radiation shielding within EXES: a vapor cooled shield tied only to the cryogen fill tubes, one attached to the liquid nitrogen reservoir, and the third attached to the liquid helium reservoir. All optics except for the entrance window/lens are attached to the liquid helium level. Baffling tubes connected to the liquid nitrogen level reduce thermal emission impinging on the internal optics. Within the liquid helium level, the optics are all tied to a rigid optics box constructed out of aluminum and the detector headerboard is isolated with G10 fiberglass and is actively maintained at a uniform temperature.

[Return to Table of Contents](#)

2.2.1 Performance

EXES delivered performance appears consistent with expectations over the flight series so far. There are some variations from observation-to-observation, but we believe the values quoted here are fair estimates of what is typical. The angular resolution of EXES will match that achieved by the telescope. For the latest sensitivities, observers are recommended to consult the online Exposure Time Calculator (ETC) at <http://iraastro.physics.ucdavis.edu/exes/etc/>. The ETC also provides the slit length as a function of wavelength and instrument configuration (and therefore whether on-slit nodding is possible or not), as well as the wavelength coverage in a single setting and echelon orders that can be targeted.

The wavelength coverage ranges from 4.5–28.3 μm . There are three resolution regimes—high, medium and low—with the exact resolving power depending on wavelength, grating angle and slit width. Generally, the resolution will be higher at shorter wavelengths in each regime. The high-resolution configurations use the echelon grating and will achieve $R = 50,000$ – $100,000$. If the cross disperser echelle angle is 35 – 65° , the configuration is called HIGH_MED and if 10 – 25° it is called HIGH_LOW. For these high-

resolution configurations, there is non-continuous spectral coverage in high-resolution configuration for $\lambda > 19 \mu\text{m}$, but the central wavelength can be tuned so that lines of interest do not fall in the gaps. The Medium configuration will use high angles on the echelle grating to achieve $R = 5,000\text{--}20,000$, and the LOW configuration will use low angles to achieve $R = 1,000\text{--}3,000$.

The HIGH_MED configuration slits are 4.5–45 arcsec long, and the HIGH_LOW slits are 1–12 arcsec long. The shorter slits in HIGH_LOW allow for more orders to be packed onto the array, thus increasing the instantaneous wavelength coverage, while maintaining the high spectral resolution (see [Figure 2-6](#) for an example). In the Medium and Low configurations the slit lengths vary from 25 to 180 arcsec depending on the number of rows to be read out.

The sensitivity of the instrument is shown in [Figures 2-1](#) through [2-4](#) for the HIGH_MED, Medium, and Low configurations for both point sources and extended sources. The Noise Equivalent Flux Density for S/N of 10σ in a clock-time (Note that the other instruments in this Handbook report sensitivities based on the total time on-source, not the clock-time. The latter includes the total time on-source + applicable overheads, excluding target acquisition and instrument set-up time.) of 900 seconds is plotted as a function of wavelength. These values have been calculated for a point source assuming image quality between 2 and 4 arcsec (FWHM) and the narrowest of the available 1.4 to 3.2 arcsec slits, both of which vary with wavelength, and take into account estimated instrument efficiency. They assume an altitude of 41,000 feet, 40° elevation, and $7 \mu\text{m}$ precipitable water vapor.

Figure 2-1.

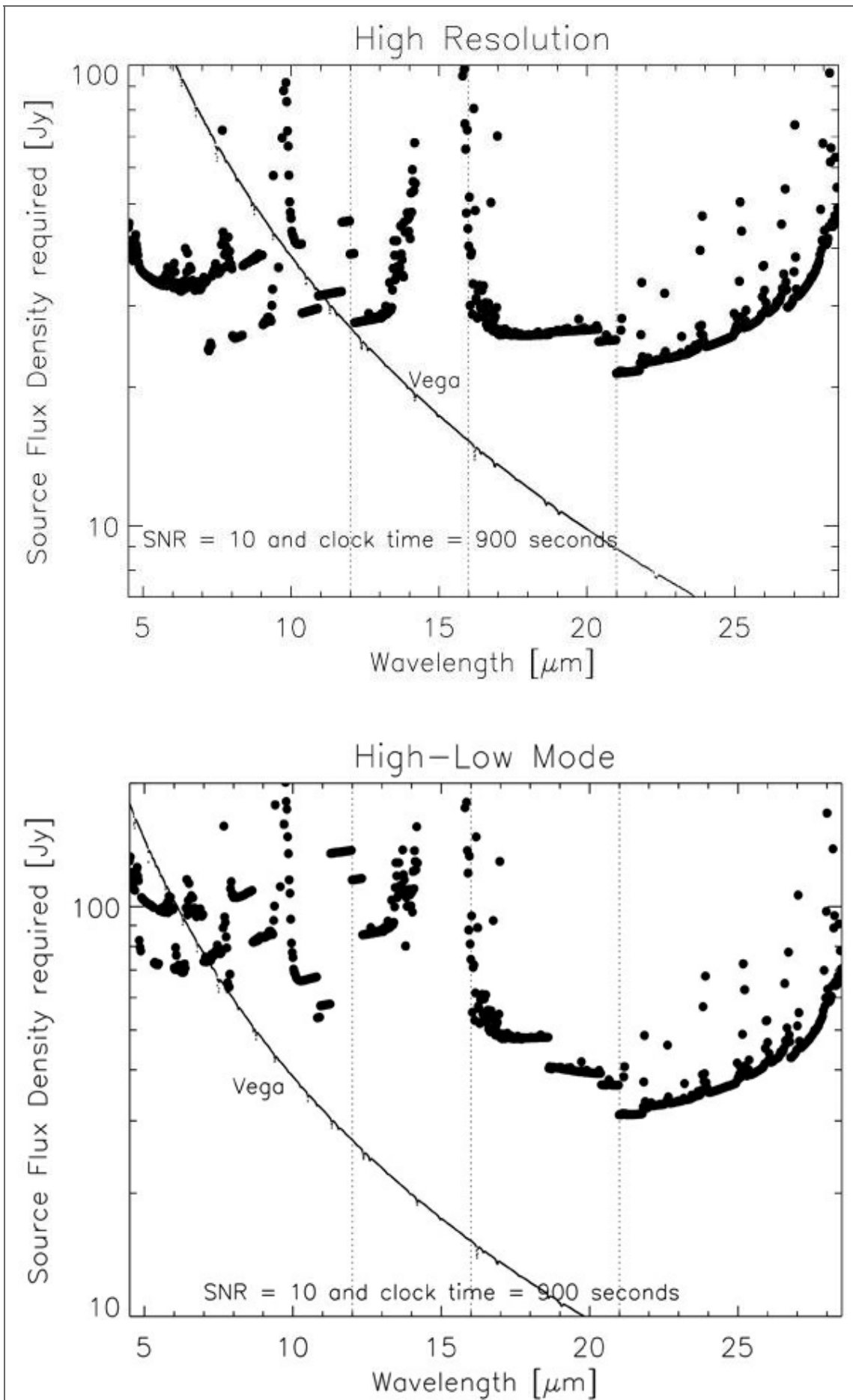


Figure 2-1. The minimum detectable point source flux as a function of wavelength for the EXES HIGH_MED (*top*) and HIGH_LOW (*bottom*) configurations, assuming the conditions mentioned above. It takes into account that on-slit nodding is not possible at all wavelengths.

The vertical dotted lines show the boundaries between the slit widths used (1.4", 1.9", 2.4", 3.2"). For precise numbers at individual wavelengths and for the HIGH_LOW configuration please use the online [ETC](#).

[Return to Table of Contents](#)

2.1.2.1 Optics

The optics consist of an entrance window/lens, fore-optics, three wheels housing the slits, deckers and filters, an echelon chamber, and a cross-dispersion chamber. The entrance window/lens (2 inches diameter) forms an image of the SOFIA telescope secondary at the liquid helium cold stop within the fore-optics. The fore-optics, including the entrance window, changes the incoming f/19 beam to f/10. After coming to a focus, the beam expands through a pupil (at the cold stop) to an ellipsoidal mirror. The light is redirected off two flat mirrors to a focus at the slit plane.

As the beam comes to a focus, it passes through the slit/filter cassette. This consists of three wheels on a common axle containing (i) filters to isolate grating orders, (ii) deckers to determine the length of the slit, and (iii) slits of different widths. The filter wheel has 12 slots that will be loaded with specific filters for each cooldown cycle based on the planned observations. Broader filters for use in the Low resolution configuration are included in four of the decker wheel slots. The decker wheel has a total of 11 features, which include continuously variable length slits, fixed length slits, pinholes, and an open position. The continuously variable slit length is provided by a cutout on the decker wheel that gets larger as a function of angle. The smallest size is about 4.5 arcsec and the largest about 45 arcsec. The slit length depends on the wavelength and the instrument configuration. With that caveat, slit lengths can range from 1 to 180 arcsec on SOFIA. The slit wheel contains six slits. On SOFIA, EXES will typically use four of them ([Table 2-1](#)). There is also a wide 9.400 slit intended for flux calibration.

Table 2-1.

Observing Configurations, Modes, Slits, and Spectral Resolutions

Configuration	Available Modes	Available Slit Widths ^a (arcseconds)	Resolving Power ^b
HIGH_MED	nod on slit ^c , nod off slit, map	1.4	112,000
		1.9	86,000
		2.4	67,000
		3.2	50,000
		1.4	112,000
		1.9	86,000

HIGH_LOW Configuration	nod off slit, map Available Modes	Available Slit Widths (arcseconds)	Resolving Power
		2.4	67,000
		3.2	50,000
Medium	nod on slit, nod off slit, map	1.4, 1.9, 2.4, 3.2	5,000-20,000 ^d
Low	nod on slit, nod off slit, map	1.4, 1.9, 2.4, 3.2	1,000-3,000 ^d

^a 1.400 slit unavailable >12 μm, 1.900 slit unavailable >16 μm, 2.400 slit unavailable >21 μm

^b Observers must check the most recent resolving powers as a function of slit width and wavelength at <http://iraastro.physics.ucdavis.edu/exes/etc/>

^c On-slit nodding not possible at all wavelengths. Observers must check this at <http://iraastro.physics.ucdavis.edu/exes/etc/>

^d Resolving power is a strong function of wavelength and slit width

After passing through the slit wheel, the beam hits a flip mirror mechanism, which is used to choose between instrument resolution configurations (Table 2-1) by either directing the beam into the echelon chamber (high-resolution) or into the cross-dispersion chamber (medium- and low-resolution). In the high-resolution configuration, the beam enters the echelon chamber and expands to an off-axis hyperboloid mirror that serves as both collimator and camera mirror for the echelon grating. The dispersed light, focused by the hyperboloid, bounces off a flat into the cross-dispersion chamber.

The cross-dispersion chamber is conceptually similar to the echelon chamber. The light expands from the input to an off-axis paraboloid that again serves as both collimator and camera mirror. The collimated beam is sent to the cross-dispersion grating which disperses the light in the plane of the grating. The camera mirror sends the light to our detector. When operating in single-order, long-slit spectral configurations—our Medium and Low resolution science configurations—the light never enters the high-resolution echelon chamber.

There is a wheel in front of the detector, which provides a lens for imaging the pupil through the instrument, and a dark slide for isolating the detector. The wheel would also be available for including transmissive optics to adjust the plate scale on the detector, if desired.

[Return to Table of Contents](#)

2.1.2.2 Detector

The detector is a Raytheon Vision Systems Si:As array with 1024x1024 pixels. The detector material is bonded to a SB 375 multiplexer. The array is mounted in a separate enclosure to reduce scattered light. The headerboard is thermally isolated from the rest of the optics box to permit active temperature control of the array. The photon fluxes in

the Low configuration will be significantly above the level intended for the array. This prevents observations at longer wavelengths and/or with wider slits. When photon fluxes allow, only a subsection of the array will be clocked out in this configuration for a faster read-out (as well as in any imaging configuration). It is expected that a quarter to half the array will be utilized in these configurations, so the effective slit length is about 60". There are other potential work-arounds that reduce the instrument sensitivity and may require extra overheads to prepare for and recover from low resolution observations. Proposers interested in low resolution observations should [contact](#) the instrument team to discuss their goals and possible options.

[Return to Table of Contents](#)

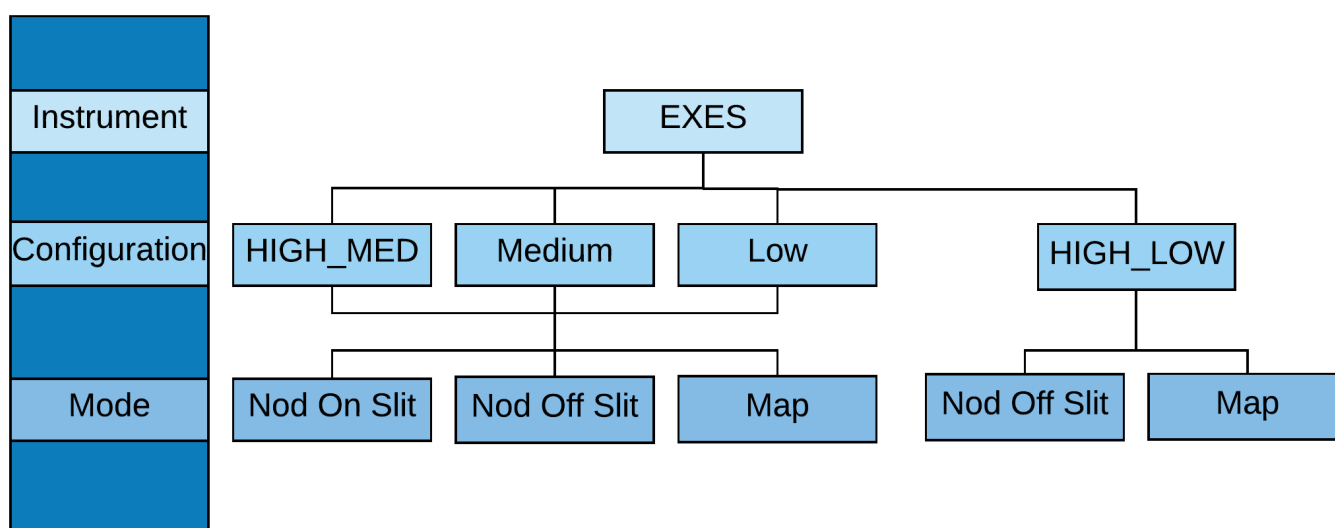
2.2 Planning Observations

Table of Contents

- 2.2 Planning Observations
 - 2.2.1 Wavelength Calibration
 - 2.2.2 Flux Calibration and Atmospheric Line Correction
 - 2.2.3 Overheads
 - 2.2.4 As a Principle Investigator Instrument

Return to the Table of Contents for this section at any time by selecting [Return to Table of Contents](#). Users may also navigate through the entire Observer's Handbook by using the complete Table of Contents menu to the right.

2.2 Planning Observations



All EXES configurations and modes are released for observations. The observing modes for EXES are summarized as follows:

Nod On Slit

The telescope is noddled along the slit at distances that keep the target within the slit length. The nod throw is half the slit length. This is the most efficient EXES mode for point sources.

Nod Off Slit

The telescope is nodded such as that the object is not on the slit. This is used for extended sources or when the PSF is larger than four times the slit length.

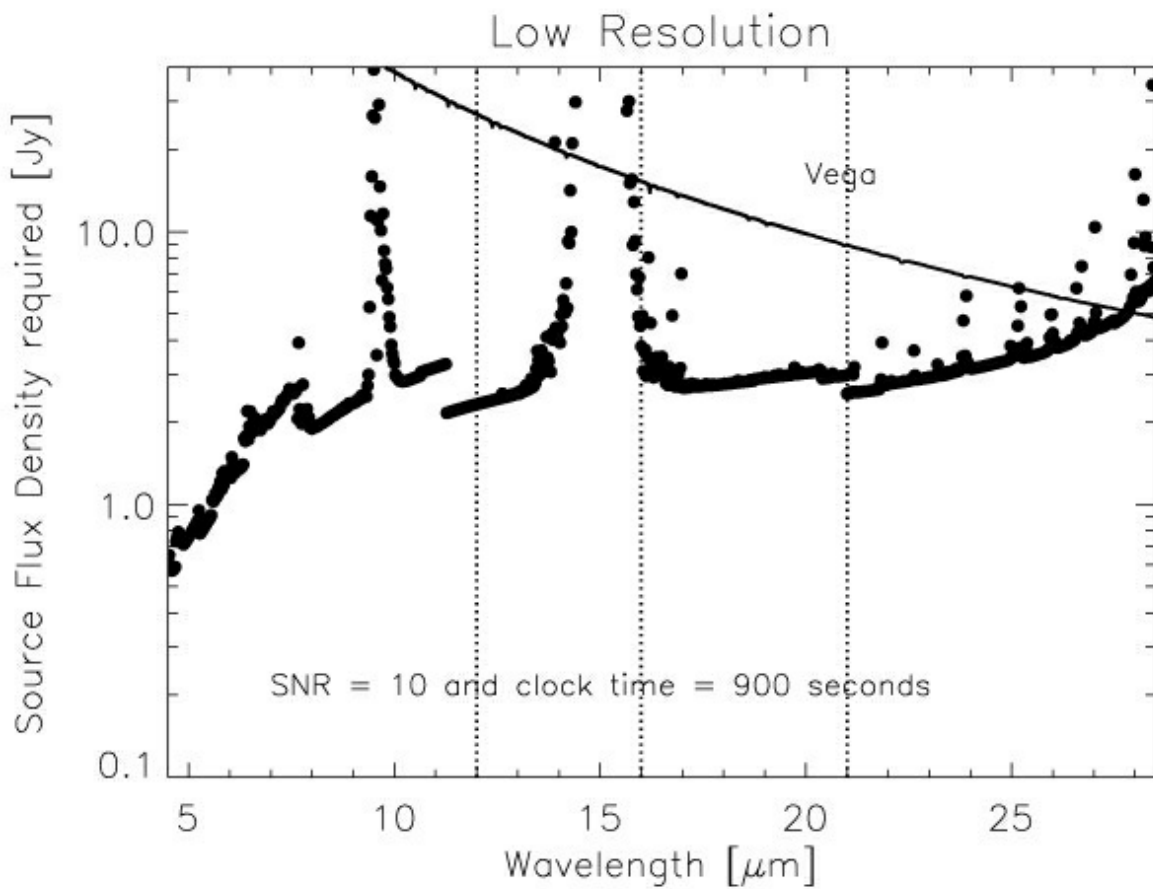
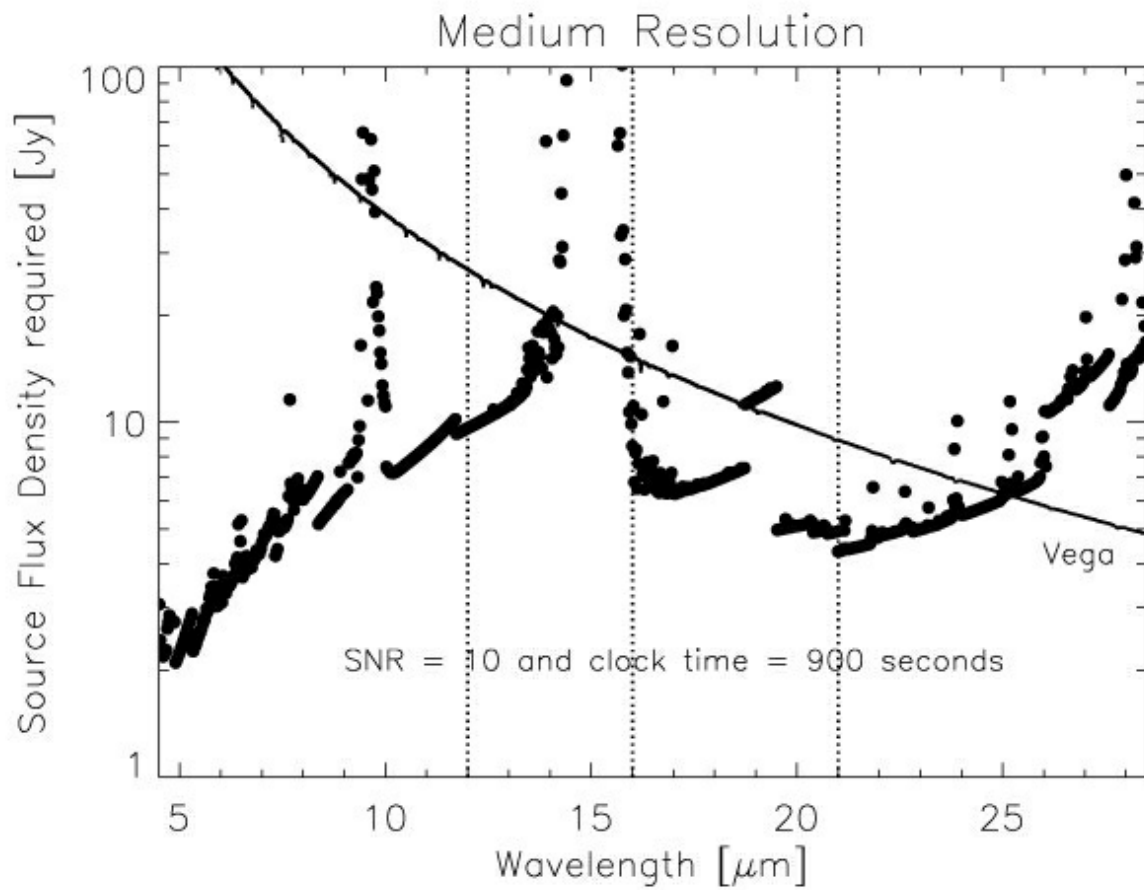
Map

The telescope is moved perpendicular to the slit while EXES takes spectra on a grid of telescope positions, which are always one dimensional stripes.

Observers are always encouraged to [contact](#) the instrument team for the latest performance results—especially for the Low configuration, which suffers from saturation effects. There are potential work-arounds that reduce the instrument sensitivity and may require extra overheads to prepare for and recover from low resolution observations. Proposers interested in low resolution observations should [contact](#) the instrument team ready to discuss their goals and hear about possible options.

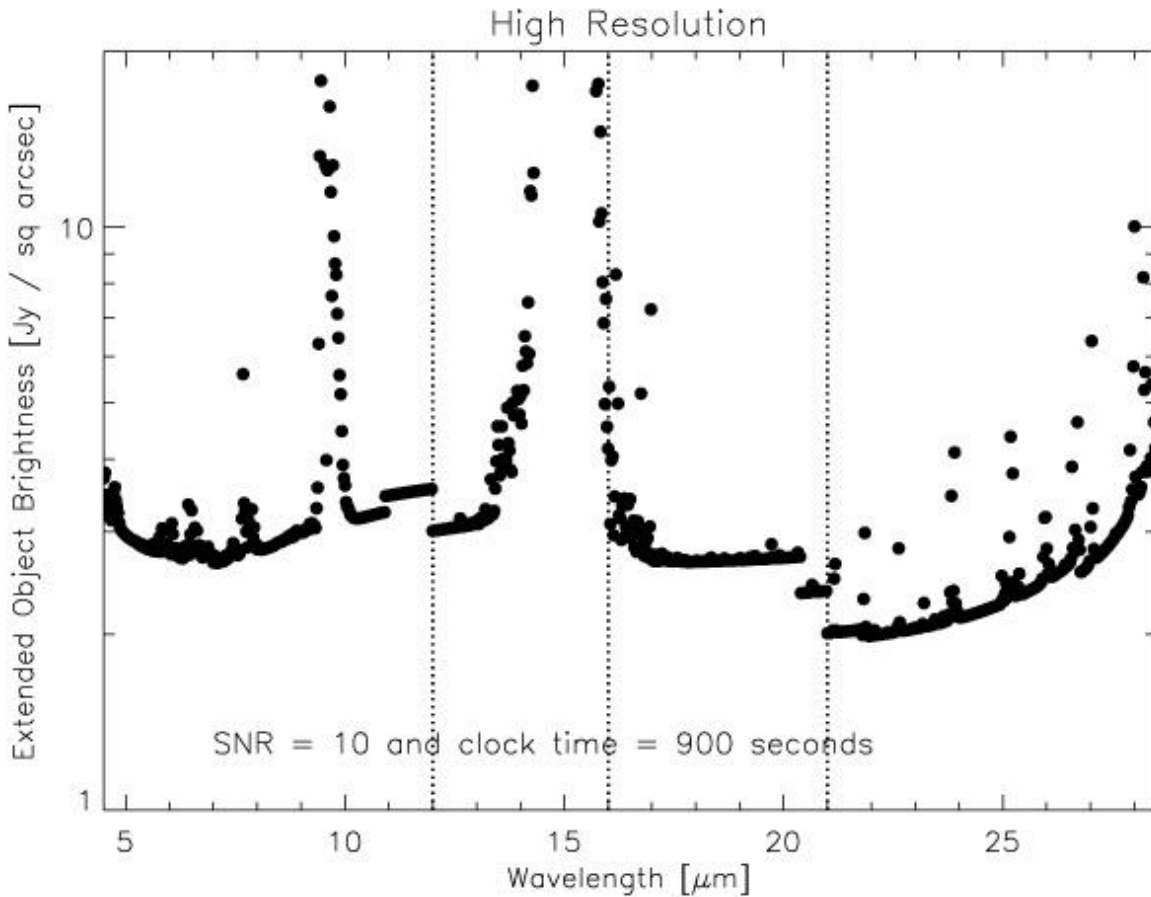
The proposer needs to supply the central wavelength, the spectroscopic configuration, the slit width, and the observing mode for each observation ([Table 2-1](#)). These parameters define the default instrument set-up. Each central wavelength specified should count as a separate observation. In addition, the proposer should estimate the clock time necessary to reach the desired S/N.

Figure 2-2.



The calculation may be based on [Figure 2-1](#) or [2-2](#) for point sources and on [Figure 2-3](#) and [2-4](#) for extended sources, noting that the minimum detectable flux $\propto (S/N) / \sqrt{t_{\text{exp}}}$. However, it is recommended that the online ETC at <http://irastro.physics.ucdavis.edu/exes/etc/> is checked as well for the latest updates.

Figure 2-3.



EXES operates in a wavelength region, parts of which are accessible from ground based telescopes. Proposers should carefully check the atmospheric transmission (using [ATRAN](#), for example) and make sure that the observations require, or would greatly benefit from, using SOFIA. The proposer should take into account the Doppler shift of the target(s) due to their motion relative to Earth. If proposers find that the atmospheric transmission at the wavelength of interest is lower than the local median (calculated over a range $\pm 0.0125 \mu\text{m}$), then more time will be required to reach the desired S/N. Higher transmission would imply shorter required times. In general, the S/N scales as $\text{transmission}/\sqrt{(1 - \text{transmission}) + 0.3}$. Note that the [online ETC](#) includes the impact of the atmosphere at precise wavelength of interest and so may differ from the figures above. The ETC provides the clock-time required to achieve the desired S/N per resolution element on a continuum object at the specific wavelength of interest and then indicates what the expected S/N should be for the entire setting.

Proposers should specify the slit width, which sets the resolving power for each configuration ([Table 2-1](#)). Note that the narrowest slit (1.4 arcsec) is only effective below $12 \mu\text{m}$ (above this wavelength no gain in resolving power is achieved, while flux is lost with respect to the wider slits). Similarly, the 1.9 arcsec slit can only be used below $16 \mu\text{m}$, and the 2.4 arcsec slit below $21 \mu\text{m}$.

Figure 2-4.

In configurations using the medium resolution grating (Medium and HIGH_MED), the single setting spectral coverage ranges between $0.03 \mu\text{m}$ at the shortest wavelengths, and $0.3 \mu\text{m}$ at longer wavelengths ([Figure 2-5](#)). For the low resolution grating (the LOW and HIGH_LOW configurations) this is $0.2\text{--}0.8 \mu\text{m}$. Note that while HIGH_LOW and HIGH_MED have the same spectral resolution, the larger wavelength coverage of

HIGH_LOW comes at the expense of a smaller slit length, which is illustrated in Figure 2-6.

Figure 2-5.

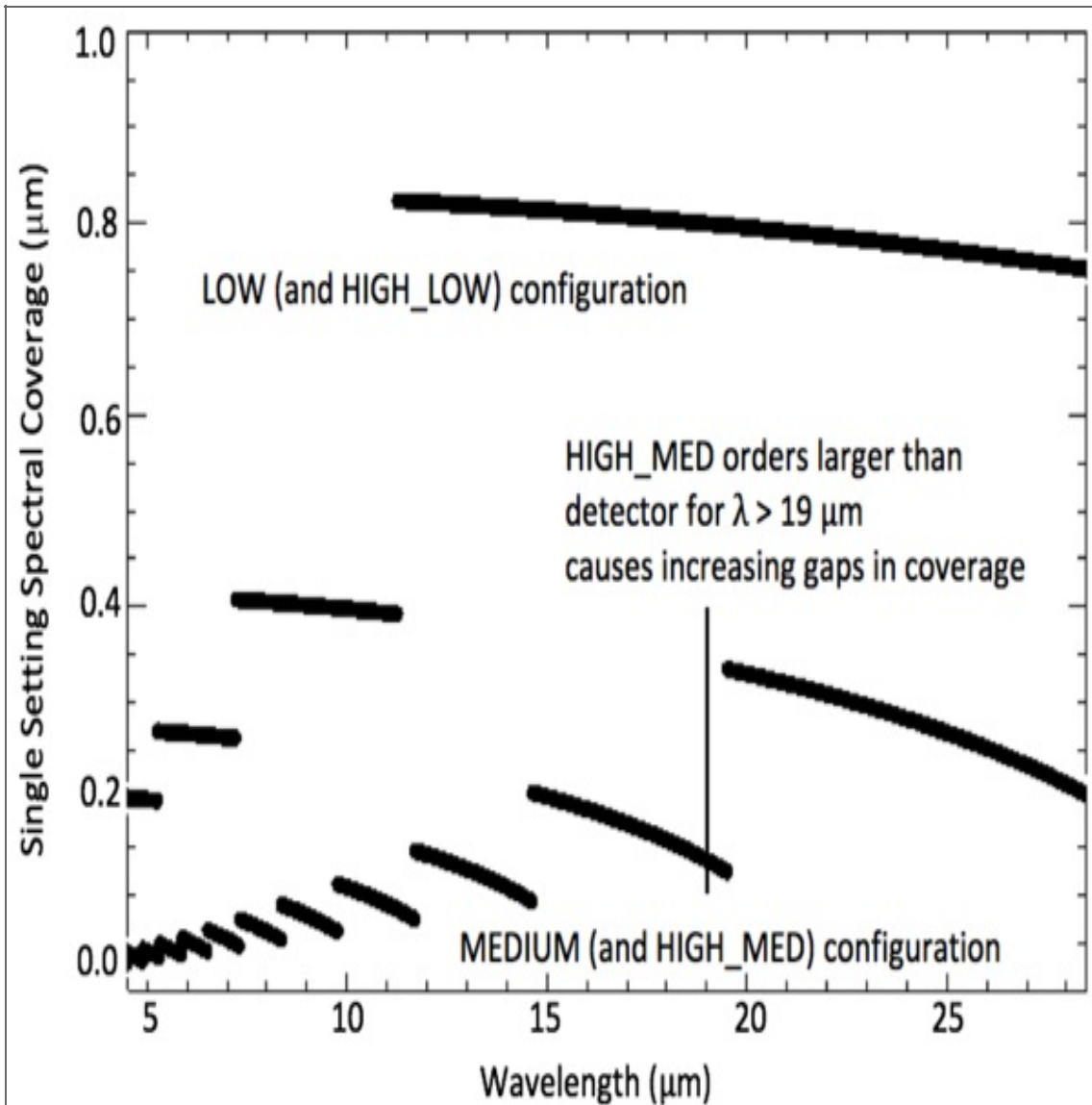


Figure 2-5. The single setting spectral coverage as a function of wavelength. Note that these values are the same for the HIGH_MED and Medium configurations, and for the HIGH_LOW and Low configurations.

Proposers should choose a single line of interest for each observation. Fine tuning of the bandpass to observe lines at the extreme edges of a single setting should be done in consultation with the EXES team to see if existing data indicates such tuning is possible.

The slit orientation on the sky depends upon the time when the target is observed and therefore the position angle cannot be specified.

Figure 2-6.

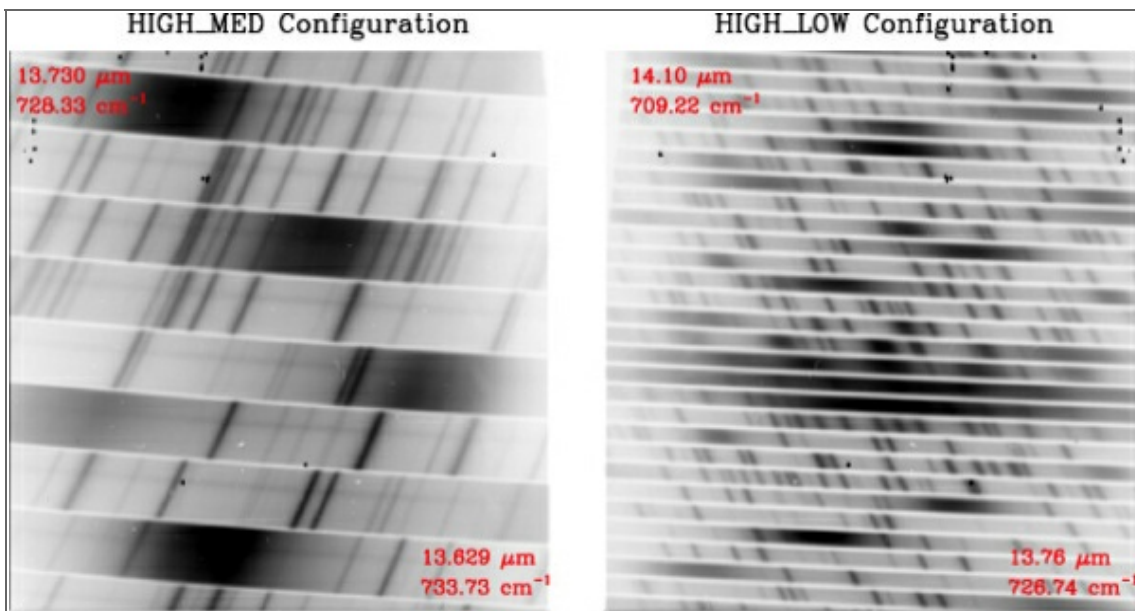


Figure 2-6. Comparison of raw 2D spectra of EXES in the HIGH_MED (*left*) and HIGH_LOW (*right*) configurations obtained during commissioning flights. The spectra are not nod-subtracted, highlighting the sky emission lines (dark). This comparison shows that, while the HIGH_MED and HIGH_LOW configurations have the same spectral resolution, HIGH_LOW has a much larger spectral coverage at the expense of a shorter slit to be able to pack more orders on the array. In contrast, the Low and Medium configurations (not shown) have the same spectral coverage as HIGH_LOW and HIGH_MED, respectively, but a lower spectral resolution without cross dispersion. The approximate start and end wavelengths are indicated in red.

EXES will not use the secondary for chopping in any of its observations. Rather, only nodding and mapping modes will be implemented.

In a nod mode (either Nod On Slit or Nod Off Slit), the telescope is moved to a new position in order to remove the sky background. For point sources observed with a sufficiently long slit, the telescope is moved such that the object remains on the slit (Nod On Slit mode). For sources larger than about a quarter of the slit length, the telescope is moved such that the object is not on the slit (Nod Off Slit mode). The time between telescope motions will depend on the sky variation, the telescope settling time, and the integration time. The goal is to maximize the signal-to-noise per clock time. For observations of point sources, the detectable flux plots (Figures 2-1 and 2-2) and the ETC include assumptions regarding whether nodding off the slit is required due to short slit lengths. For noded observations of extended objects, proposers should [contact](#) the EXES team to check if nodding on the slit is possible. If not, the observing time required should be doubled. Unless specific nod parameters are requested for such observations, the instrument team will define the nod amplitude, direction, and frequency. The sensitivities for extended source observations shown in Figures 2-3 and 2-4 assume that the source is noded off-slit and take into account the variation in spatial resolution with wavelength. The atmospheric and overhead factors for nodding are included. If the source is small relative to the slit length, then it may be possible to nod along the slit. In this case, the source brightness given in the figures is for a SNR of 10 in 450 seconds.

In Map mode, the telescope is moved sequentially such that a series of positions along straight lines on the sky (i.e. along stripes) are observed to create a map. The sky background is taken from the first positions and, depending on the size of the map, from the last positions. In general, we anticipate the telescope motions to be half the slit width to create a well-sampled map. Proposers should specify the number of steps in a map and the step size. Map steps are generally assumed to be perpendicular to the slit. The first three positions for taking data in a map must be blank sky. These could be the first three positions of the map or at a separate sky offset position specified by the user. It is recommended that additional blank sky positions are observed at the end of the map on the other side of the object. For all maps, the instrument software returns to the sky offset position for three final sky observations at the end of the observation. Proposers should specify the required clock time based on the flux limit desired, using the values in Figures 1-3 and 1-4, including any assumptions regarding binning of map positions to yield the final required SNR. The SNR for a single map position can be estimated by assuming that the required time is similar to that for nodding an extended object on slit, i.e. 10σ in 450 seconds for a given source brightness. If any spatial binning is required—at least a two-step sum is recommended—then the SNR will improve by the square root of the number of steps in the sum. The [online ETC](#) allows the user to specify the number of steps and bins according to the predicted image quality in producing a clock-time estimate.

[Return to Table of Contents](#)

2.2.1 Wavelength Calibration

Wavelength calibration with EXES will be performed by applying the grating equation to atmospheric lines observed in the source spectra. As long as there is a single telluric feature in the bandpass with depth of at least 5%, the wavelength calibration is expected to be accurate to $\cong 0.5 \text{ km s}^{-1}$.

If atmospheric models show no telluric features within the EXES instantaneous band pass for a given observation, then obtaining a good wavelength solution will require a few additional steps. Note that the absence of telluric features from SOFIA suggests the observation may be better done from the ground. First, the order sorting filter (OSF) is rotated so that a different order from the echelle is observed that includes a suitable telluric line. The grating equation can then be applied, providing wavelength calibration accuracy down to $\approx 1 \text{ km s}^{-1}$. The process of rotating the OSF, observing blank sky, and rotating the OSF back to the original orientation should take less than 5 minutes of additional time. A demonstration of this procedure can be found in Harper et al. (2009, *ApJ*, 701, 1464).

[Return to Table of Contents](#)

2.2.2 Flux Calibration and Atmospheric Line Correction

For every EXES science observation, the EXES temperature-controlled black body source and a nearby blank sky field will be observed. From these, a calibration spectrum will be constructed that will correct for response variations and provide flux calibration after division over the science observations. In principle, division by the calibration spectrum would also correct for telluric absorption lines (see Lacy et al., *PASP* volume 114, issue 792, p. 153), but this is presently not the case because of the large difference between

the blackbody and sky temperatures. The flux calibration is expected to be better than 20% but the true accuracy is currently uncertain. Experiments focused on line profile information and those that can normalize the continuum level (or use past observations for setting the continuum) will likely be more successful. Projects requesting a telluric calibration object, in particular those observing lines near strong telluric features or those observing relatively broad lines, will need to include the observation time required in their proposal. Because of the difficulty of scheduling a given telluric calibrator with the science target in a given flight, the specific calibrator will need to be chosen at the time of flight planning in consultation between the program proposer, the instrument PI, and the SMO support scientist. For wavelengths below 8–10 μm this will most likely be a hot, bright star (e.g., Vega or Sirius) and at longer wavelengths an asteroid. Galilean moons will also be considered, provided they are well separated from Jupiter. For the proposal, a separate observation entry should be entered via USPOT with name Cal_target where *target* is the name of the associate science target (e.g., IRC+10216 and Cal_IRC+10216) and given the coordinates RA:00:00:00, Dec:+00:00:00. The observing time for such a telluric standard observation will depend on the instrument configuration and wavelength observed as well as on the signal-to-noise level needed. Proposers must use the [EXES ETC](#) to estimate this, assuming a continuum brightness of 100 Jy below 10 μm and 150 Jy above 10 μm for the HIGH_MED and HIGH_LOW configurations. For the Medium and Low configurations the proposer should assume at all wavelengths a brightness of 50 Jy and 25 Jy, respectively. Proposers are urged to limit the EXES clock times on the telluric standard at a given wavelength and instrument configuration to less than about 30 minutes. Further improvement of the removal of telluric absorption features may be achieved by employing models of the Earth's atmospheric transmission.

[Return to Table of Contents](#)

2.2.3 Overheads

The treatment of overheads for EXES differs from that of most other SOFIA instruments: instead of on-source times, users are required to specify wall clock times (i.e. total elapsed time) in USPOT, which is the on-source time plus all overheads except those related to acquisition and instrument set-up. The overheads include time on empty sky in the off-slit nodding and mapping modes as well as read-out and other telescope and instrument inefficiencies. The ETC and the figures in this manual give the clock times needed. The figures in this manual only give clock times. USPOT will add an additional 15 minutes for peak-up, wavelength optimization, flux calibration, and flat field overheads in the HIGH_MED, Medium, and Low configurations and 20 minutes in HIGH_LOW. In all configurations, an extra 3 minutes of peak-up time is needed for the narrow (1.4 arcsec) slit. If no peak-up is necessary (i.e., after a wavelength change on the same target, if the source is extended, or if the continuum emission is too weak), the overheads can be reduced by using the **No Peak-Up** option in USPOT. Overheads can also be reduced if multiple sky positions are observed in the same wavelength setting. In this case, click the **No Wavelength Setup** button in USPOT. Note that the time on a given target on a single flight is limited to 90–180 minutes, so full overheads may be needed again once the sum of AOR times exceeds 90 minutes. Conversely, if a single observation takes more than 90 minutes it may need to be split into multiple AORs, each with full overheads. Please consult the EXES and SOFIA staff in these cases.

[Return to Table of Contents](#)

2.2.4 As a Principle Investigator Instrument

EXES is a Principal Investigator (PI) class instrument. The proposer is encouraged (but not required) to [contact](#) the Instrument PI before preparing or submitting the proposal, since the PI has the most up to date information about the instrument capabilities. However, it is recommended that they do so, in order to get the most up to date information about instrument capabilities. The data collection and reduction will be done by the instrument team, and it is expected that data analysis and preparation of the results for publication will be done by the proposers in collaboration with the instrument team.

[Return to Table of Contents](#)

3. FIFI-LS

- 3. FIFI-LS
 - 3.1 Specifications
 - 3.1.1 Instrument Overview
 - 3.1.1.1 Integral Field Concept
 - 3.1.1.2 Selection of the Dichroic
 - 3.1.1.3 Beam Rotator
 - 3.1.2 Performance
 - 3.1.2.1 Comparison with the PACS Spectrometer
 - 3.1.2.2 Spectral Resolution
 - 3.1.2.3 Sensitivity
 - 3.2 Planning Observations
 - 3.2.1 Observing Modes
 - 3.2.1.1 Symmetric Chop
 - 3.2.1.2 Asymmetric Chop
 - 3.2.1.3 Bright Object
 - 3.2.1.4 Spectral Scan
 - 3.2.2 Integration Time Estimates
 - 3.2.3 Spectral Dithering
 - 3.2.4 Mapping

3.1 Specifications

Table of Contents

- 3.1 Specifications
 - 3.1.1 Instrument Overview
 - 3.1.1.1 Integral Field Concept
 - 3.1.1.2 Selection of the Dichroic
 - 3.1.1.3 Beam Rotator
 - 3.1.2 Performance
 - 3.1.2.1 Comparison with the PACS Spectrometer
 - 3.1.2.2 Spectral Resolution
 - 3.1.2.3 Sensitivity

Return to this Table of Contents at any time by selecting [Return to Table of Contents](#). Users may also navigate through the entire Observer's Handbook by using the complete

Table of Contents menu to the right.

3.1 Specifications

3.1.1 Instrument Overview

The Far Infrared Field-Imaging Line Spectrometer (FIFI-LS) is an integral field, far infrared spectrometer. The instrument includes two independent, simultaneously operating grating spectrometers sharing one common field-of-view (FOV). Each spectrometer has a detector consisting of 400 pixels of Germanium Gallium-doped photoconductors. The short wavelength spectrometer (blue channel) operates at wavelengths between 50 μm and 125 μm , while the long wavelength spectrometer (red channel) covers the range from 105 μm up to 200 μm . One of two dichroics has to be selected for an observation affecting the wavelength range of both channels in the overlap region.

The projection onto the sky of the 5x5 pixel FOVs of both channels is concentric (10 arcsec offset), but the angular size of the FOVs differs. The red channel has a pixel size of 12x12 arcsec yielding a square 1 arcmin FOV and the blue channel has a pixel size of 6x6 arcsec, which yields a square 30 arcsec FOV.

The resolving power of both channels varies between 1000 and 2000 dependent on the observed wavelength. The higher values are reached towards the long wavelength ends of each spectrometer.

The detectors are cooled down to about 1.7 K with super fluid helium. The spectrometers and all mirrors are cooled down to 4 K with liquid helium. The exception is the entrance optics featuring a K-mirror (see [Section 3.1.1.3](#)) and an internal calibration source. These optical components are cooled to about 80 K with liquid nitrogen.

[Return to Table of Contents](#)

3.1.1.1 Integral Field Concept

The integral field unit (IFU) allows FIFI-LS to obtain spectra at each point in its FOV; this is in contrast to a spectrometer with a slit, which only provides spectra along the slit. Both channels in FIFI-LS have an IFU, which consists of 15 specialized mirrors to separate the two dimensional 5x5 pixel FOV into five slices (of five pixels length each) which are then reorganized along a (one dimensional) line (25x1 pixel). This line forms the entrance slit of the actual spectrometer. The diffraction grating disperses the incoming light in the spectral dimension. Finally the dispersed light reaches the 16x25 pixel detector array. The result is a data cube with 5x5 spatial pixels (spaxels) and 16 pixels in the spectral dimension. [Figure 3-1](#) shows the concept.

Figure 3-1.

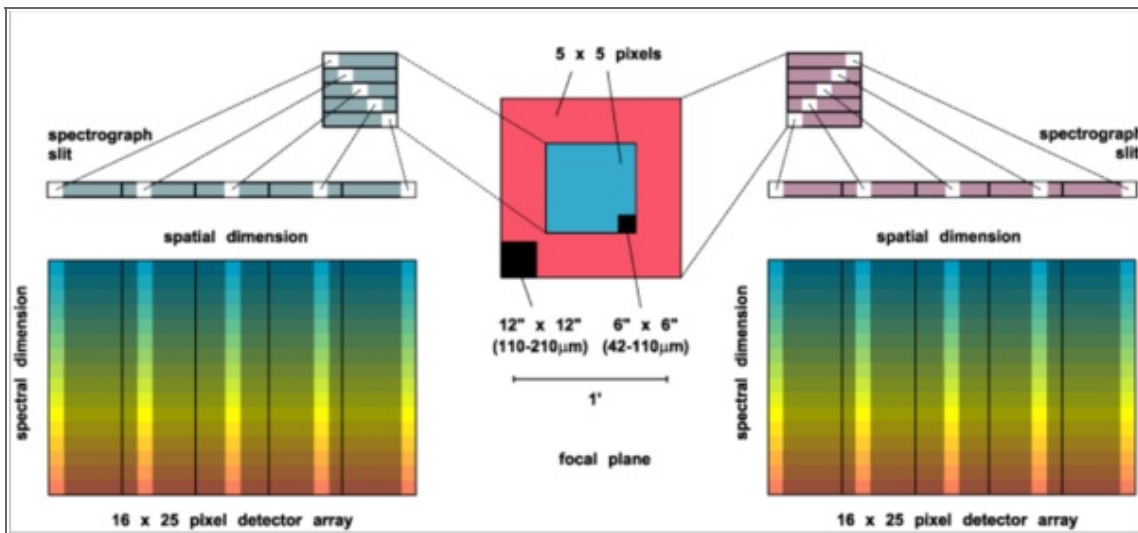


Figure 3-1. Illustration of the field imaging concept in FIFI-LS. The optics slice the rows of the 5x5 pixel field of view into a 25x1 pixel pseudo slit.

[Return to Table of Contents](#)

3.1.1.2 Selection of the Dichroic

The two channels have an overlap in their wavelength range. That is necessary because a dichroic splits the light between the two channels allowing the common FOV for both channels. The drawback is that a dichroic has a transition region where neither the transmission nor the reflection is good. Thus, FIFI-LS has two dichroics with transitions at different wavelengths. The The D105 cuts off the blue channel at about 100 μm and opens the red at about 115 μm . The D130 cuts off the blue channel at 120 μm and opens the red at 130 μm . [Figure 3-2](#) should be used to choose the best dichroic and line combinations. The proposer needs to pair up wavelengths so that each pair can be observed efficiently with one of the dichroics. Typically, the D105 is used unless a wavelength between 100 and 115 μm is observed.

Figure 3-2.

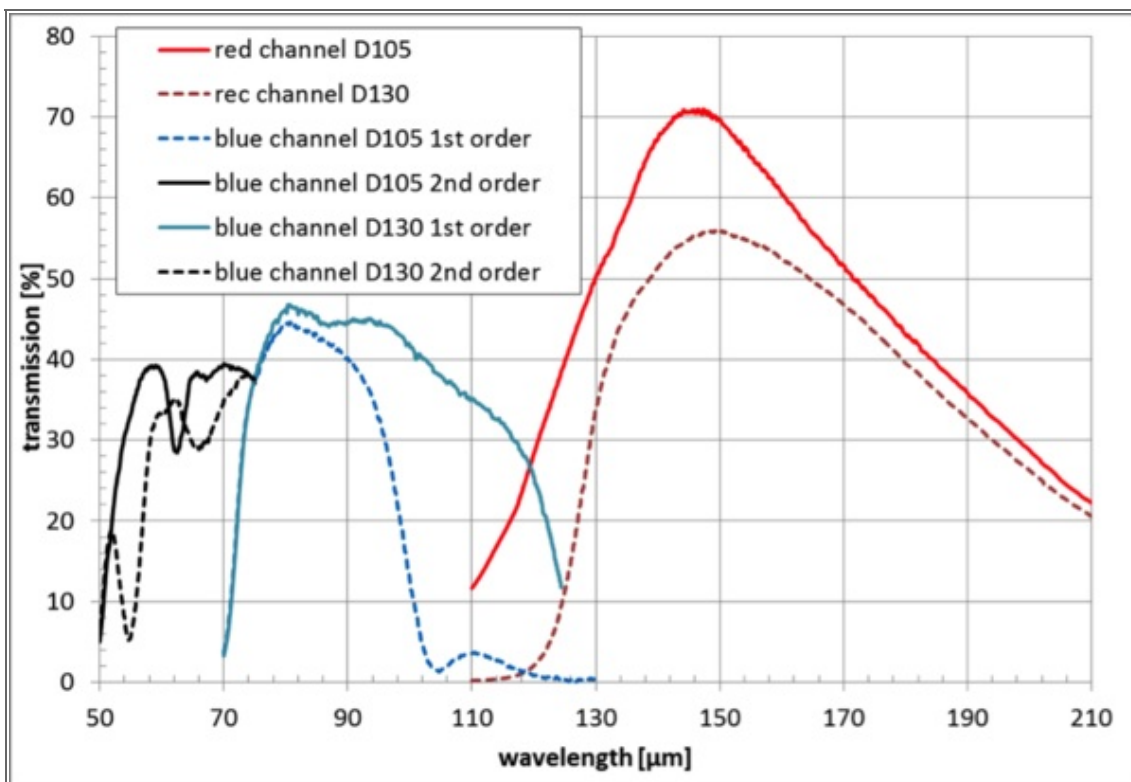


Figure 3-2. Throughput of optical system—here the transmission of the overall optical system is shown for the six possible optical configurations using two dichroic beam splitters (D105 and D130) and both grating orders (blue channel only).

[Return to Table of Contents](#)

3.1.1.3 Beam Rotator

The SOFIA telescope is essentially an Alt-Az-mounted telescope. Thus, the field of view on the sky rotates while tracking an object. However, the telescope can rotate around all three axes, but the amount it can rotate in cross-elevation and line-of-sight is limited. Thus, the normally continuous sky rotation is frozen-in for some time while the telescope is inertially stabilized. When the telescope reaches its limit in line-of-sight rotation, it needs to rewind, resulting in a rotated FOV of the telescope.

FIFI-LS has a beam rotator (K-mirror) that rotates the instrument's FOV, counteracting the sky rotation experienced by the SOFIA telescope. When a rewind happens, the FIFI-LS beam rotator will automatically rotate the FOV of the instrument, so that the position angle of the instrument's FOV on the sky is maintained. An additional benefit is that the beam rotator enables the observer to line up the FOV with e.g. the axes of a galaxy and keep the alignment. The desired position angle of the FOV can be specified in Phase II of the proposal process.

[Return to Table of Contents](#)

3.1.2 Performance

3.1.2.1 Comparison with the PACS Spectrometer

The FIFI-LS design is very similar to the Herschel/PACS-spectrometer sharing much of the design. The detectors are basically the same and the optical design is very similar (same sized gratings in Littrow configuration, same IFU). The difference is that FIFI-LS features

two grating spectrometers whereas the PACS-spectrometer had only one. The two gratings make it possible to observe two different wavelengths simultaneously and independent of each other (one in each channel). This design also allows different pixel sizes (6 arcsec vs 12 arcsec) in each spectrometer, which means a better match to the beam size. The spectral range of FIFI-LS also goes down to 51 μm whereas PACS did not routinely observe the [OIII] 52 μm line.

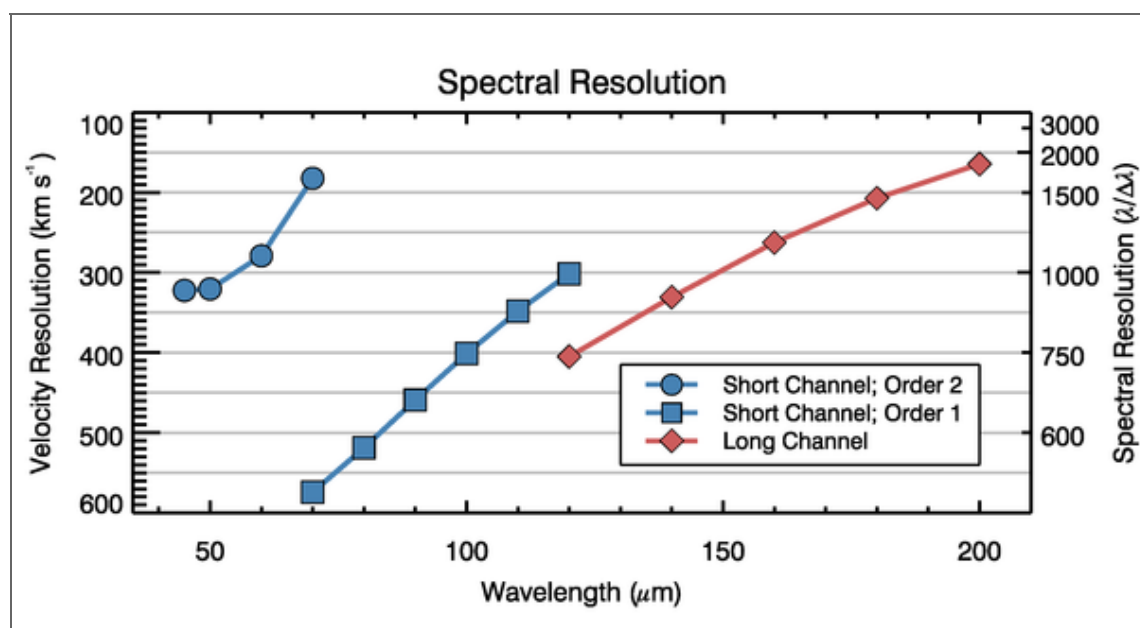
[Return to Table of Contents](#)

3.1.2.2 Spectral Resolution

The blue spectrometer operates in 1st and 2nd order. An order-sorting filter blocks the unwanted order. The red spectrometer only operates in 1st order. The spectral resolution of FIFI-LS depends on the observed wavelength. It ranges from $R = \lambda/\Delta\lambda \sim 500$ to 2000. That corresponds to a velocity resolution of 150 to 600 km/s. The top panel of [Figure 3-3](#) shows the spectral resolution in velocity resolution and in R vs. wavelength as measured in the lab.

FIFI-LS has 16 pixels in the spectral direction. The wavelength range covered by these 16 pixels also depends on the observing wavelength. The bottom panel of [Figure 3-3](#) shows the instantaneous spectral coverage or bandwidth (BW) in micron.

Figure 3-3.



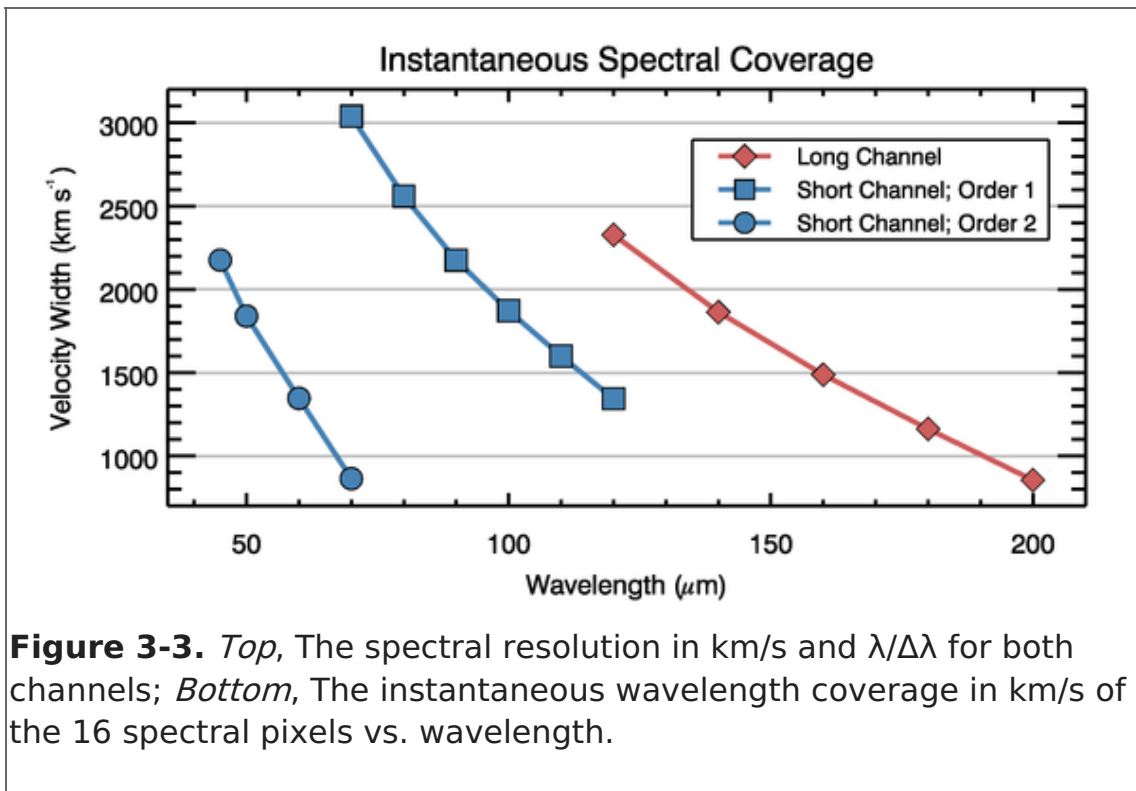


Figure 3-3. *Top*, The spectral resolution in km/s and $\lambda/\Delta\lambda$ for both channels; *Bottom*, The instantaneous wavelength coverage in km/s of the 16 spectral pixels vs. wavelength.

[Return to Table of Contents](#)

3.1.2.3 Sensitivity

FIFI-LS will operate such that the detectors are always background-limited, infrared photodetectors. Under this assumption, the overall performance of FIFI-LS as a function of wavelength has been estimated. Further assumptions about the emissivity of the telescope, optics, and baffling, the efficiency of the detectors had to be made. [Figure 3-4](#) shows the resulting sensitivities for continuum and unresolved lines as minimum detectable fluxes per pixel, i.e. detected with a signal to noise ratio (SNR) of 4 and an on-source integration time of 900 s or 15 min.

The [FIFI-LS on-line exposure time estimator](#) should be used to estimate the on-source exposure times used in proposals and observing preparation. The time estimator calculates the on-source integration time per map position for a source flux, F and a desired SNR using [Eq. 3-1](#):

(Eq.3-1)

$$t_{\text{on}} = l \left(\frac{\text{SNR}/4}{\alpha F / \text{MDF}(\lambda)} \right)^2 900 \text{ s}$$

where $\text{MDF}(\lambda)$ is either the Minimum Detectable Continuum Flux (MDCF) in Jy per pixel or the Minimum Detectable Line Flux (MDLF) in W m^{-2} per pixel at the entered wavelength (see [Figure 3-4](#)).

Figure 3-4.

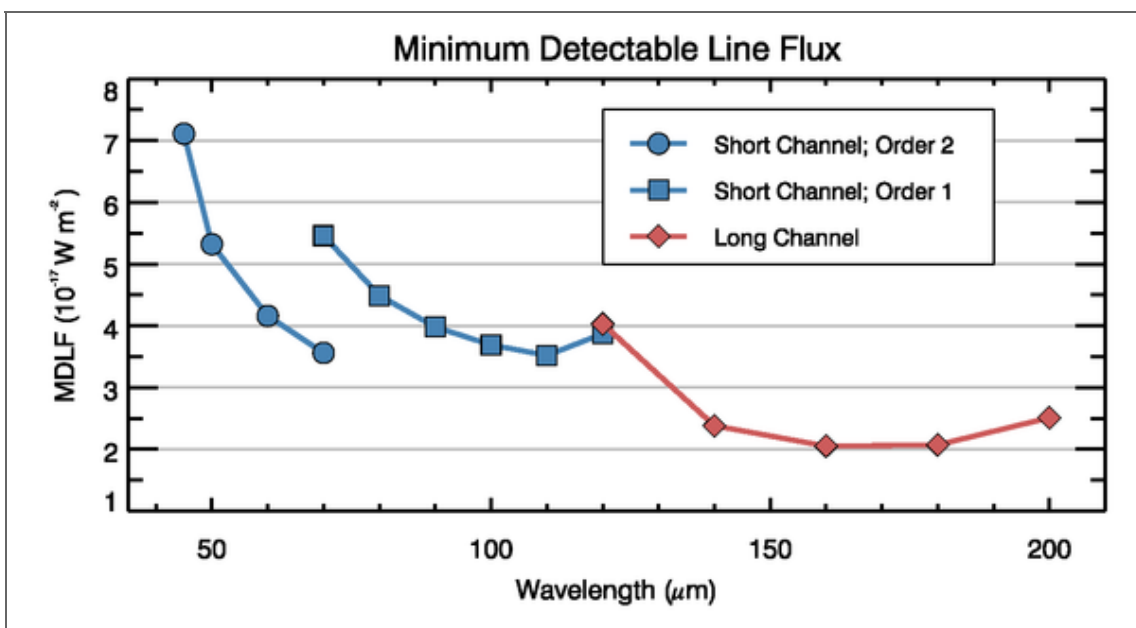
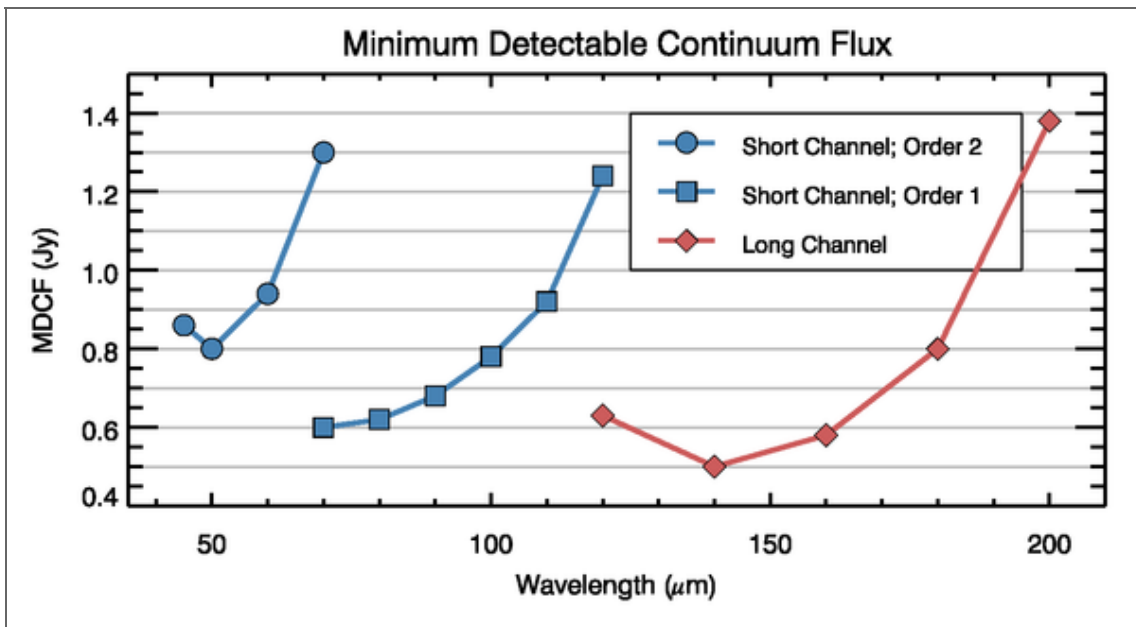


Figure 3-4. Continuum and emission line sensitivities for a monochromatic point source: The values are calculated for a SNR of 4 in 900 s. The MDCF is in Jy per pixel and the MDLF is in Wm⁻² per pixel. Both sensitivity values scale as SNR / √(t), where t is the on-source integration time.

[Return to Table of Contents](#)

3.2 Planning Observations

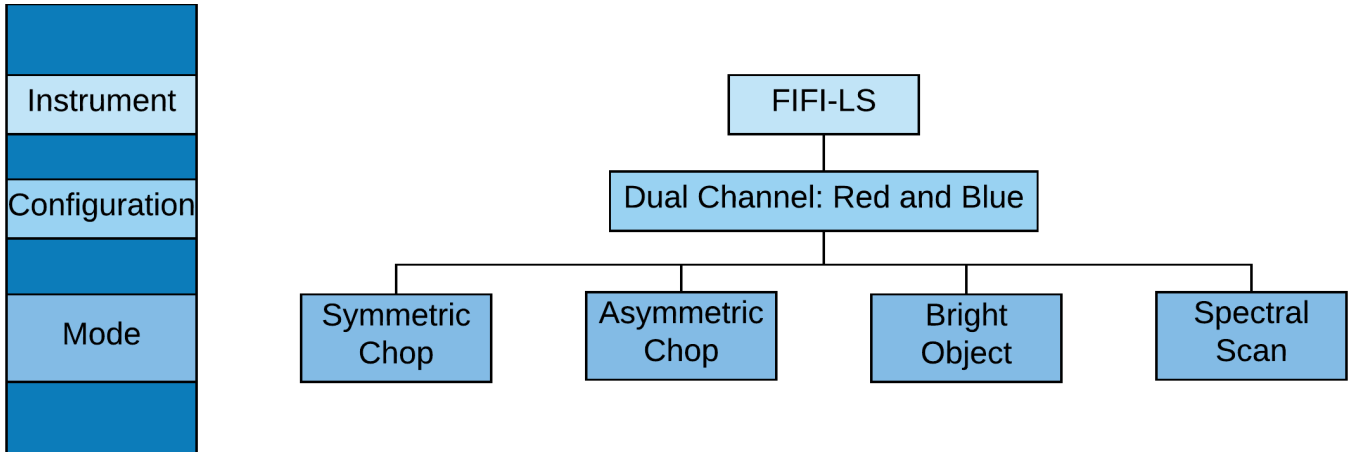
Table of Contents

- 3.2 Planning Observations
 - 3.2.1 Observing Modes
 - 3.2.1.1 Symmetric Chop
 - 3.2.1.2 Asymmetric Chop
 - 3.2.1.3 Bright Objects
 - 3.2.1.4 Spectral Scan
 - 3.2.2 Integration Time Estimates
 - 3.2.3 Spectral Dithering

3.2.4 Mapping

Return to the Table of Contents for this section at any time by selecting [Return to Table of Contents](#). Users may also navigate through the entire Observer's Handbook by using the complete Table of Contents menu to the right.

3.2. Planning Observations



3.2.1 Observing Modes

The high sky background in the far infrared requires careful subtraction. That is achieved by chopping with SOFIA's secondary mirror and by nodding the telescope. The secondary will chop at 2 Hz to efficiently remove the sky emission. To remove residual background not canceled by chopping, the telescope is nodded typically every 30 s either to move the source to the other chop-beam or to an off-position. Since the instrument telescope communications and the telescope move take 10 s, a whole nod-cycle takes typically 80 s.

The following sections describe the possible observing modes. In the discussion of the overheads, N is the number of map positions and t_{on} is the on-source exposure time per map position. The main driver to choose the observing mode is to figure out possible chop configuration. However, the details like the exact chop throw and angle and other observing details do not need to be fixed until Phase II of the proposal process. Information on how the parameters for each mode is to be entered into USPOT during Phase II of the proposal process can be found on the [FIFI-LS USPOT web page](#).

[Return to Table of Contents](#)

3.2.1.1 Symmetric Chop

If possible this observing mode should be used because it is the most efficient mode. This mode combines chopping symmetrically to the telescope's optical axis with a matched telescope nod to remove the residual telescope background. This mode is also known as nod match-chop (NMC) mode (cf. [Section 5.2.1](#)) or beam switching (BSW, cf. [Section 7.2.1](#)).

When observing using a symmetric chop, large chop amplitudes degrade the image quality due to the introduction of coma. This effect causes asymmetric smearing of the Point Spread Function (PSF) in the direction of the chop. However, the effect is small (with effect on Signal to Noise Ratio (SNR) less than 10%) in the red channel for all chop

throws and in the blue channel for total chop throws less than 5 arcmin and wavelengths longer than 63 μm . For wavelengths shorter than 63 μm , we recommend total chop throws of less than 4 arcmin. Generally, it is recommended to use a chop as small as possible, but keep the FOV in the off-positions outside of any detectable emission.

The position angle of the chop can be specified relative to equatorial coordinates or telescope coordinates (e.g. horizontal). Keep in mind that the telescope nod matched to the chop creates two off-positions symmetric to the on-position (Figure 3-5).

The total overhead in this mode is about $1.6N t_{\text{on}} + 300$ s, since the source is only observed during 50% of the observation and additional time is required for telescope moves, plus 300 s for the setup. This overhead estimate assumes that the on-source exposure time per map position t_{on} is at least 30 s. If the on-source exposure time per map position t_{on} is less than 15 s, the Bright Object mode should be used. For values of t_{on} in between, one needs to enter an alternate overhead in SPT. The total alternate overhead is $N(t_{\text{on}} + 20$ s) + 300 s.

Figure 3-5.

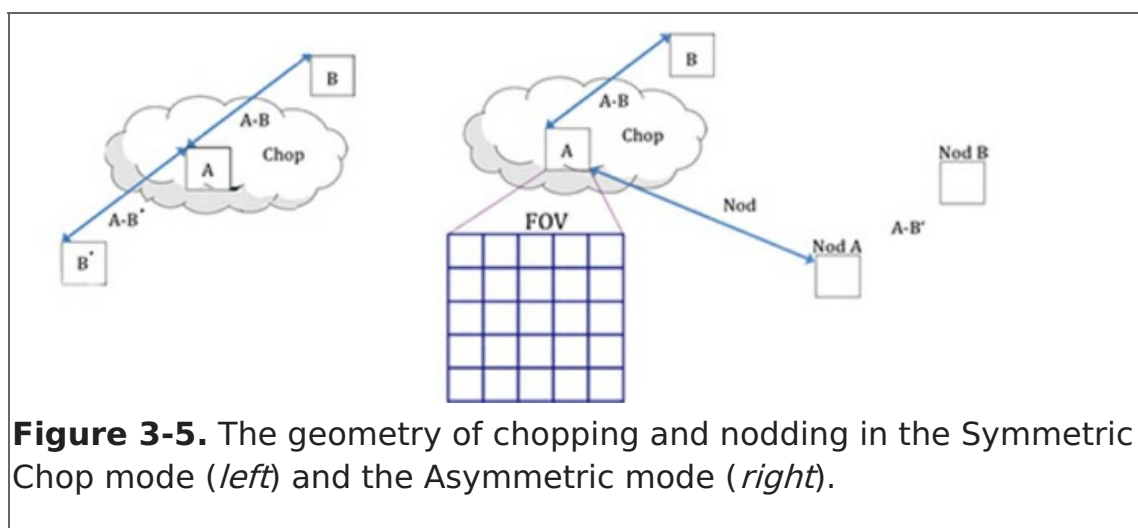


Figure 3-5. The geometry of chopping and nodding in the Symmetric Chop mode (*left*) and the Asymmetric mode (*right*).

[Return to Table of Contents](#)

3.2.1.2 Asymmetric Chop

If the target's size or environment does not allow to use the Symmetric Chop Mode, one has to use the Asymmetric Chop mode allowing larger chop throws at shorter wavelengths and is not creating symmetric off-positions around the source. The asymmetric chop keeps the on-beam on the optical axis. This results in an image unaffected by coma. Consequently, the off-beam is off-center by twice the amount compared to the symmetric chop with the same chop throw resulting in twice as much coma. But that is of no consequence as the off-beam should only see empty sky. The telescope is noded to an off-position where the same chopped observation is executed to provide the residual background subtraction. Figure 3-4 illustrates this geometry. Note that this mode is similar to FORCAST's asymmetric chop-offset-nod (C2NC2) mode (see Section 5.2.1" > Section 5.2.1).

The total overhead in this mode is about $4.2N t_{\text{on}} + 300$ s, since the source is observed during 25% of the observation plus additional time for telescope moves and 300 s for the setup. This overhead estimate assumes that the on-source exposure time per map

position t_{on} is at least 15 s. For shorter values of t_{on} , the Bright Object mode should be used.

[Return to Table of Contents](#)

3.2.1.3 Bright Objects

For very bright objects, where the estimated on-source exposure time per map position is 15 s or less, the total observing time is dominated by telescope movements. The efficiency of mapping such bright objects can be improved by observing two map positions and one off-position per nod-cycle using an asymmetric chop. In this mode, the total overhead is $3 N t_{\text{on}} + 300$ s assuming an on-source exposure times per map position of about 15 s. Please [contact](#) the Help-Desk, if you are planning shorter integration times. The overhead increases with shorter integration times and the standard overhead calculation should be overwritten with the actual overheads for such short integrations times.

[Return to Table of Contents](#)

3.2.1.4 Spectral Scan

In contrast to the other observing modes, this mode targets spectral features much wider than the bandwidth (see [Section 3.1.2.2](#)) like solid state features. The problem is a good atmospheric calibration over the whole observed wavelength range. The spectrum has to be pieced together from many different exposures. The best way to take such data and how to reduce it is still being investigated. If this observing mode is considered, please [contact](#) the Help-Desk.

[Return to Table of Contents](#)

3.2.2 Integration Time Estimates

The [FIFI-LS on-line exposure time estimator](#) should be used to estimate the on-source exposure times used in proposals and observing preparation. The time estimator requires the following input:

Observatory Altitude

(in feet; < 60,000 ft): default 38,000 ft

This value is used in ATRAN to derive the atmospheric absorption. For more details about ATRAN (see [Section 1.3](#)).

On a typical SOFIA flight, observations start at 38,000 ft or 39,000 ft and 43,000 ft are reached 3.5 h before the observations end. The default value of 38,000 ft ensures that time estimate does not underestimate the water vapor overburden. If an observation is rather sensitive to the water vapor, a higher altitude can be entered and justified in the proposal. In Phase II, select **Low** or **VeryLow** for **Requested WV Overburden** in the **Observing Condition** panel in USPOT, if the altitude used in the time estimation is 41,000 ft or 43,000 ft, respectively. Note, that this limits the schedulability of the observation to the last 5.5 h or 3.5 h of observations.

Water Vapor Overburden

(in microns; 0 if unknown): default 0

If a value of 0 is given, ATRAN assumes a typical amount of water vapor to derive the atmospheric absorption.

Telescope Elevation

(between 20 and 60 deg): default 40

For northern sources an elevation of 40° is okay, but sources south of a declination of -15° will most likely be observed at a respectively lower elevations unless an observation from the southern hemisphere is required.

Signal to Noise Ratio or Integration Time(s)

default SNR 5

Specify either a requested SNR and the required on-source exposure time is returned, or specify an on-source exposure time and the resulting SNR is returned.

Wavelength

(in microns, between 51 and 200): default 157.741 μm (rest wavelength of [CII] line)

Specify the rest wavelength of the requested transition.

Source Flux

default 2.087e-17 W m⁻² line flux (MDLF per pixel for [CII])

Specify the expected source flux *per FIFI-LS pixel* either as integrated line flux in W/m² or as continuum flux density in Jansky. Make it obvious in the technical feasibility section of the proposal that the referenced flux estimates have been converted to FIFI-LS pixels sizes.

Source Velocity

(in km/s): default 0 km/s

Enter the radial velocity of the source relative to the local standard of rest (LSR).

Input Observer Velocity

(VLSR in km/s): default 0 km/s

In many, but not all cases, the default value of zero can be used. However, if the observing wavelength is near a strong narrow telluric feature, the earth's velocity relative to the LSR becomes important, eg. for galactic sources and the [OI] line at 145.525 μm . Then either enter the velocity directly or have it computed by entering time, date, source coordinates, and SOFIA's location. The Doppler-shift due to the source's and the observatory's velocity is important to estimate the atmospheric extinction, discussed further below.

Bandwidth

default 0 km/s

Enter the desired width of the spectrum. The width should allow for sufficient baseline on both sides of the expected line/spectral feature to allow a good estimate of the underlying continuum telluric and astronomical. This value enters the time estimate as the factor *f*. If the desired spectrum is wider than the instantaneous bandwidth, *f* is the ratio of the requested width of the spectrum and the bandwidth (Figure 3-3). Otherwise *f* is equal to 1.

The time estimator calculates the on-source integration time per map position for a

source flux, F and a desired SNR using [Eq.3-1](#) (see also [Figure 3-4](#)).

The factor α is the transmission of the atmosphere for the observing wavelength derived by [ATRAN](#). The on-line time estimator includes a plot of the transmission of the atmosphere at full spectral resolution and smoothed to the spectral resolution of FIFI-LS at the observing wavelength over the bandwidth. Two integration times are calculated using the transmissions from each curve. The value derived from the unsmoothed curve applies to an observation of a very narrow line, while the value from the smoothed curve applies to a continuum source or a line broader than the instrument's spectral resolution. If the atmospheric transmission is smooth near the observing wavelength, the two values will not differ much and the more conservative or appropriate observing time should be chosen. Furthermore, the observing time will not depend strongly on the source velocity. The velocity correction can be rounded to 100km/s and the earth's velocity can be ignored.

However, if there is a telluric feature near the observing wavelength, one has to carefully check the feasibility of the observation (a special warning is displayed if the ratio of the derived observing times exceed 1.5). This usually happens when the observing wavelength is near a strong and narrow atmospheric feature. A typical example is the [OI] line at 145.525 μm , which is near a narrow and strong telluric feature at 145.513 μm or at -25 km/s relative to the [OI] line. In such a case, it is crucial to enter a good estimate of the source velocity accurate to ~ 1 km/s. The source velocity needs to be the combination of the source velocity relative to the LSR or another reference frame *and* earth's velocity relative to that reference frame, which depends on the observing date and target location. Therefore the time estimator includes a calculator for the earth's velocity relative to the LSR. It may be necessary to add a time constraint for the observation to avoid an adverse earth's velocity relative to the source.

If the observing line is near a strong and narrow telluric feature, not only the observing time estimate needs greater care, but the correction for the atmospheric absorption of an observed line flux will have a large uncertainty. To derive the correction factor, the atmospheric transmission curve would need to be integrated while weighted with the intrinsic line profile of the observed emission line with the correct relative Doppler-shift. In most cases FIFI-LS will not be able to resolve the line profile and cannot resolve the atmospheric feature. Any attempt to correct the measured line flux would depend strongly on assumptions of the source's line shape and position and assumptions of the water vapor content and shape of the telluric feature. In short, expect a large uncertainty of a line flux measured near a strong and narrow telluric feature.

The exposure time estimator returns the *on-source* exposure time *per map position* t_{on} . If mapping is planned, this values has to be multiplied with N , the number of map positions, to derive the total on-source observing time. More on mapping can be found in [Section 3.2.3](#). *The total on-source observing time $N \times t_{on}$ has to be entered into USPOT* during Phase I of the proposal process. The overhead depends on the observing mode ([Section 3.2.3](#)) and is automatically added by USPOT.

Be conservative with the time estimates! Unforeseen issues like thunderstorms or computer crashes may cut the observing time short. Better to aim for 5σ and get a 3σ result, than aim for a 3σ and then wonder, what to do with a 1.8σ signal.

[Return to Table of Contents](#)

3.2.3 Spectral Dithering

Spectral dithering is always employed for self flat-fielding and increased redundancy. Spectral dithering implemented via a grating scan. The grating is moved in small steps, so that the spectrum moves over different pixels in the spectral dimension of the detector array.

The default pattern to cover the instantaneous bandwidth (BW, [Section 3.1.2.2](#)) is to move the grating 12 steps, each corresponding to half a spectral pixel width. This pattern results in a spectrum about 30% wider than the BW. The central 70% of the BW are observed during the whole observing time reaching the full SNR, while the remaining 15% on each side of the BW should reach on average 86% of the SNR. The SNR reached on the extra 30% should still be 46% on average based on the observing time for each part of the spectrum. For wider spectral coverage, the step size and number of steps of the grating scan will be adjusted by the instrument operators to achieve the desired spectral coverage. The steps will be evenly distributed over the nod-cycles.

[Return to Table of Contents](#)

3.2.4 Mapping

Mapping is supported by all of the observing modes except the Spectral Scan. It can be done on a rectangular grid with a user-defined spacing and extent. It is also possible to supply a list of mapping positions to achieve a map with a custom shape optimized to the source geometry. For both map types, a spacing of 15 arcsec might be a good choice providing half pixel steps to yields super-resolution with a good overlap for the blue array and a very strong overlap for the red array. For very large maps fast maps, a spacing of half a red array or 30 arcsec achieves super-resolution with a good overlap for the red array and full coverage (but no overlap) for the blue array. These details need to be specified only in Phase II of the proposal process (see the [FIFI-LS USPOT](#) chapter). In Phase I, the effective map area needs to be entered in SPT and the proposal should explain the suggested mapping strategy. The on-source integration time to be entered in SPT has to be the on-source integration time per raster point multiplied by the number of raster map points $N t_{\text{on}}$.

If the source geometry allows the off-beam to be positioned symmetrically on both sides of the source, then one should use the much more efficient Symmetric Chop mode for mapping. If that is not possible the Asymmetric Chop mode has to be used. An asymmetric chop is also used in the Bright Object Mode. [Figure 3-6](#) illustrates mapping with an asymmetric chop. The off-beam (positions B1 to B3) covers an area while chopping that is the same size as the map itself. If this is undesirable, the map needs to be broken up into sub-maps with varying chop parameters to be specified in Phase II. The availability of guide stars might be another reason to break up a large map into sub-maps. In this case the sub-maps will be identified between Phase II and the actual observation by the support scientist in close collaboration with the guest investigator and the telescope operator.

When estimating the on-source integration time ([Section 3.1.2.3](#)), take into account the differing overlap of the red and blue FOV at the desired raster map spacing. The SNR

entered into the calculation of t_{on} is the SNR for a single raster map point. The final SNR for a point in the map should reach $\sqrt{x} * \text{SNR}$ with n being the number of raster points from which a point is covered by the respective FOV. For example in [Figure 3-6](#), the area of the pixel in the middle is covered by 3 FOVs while 16 pixels are covered by 2 FOVs and the outer parts of the map are covered by 1 FOV.

Figure 3-6.

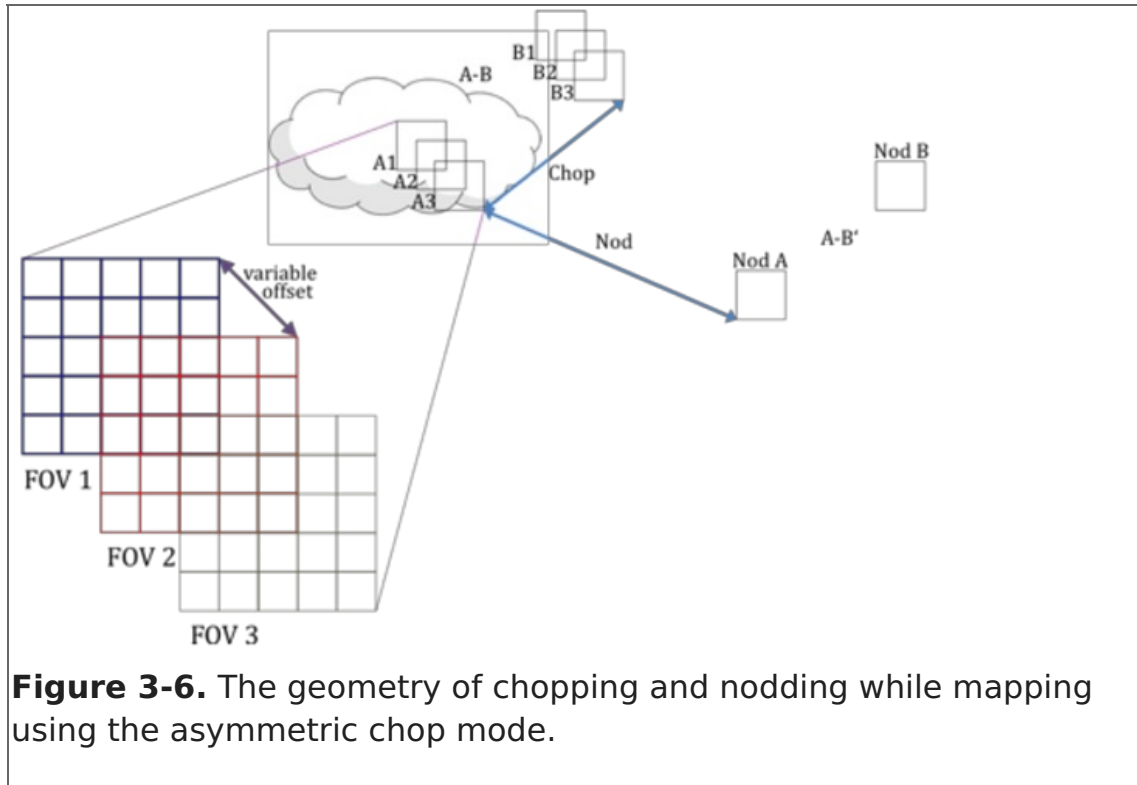


Figure 3-6. The geometry of chopping and nodding while mapping using the asymmetric chop mode.

[Return to Table of Contents](#)

4. FLITECAM

- 4. FLITECAM
 - 4.1 Specifications
 - 4.1.1 Instrument Overview
 - 4.1.1.1 Design
 - 4.1.2 Performance
 - 4.1.2.1 Camera Performance
 - 4.1.2.2 Filter Suite
 - 4.1.2.3 Imaging Sensitivities
 - 4.1.2.4 Grisms
 - 4.1.2.5 Spectroscopic Sensitivities
 - 4.2 Planning Observations
 - 4.2.1 Imaging Observations
 - 4.2.1.2 Estimation of Exposure Times
 - 4.2.2 Spectroscopic Observations
 - 4.2.2.1 Estimation of Exposure Times

4.1 Specifications

Table of Contents

- 4.1 Specifications

- 4.1.1 Instrument Overview
 - 4.1.1.1 Design
- 4.1.2 Performance
 - 4.1.2.1 Camera Performance
 - 4.1.2.2 Filter Suite
 - 4.1.2.3 Imaging Sensitivities
 - 4.1.2.4 Grisms
 - 4.1.2.5 Spectroscopic Sensitivities

Return to the Table of Contents for this section at any time by selecting [Return to Table of Contents](#). Users may also navigate through the entire Observer's Handbook by using the complete Table of Contents menu to the right.

4.1 Specifications

4.1.1 Instrument Overview

The **F**irst **L**ight **I**nfrared **T**est **C**AMera (FLITECAM) is an infrared camera operating between 1.0–5.5 μm . It consists of a 1024x1024 InSb detector with 0.475 x 0.475 arcsec pixels and uses refractive optics to provide a 8 arcmin diameter field of view. The instrument has a set of broadband filters for imaging, as well as grisms for moderate resolution spectroscopy.

Additionally, FLITECAM was designed to be co-mounted on the telescope with the **H**igh-speed **I**maging **P**hotometer for **O**ccultations (HIPO), providing simultaneous optical through near-IR (NIR) imaging capabilities. This mode is called FLIPO. Proposers wanting to use this mode can find the details of HIPO in Chapter 9.

NOTE: FLITECAM, either stand-alone or co-mounted with HIPO, is not being offered for observations in Cycle 6. Limited new observations may be requested through the Director's Discretionary Time process. Please see Section 1.0 of the [Call for Proposals](#) for a statement of the policy.

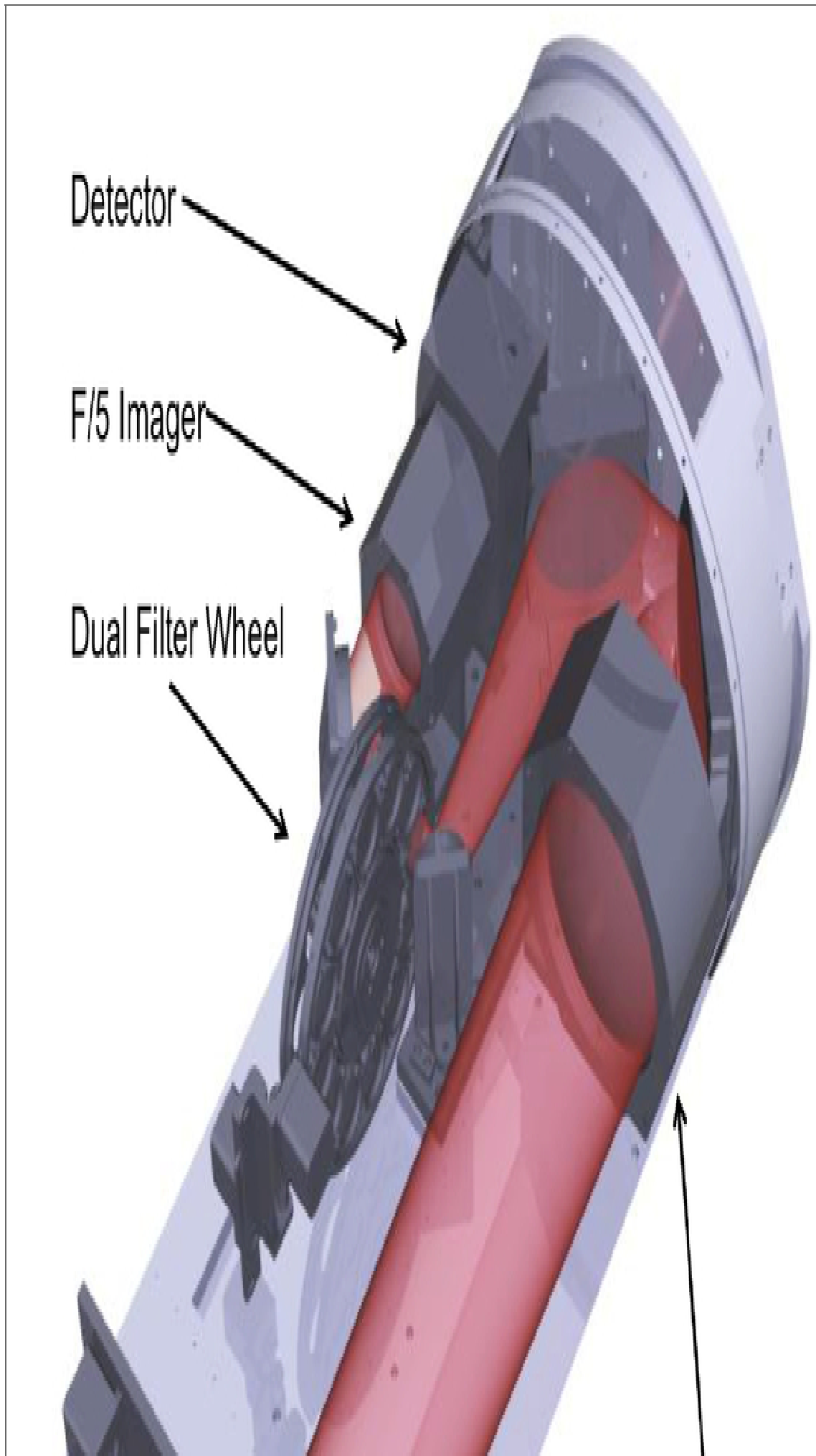
[Return to Table of Contents](#)

4.1.1.1 Design

FLITECAM consists of a cryogenically cooled near-IR (NIR) camera that can be used for both imaging and grism spectroscopy. A schematic of the optical bench is shown in [Figure 4-1](#) with a full ray trace diagram in [Figure 4-2](#). The incoming beam first passes through the entrance aperture and into the collimator assembly, a stack of custom designed lenses that allow imaging of nearly the entire 8 x 8 arcmin SOFIA field-of-view (FOV). The beam is then repositioned using three flat fold-mirrors so that it passes through the image pupil and through a pair of 12-position filter wheels. A fourth flat fold-mirror redirects the beam through the f/4.7 refractive imaging assembly, which then focusses the beam on the array.

When observing in spectroscopy mode, only minimal changes to the optical path are required. First, the slit mask is inserted into the beam immediately behind the aperture window at the telescope focus. The slit is a single 16.5 mm long slit (2 arcmin on the detector) divided in half with two different widths, one approximately 2 arcsec and the other 1 arcsec. Second, the chosen grism and order sorting filter (located in filter wheel #2 and #1, respectively) are set in place. Details are presented in [Section 4.1.2.4](#).

Figure 4-1.



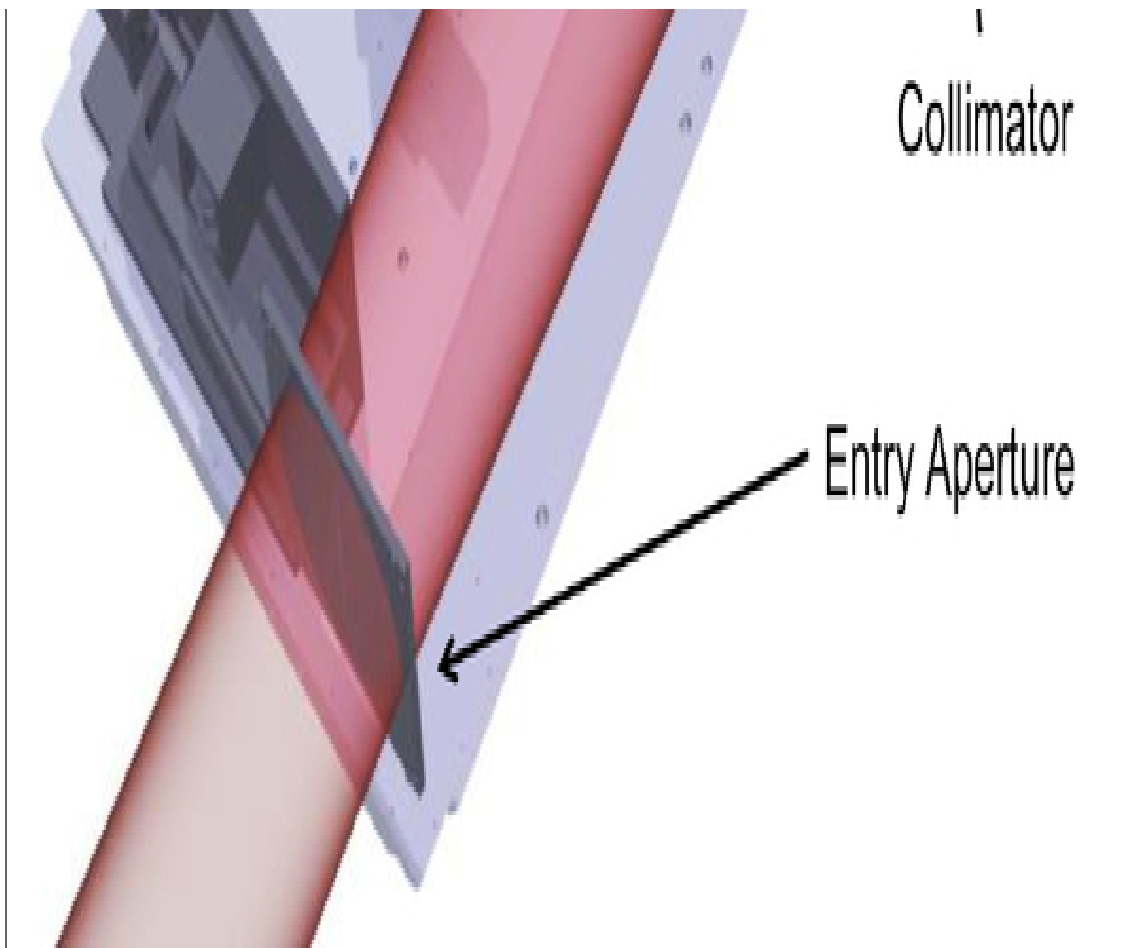
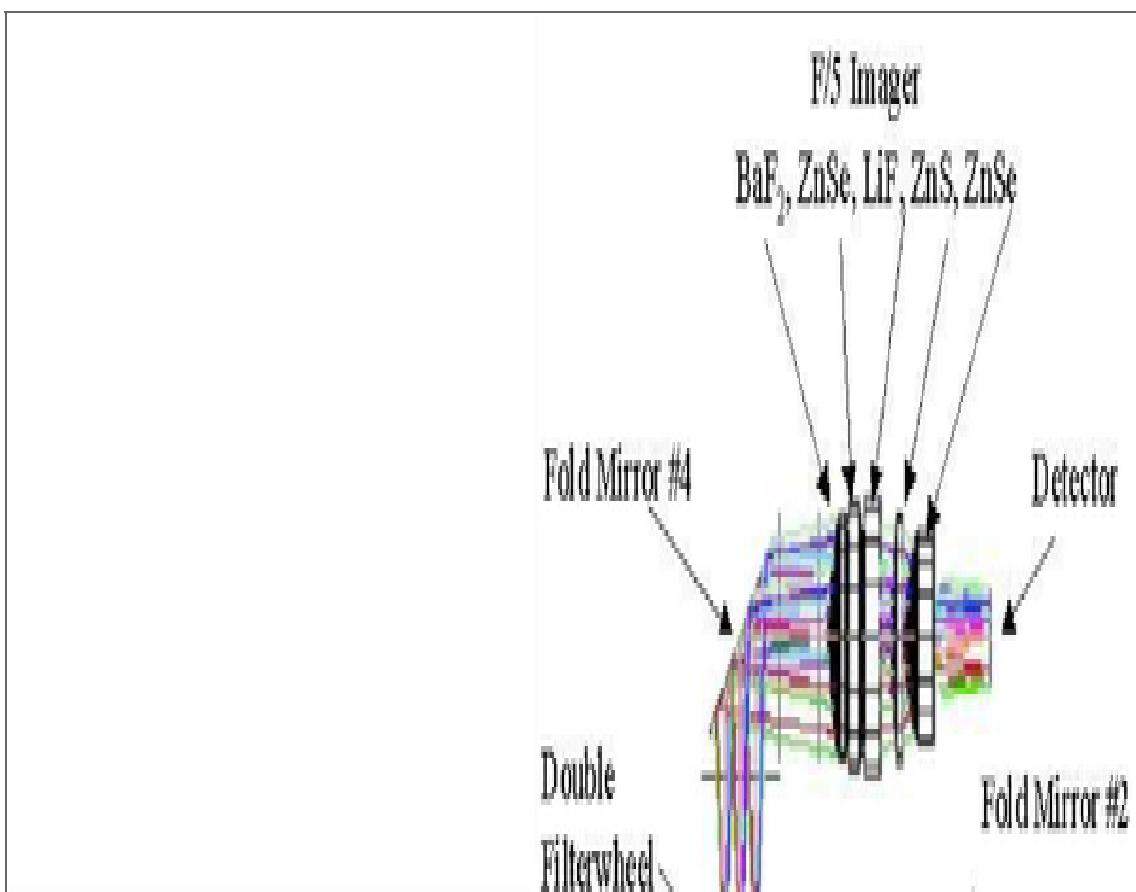


Figure 4-1. This is a block diagram of the front end of the FLITECAM instrument with labels of important components.

Figure 4-2.



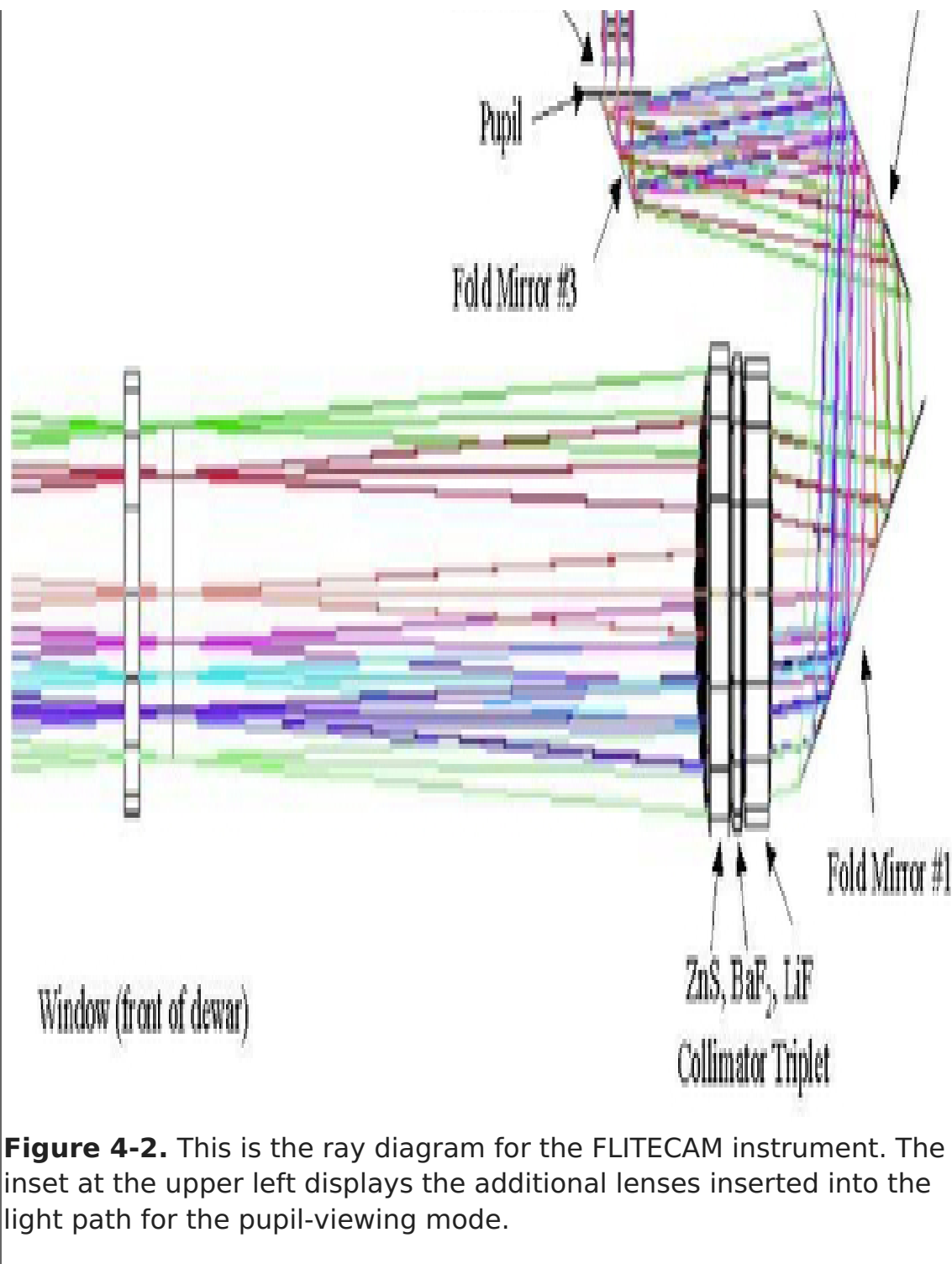


Figure 4-2. This is the ray diagram for the FLITECAM instrument. The inset at the upper left displays the additional lenses inserted into the light path for the pupil-viewing mode.

[Return to Table of Contents](#)

4.1.2 Performance

4.1.2.1 Camera Performance

The FLITECAM detector is a 1024x1024 pixel indium antimonide (InSb) Raytheon ALADDIN III array cryogenically cooled to 30 K. The detector has 27 μ pixels which translate to a plate scale of 0.475" per pixel, resulting in a nearly 8 arcmin square FOV. The detector is optimized for use between 1-5.5 microns, and has a read noise of approximately 40 e^- and dark current $\leq 1 e^- \text{ sec}^{-1}$.

The on-axis image quality (IQ) of the camera is excellent and images obtained with FLITECAM are expected to be diffraction limited from 3-5.5 μm . From 1-3 μm , the IQ will be limited by contributions from the telescope optics, telescope jitter, shear layer seeing,

and the diffraction limit. Ground based tests under the best conditions at the Lick Observatory indicated that the IQ is stable within 1.5' of the optical axis, but that beyond this distance, coma begins to appear. The extent of the coma has not been parameterized.

The detector well depth is relatively shallow ($\sim 80,000 e^-$) which, when combined with the detector quantum efficiency (QE), may necessitate relatively short exposure times, particularly on bright sources or in regions of high sky background. The shortest exposure time available for a full 1024x1024 detector readout is 0.2 seconds. However, faster readout times can be achieved using sub-arrays—0.08 seconds for a 512x512 sub-frame and 0.015 sec (~ 67 Hz) for a 64x64 pixel sub-frame. These subarrays are required to be symmetric and relative to the center of the detector. An additional "movie" mode is available to sample a single 512x512 quadrant at ~ 0.08 seconds without any deadtime between images, or down to the 32x32 sub-frame (closest to the detector center) at < 0.015 seconds. Users interested in these modes should consult the FLITECAM Instrument Scientist via the SOFIA Help desk (sofia_help@sofia.usra.edu).

Care must be taken not to over-expose the detector since charge persistence can be a significant problem for InSb arrays. If the detector is over-exposed, it is necessary to take several long exposures (~ 5 minutes each) of blanks mounted in the filter wheel to allow the detector to recover. To help mitigate the problem of accidental saturation of the detector, filter changes are carefully orchestrated to ensure that the sky is never viewed through the two open filter wheel positions.

[Return to Table of Contents](#)

4.1.2.2 Filter Suite

The core of the FLITECAM filter suite is a set of standard Barr bandpass filters used for imaging at J, H, K, L, and M, which are all located in filter wheel #1. In addition, filter wheel #2 holds a selection of specialty, narrow-band imaging filters, including Paschen α , Paschen α continuum, an ice filter centered on the 3.07 μm H₂O ice feature, a polycyclic aromatic hydrocarbon (PAH) filter centered on the prominent 3.3 μm feature, L_{narrow}, and M_{narrow}. Finally, there are a number of order sorting filters (OSFs) for use with the grisms, including J and H (both dual purpose), K_{wide}, K_{long}, and "L+M". Additional details of the OSFs are given in [Section 4.2.3.4](#).

As the bulk of the instrument commissioning was performed in the combined FLITECAM/HIPO (FLIPO) mode, some of the FLITECAM only observation modes lack detailed performance characteristics. This is due to the lack of circulation of stratospheric air down the Naysmyth tube which keeps the FLIPO foreoptics at cabin temperature, greatly increasing the observed background.

In the combined FLITECAM/HIPO configuration, imaging observations past 3 microns are required to use increasingly small subarrays; spectroscopic observations past 4 μm are not possible at all. In the FLITECAM-solo configuration, however, full-frame imaging observations are possible out to 4 μm , and the full suite of FLITECAM grisms are available.

The central wavelengths and band widths of the available imaging filters are provided in

Table 4-1. This table also includes the sensitivity values (Minimum Detectable Continuum Flux; MDCF) discussed in [Section 4.1.2.3](#). Filters that will only be available on a shared risk basis during Cycle 6 are indicated. [Figure 4-3](#) displays the transmission profiles (normalized to their peak transmission) for the imaging filters over-plotted on an ATRAN model of the atmospheric transmission. The filter transmission curves are available and linked in the last column of [Table 4-1](#) below.

Table 4-1

FLITECAM Filter Characteristics

Name	Bandpass	λ_{eff} (μm)	Peak Trans. (%)	Band- width ^a (μm)	R ^b	MDCF (μJy)		Profile
FLITECAM	FLIPO							
Standard Filters								
FLT_J	J	1.239	93.7	0.293	0.36	25.7	27.4	PNG DAT
FLT_H	H	1.631	95.3	0.305	0.50	33.5	35.7	PNG DAT
FLT_K	K	2.104	95.4	0.395	0.83	38.7	57.5	PNG DAT
FLT_Lprime	L'	3.855	93.5	0.7	2.70	-	-	PNG DAT
FLT_L	L ^c	3.53	94.1	0.65	2.29	440	-	PNG DAT
FLT_M	M ^c	4.838	91.8	0.645	3.12	2720	-	PNG DAT
Specialty Filters								
FLT_Pa	Pa α	1.874	84.2	0.033	0.06	179	195	PNG DAT
FLT_Pa_cont	Pa α Cont.	1.9	88.3	0.033	0.06	178	195	PNG DAT
FLT_ICE_308	Ice ^c	3.049	88.1	0.191	0.58	504	1130	PNG DAT
FLT_PAH_329	PAH ^c	3.302	91.4	0.115	0.38	1070	2260	PNG DAT

Name	Bandpass	λ (μm)	Peak Trans. (%)	Band- width (μm)	R	MDCF (μJy)		Profile
FLT_NbL	L _{narrow} ^c	3.602	90.5	0.231	0.83	1010	2110	PNG DAT
FLT_NbM	M _{narrow} ^c	4.804	89.5	0.19	0.91	5430	-	PNG DAT
Order Sorting Filters^d								
Hwide	H _{wide}	1.794	97.1	0.587	1.05	-	-	PNG DAT
Kwide	K _{wide}	2.299	96	0.882	2.03	-	-	PNG DAT
Klong	K _{long}	2.45	95.5	0.55	1.35	-	-	PNG DAT
L+M	L+M	4.11	92.5	2.715	11.16	-	-	PNG DAT

^a Bandwidth for transmission level is >5%

^b $R = \lambda/\Delta\lambda$

^c Will be offered as Shared Risk during Cycle 6

^d Will not be available for imaging

Figure 4-3.

FLITECAM Imaging Filters

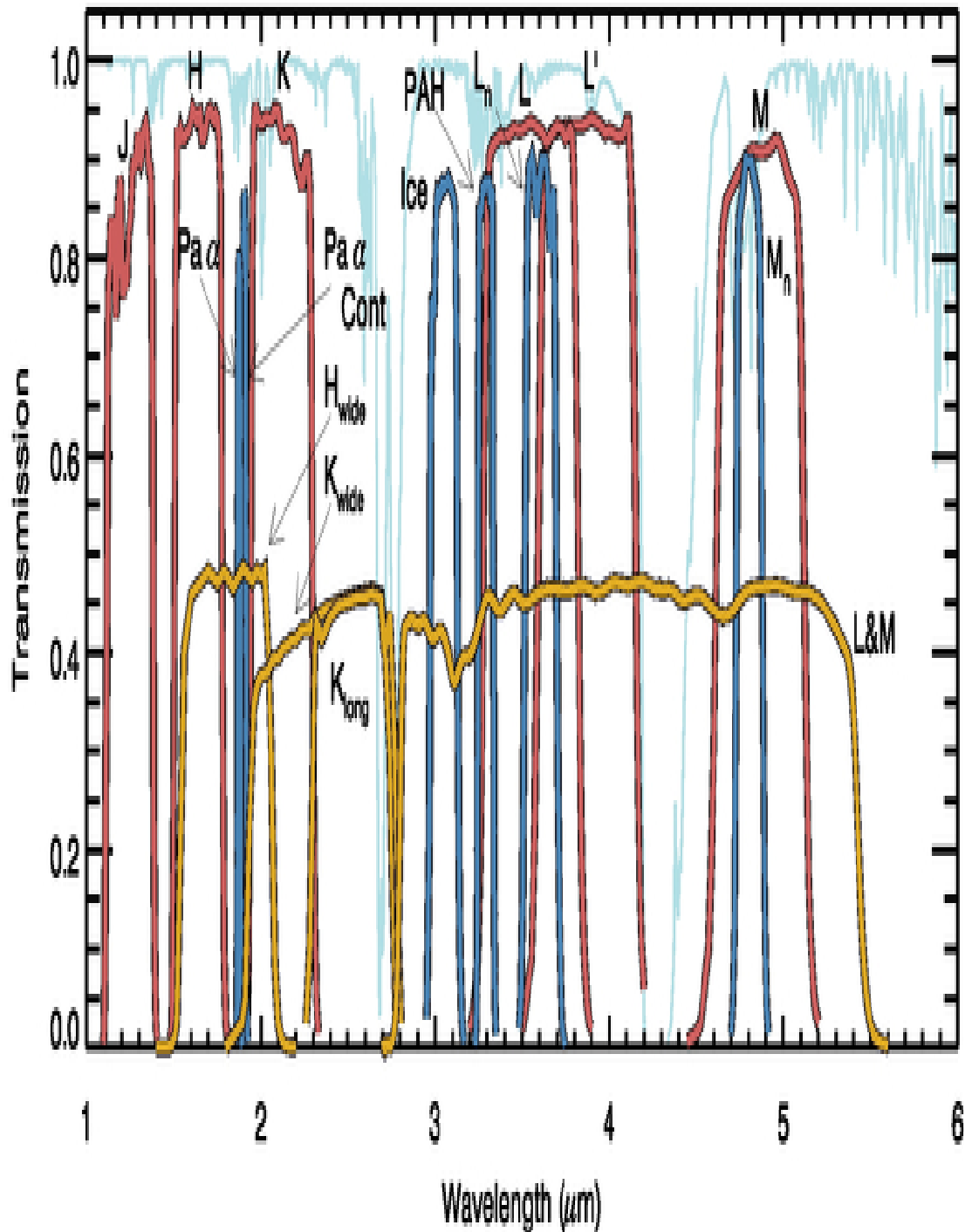


Figure 4-3. Plotted here are the FLITECAM filter transmission curves overlaid on an ATRAN model of the atmospheric transmission across the FLITECAM bandpass assuming a zenith angle of 45 degrees and 7 μm of precipitable water vapor. The transmission profiles of the standard filters are shown in red, specialty filters are shown in blue, and OSFs in gold. The OSF transmission profiles have been scaled by 50% for clarity.

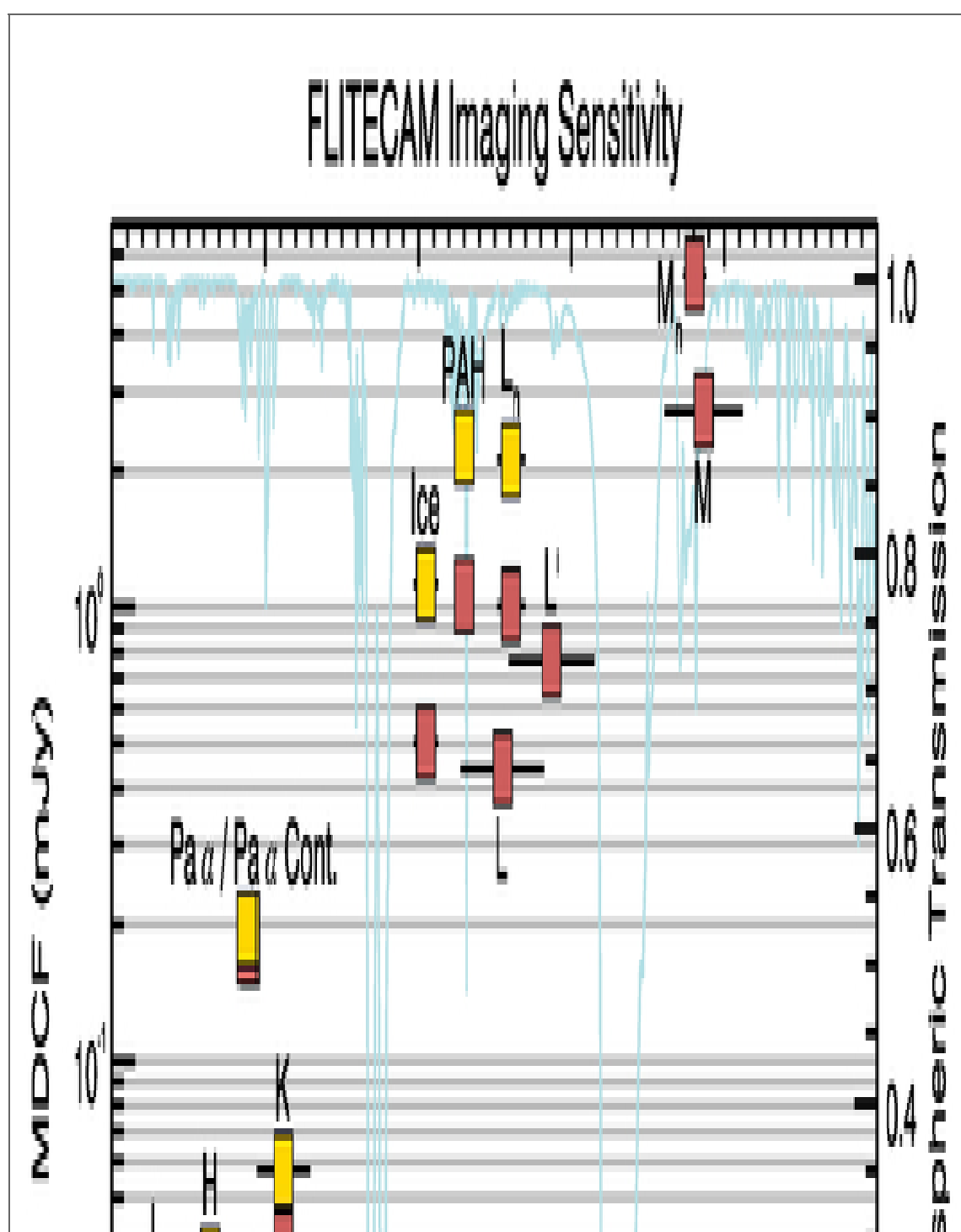
[Return to Table of Contents](#)

4.1.2.3 Imaging Sensitivities

The Minimum Detectable Continuum Flux (MDCF; 80% enclosed energy) in μJy needed to get $S/N = 4$ in 900 s has been estimated for each filter for an altitude of 41,000 feet (7.3 μm of precipitable water vapor) from a model of the instrument and the atmosphere. The values are presented in Table 4-1 above and are plotted in Figure 4-4. The horizontal bars on the data in the figure indicate the effective bandpass at each wavelength. At the shorter wavelengths the bandpass is sometimes narrower than the symbol size.

Atmospheric transmission affects sensitivity, particularly at wavelengths $> 4 \mu\text{m}$, depending on the water vapor overburden. In addition to the theoretical sensitivity values for FLITECAM we have included the as-measured imaging sensitivities in the FLIPO (combined HIPO+FLITECAM) mode. **Until the instrument has been more accurately characterized at these longer wavelengths, the L and M band filters will be offered on a *shared risk basis*.**

Figure 4-4.



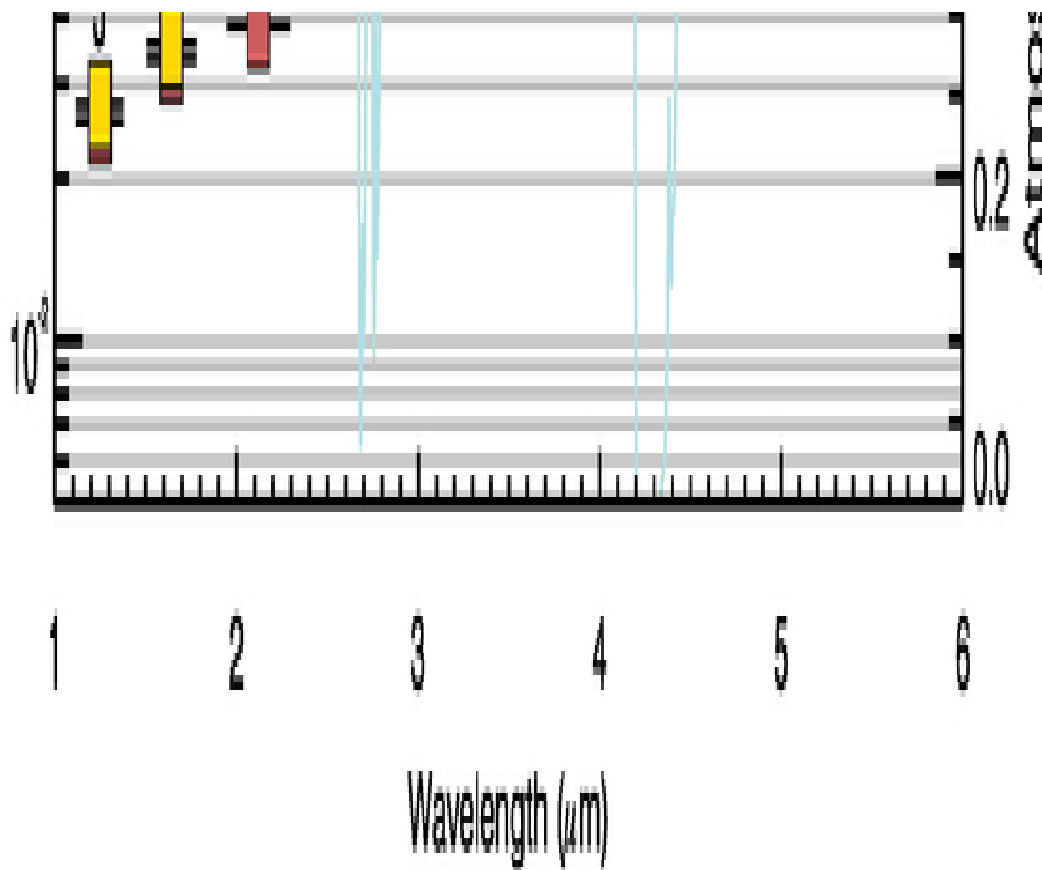


Figure 4-4. Theoretical FLITECAM imaging sensitivities for a continuum point source at the effective wavelengths of the FLITECAM filters listed above (red boxes). Yellow boxes indicate the imaging sensitivities for the FLIPO configuration (i.e. FLITECAM co-mounted with HIPO). The values reported are for a S/N of 4 in 900 seconds at water vapor overburdens of 7 μm. The horizontal bars correspond to the photometric band pass.

[Return to Table of Contents](#)

4.1.2.4 Grisms

A selection of three grisms are available in FLITECAM to provide medium resolution spectroscopic capabilities across the entire 1–5.5 μm wavelength range. The grisms are mounted in filter wheel #2 and are used along with Order Sorting Filters (OSFs) mounted in filter wheel #1 (see [Table 4-1](#)) to prevent order contamination. A summary of the grism properties is provided in [Table 4-2](#).

Grisms were chosen for use in FLITECAM since they minimize the changes necessary to the optical path while still allowing moderate spectral resolution. The grisms are made of direct-ruled (i.e. etched) KRS-5 (thallium bromiodide) material that provides a relatively high index of refraction ($n \sim 2.4$) without the significant absorption features that plague grisms with adhered transmission gratings. The three grisms were fabricated by Carl-Zeiss (Jena, Germany) each with an apex angle of 34.4°, but with different groove spacings to allow coverage of the entire 1–5.5 μm band (see [Table 4-2](#)).

Table 4-2

Grism Characteristics

Name ^a	Grism	Sep. (l/mm)	Order	OSF ^b	Coverage (μm)	High-Res R	Low-Res R
FLT_A1_LM	A	162.75	1	L+M ^d	4.395-5.533	--	--
FLT_A2_KL			2	K _{long}	2.270-2.722	1690	1140
FLT_A3_Hw			3	H _{wide}	1.550-1.828	1710	1290
FLT_B1_LM	B	217	1	L+M ^d	3.303-4.074	1780	1200
FLT_B2_Hw			2	H _{wide}	1.675-2.053	1750	1320
FLT_B3_J			3	J	1.140-1.385	1720	1425
FLT_C2_LM	C ^e	130.2	2	L+M	2.779-3.399	1670	1300
FLT_C3_Kw			3	K _{wide}	1.910-2.276	1650	1390
FLT_C4_H			4	H	1.500-1.718	1640	1400

^a Order Sorting Filter

^b Identifier used in the USPOT tool

^c $R = \lambda/\Delta\lambda$

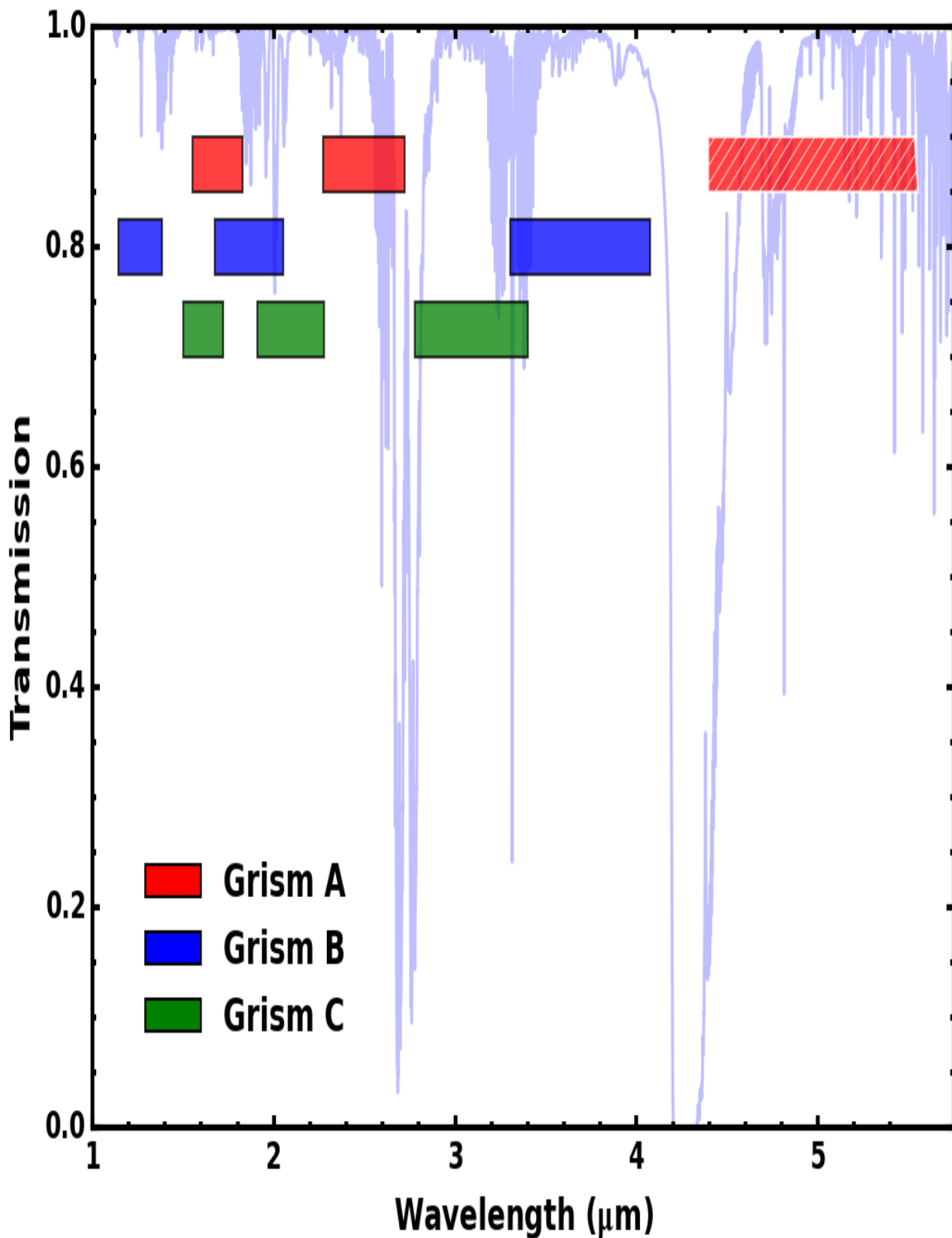
^d This combination of Grism and OSF will be available on a Shared Risk basis during Cycle 6.

^e The C Grism suffers from excess light at the blue end of each order. This issue is under investigation at the time of this writing.

The FLITECAM slit mask is mounted in a fixed slide mechanism at the telescope focus, immediately inside the entrance window to the dewar.

No calibration lamps are installed in FLITECAM. Consequently, wavelength calibration will be performed using atmospheric absorption lines.

Figure 4-5.



[Return to Table of Contents](#)

4.1.2.5 Spectroscopic Sensitivities

Figure 4-6 presents the *expected* continuum point source sensitivities for the FLITECAM grisms combined with an ATRAN model of the atmospheric transmission. The Minimum Detectable Continuum Flux (MDCF; 80% enclosed energy) in Jy needed for a S/N of 4 in 900 s at a water vapor overburden of 7.3 μm , an altitude of 41K feet, and an elevation

angle of 45° (i.e. at an airmass of 1.4) is shown.

Figure 4-6.

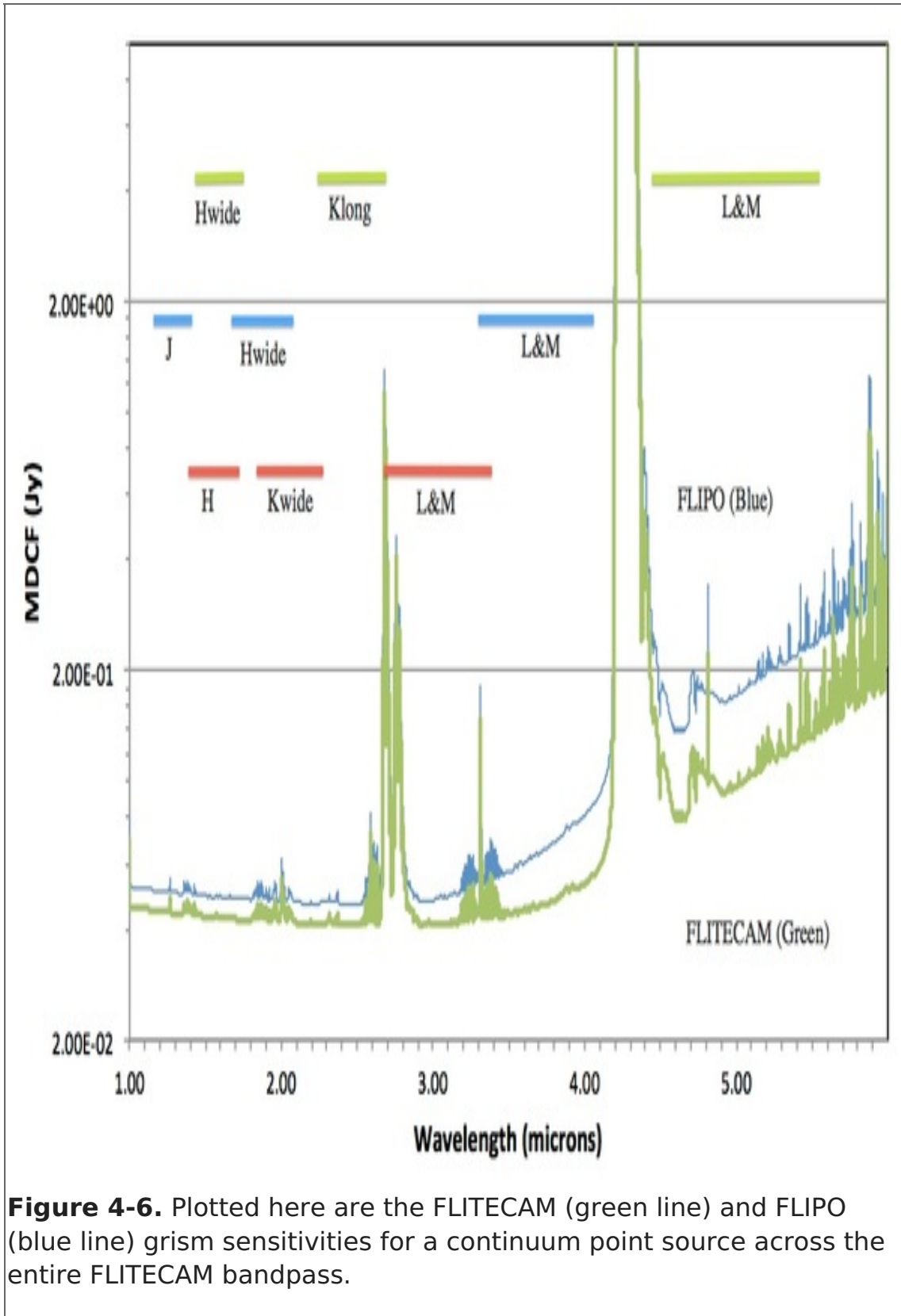


Figure 4-6. Plotted here are the FLITECAM (green line) and FLIPO (blue line) grism sensitivities for a continuum point source across the entire FLITECAM bandpass.

[Return to Table of Contents](#)

4.2 Planning Observations

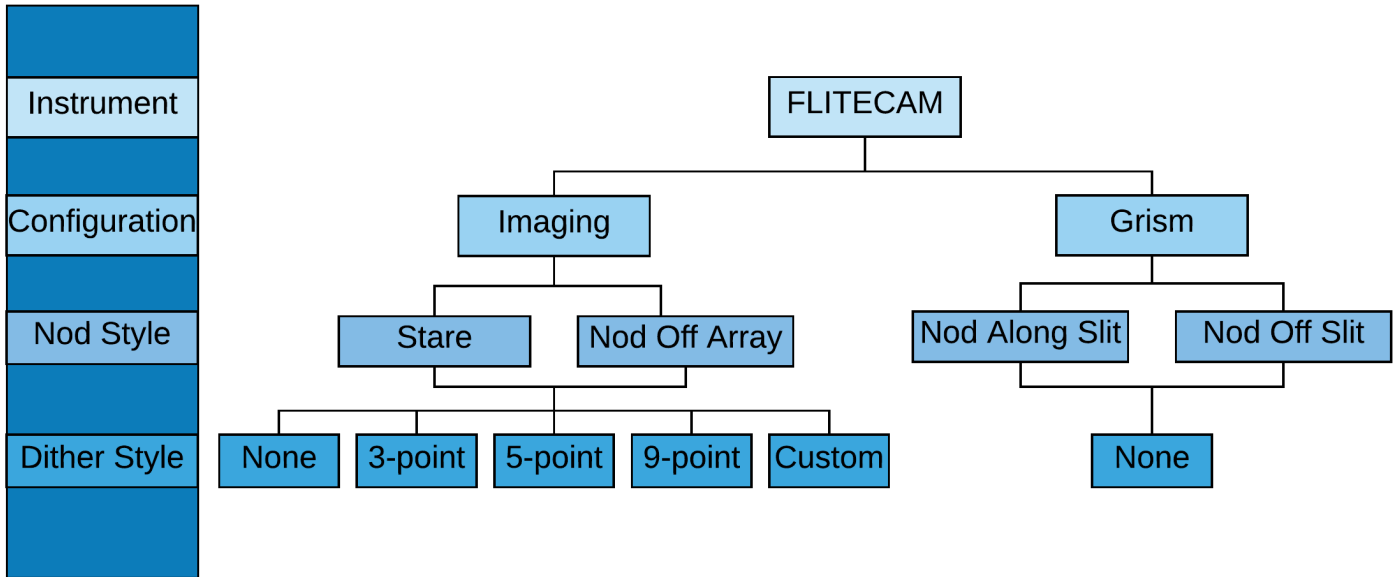
[Table of Contents](#)

- 4.2 Planning Observations
 - 4.2.1 Imaging Observations

- 4.2.1.1 Estimation of Exposure Times
- 4.2.2 Spectroscopic Observations
 - 4.2.2.1 Estimation of Expousre Times

Return to the Table of Contents for this section at any time by selecting [Return to Table of Contents](#). Users may also navigate through the entire Observer's Handbook by using the complete Table of Contents menu to the right.

4.2 Planning Observations



4.2.1 Imaging Observations

FLITECAM Imaging observations can be obtained in two different modes: STARE (with or without dithers) and Nod Off Array. The choice depends on the target and astronomical background. Chopping is not supported with FLITECAM.

Stare Mode

STARE mode observations involve a single telescope pointing centered on the source with dither pattern relative to it to facilitate background subtraction and image calibration. Dithering can be performed by selecting from pre-programmed dither patterns, or by defining a custom pattern. Observational experience has shown that STARE observations without dithers are particularly challenging with FLITECAM due to thermal background issues. Therefore, we recommend using dithers with *at least* 9 points, particularly longward of 2.2 μm .

Nod Off Array Mode

If the science target is extended or if it is located in a crowded region or region of extended emission, dithering alone may not be able to produce a suitable sky background frame. In this case the proposer may elect to observe using Nod Off Array mode which will complete a dither on-source and then nod the telescope to a defined sky position and complete a dither there as well. Selection of the nod direction and amplitude depends on the field of view around the target and will need to be chosen carefully to access a clean sky position and allow proper background subtraction.

The observing efficiency for FLITECAM STARE mode observations with dithering is

expected to be on the order of 70%. Observations in Nod Off Array mode are expected to result in a decrease in observing efficiency to around 35%. However, these efficiencies are built-in to USPOT and do not need to be specified by the proposer.

[Return to Table of Contents](#)

4.2.1.1 Estimation of Exposure Times

The exposure times for FLITECAM imaging observations should be estimated using the on-line exposure time calculator, [SITE](#). SITE can be used to calculate the signal-to-noise ratio (S/N) for a given total integration time, or to calculate the total integration time required to achieve a specified S/N. The format of the S/N values output by SITE depends on the source type. For Point Sources, the reported S/N is per resolution element, but for Extended Sources, it is the S/N per pixel. The total integration time used by SITE corresponds to the time actually spent integrating on-source without overheads. These integration times are used as input for SPT and for SSPOT, both of which will automatically calculate the necessary overheads.

[Return to Table of Contents](#)

4.2.2 Spectroscopic Observations

Spectroscopic observations with the FLITECAM grisms may be obtained with either an ABBA or an AB nod pattern that is either on-slit (Nod Along Slit) or off-slit (Nod Off Slit). The final choice of nod pattern may be determined by the observation's flight plan (Line-of-Sight rate) and will be communicated by the FLITECAM Instrument Scientist before flight.

Guiding during spectroscopic observations will be conducted with either the telescope guide cameras or with HIPO, if FLITECAM and HIPO are co-mounted in the FLIPO configuration (see Chapter 8).

It is important to note that due to the fixed position of the grisms/slits in the filter/aperture wheels, the orientation of the slit on the sky will be dependent on the flight plan and will not be able to be predetermined. Further, the slit orientation rotates on the sky with each telescope Line-of-Sight (LOS) rewind. These limitations may be especially important to consider when proposing observations of extended objects.

[Return to Table of Contents](#)

4.2.2.1 Estimation of Exposure Times

The exposure times for FLITECAM grism mode spectroscopic observations should be estimated using the [online exposure time calculator](#). This calculator can be used to calculate the signal-to-noise ratio (S/N) for a given total integration time, to calculate the total integration time required to achieve a specified S/N, or to estimate the limiting flux for a desired S/N. For both imaging and spectroscopy modes, the estimated total integration time from the respective calculators should be used as the time for an observation in USPOT. *Remember, overheads should not be included, as USPOT calculates them independently.*

[Return to Table of Contents](#)

5. FORCAST

- 5. FORCAST
 - 5.1 Specifications
 - 5.1.1 Instrument Overview
 - 5.1.1.1 Design
 - 5.1.2 Performance
 - 5.1.2.1 Camera Performance
 - 5.1.2.2 Filter Suite
 - 5.1.2.3 Imaging Sensitivity
 - 5.1.2.4 Grisms
 - 5.1.2.5 Spectroscopic Sensitivity
 - 5.2 Planning Observations
 - 5.2.1 Imaging Observations
 - 5.2.1.1 Estimation of Exposure Times
 - 5.2.2 Spectroscopic Observations
 - 5.2.2.1 Estimation of Exposure Times

5.1 Specifications

Table of Contents

- 5.1 Specifications
 - 5.1.1 Instrument Overview
 - 5.1.1.1 Design
 - 5.1.2 Performance
 - 5.1.2.1 Camera Performance
 - 5.1.2.2 Filter Suite
 - 5.1.2.3 Imaging Sensitivities
 - 5.1.2.4 Grisms
 - 5.1.2.5 Spectroscopic Sensitivity

Return to the Table of Contents for this section at any time by selecting [Return to Table of Contents](#). Users may also navigate through the entire Observer's Handbook by using the complete Table of Contents menu to the right.

5.1 Specifications

5.1.1 Instrument Overview

The **F**aint **O**bject **i**nfra**R**ed **C**amera for the **S**O**F**I**A** **T**elescope (FORCAST) is a dual-channel mid-infrared camera and spectrograph sensitive from 5–40 μm . Each channel consists of a 256x256 pixel array that yields a 3.4x3.2 arcmin instantaneous field-of-view with 0.768 arcsec pixels, after distortion correction. The Short Wavelength Channel (SWC) uses a Si:As blocked-impurity band (BIB) array optimized for $\lambda < 25 \mu\text{m}$, while the Long Wavelength Channel's (LWC) Si:Sb BIB array is optimized for $\lambda > 25 \mu\text{m}$. Observations can be made through either of the two channels individually or, by use of a dichroic mirror, with both channels simultaneously across most of the range. Spectroscopy is also possible using a suite of six grisms, which provide coverage from 5–40 μm with a low spectral resolution of $R = \lambda/\Delta\lambda \sim 200$. The instrument has space for cross dispersing grisms allowing for high resolution cross-dispersed (XD) spectroscopy at $R \sim 800\text{--}1200$ in the 5–14 μm range. The availability of the XD configuration during a given cycle is published in the Call-for-Proposals.

5.1.1.1 Design

The FORCAST instrument is composed of two cryogenically cooled cameras of functionally identical design. A schematic of the instrument layout is provided in [Figure 5-1](#) below. Light from the SOFIA telescope enters the dewar through a 7.6 cm (3.0 in) caesium iodide (CsI) window and cold stop and is focused at the field stop, where a six position aperture wheel is located. The wheel holds the imaging aperture, the slits used for spectroscopy, and a collection of field masks for instrument characterization. The light then passes to the collimator mirror (an off-axis hyperboloid) before striking the first fold mirror, which redirects the light into the LHe-cooled portion of the cryostat.

The incoming beam then reaches a four-position slide, which includes an open position, a mirror, and two dichroics, one for normal use and the other as a spare. The open position passes the beam to a second fold mirror, which sends the beam to the LWC, while the mirror redirects the light to the SWC. The magnesium oxide (MgO) dichroic reflects light below 26 μm to the SWC and passes light from 26–40 μm to the LWC. The light then passes through a Lyot stop at which are located two filter wheels of six positions each, allowing combinations of up to 10 separate filters and grisms per channel. Well characterized, off-the-shelf filters can be used, since the filter wheel apertures have a standard 25 mm diameter (see [Section 5.1.2.2](#)).

Finally, the incoming beam enters the camera block and passes through the camera optics. These two-element catoptric systems are composed of an off-axis hyperboloid mirror and an off-axis ellipsoid mirror that focuses the light on the focal plane array. Also included is an insertable pupil viewer that images the Lyot stop on the arrays to facilitate alignment of the collimator mirror with the telescope optical axis and to allow characterization of the emissivity of both the sky and telescope.

Figure 5-1.

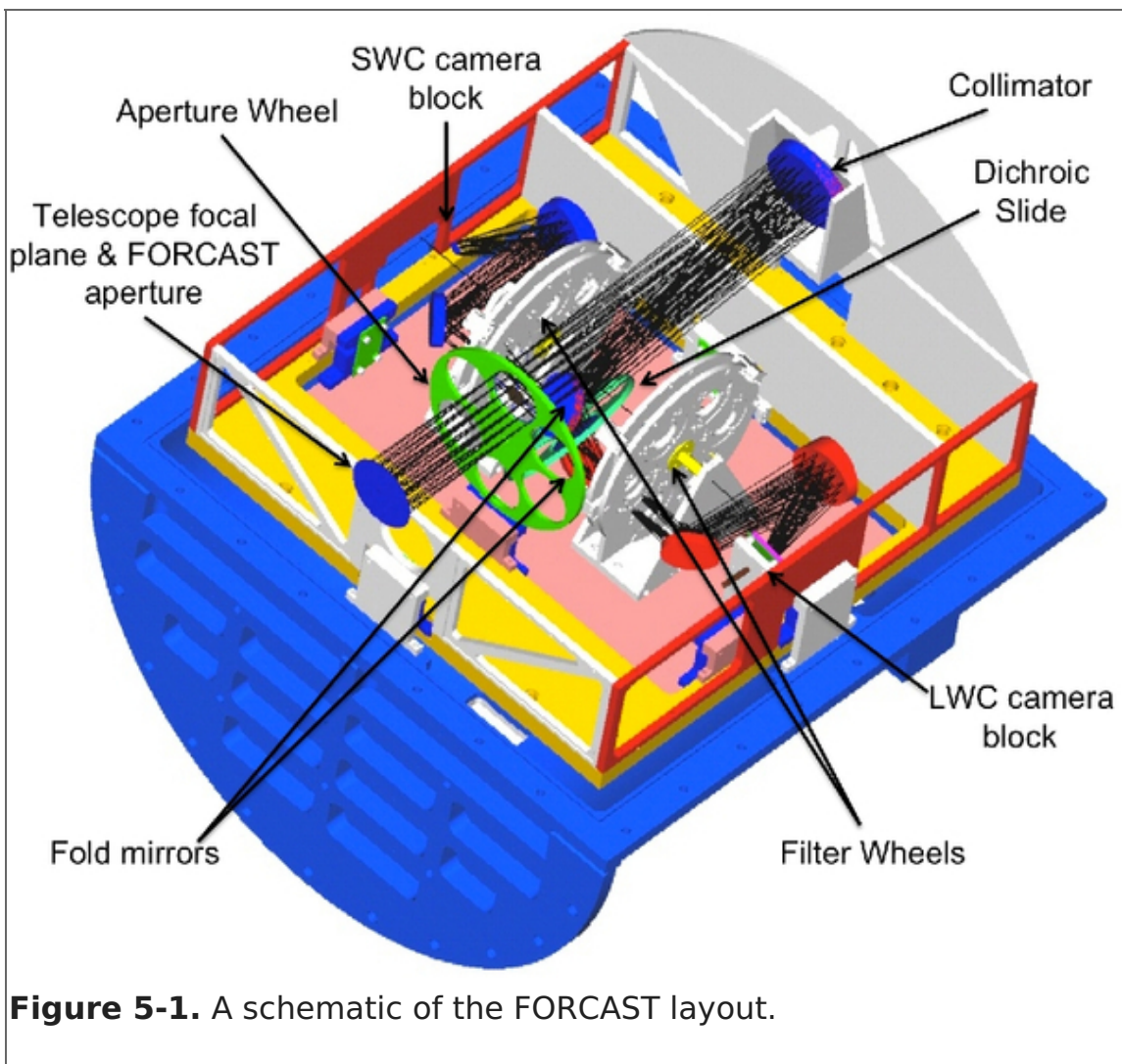


Figure 5-1. A schematic of the FORCAST layout.

[Return to Table of Contents](#)

5.1.2 Performance

5.1.2.1 Camera Performance

The SWC and LWC arrays were selected to optimize performance across the 5–40 μm bandpass. Both arrays have a quantum efficiency (QE) greater than 25% over most of their spectral range. The cameras can be operated with variable frame rates and in either high or low capacitance modes (which are characterized by well depths of 1.8×10^7 and 1.9×10^6 e⁻ respectively), depending upon the sky background and source brightness.

The best measured image quality (IQ) obtained by FORCAST on SOFIA is in the 7–11 μm range with a FWHM PSF (point spread function) of ~ 2.7 arcsec. This measured image quality in-flight is limited by telescope jitter arising from vibrations of the telescope itself (e.g., due to wind loading in the cavity), turbulence, and tracking accuracy. Presented in [Figure 5-2](#) is a sample of FWHM IQ measurements made during a single observatory characterization flight during the winter of 2010 in comparison to the theoretical diffraction limit calculated for a 2.5 m primary with a 14% central obstruction combined with the FWHM telescope jitter, here assumed to be 2.08 arcsec (1.25 arcsec rms).

Figure 5-2.

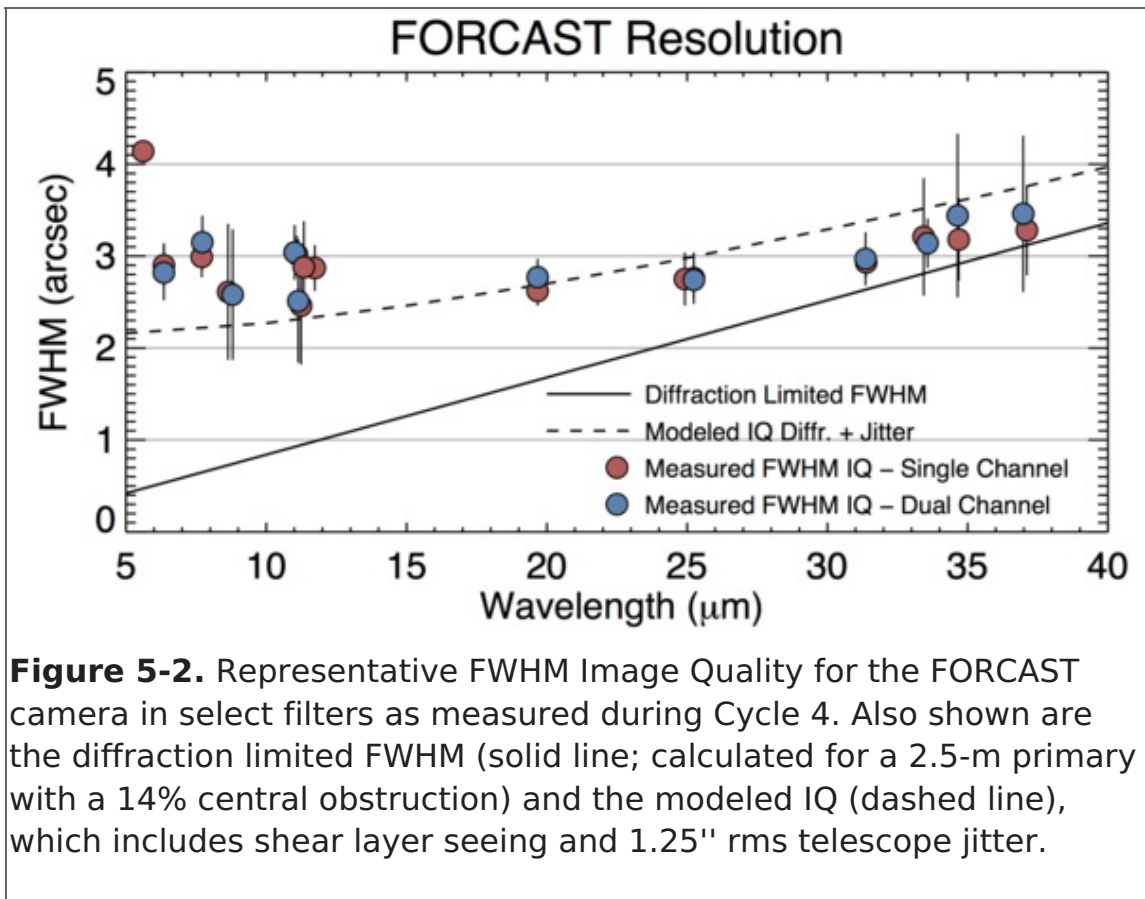


Figure 5-2. Representative FWHM Image Quality for the FORCAST camera in select filters as measured during Cycle 4. Also shown are the diffraction limited FWHM (solid line; calculated for a 2.5-m primary with a 14% central obstruction) and the modeled IQ (dashed line), which includes shear layer seeing and 1.25" rms telescope jitter.

[Return to Table of Contents](#)

5.1.2.2 Filter Suite

Imaging with FORCAST can be performed in either a single channel or in both the SWC and LWC channels simultaneously (dual channel configuration). In a single channel configuration, any one of the available filters may be used. In the dual channel configuration, a dichroic is used to split the incoming beam, directing it to both the SWC and LWC.

The dichroic reduces the overall throughput. [Table 5-1](#) shows the throughput with the dichroic in (dual channel configuration) relative to that for the single channel configuration. The degradation of the system throughput by the dichroic can have a significant effect on the instrument sensitivities as discussed in more detail in [Section 5.1.2.3](#). In addition, since there are more short wavelength filters available than slots in the SWC filter wheels, some short wave filters will be housed in the LWC. The final filter wheel configuration for each observing cycle will be driven by proposal pressure. Depending on the final filter configuration, it is possible that not all LWC filters will be able to be used in the dual channel configuration due to the cutoff in the dichroic transmission at short wavelengths.

Table 5-1: Dichroic Throughput

Dichroic Throughput

Bandpass	Throughput
5-10 μm	60%
11-25μm	85%

Bandpass	Throughput
25-40 μm	40%

The filters in the SWC are standard Optical Coating Laboratory, Inc. (OCLI) thin-film interference filters. These filters are stacked with blocking filters to prevent light leaks. The only exception is the 25.4 μm (FOR_F253) University of Reading filter, which is a custom double half-wave (three mesh) scattering filter stacked with a diamond scattering blocking filter to provide blue-light rejection. The 33.6 (FOR_F336), 34.7 (FOR_F347), and 37.1 μm (FOR_F371) filters in the LWC are LakeShore custom double half-wave (three mesh) scattering filters. The 31.5 μm filter is a Fabry-Perot Interferometer filter.

The central wavelengths, bandwidths, and the typical FWHM IQ in each of the filters are given in [Table 5-2](#) below. The first column under the Imaging FWHM column (single channel) heading presents the best measured FWHM IQ in single channel configuration. These values are representative of the IQ observed since Cycle 3. The second column (dual channel) contains the average measured FWHM IQ in dual channel configuration. Not all of the filters have measured IQ values, but we expect that they will be comparable to those with measured values that are of similar λ_{eff} . [Figure 5-3](#) shows the filter transmission profiles (normalized to their peak transmission) over-plotted on an ATRAN model of the atmospheric transmission. The filter transmission curves (text tables) are available as a zip file or individually from [Table 5-2](#).

Due to the limited number of slots available in the filter wheels, not all of the filters listed in [Table 5-2](#) are available at any one time. For Cycle 6, there will be a nominal filter set (indicated by ***bold italic type*** in [Table 5-2](#)). Other filters can be requested for use, but a convincing scientific argument must be made to justify swapping out the existing filters. A filter swap during the cycle may be permitted dependent upon proposal pressure; more details are available in the [Call for Proposals](#).

Table 5-2: Filter Characteristics

Filter Characteristics

Channel	Filter	λ_{eff} (μm)	$\Delta\lambda$ (μm)	Imaging FWHM (arcsec)		Profiles
Single Channel	Dual Channel					
	FOR_F054	5.4	0.16	– ^b	–	txt file
	<i>FOR_F056</i>	<i>5.6</i>	<i>0.08</i>	–	–	–
	<i>FOR_F064</i>	<i>6.4^a</i>	<i>0.14</i>	<i>2.9</i>	<i>2.9</i>	txt file
	FOR_F066	6.6	0.24	2.9	3.1	txt file
	<i>FOR_F077</i>	<i>7.7</i>	<i>0.47</i>	3.0	3.0	txt file

Channel	Filter	λ (μm)	$\Delta\lambda$ (μm)	Imaging FWHM (arcsec)		Profiles
	<i>FOR_F088</i>	<i>8.8</i>	<i>0.41</i>	-	-	-
	<i>FOR_F111</i>	<i>11.1</i>	<i>0.95</i>	<i>2.8</i>	<i>2.9</i>	txt file
	<i>FOR_F112</i>	<i>11.2</i>	<i>2.7</i>	-	-	-
	<i>FOR_F197</i>	<i>19.7</i>	<i>5.5</i>	<i>2.4</i>	<i>2.5</i>	txt file
	<i>FOR_F253</i>	<i>25.3</i>	<i>1.86</i>	<i>2.3</i>	<i>2.1</i>	-
LWC	FOR_F113	11.3	0.24	2.6	-	txt file
	FOR_F118	11.8	0.74	2.6	-	-
	FOR_F242	24.2	2.9	2.6	-	txt file
	<i>FOR_F315</i>	<i>31.5</i>	<i>5.7</i>	<i>2.8</i>	<i>2.8</i>	txt file
	<i>FOR_F336</i>	<i>33.6</i>	<i>1.9</i>	<i>3.1</i>	<i>3.3</i>	txt file
	<i>FOR_F348</i>	<i>34.8</i>	<i>3.8</i>	<i>3.1</i>	<i>3.0</i>	txt file
	<i>FOR_F371</i>	<i>37.1</i>	<i>3.3</i>	<i>2.9</i>	<i>3.4</i>	txt file

^a Entries in blue are expected to be part of the default filter set for Cycle 6.

^b IQ values for some filters have not been measured at this time, but it is expected that they will be similar to those of similar λ_{eff} with measured values.

Figure 5-3.

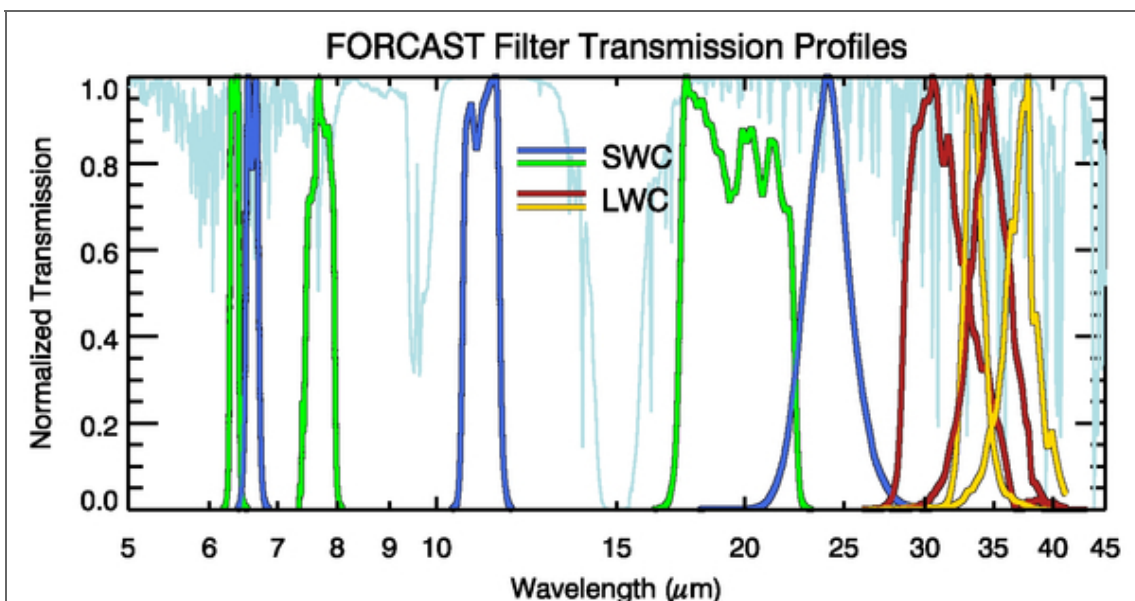


Figure 5-3. FORCAST filter transmission profiles along with an ATRAN model of the atmospheric transmission across the FORCAST band

(assuming a zenith angle of 45 degrees and 7 μm of precipitable water vapor). For clarity the filter profiles have been normalized to their peak transmission. SWC filters alternate between green and blue, while LWC filters alternate between red and yellow.

[Return to Table of Contents](#)

5.1.2.3 Imaging Sensitivities

The FORCAST imaging sensitivities for a continuum point source for each filter are presented in [Table 5-3](#) and [Figure 5-4](#). The Minimum Detectable Continuum Flux (MDCF; 80% enclosed energy) in mJy needed to obtain a $S/N = 4$ in 900 seconds of on-source integration time is plotted versus wavelength. The MDCF scales roughly as $(S/N) / \sqrt{t}$ where t = net integration time. The horizontal bars indicate the effective bandpass at each wavelength. At the shorter wavelengths the bandpass is sometimes narrower than the symbol size.

Atmospheric transmission will affect sensitivity, depending on water vapor overburden. The sensitivity is also affected by telescope emissivity, estimated to be 15% for [Figure 5-4](#).

Observations with FORCAST are performed using standard IR chop-nod techniques. Chop/nod amplitudes can be chosen such as that they are small enough to leave the source on the array in each position or large enough that the source is positioned off the chip for one of the chop positions. For background-limited observations, as is the case with FORCAST on SOFIA, chopping and nodding off-chip in nod-match-chop (NMC; see [Section 5.2.1](#)) will generally result in the same signal to noise (S/N) as chopping and nodding on-chip in nod-perp-chop (NPC; see [Section 5.2.1](#)). Calculations of S/N for various chop-nod scenarios are provided [here](#).

Table 5-3: Filter Sensitivities

Filter Sensitivities

Filter	Channel	Single Chan. MDCF (mJy)	Dual Chan. MDCF (mJy)
FOR_F054 ^a	SWC	41.5	57.5
FOR_F056 ^b	SWC	48.9	22.5
FOR_F064	SWC	52.5	59.5
FOR_F066	SWC	58.8	77.7
FOR_F077	SWC	54.7	66.6
FOR_F088 ^a	LWC	63.0	65.7
FOR_F111 ^a	SWC	90.2	97.1

Filter	Channel	Single Chan. MDCF (mJy)	Dual Chan. MDCF (mJy)
FOR_F112 ^a	SWC	50.0	63.4
FOR_F113 ^a	LWC	206	-
FOR_F118 ^a	LWC	123	-
FOR_F197	SWC	73.5	77.4
FOR_F242	LWC	97.9	-
FOR_F253	SWC	150	158
FOR_F315	LWC	126	171
FOR_F336	LWC	265	380
FOR_F348	LWC	180	257
FOR_F371	LWC	245	376

^a MDCF values shown are those measured from Cycle 4 data.

^b No observations were available to test the theoretical MDCF values.

Figure 5-4.

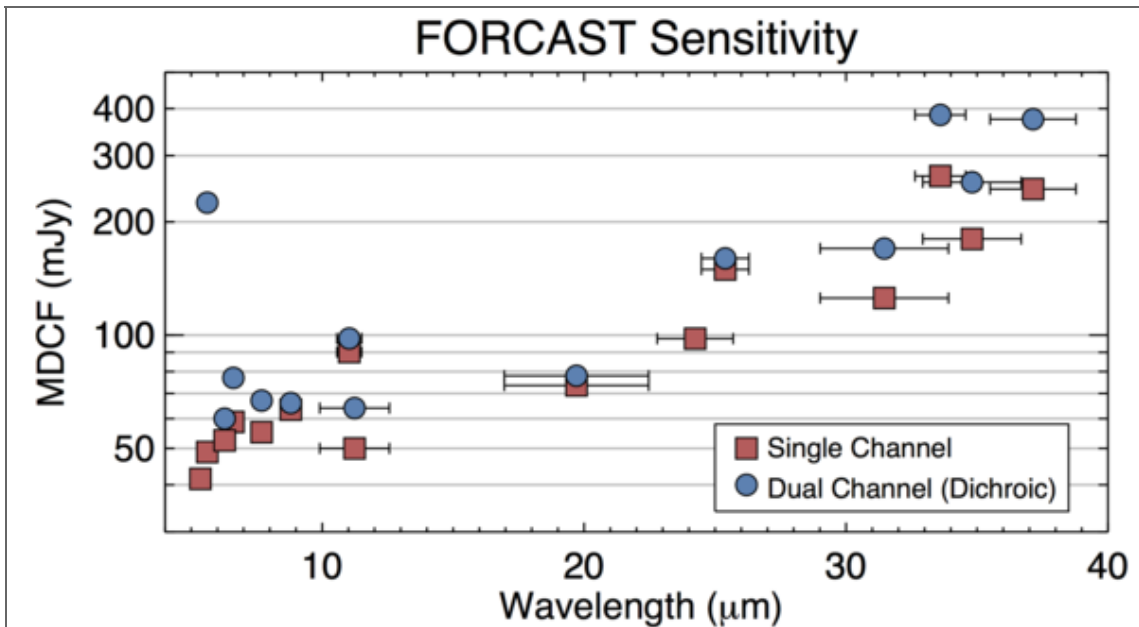


Figure 5-4. Cycle 6 continuum point source sensitivities for single and dual channel modes. Values are for S/N = 4 in 900 s under nominal conditions. Investigators are encouraged to use the SOFIA Integration Time Calculator ([SITE](#)) for their calculations.

5.1.2.4 Grisms

The suite of 6 grisms available for FORCAST provide low to medium resolution coverage throughout most of the range from 5–40 μm (see [Table 5-4](#)). The grisms are situated in the four filter wheels: two in each SWC wheel and one in each LWC wheel. The arrangement is chosen to minimize the impact on the imaging capabilities of the instrument. The grisms are blazed, diffraction gratings used in transmission and stacked with blocking filters to prevent order contamination. A summary of the grism properties is provided in [Table 5-4](#). *Note that during Cycle 6, the cross-dispersed XD configuration will not be available. The information on XD configuration below is for informational purposes, only.*

Grisms FOR_G063, FOR_G227, FOR_G329, and the FOR_XG063 dispersing grism provided by the University of Texas at Austin, are made of silicon to take advantage of its high index of refraction, which allows optimum spectral resolution. However, these grisms suffer from various absorption artifacts precluding their use in the 8–17 μm window. Coverage in this region is provided by the FOR_G111 grism (and its cross-dispersing counterpart), constructed of KRS-5 (thallium bromoiodide) by Carl-Zeiss (Jena, Germany). These latter two grisms have a lower spectral resolution due to the lower index of refraction of the KRS-5 material.

Three slits have been designed for FORCAST: two long slits (2.4 x 191 arcsec, 4.7 x 191 arcsec) and a short slit (2.4 x 11.2 arcsec). The narrow slits yield higher resolution data. All of the slits are located in the aperture wheel of the instrument. The cross-dispersed spectra are obtained by using the short slit and passing the beam first through the low-resolution grism (either FOR_G063 or FOR_G111), followed by a disperser.

Although grisms are available in both cameras, during Cycle 6 grism spectroscopy will be available only in single channel configuration.

It is important to note that due to the fixed position of the slits in the aperture wheels, the lack of a field de-rotator, and the fact that SOFIA behaves in many respects as an Alt-Az telescope, the orientation of the slit on the sky will be dependent on the flight plan and will not be able to be predetermined. Furthermore, the slit orientation rotates on the sky with each telescope Line-of-Sight (LOS) rewind (see [Section 1.2.4](#)). These limitations may be especially important to consider when proposing observations of extended objects.

Table 5-4: Grism Characteristics

Grism Characteristics

Channel	Grism	Material	Groove Sep. (μm)	Prism Angle ($^\circ$)	Order	Coverage (μm)	R ($\lambda/\Delta\lambda$) ^a
	FOR_G063	Si	25	6.16	1	4.9 - 8.0	120 ^c /180
	FOR_XG063 ^b	Si	87	32.6	15 - 23	4.9 - 8.0	1170 ^d

SWC Channel	Grism	Material	Groove Sep. (μm)	Prism Angle (°)	Order	Coverage (μm)	R (λ/Δλ)
	FOR_G111	KRS-5	32	15.2	1	8.4 - 13.7	130 ^c /260
LWC	FOR_G227	Si	87	6.16	1	17.6 - 27.7	110/120
	FOR_G329	Si	142	11.07	2	28.7 - 37.1	160/170

^a For the 4.7" x 191" and the 2.4" x 191" slits, respectively

^b Not available during Cycle 6

^c The resolution of the long, narrow-slit modes is dependent on (and varies slightly with) the in-flight IQ

^d Only available with the 2.4" x 11.2" slit

[Return to Table of Contents](#)

5.1.2.5 Spectroscopic Sensitivity

Tables 5-5 and 5-6 provide samples of the MDCF and Minimum Detectable Line Flux (MDLF) calculated at three different wavelengths across each grism bandpass for each of FORCAST's spectroscopic configurations. The data are provided for point sources only. The MDCF and MDLF estimates are for the raw integration time of 900 seconds and do not include observing overheads, but do account for a two-position chop (perpendicular to the slit).

Figure 5-5 presents the continuum point source sensitivities for the FORCAST grisms. The plots are the MDCF in Jy needed for a S/N of 4 in 900 seconds at a water vapor overburden of 7 μm, an altitude of 41K feet, and a zenith angle of 60°. The rapid variations with λ are due to discrete atmospheric absorption features (as computed by ATRAN).

To determine the required integration time necessary to achieve a desired S/N ratio for a given source flux, the [FORCAST online grism exposure time calculator](#) should be used. The on-line calculator also allows for calculation of the limiting flux for a given integration time and required S/N. Since FORCAST observations are background limited, the values given in Tables 5-5 and 5-6 and Figure 5-5 can be used to make an estimate of the required integration time using Equation 5-1:

(Eq. 5-1)

$$\frac{[S/N]_{\text{req}}}{4} = \frac{F_{\text{src}} \cdot \sqrt{t_{\text{exp}}}}{\text{MDCF} \cdot \sqrt{900}}$$

where $[S/N]_{\text{req}}$ is the desired signal-to-noise ratio, F_{src} is the continuum flux of the target,

t_{exp} is the exposure time on source (without taking into consideration observational overheads), and the MDCF is taken from the tables for the point-source sensitivities or estimated from the figures. For emission lines, simply use the line flux for F_{src} and use the MDLF value instead of the MDCF. *However, these tables may not contain the most recent or best determined sensitivity values and therefore the on-line calculator results should be used in the actual proposal.*

Table 5-5: Long Slit Point Source Sensitivities

Long Slit Point Source Sensitivities

Grism	λ (μm)	R = ($\lambda/\Delta\lambda$)	MDCF (mJy)	MDLF (W m^{-2})	R= ($\lambda/\Delta\lambda$)	MDCF (mJy)	MDLF (W m^{-2})
		4.7" Slit			2.4" Slit		
FOR_G063	5.1	120	79	2.3E-16	180	98	2.9E-16
FOR_G063	6.4	120	219	5.2E-16	180	268	6.3E-16
FOR_G063	7.7	120	496	5.2E-16	180	724	6.3E-16
FOR_G111	8.6	130	419	4.9E-16	300	532	6.2E-16
FOR_G111	11.0	130	449	4.1E-16	300	575	5.2E-16
FOR_G111	13.2	130	593	4.5E-16	300	764	5.8E-16
FOR_G227	17.8	110	715	8.6E-16	140	936	1.1E-15
FOR_G227	22.8	110	834	7.9E-16	140	989	9.3E-16
FOR_G227	27.2	110	1979	1.6E-15	140	2586	2.0E-15
FOR_G329	28.9	160	1365	6.5E-16	220 ^a	1899	9.0E-16
FOR_G329	34.1	160	1408	5.6E-16	220 ^a	1994	8.0E-16
FOR_G329	37.0	160	1763	5.6E-16	220 ^a	2439	8.0E-16

^a The 2.4 arcsec long slit mode for G329 will not be available during Cycle 6.

Table 5-6: Cross-Dispersed Point Source Sensitivities^a

Cross-Dispersed Point Source Sensitivities^a

Grism	λ (μm)	$R = (\lambda/\Delta\lambda)$	MDCF (mJy)	MDLF (W m^{-2})
2.4" x 11.2" Slit				
FOR_XG063	5.1	1200	238	1.2E-16
FOR_XG063	6.4	1200	703	2.8E-16
FOR_XG063	7.7	1200	918	3.0E-16

^a XD configurations are not available during Cycle 6

Figure 5-5.

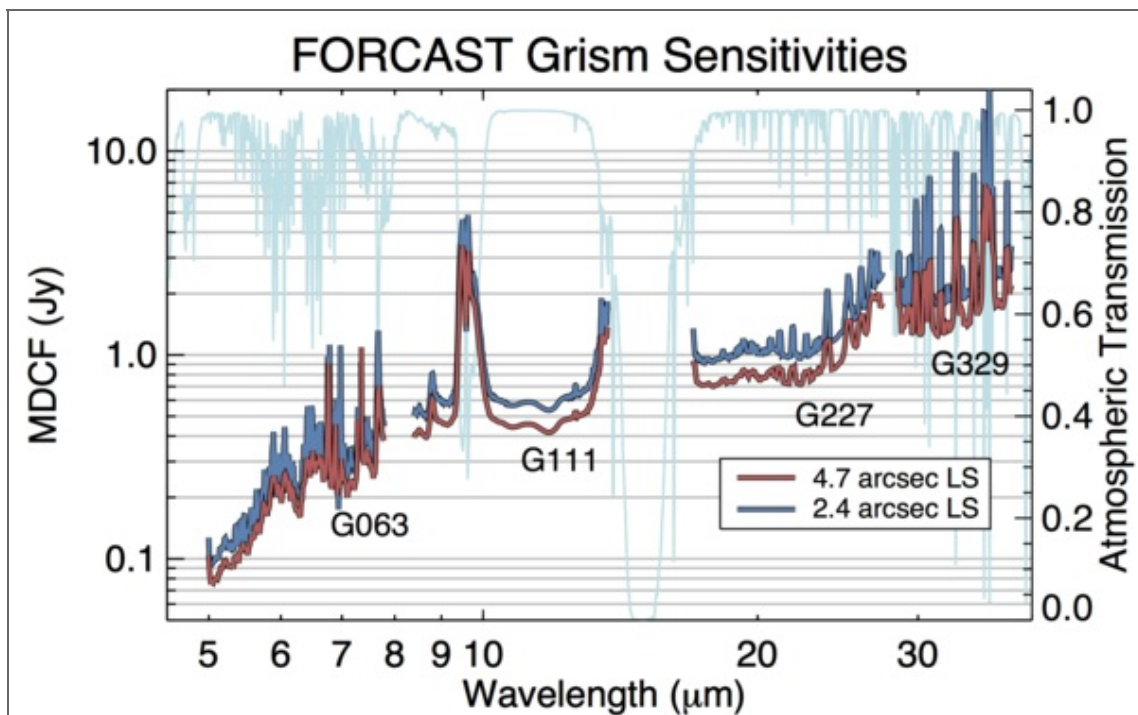


Figure 5-5. Cycle 6 grism continuum point source sensitivities for both wide and narrow long slits overlaid on an atmospheric transmission model (light blue). Values are for $S/N = 4$ in 900 s under nominal conditions.

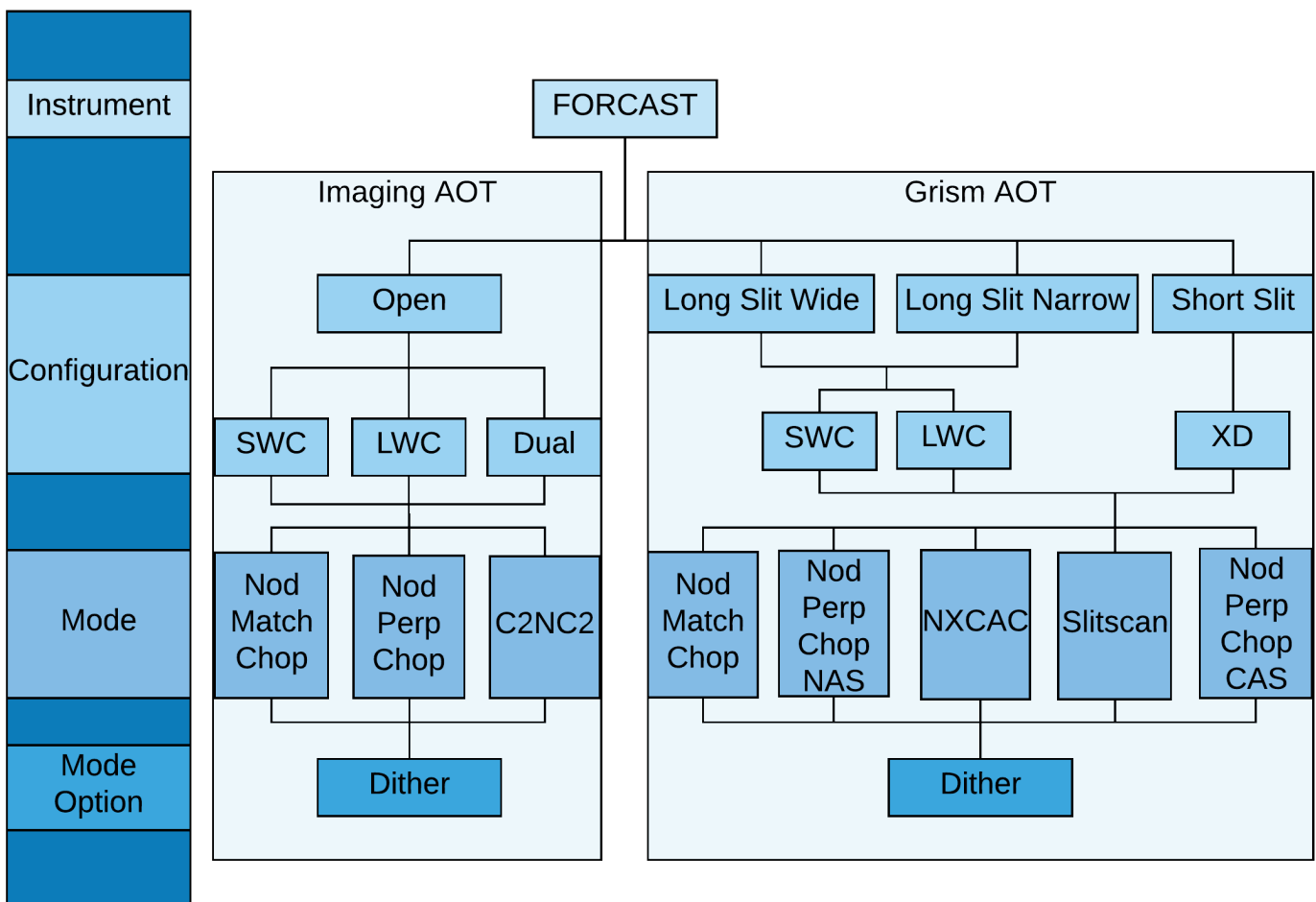
5.2 Planning Observations

Table of Contents

- 5.2 Planning Observations
 - 5.2.1 Imaging Observations
 - 5.2.1.1 Estimation of Exposure Times
 - 5.2.2 Spectroscopic Observations
 - 5.2.2.1 Estimation of Exposure Times

Return to the Table of Contents for this section at any time by selecting [Return to Table of Contents](#). Users may also navigate through the Handbook using the Table of Contents menu to the right.

5.2 Planning Observations



As is the case with ground based observations at mid-IR wavelengths, individual FORCAST exposures will be dominated by the sky and telescope background. Therefore chopping and nodding are essential for each observation. Selection of the observing mode and its parameters, including the distance and direction of chop and nod throws, depend on the details of the field of view around the target. The source(s) of interest may be surrounded by other IR-bright sources or may lie in a region of extended emission, which needs to be avoided to ensure proper background subtraction.

Presented in this section is a discussion of how to best plan FORCAST observations in order to optimize the success of observations.

5.2.1 Imaging Observations

Proposers are strongly encouraged to familiarize themselves with the basics of techniques for performing background limited observations covered in [Section 1.3](#). In brief, the imaging observation modes for FORCAST include the following:

NMC Mode

Nod Match Chop mode consists of a chop symmetric about the optical axis of the telescope with one of the two chop positions centered on the target. The nod throw is oriented 180° from the chop, i.e. anti-parallel, such that when the telescope nods, the source is located in the opposite chop position. The chop/nod subtraction results in two negative beams on either side of the positive beam, which is the sum of the source intensity in both nod positions and therefore has twice the intensity of either negative beam. This mode uses the standard ABBA nod cadence. An example of an observation taken in this mode is presented in the left panel of [Figure 5-7](#).

NPC Mode

Similar to NMC, Nod Perpendicular to Chop mode also uses a chop that is symmetric about the optical axis, but in this case the nod is perpendicular to the chop. The final images produced using NPC show four sources arranged in a parallelogram with alternating positive and negative beams. Unlike NMC, each beam in NPC has the same relative intensity. This mode also uses the standard ABBA nod cadence. The right side of [Figure 5-7](#) shows data obtained using NPC. *This mode will not be supported in Cycle 6.*

C2NC2 Mode

In Chop-Offset Nod mode, the chop throw is asymmetric, such that one chop position is centered on the optical axis (and the target) while the second (sky) position is off-axis. Rather than nodding, the telescope then slews to an offset position free of sources or significant background and the same chop pattern is repeated. Observations in C2NC2 mode follow a nod cadence of ABA and, by default, are dithered to remove correlated noise. This mode is particularly useful for large extended objects, smaller objects that are situated within crowded fields, or regions of diffuse emission with only limited sky positions suitable for background removal.

Since only a single chop position out of a full chop/nod cycle is on source, NMC and NPC have a much greater efficiency than C2NC2. A sample mosaic demonstrating how a C2NC2 observation might be designed for a large, extended object is provided in [Figure 5-8](#), and it is immediately apparent from the figure that C2NC2 has an efficiency of only ~20%. However, while mosaicking can be performed for any of the available observing modes, proposers should keep in mind that the effects of coma may compromise the image severely for fields requiring large chop amplitudes when chopping symmetrically (NMC or NPC modes). If the source has an angular extent large enough that multiple pointings are required, the central position of each FORCAST field must be specified, with due consideration of the desired overlap of the individual frames. For more on mosaicking, see [Section 5.3.1.2b](#) in the [USPOT Manual](#).

Figure 5-7.

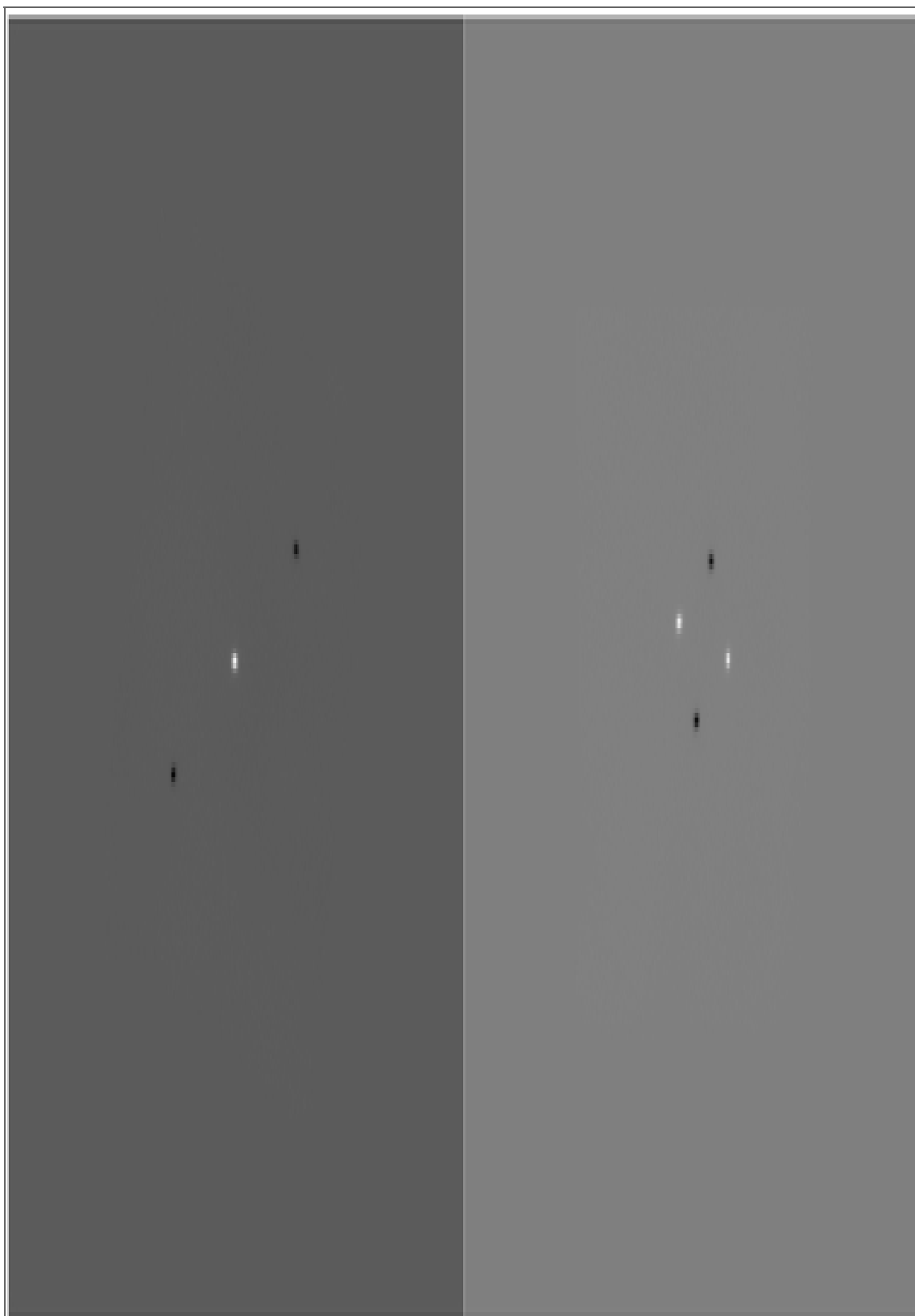
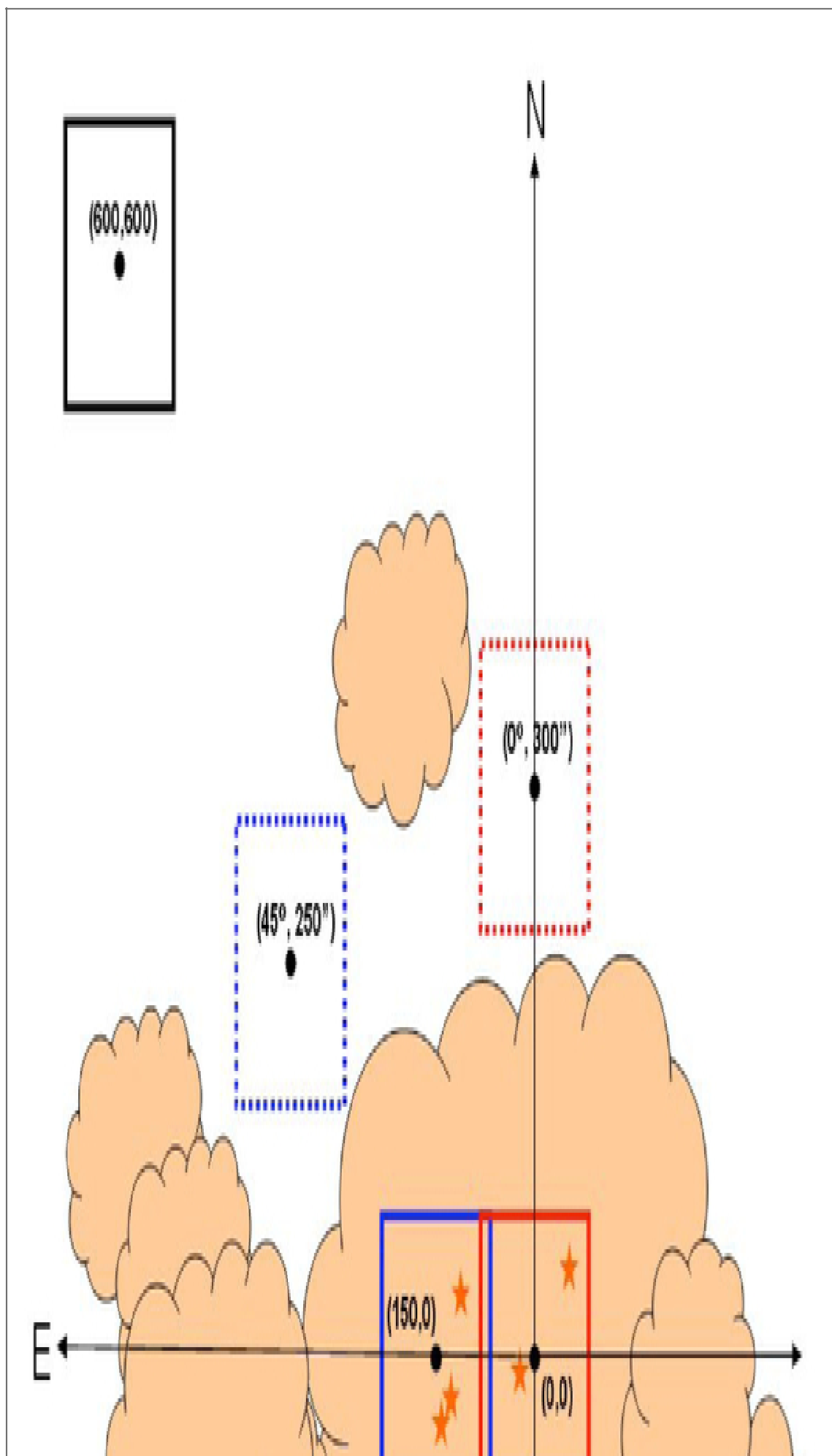


Figure 5-7. Each source position (*solid line*) with its associated asymmetric chop position (*dashed line*) have matching colors. After a full chop cycle at each position, the telescope is slewed to a location off of the source, shown in black and labeled with the coordinates (600, 600). The chop throw and angle at that position is the same as it is for the source position to which it is referenced (not shown in the figure).

Figure 5-8.



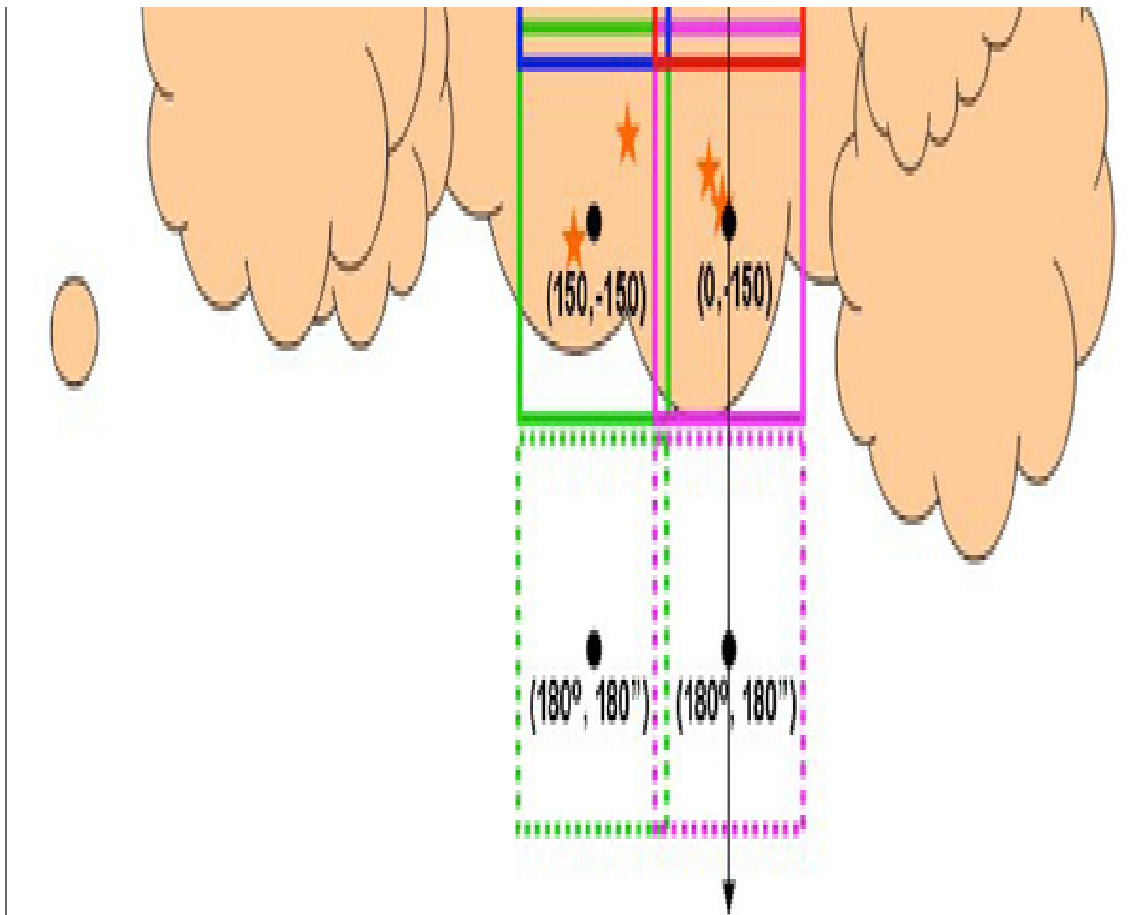


Figure 5-8. Cartoon of a C2NC2 mode FORCAST observation with mosaic.

Once a proposal has been accepted, the proposer, in collaboration with the SMO instrument scientist, will specify the details of chopping and nodding for each observation using the SOFIA observation preparation tool (USPOT). Experienced proposers are encouraged to design their observations using USPOT *before* writing their proposals to prevent the loss of observing time that might occur if, during Phase II, the observations are discovered to be more challenging than expected.

Following are a few of the most important issues to consider when preparing a FORCAST Imaging proposal:

- It is recommended that a near-IR or mid-IR database (e.g., 2MASS, *Spitzer*, *WISE*, MSX or IRAS) be checked to see if the target of interest is near other IR sources of emission. In the case of extended sources, where **on-chip** (i.e., on the detector array) chop and nod is not possible, it is necessary to pick areas free of IR emission for the chop and nod positions to get proper background subtracted images.
- If the IR emission from the region surrounding the source is restricted to a region smaller than half the FORCAST field of view (i.e. ~ 1.6 arcmin) then the chop and nod can be done on-chip. Observations performed in NMC mode either on-chip or off-chip yield a S/N equal to or slightly better than that obtained in NPC mode. For additional discussion of this point, see the calculations of S/N for various FORCAST chop-nod scenarios provided [here](#).
- When using a symmetric chop, chopping and nodding can be performed in any

direction for chop throws less than 584 arcsec.

- When observing in one of the symmetric chop modes, large chop amplitudes may degrade the image quality due to the introduction of coma. This effect causes asymmetric smearing of the PSF parallel to the direction of the chop at a level of 2 arcsec per 1 arcmin of chop amplitude.
- When using an asymmetric chop, the maximum possible chop throw is 420 arcsec. However, some chop angles (as measured in the instrument reference frame) are not allowed for asymmetric chop throws between 250 arcsec and 420 arcsec. Since the orientation of the instrument relative to the sky will not be known until the flight plan is generated, Those requesting chop throws between 250–420 arcsec are required to specify a range of possible chop angles from which the instrument scientists can choose when the flight plan is finalized.
- For large, extended objects, it may not be possible to obtain clean background positions due to these limitations on the chop throw.

There are some additional considerations for observations of faint targets.

- Currently, the longest nod dwell time (that is, the time spent in either the nod A or nod B position) for FORCAST is 30 sec in the SWC-only and dual channel configurations and up to 120 sec in the LWC-only configurations (depending on the filter). Run the exposure time estimator to determine if the object will be visible in a single A-B chop-subtracted, nod-subtracted pair, with an exposure time of 30 sec in each nod position. If the object is bright enough to be detectable with S/N greater than a few, it is recommended that dithering be used when observing in NMC or NPC mode. The dithering will mitigate the effects of bad pixels when the individual exposures are co-added.
- If the object is not visible in a single A-B chop/nod-subtracted pair, with a nod dwell time of 30 sec in each nod position (60 sec integration), then dithering should *not* be used.

[Return to Table of Contents](#)

5.2.1.1 Estimation of Exposure Times

The exposure times for FORCAST imaging observations should be estimated using the on-line exposure time calculator, [SITE](#). SITE can be used to calculate the signal-to-noise ratio (S/N) for a given total integration time, or to calculate the total integration time required to achieve a specified S/N. The total integration time used by SITE corresponds to the time actually spent integrating on-source without overheads. These integration times are used as input for USPOT, which will automatically calculate the necessary overheads. The format of the S/N values output by SITE depends on the source type. For Point Sources, the reported S/N is per resolution element, but for Extended Sources, it is the S/N per pixel.

For mosaic observations the total integration time required for a single field should be multiplied by the number of fields in the mosaic to obtain the total time, which is to be entered in USPOT.

An important consideration in planning observations is whether FORCAST should be used in single channel configuration, or in a dual channel configuration, since one gains the extra filter observation at the cost of lower system throughput in the individual bands.

On the SITE form, a single channel configuration is specified by selecting the filter of interest for one channel and selecting **None** on the other channel in the Instrument properties section.

[Return to Table of Contents](#)

5.2.2 Spectroscopic Observations

Proposers are strongly encouraged to familiarize themselves with the basics of techniques for performing background limited observations covered in [Section 1.3](#). In brief, the spectroscopic observation modes for FORCAST include the following:

NMC Mode

As with FORCAST imaging observations, Nod Match Chop mode consists of a chop symmetric about the optical axis of the telescope with one of the two chop positions centered on the target. See [Section 5.2.1](#) or [Section 1.3](#).

NPC CAS and NPC NAS Modes

Grism Nod Perpendicular to Chop observations can be performed either in a Chop Along Slit mode (NPC CAS) or Nod Along Slit mode (NPC NAS). As with FORCAST imaging observations, FORCAST's grism NPC modes also implement a chop that is symmetric about the optical axis—however, unlike in NMC mode, the nod is perpendicular to the chop. The final images produced using NPC CAS or NAS show two sources arranged along the slit with one positive and one negative beam. Unlike NMC, each beam in NPC has the same relative intensity.

NXCAC Mode

Nod not related to Chop with Asymmetric Chop mode is the grism version of C2NC2, i.e., an asymmetric chop with dithering along the slit. See [Section 5.2.1](#) or [Section 1.3](#).

Slitscan Mode

In Slitscan mode, the slit is moved across a target in discrete steps using dithers perpendicular to the slit axis to yield a spectroscopic map of an entire area of sky.

During Cycle 6, grism spectroscopy with FORCAST will only be available in single channel, long-slit configurations (SWC and LWC). By default, observations will be set up using NMC aligned along the slit in Long Slit configurations and perpendicular to the slit in XD configuration. Due to the size of the PSF, neither chopping or nodding along the slit nor dithering are possible for high-resolution XD observations. For larger sources and for targets embedded in crowded fields it is advised to use C2NC2 mode.

The observing efficiency for FORCAST spectroscopic observations depends on a number of factors, including the observing mode, chop frequency and nod cadence, the detector frame rate, and LOS rewind cadence. The typical observing efficiency as measured from NMC and NPC observations is 50–75% of clock time. Work is ongoing to optimize the mode-dependent efficiency values. These efficiency estimates are built-in to USPOT and do not need to be specified.

It is important to note that due to the fixed position of the gratings/slits in the filter/aperture wheels, the orientation of the slit on the sky will be dependent on the flight

plan and will not be able to be predetermined. Further, the slit orientation rotates on the sky with each telescope Line-of-Sight (LOS) rewind (Section 1.1). These limitations may be especially important to consider when proposing observations of extended objects.

[Return to Table of Contents](#)

5.2.2.1 Estimation of Exposure Times

The exposure times for FORCAST Grism spectroscopic observations should be estimated using the online [FORCAST Grism Exposure Time Calculator](#) tool. This calculator can be used to calculate the signal-to-noise ratio (S/N) for a given total integration time, to calculate the total integration time required to achieve a specified S/N, or to estimate the limiting flux for a desired S/N.

In either case, *overheads should not be included*, as USPOT calculates them independently.

[Return to Table of Contents](#)

6. FPI+

- 6. FPI+
 - 6.1 Specifications
 - 6.1.1 Instrument Overview
 - 6.1.1.1 Design
 - 6.1.1.2 Angular Resolution
 - 6.1.2 Performance
 - 6.1.2.1 Filter Suite
 - 6.1.2.2 Imaging Sensitivities
 - 6.1.2.3 Camera Performance
 - 6.2 Planning Observations
 - 6.2.1 Observing Modes
 - 6.2.2 Estimation of Exposure Times
 - 6.2.3 Overheads

6.1 Specifications

Table of Contents

- 6.1 Specifications
 - 6.1.1 Instrument Overview
 - 6.1.1.1 Design
 - 6.1.1.2 Angular Resolution
 - 6.1.2 Performance
 - 6.1.2.1 Filter Suite
 - 6.1.2.2 Imaging Sensitivities
 - 6.1.2.3 Camera Performance

Return to the Table of Contents for this section at any time by selecting [Return to Table of Contents](#) . Users may also navigate through the entire Observer's Handbook by using the complete Table of Contents menu to the right.

6.1 Specifications

6.1.1 Instrument Overview

The Focal Plane Imager (FPI) is the standard tracking camera for the SOFIA telescope. Since an imager upgrade in 2013, the FPI uses a science grade CCD sensor and is referred to as FPI+ (FPI_PLUS). Since the FPI+ is a subsystem of the SOFIA tracking system, it is permanently installed on the telescope. Therefore, it can be operated on every observing flight, either stand-alone or in parallel with any science instrument that is mounted on the telescope.

As a science instrument, the FPI+ is intended to be used as a fast framerate imaging photometer in the visual wavelength range. The highly configurable readout modes of the camera can be adapted to the proposed observation needs. Examples for the scientific use of the FPI+ include observations of stellar occultations and exo-planet transits. The observations of stellar occultations benefit from SOFIA's mobility, e.g. the abilities to fly into the shadow path and to avoid cloud cover. The observation of exo-planet transits benefit from the much reduced scintillation noise at flight altitude, resulting in higher signal-to-noise ratios in the light curves compared to ground based measurements.

[Return to Table of Contents](#)

6.1.1.1 Design

Most of the visual light passes SOFIA's tertiary beam splitter (M3-1) before it is reflected into the Nasmyth tube by the fully-reflective tertiary (M3-2). A significant amount of visual light is not transmitted, but rather absorbed or reflected along with the longer, infrared wavelengths. However, in the range between 480 nm to 800 nm, where the visual-light CCD cameras are most sensitive, more than 50% of the light is transmitted to the FPI+. The visual light continues through a set of four silver-coated folding mirrors inside the so called *delay line assembly* of the telescope. This setup allows focusing the FPI+ independently from the instrument at the telescope science instrument flange. A pair of windows is installed between the Nasmyth tube and the delay line that create the boundary between the stratospheric conditions in the telescope cavity and cabin conditions inside the delay line assembly. Two eyepiece lenses are used to collimate the telescope beam. Close to the camera is a pellicle beam splitter made of a nitrocellulose membrane with 85% transmission. The beam splitter can be used to reflect a reticle into the light path for camera alignment purposes. The last optical element in front of the camera is an industrial ZEISS 1.4/85 mm Planar T* IR photo lens.

A double-carousel, filter wheel with six positions on each carousel is installed between the reticle beam splitter and the ZEISS lens.

[Return to Table of Contents](#)

6.1.1.2 Angular Resolution

The CCD sensor of the FPI+ is an e2v CCD201-20 1024 x 1024 pixel frame transfer EMCCD with a plate scale of 0.51 arcsec/pix and a square field of view (FOV) of 8.7 x 8.7 arcmin. The unvignetted FOV is a circular beam of approx. 9 arcmin diameter centered on the FPI+ sensor. Pixel binning of 2x2, 4x4, etc. is available and can be used to increase the frame rate and reduce the effective readout noise. In flight, the seeing blur size of the observatory is at about 4 arcsec diameter. Therefore, a reduction of the

angular resolution by binning up to 4x4 (2x2 arcsec²) still provides critical sampling of the seeing element.

The image quality in visible wavelengths on SOFIA is dominated by seeing and image motion effects. A wavelength dependent analysis of the image quality for the visual wavelength range has been done by the HIPO team.

[Return to Table of Contents](#)

6.1.2 Performance

6.1.2.1 Filter Suite

The wavelength range of the FPI+ is 360 nm to 1100 nm. Six spectral filters are available within this range. These are five Sloan Digital Sky Survey filters u'g'r'i'z' and a Schott RG1000 near-IR cut-on filter. Additionally, three neutral density (ND) filters can be used to attenuate bright stars. The ND filters are required for the tracking function of the FPI+ and the optical densities are chosen in such a way that stars within the brightness range of $0 < V \text{ mag} < 16$ can be imaged with an exposure time of 1 second. The Daylight filter is also a requirement for telescope tracking to be able to acquire bright guide stars in twilight.

Table 6-1.

Filter Wheel Configuration

Carousel 1	Carousel 2
OPEN	OPEN
Sloan u'	ND 1
Sloan g'	ND 2
Sloan r'	ND 3
Sloan I'	Daylight
Sloan z'	Blocked

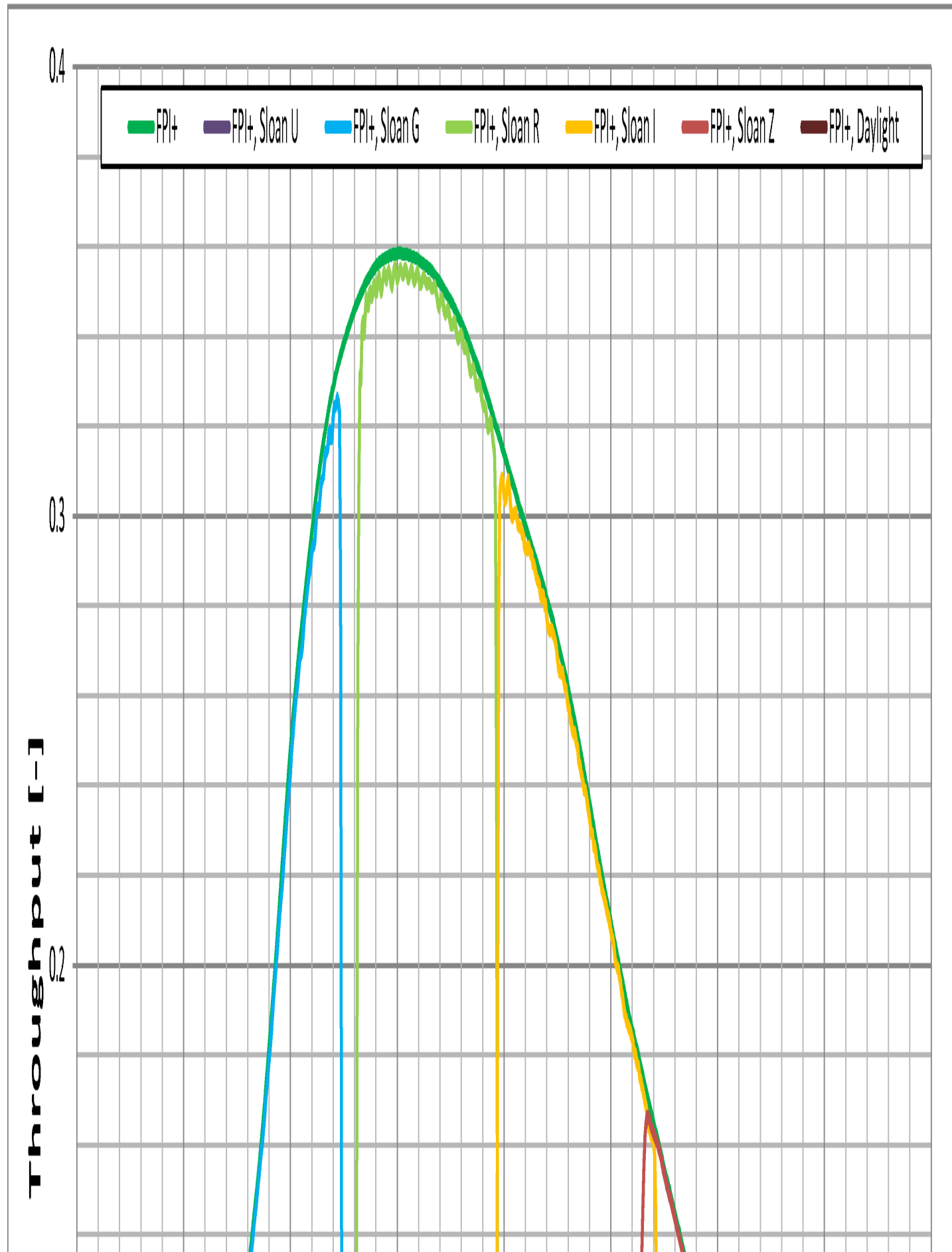
Table 6-1 shows the configuration of the FPI+ double filter wheel. Filters from carousel one and two can be combined freely with a few exceptions. The daylight tracking filter from carousel two can only be used with the OPEN position of carousel one to avoid non-overlapping wavelength bands. The Blocked position cannot be selected for observations, but instead is used for taking calibration data (bias frames, dark frames).

Filter Throughput

Figure 6-1 shows a plot of the FPI+ total system throughput, which includes a model for atmospheric extinction, the calculated SOFIA telescope throughput, and the instrument quantum efficiency. The filter spectral response has been measured and is added to the plot. At the wavelengths where the Sloan u' filter is transparent, other elements in the

FPI+ light path (dichroic tertiary mirror, protected silver coatings, ZEISS lens) are nearly opaque. This results in a very low throughput ($\sim 0.5\%$) for the selection of the FPI+ with the Sloan u' filter.

Figure 6-1.



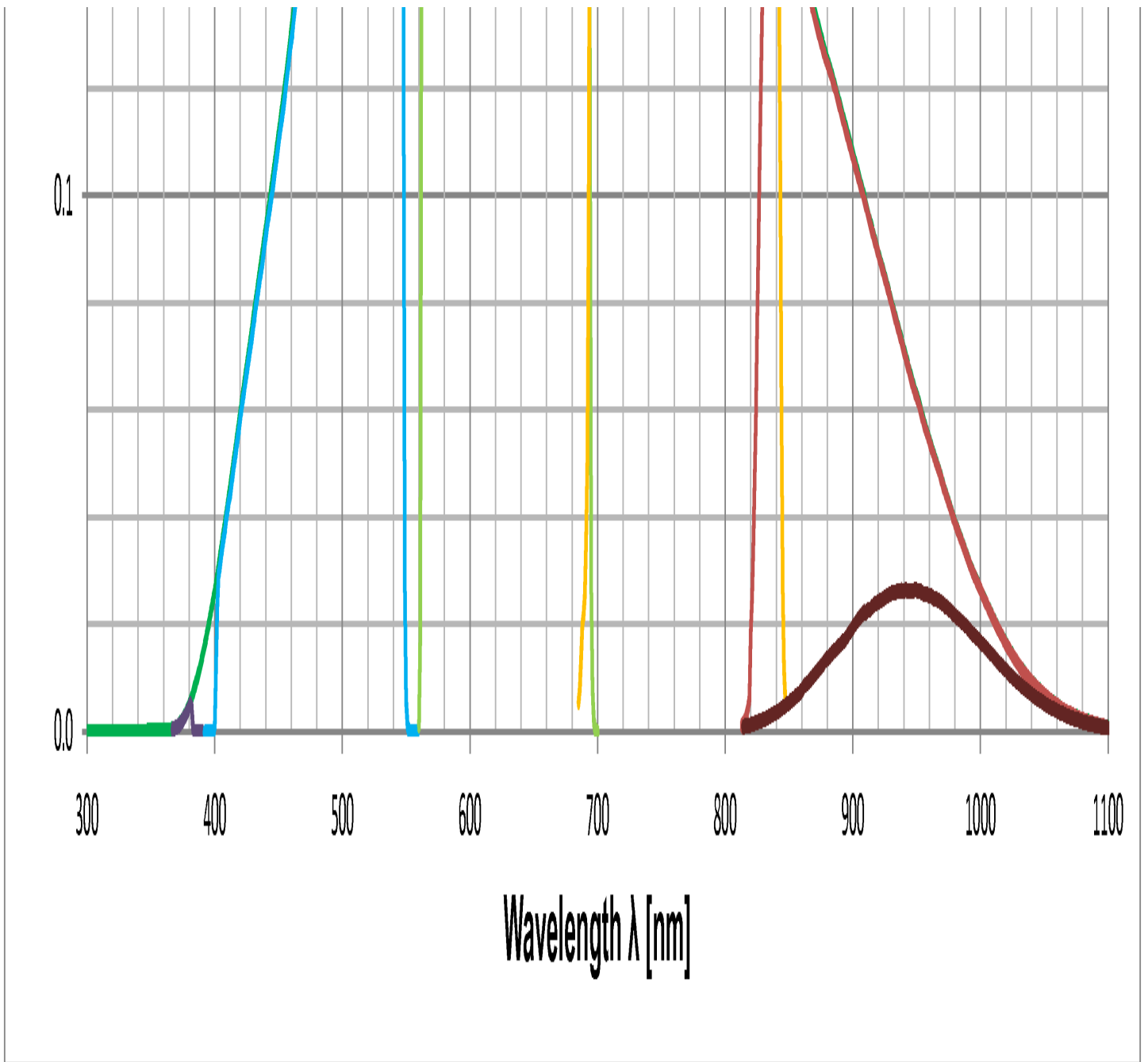


Figure 6-2 is a plot of the neutral density filter transmittance vs. wavelength for the three installed ND filters. Over the entire wavelength range of the FPI+, the ND filters have the average optical density listed in Table 6-1. However, there is a wavelength dependence of the optical density of all ND filters that has to be considered when using the ND filters in conjunction with the Sloan filters. All filters are par focal despite their different thicknesses, because they are installed in the parallel beam in front of the Zeiss lens.

Figure 6-2.

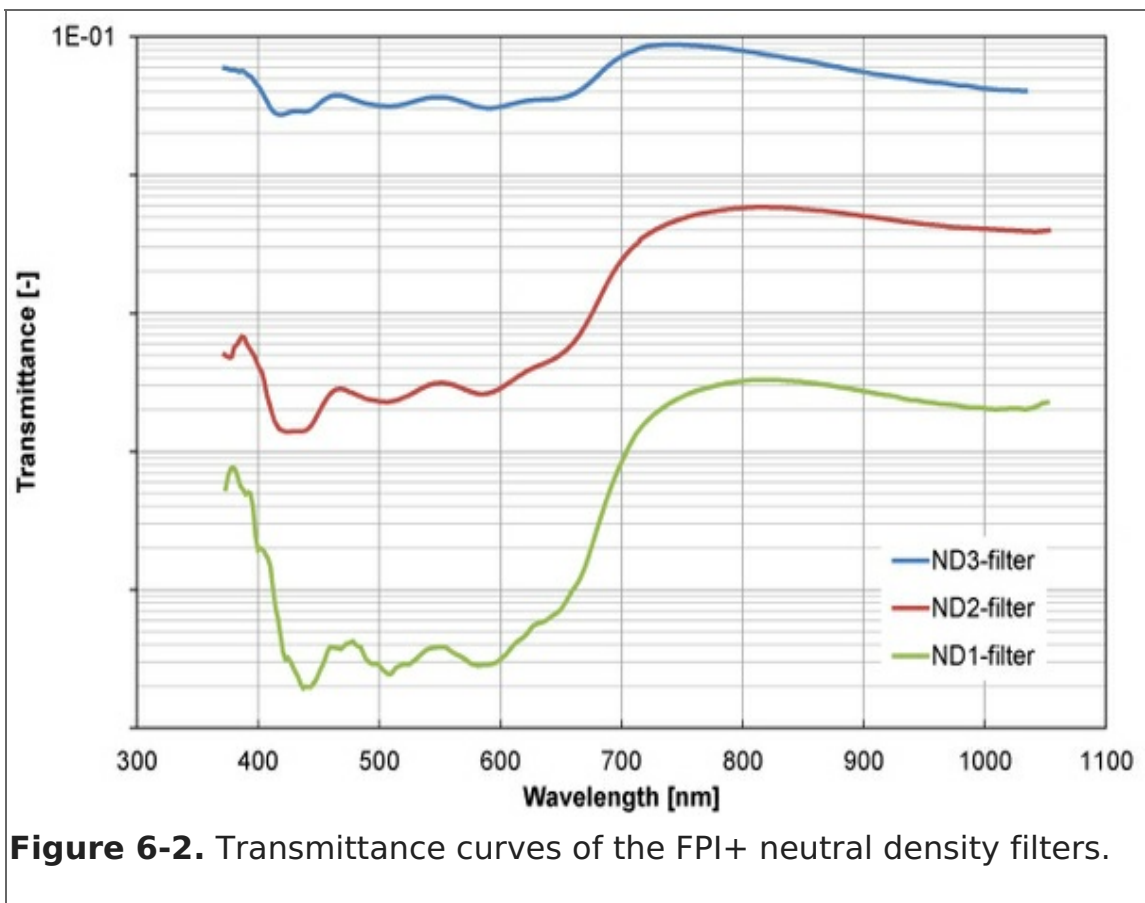


Table 6-2.

Neutral Density Filter Properties

Filter name	Glass Type	Thickness	Average Optical Density
ND1	Schott NG9	4.0mm	4
ND2	Schott NG3	3.5mm	2.6
ND3	Schott NG4	2.8mm	1.3

[Return to Table of Contents](#)

6.1.2.2 Imaging Sensitivities

The instrument sensitivity and resolution is provided to analyze the feasibility of scientific investigations. The sensitivity of the FPI+ in its different Sloan filters was measured in-flight as part of the camera upgrade verification. The selected star field had targets with a wide range in V mag brightness ($11.1 < V \text{ mag} < 16.7$). The full-frame images were acquired with an exposure time of one second without pixel binning. The SNR values in [Figure 6-3](#) are calculated with the measured signal values and the known noise sources. Displayed are the results of the OPEN configuration and the Sloan filters u' , g' , r' , i' , z' and DAYLIGHT.

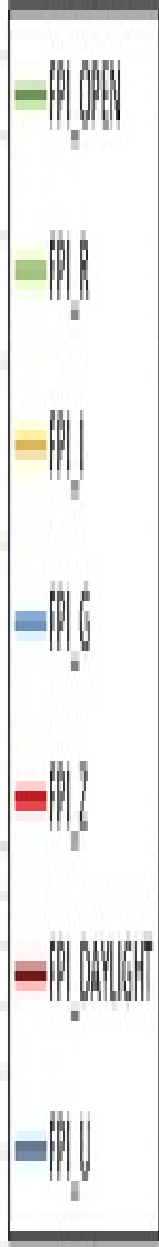
Figure 6-3.

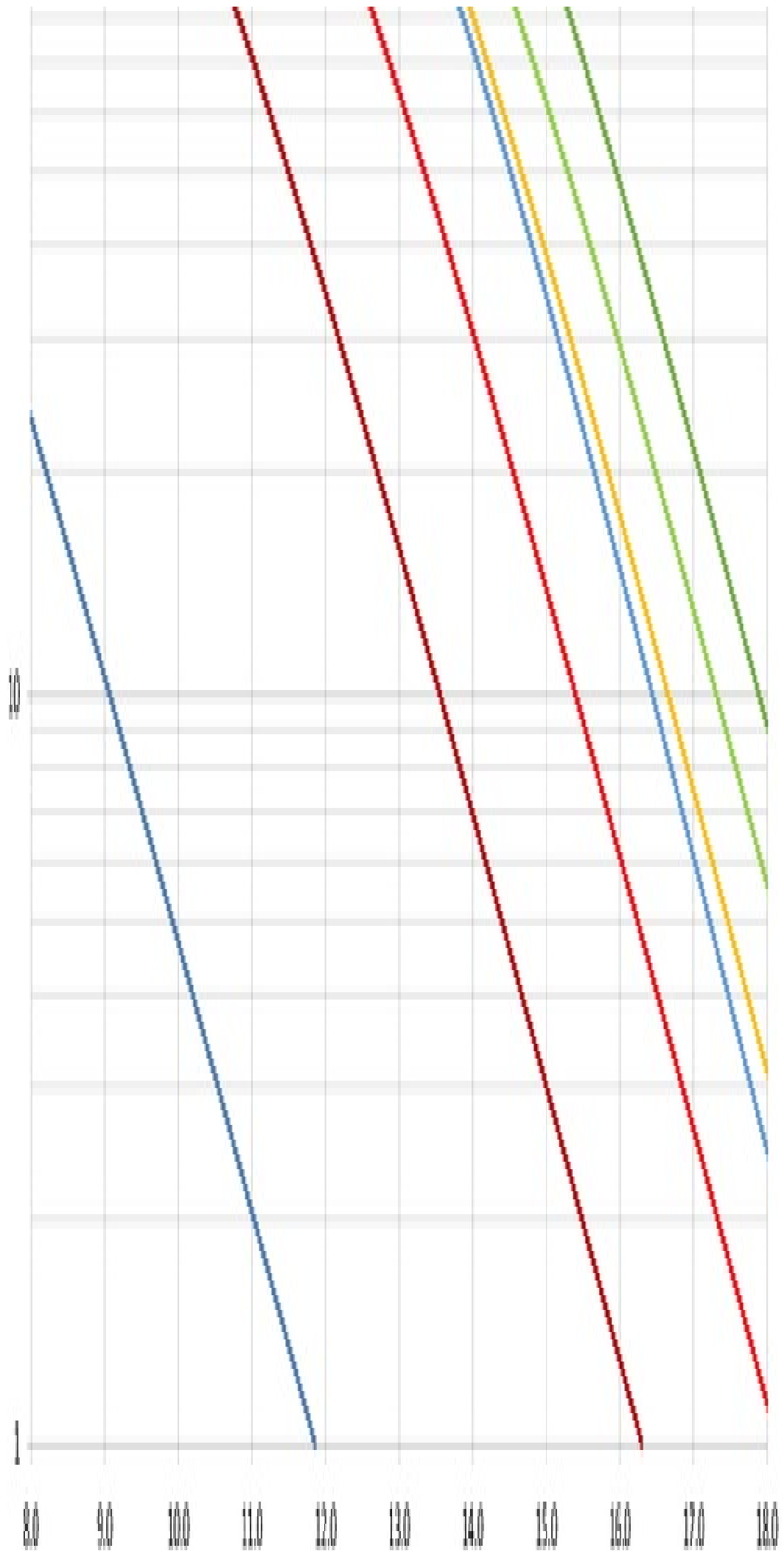


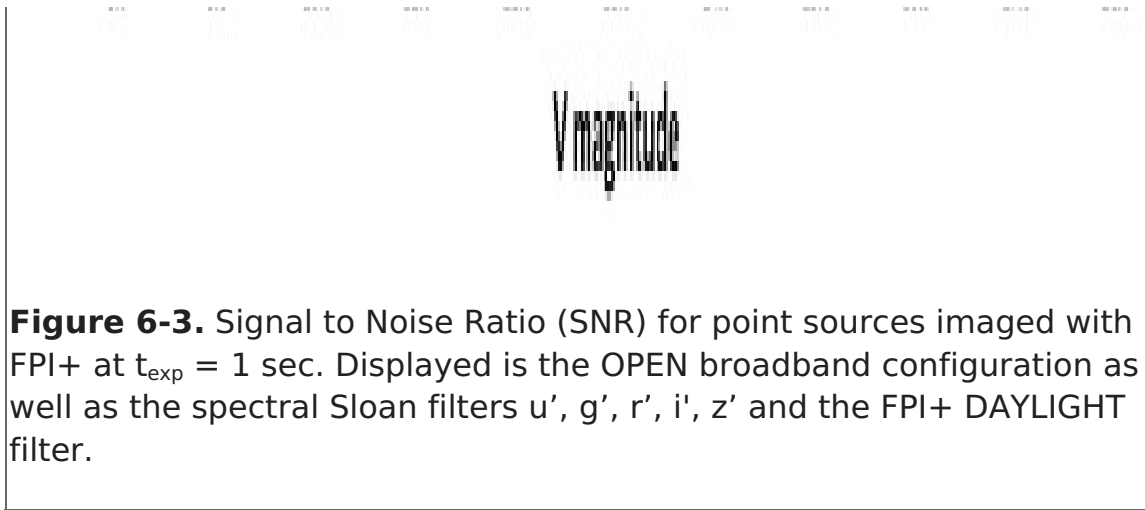
IS - 2718

1000

100







[Return to Table of Contents](#)

6.1.2.3 Camera Performance

Table 6-3.

Camera Modes and Performance

FPI+ Observing Mode	Horizontal Clock Rate	Bit Depth	Gain [e-/DU]	Minimum Read Noise	FPI+ Tracking Possible
FAST_STARE	10 MHz	14 bit	10.7	45.9 e-rms	No
FPI_TRACK_MEDIUM_STARE	5 MHz	14 bit	8.9	36.1 e-rms	Yes
FPI_TRACK_SLOW_STARE	1 MHz	16 bit	0.7	6.0 e-rms	Yes

With the camera's multi-stage thermo-electric cooler, it is possible to achieve sensor temperatures of 100°C below ambient temperature. The measured dark current rate at a sensor temperature of -85°C , the recommended setting, is 0.001 e-/pixel/second.

The frame rates listed in [Table 6-4](#) are for the full frame. When sub-frames are used (without FPI+ tracking) the achievable rates can be increased. The frame rate then depends on the sub-frame size and its position on the sensor.

Table 6-4.

Frame Rates (frames per sec) for the Acquisition of Full Frames

	FAST_STARE	MEDIUM_STARE	SLOW_STARE
1x1	8.9	3.8	0.9
2x2	17.5	6.9	1.7

	FAST_STARE	MEDIUM_STARE	SLOW_STARE
4x4	33.6	11	3.2

[Return to Table of Contents](#)

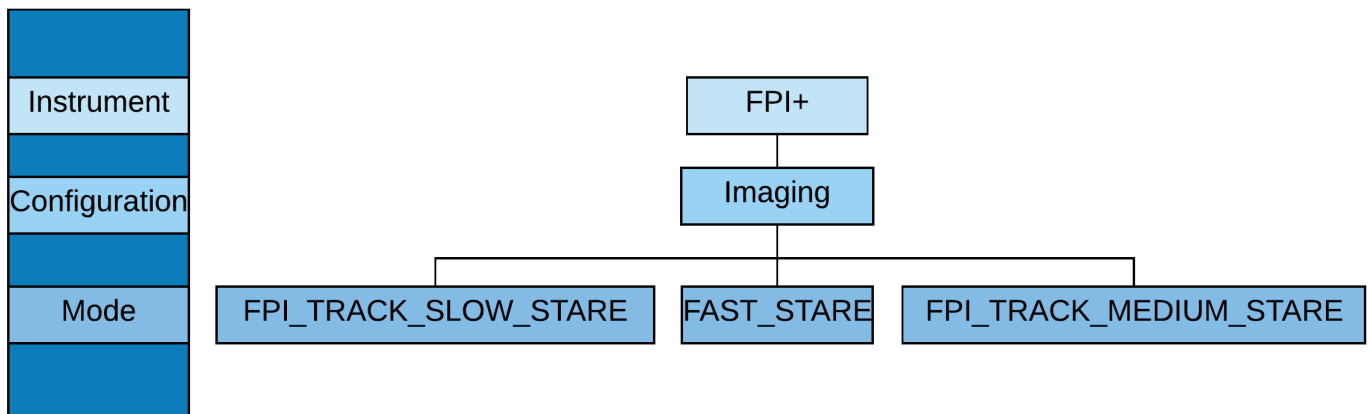
6.2 Planning Observations

Table of Contents

- 6.2 Planning Observations
 - 6.2.1 Observing Modes
 - 6.2.2 Estimation of Exposure Times
 - 6.2.3 Overheads

Return to the Table of Contents for this section at any time by selecting [Return to Table of Contents](#). Users may also navigate through the entire Observer's Handbook by using the complete Table of Contents menu to the right.

6.2 Planning Observations



6.2.1 Observing Modes

FPI+ is the standard tracking camera for the SOFIA telescope, and therefore does not require background elimination techniques to be employed. The FPI+ science instrument offers one imaging configuration with three observing modes: FPI_TRACK_SLOW_STARE, FPI_TRACK_MEDIUM_STARE and FAST_STARE. There is no slit for spectroscopy available. The observing modes are described below.

FPI_TRACK_SLOW_STARE (1 MHz)

Allows image acquisition while tracking on the same images. The parallel tracking requires a reasonably bright guide star in the field of view and exposure times should not exceed 4000 milliseconds.

FPI_TRACK_MEDIUM_STARE (5MHz)

The higher readout rate results in a higher associated readout noise but also in faster frame rates. The parallel tracking requires a reasonably bright guide star in the field of view and exposure times should not exceed 4000 milliseconds.

FPI_TRACK_FAST_STARE (10 MHz)

The fastest readout currently possible with FPI+. This mode does not allow FPI+ tracking on the science images--however FFI tracking can be used.

The two slower observing modes offer, but do not require, tracking in the FPI+ in parallel to the acquisition of science data. However, simultaneous FPI+ tracking does impose certain restrictions on the camera acquisition setting. Acquisition setting restrictions for simultaneous FPI+ tracking are as follows:

- Image frame size: Full frame
- Pixel binning: 1x1, 2x2, 4x4
- Exposure time: between 100 and 4,000 ms for best tracking performance
- Target: Track star available in FPI+ field of view

With simultaneous FPI+ tracking, a target position accuracy of 0.17 arcsec rms has been measured over a two hour time period. There is no positional drift of the target evident.

Alternatively, all of the three observing modes can be used with tracking in the Fine Field Imager (FFI; the tracking camera on the telescope front ring) or without any tracking at all. This allows the selection of an arbitrary sub-frame and binning factors along with the choice of very short (or longer) exposure times in the FPI+. With FFI tracking, positional drifts of the target of 3.9 arcsec per hour have been observed.

[Return to Table of Contents](#)

6.2.2 Estimation of Exposure Times

The sensitivities of the FPI+ with all spectral filter options have been implemented into the SOFIA Instrument Time Estimator ([SITE](#)). This online tool allows the estimation of exposure times to achieve a desired signal to noise ratio.

[Return to Table of Contents](#)

6.2.3 Overheads

Generally, observations can be set up very efficiently and overheads are small. For each observation, bias frames and dark frames will be acquired for image calibration. These calibration acquisitions will result in additional overheads.

The overhead is the instrument set-up time per observation in minutes. It is calculated with:

$$\text{Overhead} = A * \text{Repeat} + B$$

where A = 0.013 sec, B = 200 sec, and Repeat is the total number of acquisitions with the specified exposure time.

The entire duration of the observation is:

$$\text{Duration} = \text{ExposureTime} * \text{Repeat} + \text{Overhead}$$

Observations are done in the frame transfer mode. This means parameter A represents the time for the charge transfer on the sensor and has a value of 1 to 3.4 μ s.

The setup time is less than 20 seconds and approximately 3 minutes should be planned for the acquisition of bias and dark calibration frames.

[Return to Table of Contents](#)

7. GREAT

- 7. GREAT
 - 7.1 Specifications
 - 7.1.1 Instrument Overview
 - 7.1.1.1 Design
 - 7.1.1.2 Configurations
 - 7.1.2 Performance
 - 7.1.2.1 Imaging Sensitivities
 - 7.2 Planning Observations
 - 7.2.1 Observing Modes Overview
 - 7.2.1.1 AOT's
 - 7.2.1.2 Spectroscopic Stability Limitations
 - 7.2.2 Estimation of Exposure Times
 - 7.2.3 OTF Technical Details
 - 7.2.3.1 Coordinates and Array Geometry
 - 7.2.3.2 OTF Mapping
 - 7.2.3.2a upGREAT LFA Channel
 - 7.2.3.2.b 4GREAT L1 Channel
 - 7.2.3.3 OTF Array Mapping
 - 7.2.3.3a upGREAT LFA Channel

7.1 Specifications

Table of Contents

- 7.1 Specifications
 - 7.1.1 Instrument Overview
 - 7.1.1.1 Design
 - 7.1.1.2 Configurations
 - 7.1.2 Performance
 - 7.1.2.1 Imaging Sensitivities

Return to the Table of Contents for this section at any time by selecting [Return to Table of Contents](#). Users may also navigate through the entire Observer's Handbook by using the complete Table of Contents menu to the right.

7.1 Specifications

7.1.1 Instrument Overview

The **G**erman **R**Eceiver for **A**stronomy at **T**erahertz Frequencies (GREAT) is a dual channel heterodyne instrument that will provide high resolution spectra (up to $R = 10^8$) in several frequency windows in the 1.25–5 THz range.

The front-end unit consists of two independent dewars that operate simultaneously. Each dewar contains one of the following channels:

upGREAT Low Frequency Array (LFA)

The LFA is a 14-pixel array (two polarizations and times; 7 pixels) arranged in a hexagonal geometry with a central beam. The current tuning range of the LFA is approximately 1.830–2.006 THz.

upGREAT High Frequency Array (HFA)

The HFA is a 7-pixel array arranged in a hexagonal geometry with a central beam. The tuning range of the HFA is limited to the [OI] frequency of 4.74477749 THz (+/- 100 km/s LSR velocity).

4GREAT

4GREAT consists of four co-aligned (to within a few arcsec) pixels at four different frequencies. The tuning ranges of these pixels are 490–635 GHz (Herschel/HIFI band 1), 890–1100 GHz (Herschel/HIFI band 4), 1240–1500 GHz (GREAT L1 channel), and 2490–2590 GHz (GREAT M channel). Only the L1 and M channels will be offered for Cycle 6.

The GREAT instrument uses Fast Fourier Transform (FFT) spectrometers as backends. Each XFFTS spectrometer has a bandwidth of 2.5 GHz and 64,000 channels, providing a resolution of 44 kHz. The beam size is close to the diffraction limit—about 14 arcsec at 160 μm .

A detailed description of the GREAT instrument and its performance during Basic Science can be found in the GREAT special issue (Heyminck et al. 2012, *A&A*, 542, L1). The LFA is described in Risacher et al. 2016 (*A&A*, 595, A34). Because the instrument is regularly being upgraded and its performance improved, always check the [GREAT website](#) for the latest information.

[Return to Table of Contents](#)

7.1.1.1 Design

Heterodyne receivers work by mixing the signal from a source at a given frequency ν_s with that from a local oscillator (LO) at a specified (and precisely controlled) frequency ν_{LO} and amplifying the result. The mixing results in two frequency bands, called the signal and the image bands, located symmetrically on either side of ν_{LO} and separated from ν_{LO} by the intermediate frequency $\nu_{\text{IF}} = |\nu_s - \nu_{\text{LO}}|$. GREAT operates in double sideband mode, i.e. both the image and signal bands are equally sensitive to incoming radiation. By definition the spectral line of interest is always placed in the signal band, which can be chosen to be either above (Upper Sideband, USB) or below the LO frequency (Lower Sideband, LSB); see [Figure 7-1](#). For sources rich in spectral lines, care has to be taken so that a spectral line in the image band does not overlap or blend with the line in the signal band.

Figure 7-1.

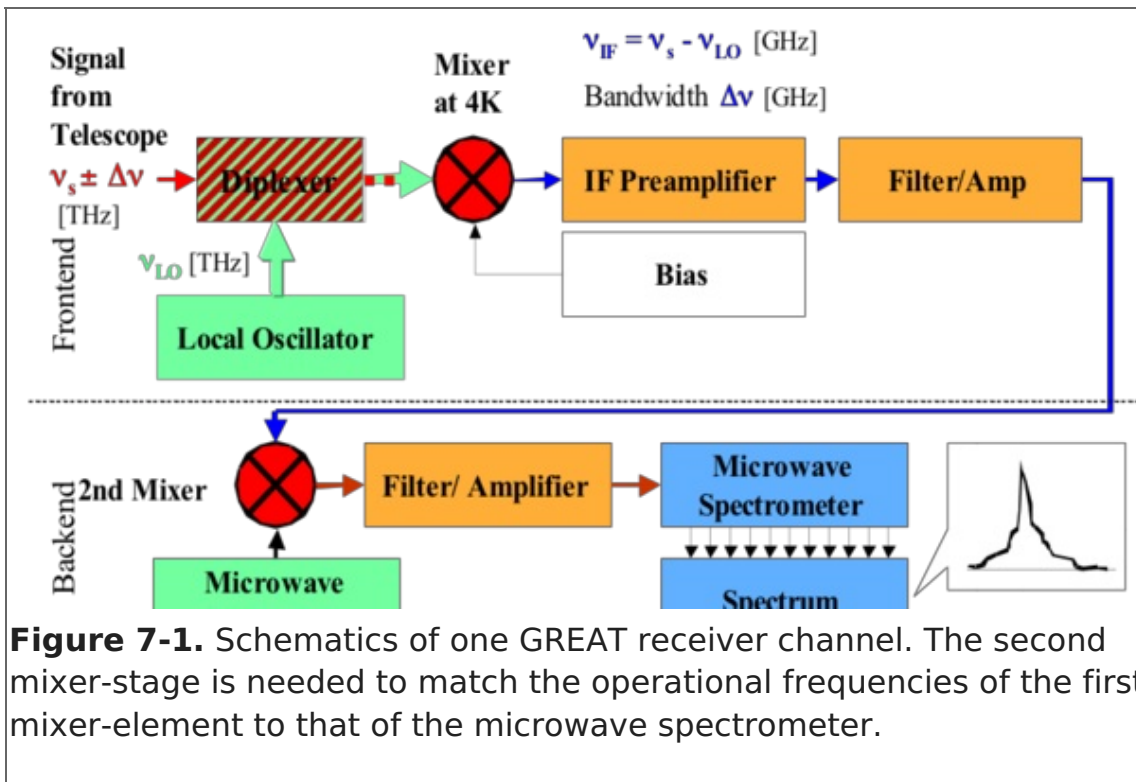


Figure 7-1. Schematics of one GREAT receiver channel. The second mixer-stage is needed to match the operational frequencies of the first mixer-element to that of the microwave spectrometer.

[Return to Table of Contents](#)

7.1.1.2 Configurations

The channels that are currently operational are listed in [Table 7-1](#). Not every frequency in each tuning range has been checked, so there may be gaps where the LOs do not provide enough power to pump the mixer.

Table 7-1: GREAT Configurations

GREAT Configurations

Front-End	Frequencies (GHz)	Lines of Interest	DSB ⁵ Receiver Temperatures (K)
upGREAT LFA	1830–2006	[CII], CO 16-15, OH $^2\Pi_{1/2}$	1000
upGREAT HFA	4744.77749	[OI]	1100
4GREAT	490–635 ¹	NH ₃ , [CI]	--
	890–1100 ²	CH, CS	--
	1240–1500 ³	[NII], CO, OD, SH, H ₂ D ⁺	800
	2490–2590 ⁴	¹⁸ OH $^2\Pi_{3/2}$	1500

¹Herschel/HIFI Band 1; not offered in Cycle 6

²Herschel/HIFI Band 4; not offered in Cycle 6

³GREAT L1 channel

⁴GREAT M channel

⁵DSB = Dual Sideband

In Cycle 6, GREAT offers two configurations:

upGREAT LFA with upGREAT HFA

This configuration employs the Low Frequency Array (LFA) in one dewar and the High Frequency Array (HFA) in the second dewar. The LFA array consists of 2 x 7 pixels (H and V polarizations) and the HFA consists of seven pixels. At the frequency of the CII line, 1900.536 GHz, the frequency coverage of both LFA polarizations overlap and all 14 pixels are in operation. At higher and lower frequencies, only one LFA polarization will be available and only seven LFA pixels can be operated at a given time.

4GREAT with upGREAT HFA

This configuration implements 4GREAT in one dewar and the HFA in the second dewar. The 4GREAT pixels are aligned on the sky to within several arcseconds.

Each of the two installed mixers is provided with XFFTS Fast Fourier Transform spectrometers. The XFFTS has a 2.5 GHz bandwidth and 64,000 channels, providing a resolution of 44 kHz.

The usable instantaneous bandwidth is generally less than that covered by the XFFTS, generally about 1-1.5 GHz. The tuning range of the HFA is limited because the LO (a Quantum Cascade Laser) can only be tuned in discrete steps.

[Return to Table of Contents](#)

7.1.2 Performance

7.1.2.1 Imaging Sensitivities

The GREAT sensitivities and integration times are calculated with the [GREAT time estimator](#). Presented here are the background of these calculations and some worked out examples. Because of the way a heterodyne receiver is calibrated (by measuring the receiver temperature, T_{rx} , with a hot and a cold load), the logical intensity unit for a heterodyne observation is temperature, expressed in Kelvin (K). Either the antenna temperature, T_A^* (the asterisk refers to values after correction for sky transmission, telescope losses and rearward spillover, see e.g. Kutner and Ulich, ApJ, 250, 341 (1981)) or the main beam brightness temperature, T_{mb} , are used. Similarly, the noise is expressed in temperature units as well, ΔT_A^* or ΔT_{mb} , and the sensitivity (or signal-to-noise ratio) of the observations is given by the ratio of the source temperature and the rms temperature of the spectrum. In order to calculate these quantities, we first must estimate the single sideband (SSB) system temperature, T_{sys} , which also includes losses from the atmosphere and the telescope. T_{sys} is given by:

(Eq.7-1)

$$T_{sys} = 2 \times [T_{rx} + \eta_{tel} \times T_{sky} + \eta_{tel} \times T_s + T_{tel}] / (\eta_{tel} \times \eta_{sky})$$

where

T_{rx} is the dual sideband (DSB) receiver temperature

T_{sky} is the radiation temperature of the sky

T_s is the continuum temperature of the source; This term is usually completely negligible (unless observing an extremely bright object such as Jupiter, Saturn, or Sgr B2) and is therefore set to 0 in the GREAT time estimator.

T_{tel} is the Rayleigh-Jeans telescope temperature

η_{sky} is the fraction of radiation transmitted through the atmosphere

η_{tel} is the efficiency of the telescope, which includes ohmic losses and spillover

The factor 2 in [Equation 7-1](#) assumes that the noise temperature is the same in both signal and image band, which is true for the HEB mixers used by GREAT. The transmission of the atmosphere, η_{sky} , at the altitude, observing frequency, and airmass that we plan to observe at can be estimated using the atmospheric transmission code [ATRAN](#). The GREAT time estimator calls ATRAN directly, so those estimating the integration time needed by using the time estimator have no need to run ATRAN separately. T_{sky} depends on η_{sky} and the ambient temperature of the sky (T_{amb}) where the signal is absorbed and can be derived from [Equation 7-2](#).

(Eq. 7-2)

$$T_{sky} = J(T_{amb}) \times (1 - \eta_{sky})$$

where $J(T_{amb})$ is the mean Rayleigh-Jeans (R-J) temperature of the atmosphere, which we assume to have a physical temperature of 220 K at 41,000 ft, resulting in $J(T_{amb}) = 177.5$ K at 1.9 THz. Likewise the telescope temperature, T_{tel} , is related to η_{tel} by [Equation 7-3](#):

(Eq. 7-3)

$$T_{tel} = J_{tel} \times (1 - \eta_{tel})$$

where J_{tel} is the radiation temperature of the telescope, with a physical temperature ~ 230 K ($J_{tel} = 187.4$ K at 1.9 THz). If we assume an η_{tel} of 0.92, then $T_{tel} = 14.8$ K.

As an example, let us calculate the system temperature at the [CII] fine structure line at 157.74 μm (1.9005369 THz). In this example we calculate what we would have at the beginning of a flight, when we are still at low altitude. We therefore assume that we fly at an altitude of 39,000 ft and observe at an elevation of 30 degree. For a standard atmospheric model this corresponds to a transmission of $\sim 76\%$, which gives $T_{sky} = 42.6$ K. For a receiver temperature $T_{rc} = 1100$ K, [Equation 7-1](#) therefore predicts a single sideband system temperature $T_{sys} = 3301$ K when observing the sky.

Now we are ready to calculate the sensitivity. The rms antenna temperature, (corrected for the atmospheric absorption, and telescope losses), ΔT_A^* , for both position switching and beam switching is given by [Equation 7-4](#)

(Eq. 7-4)

$$\Delta T_A^* = (2 \times T_{sys} \times \kappa) \times (t \times \Delta\nu)^{-0.5}$$

where κ is the backend degradation factor, t is the total integration time of the number of on and off pairs that we plan to take, and $\Delta\nu$ is the frequency resolution of our spectra. Strictly speaking, $\Delta\nu$ is the noise bandwidth, which can be slightly different than the frequency resolution, depending on the design of the spectrometer. For our example we

expect the Full Width Half Maximum (FWHM) of the line to be a few km/s, and we will therefore calculate the rms for a velocity resolution of 1 km/s, corresponding to a frequency resolution of 6.3 MHz. Since the GREAT backends have much higher resolution, this is not a problem. We can easily bin the spectrum to our desired velocity resolution. For an observation with three pairs of 40 seconds in each beam, or $t = 4$ min, and assuming the backend degradation factor $k=1$, we then find $\Delta T_A^* = 0.17$ K, which is the one sigma rms antenna temperature.

To convert antenna temperature to brightness temperature T_R^* , we have to make one more correction as shown in [Equation 7-5](#):

(Eq. 7-5)

$$T_R^* = T_A^* / \eta_{fss}$$

where η_{fss} is the forward scattering efficiency, usually measured for a very extended source (like the Moon). For GREAT $\eta_{fss} = 0.97$. Therefore our brightness rms temperature, $\Delta T_R^* = 0.18$ K⁵. Note: The GREAT time estimator assumes the line temperature in T_R^* , and *not in main beam brightness temperature*, $T_{mb} = T_R^* / \eta_{MB}$, which is for a source that just fills the main beam.

If we want to express our results in flux density, S_n , rather than brightness temperature, we can convert antenna temperature, T_A , to flux density, S_v , using the standard relation given in [Equation 7-6](#):

(Eq. 7-6)

$$S_v = 2 \times \kappa \times \eta_{fss} \times T_A^* / A_{eff}$$

where κ is the Boltzmann constant, and A_{eff} is the effective area of the telescope. A_{eff} is related to the geometrical surface area of the telescope, A_g , by the aperture efficiency, η_a ,

i.e. $A_{eff} = \eta_a \times A_g$. For the measured main beam efficiency in early April 2013 (0.67) and a Half Power Beam Width (HPBW) of ~ 14.1 arcsec (± 0.3 arcsec) an aperture efficiency⁶ of 55 \pm 2 % is derived. [Equation 7-7](#) yields the following simple form for the 2.5 m SOFIA telescope:

(Eq. 7-7)

$$S \text{ (Jy)} = 971 \times T_A^* \text{ (K)} \text{ or within errors } \sim 1000 \times T_A^* \text{ (K)}$$

Normally we use Jy only for spatially unresolved sources, but we can also use [Equation 7-7](#) to convert line intensities into W/m^2 , which maybe a more familiar unit for the far infrared community. If we assume that the [CII] line we are observing is a Gaussian with a Full Width Half Maximum (FWHM) of $= 5$ km/s, i.e. 31.8 MHz, the integrated line intensity is given by $1.065 \times T_{peak} \times \Delta\nu$, where $\Delta\nu = 31.8$ MHz. If we take T_{peak} equal to our rms antenna temperature, we find using [Equation 7-7](#) that our four minute integration therefore corresponds to a one sigma brightness limit of $\sim 6.1 \cdot 10^{-17}$ W/m^2 for a 5 km/s wide line observed with 1 km/s resolution. If we only aim for a detection, we can probably degrade the resolution to 2 km/s. In this case we gain a square root of 2, and therefore our one sigma detection limit is $4.3 \cdot 10^{-17}$ W/m^2 .

This is the reverse of what is typical when writing a proposal, when the proposer has an

estimate how wide and how bright the line is expected to be and knows what signal to noise is needed for the analysis. Assume we want to observe the [CII] 158 μm line in T Tauri, a young low-mass star. Podio et al. (2012, A&A, 545, A44) find a line intensity of $7.5 \cdot 10^{-16} \text{ W m}^{-2}$ for the Herschel PACS observations, which are unresolved in velocity (the PACS velocity resolution is $\sim 240 \text{ km/s}$ for [CII]). Here we want to velocity resolve the line to see if it is outflow dominated or whether it is emitted from a circumstellar disk or both. We therefore need a velocity resolution of 1 km/s or better. If we assume that the line is outflow dominated with a FWHM of say 20 km/s (127.2 MHz; little or no contribution from the circumstellar disk) we get a peak antenna temperature (using Equation 7-7) of 0.52 K or a radiation temperature $T_R^* = 0.55 \text{ K}$. In this case we want a SNR of at least 10 and a velocity resolution of 1 km/s or better. Let's check whether it is feasible. If we plug in the values we have in the GREAT time estimator (assume 40 degrees elevation, standard atmosphere, and we fly at 41,000 ft) or we can estimate it from the equations given above.

With these assumptions ATRAN gives us an atmospheric transmission of 0.86 integrated over the receiver band-pass. The receiver temperature is 1100 K (DSB). Using Equation 7-2, we find that the sky only adds 24.9 K to the system temperature and from Equation 7-1 we therefore get $T_{\text{sys}} = 2881 \text{ K}$. Since we want to reach a signal to noise of 10, the rms antenna temperature $\Delta T_A^* = 0.052 \text{ K}$. We can now solve for the integration time using Equation 7-4, where we set $\Delta\nu = 6.338 \text{ MHz}$ (1 km/s resolution). In this case $t = 1937 \text{ sec}$ or 32.3 min. The PACS observations show the emission to be compact, so we can do the observations in Dual Beam Switching Mode (DBS; see Section 7.2.1.1), with a chop throw of 60 arcsecond. Both DBS and Total Power (TP) modes are currently estimated to have an overhead of 100% and a setup time for tuning and calibration of two minutes (which get added when entering the observations in USPOT, the SOFIA proposal tool). Our observation would therefore take 60 minutes, which is completely feasible. The GREAT exposure time calculator gives $t = 1930 \text{ sec}$. The difference is negligible.

Sensitivity calculations for an On-the-Fly (OTF) map, when data are taken while the telescope is scanning), are done a bit differently. For example, for an OTF map of the [CII] line (Half Power Beam Width, HPBW $\sim 14 \text{ arcsec}$), we need to sample the beam about every 7 arcsec. If we read out the average once per second, for example, this means that we scan with a rate of 7 arcsec/second. To do a 3 arcmin scan will therefore take 26 sec, resulting in 26 map points, let us make it 27, to get an odd number of points. We therefore need to spend (1 second) * $(\sqrt{27}) = 5.2 \text{ seconds}$ on the reference position in total power mode. We ignore the time it takes the telescope to slew to the next row and any time needed for calibration. For a 3 x 3 arcmin² map, i.e. 27 x 27 positions with a cell size of 7 x 7 arcsec². The integration time for each row is therefore 5.2 + 27 seconds or 32.2 seconds/row. The total integration time for the map is therefore 14.5 minutes. We definitely want to do one repeat, so the total integration time is therefore 29 minutes. For all observing modes, we assume a 100% overhead and 2-minute setup for tuning and calibration. The total duration of the two maps is therefore 61.9 minutes. Thus, a 3 x 3 arcmin² map in the [C II] line is entirely feasible.

Our 3 by 3 arcmin² map with one repeat has an integration time of 2 seconds per map point. For typical observing conditions (41,000 feet, 30 degrees elevation) the GREAT time estimator (settings: TP OTF map, Non=27, Classic OTF; see Section 7.2.3) gives us

an rms temperature/map point of 0.9 K for a velocity resolution of 1 km/s.

[Return to Table of Contents](#)

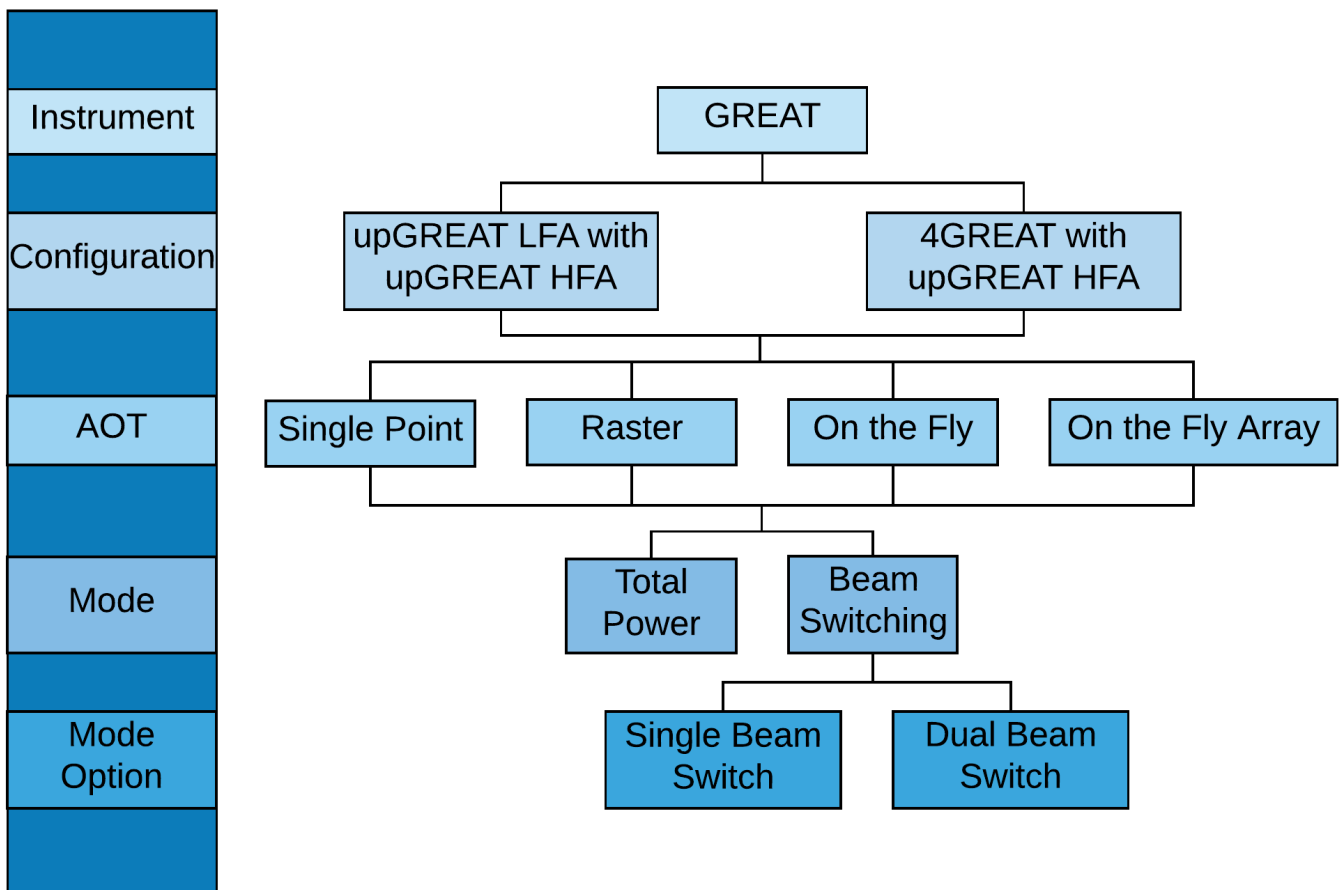
7.2 Planning Observations

Table of Contents

- 7.2 Planning Observations
 - 7.2.1 Observing Modes Overview
 - 7.2.1.1 AOTs
 - 7.2.1.2 Spectroscopic Stability Limitations
 - 7.2.2 Estimation of Exposure Times
 - 7.2.3 OTF Technical Details
 - 7.2.3.1 Coordinates and Array Geometry
 - 7.2.3.2 OTF Mapping
 - 7.2.3.2a upGREAT LFA Channel
 - 7.2.3.2b 4GREAT L1 Channel
 - 7.2.3.3 OTF Array Mapping
 - 7.2.3.3a upGREAT LFA Channel

Return to the Table of Contents for this section at any time by selecting [Return to Table of Contents](#). Users may also navigate through the entire Observer's Handbook by using the complete Table of Contents menu to the right.

7.2 Planning Observations



This section describes the GREAT instrument and the available observing modes. It also contains the information required to estimate observing times in individual modes and

examples of each.

If the frequency of interest has not already been used by GREAT, please [contact](#) the GREAT team to ensure that observing the line is feasible. There may be gaps where the broadband Local Oscillators do not provide enough power to pump the mixers.

Note: Allan variance affects the capabilities of GREAT and requires special attention when planning observations, see [Section 7.2.1.3](#) for details.

[Return to Table of Contents](#)

7.2.1 Observing Modes Overview

Two main observing modes are currently offered: Total Power (TP) and Beam Switching (BSW), the latter of which is available in either Single Beam Switching (SBS) or Dual Beam Switching modes (DBS).

Total Power Mode

In Total Power mode, the telescope alternates between the target and a nearby reference position that is free of emission. From the difference of the target and reference spectra, often called ON-OFF, the GREAT software produces a spectrum, which is largely corrected for atmospheric and instrumental effects. The integration time in this mode depends on the stability of the receiver and how fast the atmosphere fluctuates. The on-source time is typically ≤ 30 seconds, but can be adjusted during the flight if necessary. If shorter integration times are used, one gets a better cancellation of the sky fluctuations, but adds to overheads and therefore reduces the observing efficiency. The ON-OFF cycle is repeated until the required sensitivity is reached.

Total Power mode is used when observing one or a few positions in an extended source or crowded region, such as a large molecular cloud. If the reference position is far from the target position, e.g., 30 arcmin or more, changes in the sky background will result in poor baselines. If the reference position cannot be identified to within 30 arcmin from the source position, an intermediate reference position may be selected for the observations and used to measure this intermediate reference position relative to the far-away, clean reference position. Any contamination in the original spectrum due to emission in the intermediate reference position can then be added back into the data.

Beam Switching Mode

In SBS mode, the secondary mirror is chopping between the target (signal) and a sky position (reference) that is determined by a chop throw and a chop angle. In DBS mode, the telescope then nods so that the beam that was on the reference position is on the source, and the beam that was on the source is at a new reference position (at the distance of the chop throw, and at the chop angle + 180 degrees). Thus, in SBS mode, there is a single reference position, while in DBS mode, there are two reference positions that are equidistant and on opposite sides of the source.

Chopping in either BSW mode is typically done at a rate between 1 and 2.5 Hz. The maximum chop throw should be < 5 arcmin, set by the limits of the chopping

secondary. Because the time between the on- and off-source measurements is small (usually ~ 1 s), this mode results in better sky cancellation and hence better baseline stability. Beam switching is typically used for point or compact sources, because the chop throw has to be larger than half of the source size. Smaller chop throws (60–120 arcsec) are preferred, as large chop throws distort the beam (coma) and uncertainties in the chop throw result in pointing errors if there is a difference between the chop throw and the nod.

[Return to Table of Contents](#)

7.2.1.1 AOTs

GREAT offers four standard methods of observation through Astronomical Observation Templates (AOTs) in USPOT: Single Point, Raster Mapping, On the Fly (OTF) Mapping, and OTF Array Mapping. Each AOT is run in either Total Power or Beam Switching mode.

Single Point

Single Point is used for integrations at a single position on the sky. It is typically used to observe faint sources that require long integration times, or for point sources (sources that are smaller than the beam).

Raster

Raster mapping is essentially a collection of single point observations used for creating small maps or strips, where one needs relatively long integration times per map point. A typical example would be a small 3 x 3 map (9 points) with 30 seconds per map point.

In Total Power mode, the telescope nods to a single OFF position away from the source--which is temporally expensive and results in worse baselines. Total Power mode however is very useful in cases where there is a lot of clutter in the region immediately surrounding the source.

In BSW, the telescope can more quickly chop then adjust the secondary to form a pseudo map off-source.

On the Fly and On the Fly Array

In an OTF map, the telescope scans along a row, while the backends are continuously integrating the incoming signal. An average is recorded after the telescope has moved a fraction (typically half to one third) of the beam size. Each average therefore corresponds to a point on the sky with a finite width.

In Total Power mode, each scan is preceded by a measurement of a reference position, where it integrates \sqrt{N} times the integration time per point, where N is the number of points in a row. After a row is completed, the telescope steps about half a beam width in the orthogonal direction and begins a new scan along with reference measurement.

In Beam Switching mode, the telescope chops while scanning. After a row is completed, the telescope steps about half a beam width in the orthogonal direction and begins a new scan. Note that no additional dedicated reference measurement is

needed as in Total Power mode.

This process is repeated until a map of the desired size is constructed. The entire map is repeated until the required sensitivity is reached. An individual map must be rectangular. For a uniform map, the spacing between points along a row (the step size) and the spacing between rows is specified to be the same. When the spacing between rows is specified to be of different values, it is an OTF Array map.

OTF observations are particularly efficient for larger maps of bright lines--however, even for a small map OTF is more efficient as long as the line is bright enough so that one can reach the required signal to noise within several repeats of the map.

When performing observations in Total Power mode, OTF mapping is more efficient than Raster mapping only if the integration time per position is small. Thus, OTF is the preferred mode when mapping the distribution of a relatively bright line over a large area (e.g., a map of the [C II] 158 μm line in a molecular cloud). For faint emission, it is often better to use Raster mapping. The size of the scan is limited by the stability of the receiver and atmosphere and the time spent on the scan is therefore typically limited to less than 30 seconds (20 seconds for the H channel or HFA) in Total Power mode. The typical integration time per position is 1 second per map point, and is usually between 0.3 and 2.0 seconds. For a large map one therefore has to break up the map into a number of sub-maps.

[Return to Table of Contents](#)

7.2.1.2 Spectroscopic Stability Limitations

The spectroscopic stability (Allan variance) sets limits to the operation of a heterodyne instrument like GREAT.

BSW mode typically operates with 2.5 Hz, and therefore limitations are mainly set by the atmospheric stability and long integrations are typically performed. As such, integrations with 30 sec phase times are typically implemented for Single Point and OTF observations to achieve optimum spectroscopic stability. For weak and/or broad-line projects, DBS is recommended. No noticeable performance degradation has been observed from using SBS instead of DBS for other projects.

If TP mode observations are requested, the situation becomes complicated and multi-dimensional: science with linewidth more than a few 100 MHz and position changes greater than 10-15 arcmin between the ON and OFF positions become increasingly difficult, though not impossible. The actual impacts will depend on frequency, weather conditions, stability of the sky, elevation of the observation, and on the detector used. [Contact](#) a GREAT Instrument Scientist to discuss possible mitigations and their impact on the overheads to be assumed.

[Return to Table of Contents](#)

7.2.2 Estimation of Exposure Times

Estimations of exposure times for GREAT can be made using the SOFIA Instrument Time Estimator ([SITE](#)). [SITE](#) is a web-based tool that calculates either the signal-to-noise ratio

for a given line brightness and integration time, or the integration time needed to reach a certain RMS noise level for either one point on the sky or per map position for an OTF map in Total Power mode. These integration times do not include tuning, chopping, slewing, and other observatory overheads. The total time, including all overheads, is determined in USPOT after entering the time calculated by [SITE](#).

As is the case for other heterodyne receivers that use hot and cold loads to measure the receiver temperature, the intensity units are Kelvin (K). The intensity scale used in [SITE](#) is brightness temperature T_R^* . This relates to the measured antenna temperature as $T_A^* = T_R^* \eta_{fss}$ and the main beam temperature (corrected for losses in the side lobes) as $T_{MB} = T_R^* / \eta_{fss}$. For GREAT, $\eta_{fss} = 0.97$ and in bands L1, L2/LFA, and H/HFA hMB is in the range of 0.65 to 0.70. A detailed description of the GREAT intensity calibration is given in [Section 7.1.2.2](#). It also contains worked out examples for different observing modes and unit conversions.

[SITE](#) is also useful to determine in which sideband the line of interest is best put, taking into account the atmospheric transmission. System temperatures for the line in the USB or LSB are given, as well as a plot showing the line locations for either LO tuning in comparison with the atmospheric transmission.

[Return to Table of Contents](#)

7.2.3 OTF Technical Details

In general, OTF schemes are flexible and the detailed map parameters will depend on the goals of the project. The two OTF mapping options for upGREAT are the classic OTF (which can be used with the upGREAT arrays or the single-pixel GREAT channels) and OTF Array (which can only be used with the LFA or HFA).

Both AOTs can be executed as either Beam Switching mode or Total Power mode. Some things to consider when deciding between these two modes are:

Efficiency

BSW maps spend an equal amount of time on the ON and OFF positions. In contrast, Total Power maps spend less time on the OFF position and are therefore more efficient.

Baseline Stability

BSW observations have better baseline stability. If the source is expected to have faint and/or wide lines, then BSW would be preferred. If the source is expected to have bright and/or narrow lines, then the baseline quality is less of an issue.

Reference positions

For a BSW map, there needs to be an emission-free region on the sky that is the same size as the OTF map and within a few arcminutes of the map. This can sometimes be a challenge, especially in crowded regions. For Total Power maps, only single emission-free reference position is needed, and it can be farther away from the map (up to 30 arcmin, although baselines will be better for closer reference positions).

[Return to Table of Contents](#)

7.2.3.1 Coordinates and Array Geometry

Because upGREAT maps can be rotated relative to standard sky coordinates (e.g., J2000), they have their own coordinate system, defined by x and y . With a map rotation of 0 degrees, the $+x$ axis is aligned with the $+RA$ axis, and the $+y$ axis is aligned with the $+Dec$ axis (Fig. 7-2). Map rotation angle increases in the counter-clockwise direction, and the map angle can range from -360° to $+360^\circ$. Scans in the x -direction are parallel to the x -axis, and scans in the y -direction are parallel to the y -axis.

Figure 7-2.

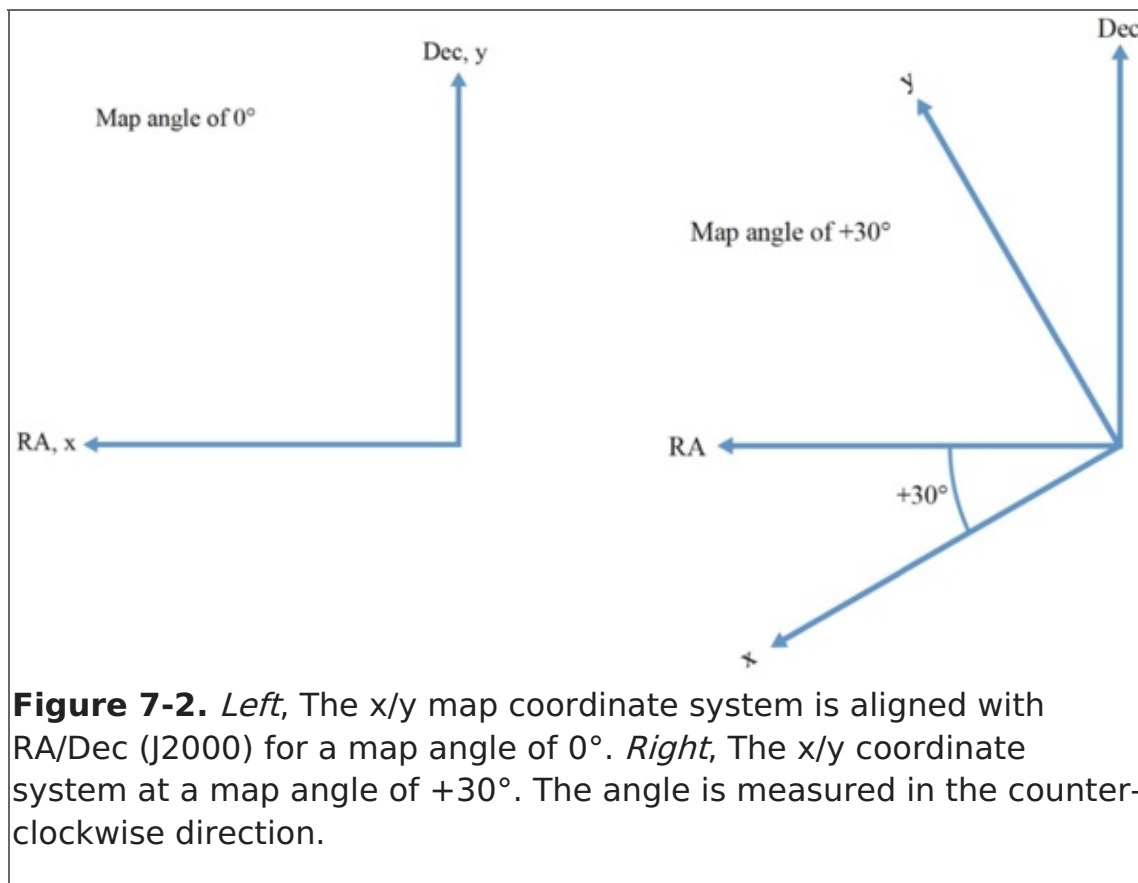


Figure 7-2. *Left*, The x/y map coordinate system is aligned with RA/Dec (J2000) for a map angle of 0° . *Right*, The x/y coordinate system at a map angle of $+30^\circ$. The angle is measured in the counter-clockwise direction.

The upGREAT Low Frequency Array (2x7 beam, H and V polarizations) and High Frequency Array (HFA) are arranged in a hexagonal pattern with a central beam. The spacings between the beams are approximately 2 beam widths (31.7 arcsec for the LFA, 13.8 arcsec for the HFA). For efficient mapping, the array is typically rotated by 19.1 degrees relative to the scan direction, resulting in a projected pixel spacing of 10.4 arcsec for the LFA and 4.6 arcsec for the HFA (see Fig. 7-3). The array can be rotated independent of scanning direction for maximum flexibility of observation planning.

Figure 7-3.

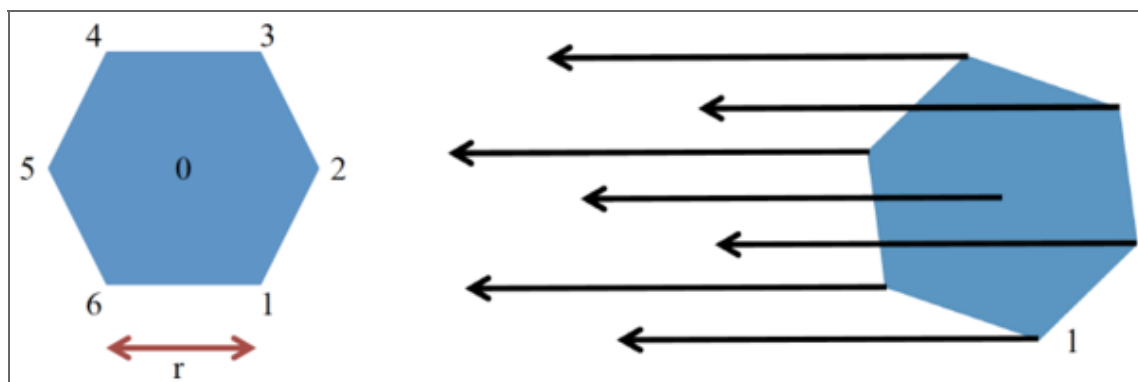


Figure 7-3. *Left*, The configuration of an upGREAT array. The numbers 0-6 mark the pixel numbers of the array, and the separation between the pixels, r , is 31.7 arcsec for the LFA, and 13.8 arcsec for the HFA. *Right*, An upGREAT array, rotated by -19.1° (pixel 1 is labeled) with arrows indicating the scan direction. The projected pixel spacing perpendicular to the scan direction is 10.4 arcsec for the LFA, and 4.6 arcsec for the HFA.

When creating a mapping strategy, observers will have to weigh many factors, including the area to be mapped, the required integration time per point, and of course the scientific objectives. Examples given in [Section 7.2.3.2](#) result in fully (or overly) sampled maps of the central region, but require different amounts of time to complete, and have very different integration times and coverage outside of the central region. In the [Section 7.2.3.2a](#), a point in the central region may be mapped by only a few pixels, while in the [Section 7.2.3.2b](#), the entire central region is mapped by each pixel. These are all important pieces of information to consider when planning mapping observations with upGREAT.

[Return to Table of Contents](#)

7.2.3.2 OTF Mapping

The classic OTF mapping is possible with either an upGREAT array or a single-pixel channel, and is the only OTF mapping option with a single pixel. In classic OTF mapping, each pixel makes a rectangular map based on the step size along the scan row, and the spacing between the scan rows. In the case of an upGREAT array, the result is seven rectangular maps; the amount of overlap between the maps depends on the map parameters (see [Section 7.2.3.2a](#)). In the case of a single-pixel GREAT channel, the result is a single rectangular map (see [Section 7.2.3.2b](#)).

[Return to Table of Contents](#)

7.2.3.2a upGREAT LFA Channel

In this example, we design an observation using the LFA such that the final map is composed of 14 fully sampled maps (one from each of the 2x7 pixels) of the central region. To ensure that all pixels cover the central region of the map during each scan, the scans start and end $\frac{1}{2}$ of the array width before and after the central region in the x (RA) direction.

In addition, the top of the array is aligned with the bottom of the map, and each subsequent row is one step size (~ 6 arcseconds for the LFA) above the prior one (see [Fig. 7-4](#)). We use a 6 arcsecond step size along the row, which will result in a fully sampled map. We continue to make rows until the bottom of the array is aligned with the top of the map.

For this map, a scan length of 140 arcsec is sufficient to cover the central region and half of the array width before and after the central region. This scan length is also a multiple of the step size, which is a requirement for upGREAT maps. Based on the selected scan length and step size, each scan will have 20 points. Here we again select an integration time of 1 second per point, so each scan will take 20 seconds. The off position will

require $\sqrt{20} \approx 4.5$ seconds, for a total of 24.5 seconds per scan. The entire map (including starting the map half of the array width below the central region and ending the map $\frac{1}{2}$ of the array width above the central region) is made up of 20 rows. Thus, the total on+off time for the entire map is 490 seconds; after including a factor of 2 for overhead, the whole map takes about 17 minutes. Every point within the central region would have an integration time of 14 seconds (the combination of 2 polarizations x 7 maps, one for each pixel, with an integration time of 1 second each).

Figure 7-4.

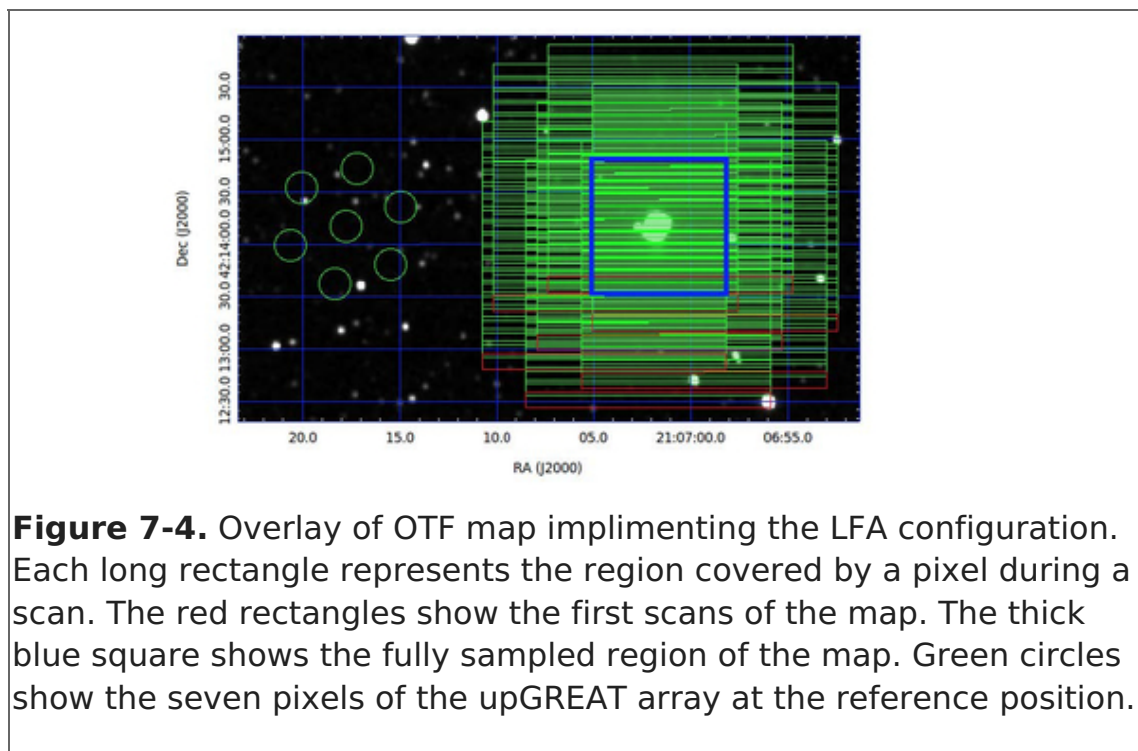


Figure 7-4. Overlay of OTF map implementing the LFA configuration. Each long rectangle represents the region covered by a pixel during a scan. The red rectangles show the first scans of the map. The thick blue square shows the fully sampled region of the map. Green circles show the seven pixels of the upGREAT array at the reference position.

Note: In this example, if the other channel used for observing is a single pixel, a rectangular map will be created in this channel as well. Whether or not this map is fully sampled will depend on the frequency of the other channel and the step size used in the map.

[Return to Table of Contents](#)

7.2.3.2b 4GREAT L1 Channel

In this example, we want to make a fully-sampled map of the filamentary cloud shown in [Fig. 7-5](#) using L1, a single pixel channel. For this map, a rectangle of ~ 240 arcsec by ~ 128 arcsec, rotated by an angle of 45 degrees CCW, would cover the area of interest. If we select a step size of 8 arcseconds, which would result in a fully-sampled map, we could scan in the long direction, with 30 ($240 \text{ arcsec} / 8 \text{ arcsec/dump}$) dumps along the scan row and 16 rows ($128 \text{ arcsec} / 8 \text{ arcsec between rows}$). To keep the scan duration within 30 seconds, we select a dump time of 1 second per point. The off position will require $\sqrt{30} * 1 \text{ second} \approx 5.5$ seconds, for a total of 35.5 seconds per scan. Thus, the total on+off time for the entire map is 568 seconds; after including a factor of 2 for overhead, the whole map takes about 19 minutes. Every point within the map would have an integration time of 1 second.

Figure 7-5.

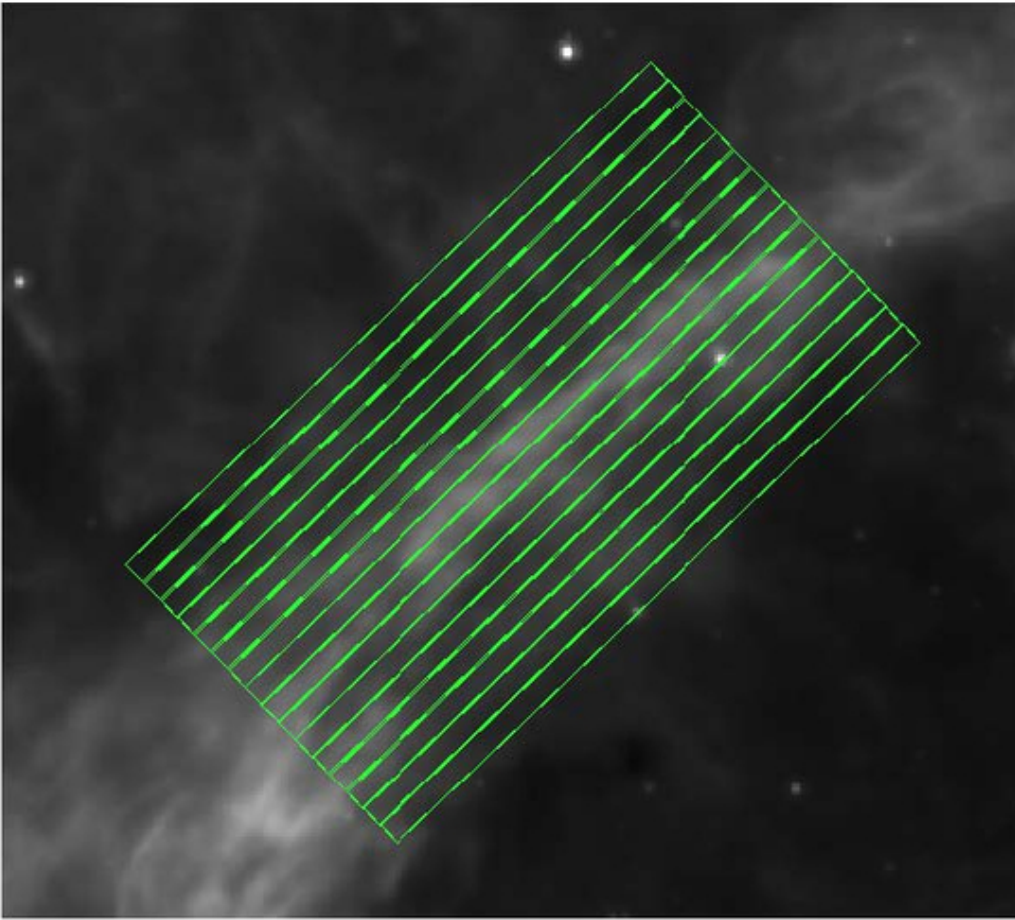


Figure 7-5. Overlay of OTF map in the L1 configuration. Each long rectangle represents the region covered by a pixel during a scan. This map is rotated by 45 degrees (CCW) to match the morphology of the filamentary cloud.

[Return to Table of Contents](#)

7.2.3.3 OTF Array Mapping

The basic unit of the upGREAT array mapping scheme is referred to as a block, which consists of a single or multiple scans of the same length, in the same direction (Fig. 7-6). For both the LFA and the HFA, the projected pixel spacing (after rotating the array by -19.1°) is such that a single scan results in an under-sampled map. To create a fully sampled map, it is necessary to make at least one more scan to fill in the gaps between pixels. The default behavior is to make a second scan, creating a fully sampled map and completing the block. It is possible, however, to scan only a single time (creating an under-sampled map), or more than two times (creating an oversampled map), depending on the goals of the project.

Figure 7-6.

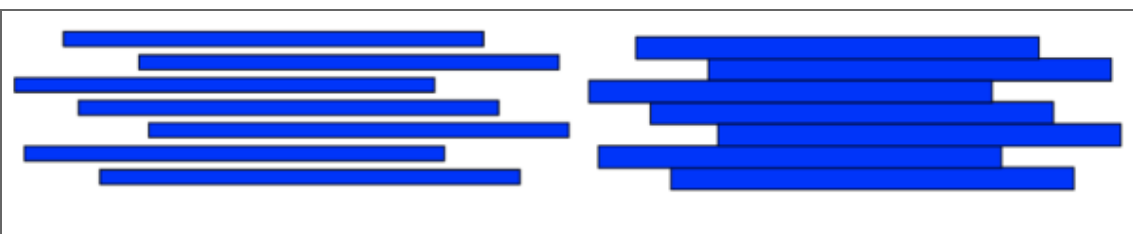


Figure 7-6. *Left*, A block that consists of a single scan of the rotated array. The gaps between the scans indicate an under-sampled map. *Right*, A block that consists of two scans. This block is fully sampled in the direction perpendicular to the scan direction. The second scan fills in the gaps in the single-scan block.

A single map can consist of any number of blocks, and can scan in the x- or y- direction, or both. The parameters of the x- and y-direction scans are independent, but can be used in concert to create fully sampled maps of a region, scanning in both directions (Fig. 7-7). Scanning in both directions helps to minimize the striping effects that can be caused by the different characteristics of the array pixels.

Figure 7-7.

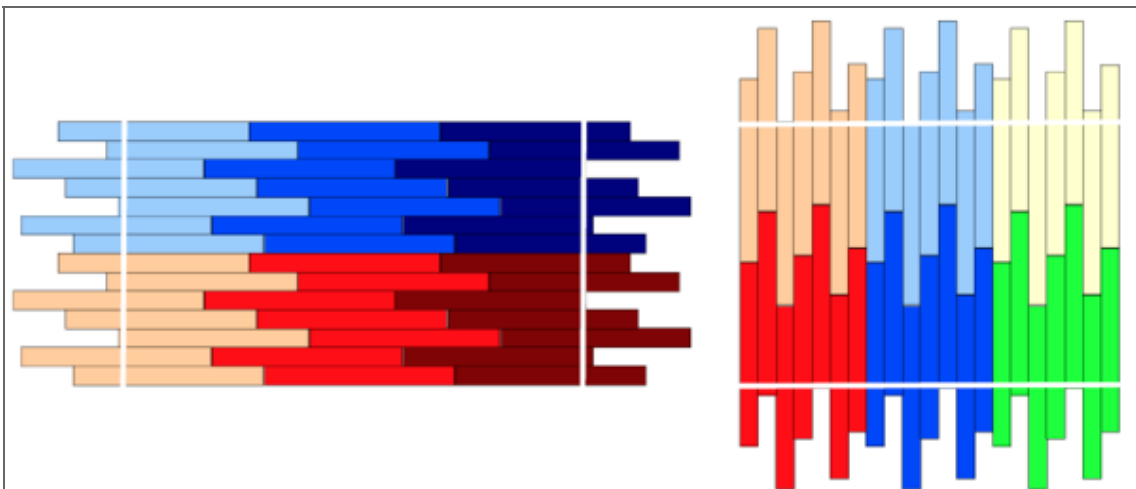


Fig. 7-7. *Left*, A map composed of six blocks scanning in the x-direction. There are 3 blocks along the scan direction, and 2 blocks perpendicular to the scan direction. The region interior to the two vertical white lines shows the inner coverage region. *Right*, A map composed of six blocks scanning in the y-direction. There are 2 blocks along the scan direction, and 3 blocks perpendicular to the scan direction. The region interior to the two horizontal white lines shows the inner coverage region. Maps scanning in both directions can be set up to align the inner coverage regions of the two maps.

To calculate the size of the inner coverage region along the scan direction:

$$\text{inner coverage} = [(\text{block length}) * (\# \text{ of blocks in scan direction}) - 1] * (\text{array size})$$

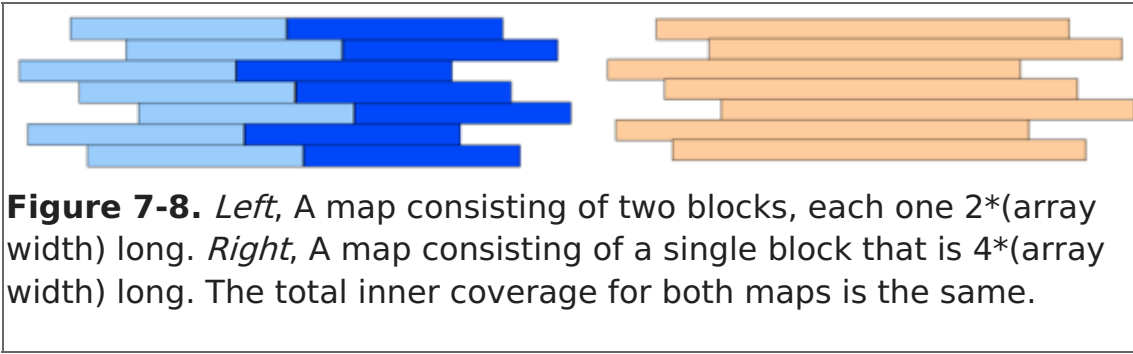
where block length is in units of the array size.

To calculate size of the inner coverage region perpendicular to the scan direction:

$$\text{inner coverage} = (\# \text{ of blocks perpendicular to scan direction}) * (\text{array size})$$

Because of the flexibility of the mapping scheme, there can be multiple ways to observe the same region. For example, the two setups in Fig. 7-8 both fully cover the same area. Some important factors in determining the proper setup between these two options are the desired integration time per point, the step size between the points, and the duration of a single scan.

Figure 7-8.



[Return to Table of Contents](#)

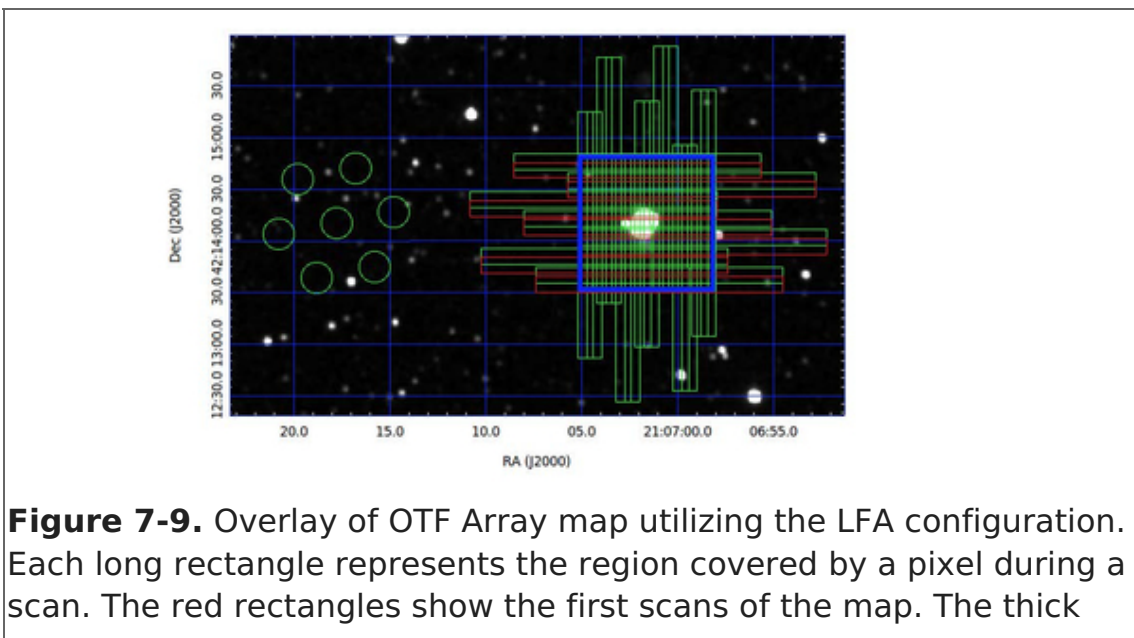
7.2.3.3a upGREAT LFA Channel

In this example, the rotated array makes four total scans—two in the x- (RA) direction and two in the y- (Dec) direction [Fig. 7-9](#). Because the projected pixel separation of 11 arcsec is larger than required to Nyquist sample the 14-arcsec beam at 1.9 THz, two scans in each direction are required to fully sample the area. These scans are separated by 5.5 arcsec (1/2 of the projected pixel separation), resulting in a slightly oversampled map.

To ensure that all pixels cover a part of the central region of the map during each scan, the scans start and end $\frac{1}{2}$ of the array width before and after the central region. To get evenly spaced sampling, we select a 5.5 arcsecond step size along the rows. This step size, along with the $\frac{1}{2}$ array length added to the beginning and end of the scan, results in a total scan length of 143 arcseconds (26 steps).

If we select 1 second integration time per point, each scan will take 26 seconds, and the off integration for each scan will take $\sqrt{26} \approx 5$ seconds. Thus, for the 4 scans that comprise the map, the total on+off time will be approximately 125 seconds. Including a factor of two for overhead, the total time for this map would be a little over four minutes, and each position in the central region of the map would have an integration time of ~ 4 seconds (2 seconds from each polarization).

Figure 7-9.



blue square shows the fully sampled region of the map. Green circles show the 2x7 pixels of the upGREAT array in the off position.

Note: In this example, if the other channel used for observing is a single-pixel, only an irregularly spaced map will be created in this channel. The shape of this will match the region traced out by the center array pixel.

[Return to Table of Contents](#)

8. HAWC+

- 8. HAWC+
 - 8.1 Specifications
 - 8.1.1 Instrument Overview
 - 8.1.1.1 Design
 - 8.1.2 Performance
 - 8.1.2.1 Filters
 - 8.1.2.2 Total Intensity Imaging Sensitivities
 - 8.1.2.3 Polarimetry Imaging Sensitivities
 - 8.2 Planning Observations
 - 8.2.1 Total Intensity Observations
 - 8.2.1.1 On the Fly Mapping
 - 8.2.1.1a Lissajous
 - 8.2.1.1b Box
 - 8.2.1.2 Nod Match Chop
 - 8.2.2 Polarimetry Observations
 - 8.2.2.1 Nod Match Chop

8.1 Specifications

Table of Contents

- 8.1 Specifications
 - 8.1.1 Instrument Overview
 - 8.1.1.1 Design
 - 8.1.2 Performance
 - 8.1.2.1 Filters
 - 8.1.2.2 Total Intensity Imaging Sensitivities
 - 8.1.2.3 Polarimetry Imaging Sensitivities

Return to the Table of Contents for this section at any time by selecting [Return to Table of Contents](#). Users may also navigate through the entire Observer's Handbook by using the complete Table of Contents menu to the right.

8.1 Specifications

8.1.1 Instrument Overview

The High-resolution Airborne Wideband Camera (HAWC+) is a multi-wavelength far-infrared imager and polarimeter with continuum bandpasses from 40 μm to 300 μm . HAWC+ Total Intensity Imaging uses a filter wheel and a polarizing grid to split incoming light into two orthogonal components of lineal polarization, the reflected (R) and

transmitted (T) rays. For Polarimetry Imaging, a rotating half-wave plate (HWP) is introduced before the filter wheels. The current state of the instrument includes a 64x40 array measuring the R polarization state and a 32x40 array for the T polarization state. HAWC+ observations are diffraction-limited with a spatial resolution of 5 to 20 arcsec and a field of view (FOV) of 2 to 8 arcmin. HAWC+ is currently not offering observations at 63 μm (Band B).

[Return to Table of Contents](#)

8.1.1.1 Design

A schematic of the HAWC+ optical design is shown in [Figure 8-1](#). Prior to entering the HAWC+ cryostat, light from the SOFIA telescope enters the set of warm fore-optics mounted outside the cryostat. The light is reflected from a folding mirror to a field mirror, capable of imaging the SOFIA pupil at the cold pupil inside the HAWC+ cryostat. After the fore-optics, light enters the cryostat through a 7.6 cm diameter high-density polyethylene (HDPE) window, then passing through a cold pupil on a rotatable carousel, a near-infrared blocking filters to define each bandpass and lenses designed to optimize the plate scale. The pupil carousel and the filter wheel are at a temperature of ~ 10 K. The carousel contains eight aperture positions, four of which contain half wave plates (HWPs) for HAWC+ bands, an open aperture whose diameter is matched to the SOFIA pupil, and three aperture options meant only for instrument alignment tests.

After the pupil carousel, the light passes through a wire grid that reflects one component of linear polarization and transmits the orthogonal component to the detector arrays (R and T arrays, respectively—see [Figure 8-2](#)). The polarizing grid is heat-sunk to the HAWC+ 1 Kelvin stage.

To perform polarimetry observations, a HWP matched to the band-pass is rotated (usually through four discrete angles) to modulate the incident light and allow computation of the Stokes parameters. The total intensity can be measured simply by removing the HWPs from the optical path and using the open pupil position, then summing the signal from the R & T arrays.

The 64x40 HAWC+ detector array is composed of two co-mounted 32x40 subarrays from NASA/GSFC and NIST. The detectors are superconducting transition-edge sensor (TES) thermometers on membranes with a wide-band absorber coating. The detector array is indium bump bonded to a matched array of superconducting quantum interference device (SQUID) amplifiers, all cooled to an operating temperature of ~ 0.2 K in flight.

Figure 8-1.

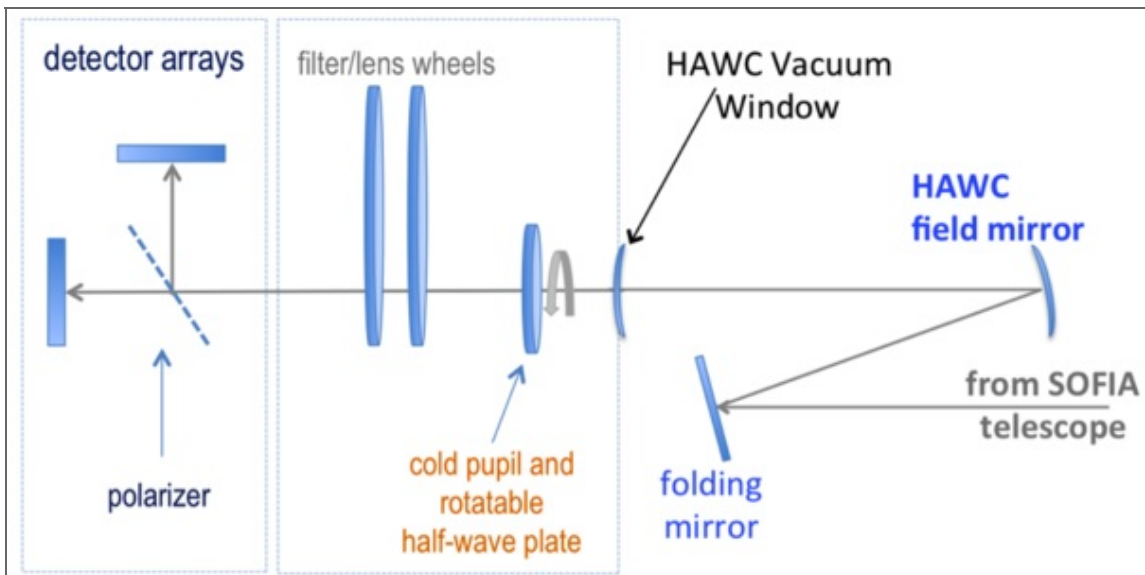


Figure 8-1. Schematic of the HAWC+ optics. Light from the SOFIA telescope is incident from the right. The field and folding mirrors are mounted on the HAWC+ cryostat but extend into the SOFIA Nasmyth tube. At the polarizing grid the light is split into two orthogonal components of linear polarization and detected at the two separate arrays.

Figure 8-2.

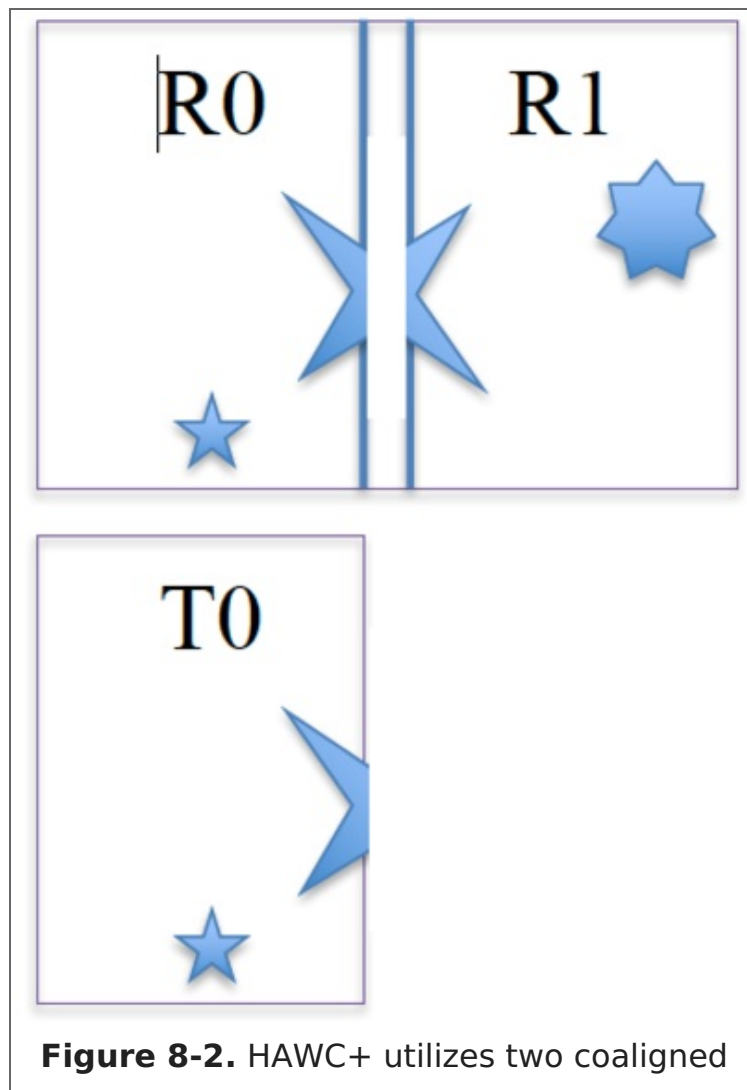


Figure 8-2. HAWC+ utilizes two coaligned

arrays of TES detectors, each array receiving polarized light from the source either by reflection (the R array) or transmission (the T array). The R array is populated with two 32x40 subarrays separated by 2.0 pixels, referred to as R0 (*top left*) and R1 (*top right*). The arrays are coaligned such that R0 and T0 (*bottom left*) observe the same patch of sky. Polarization observations are only supported using the R0 and T0 subarrays, and therefore observations are limited to the left half of the nominal field of view, or 32x40 pixels. Total intensity observations are supported using the combined R0 and R1 field of view, or 64x40 pixels with a 2.0 pixel gap between them.

[Return to Table of Contents](#)

8.1.2 Performance

The absorbing coatings on the HAWC+ detector arrays were optimized to produce about 50% efficiency across the wide (40–300 μm) range of bandpasses. The TESs were designed to optimize the sensor time constants and background power at which they saturate, with the goal being operation at both laboratory and stratospheric background levels. The final design includes a superconducting transition temperature of ~ 0.3 K and a detector yield of $> 50\%$. Measurements of detector noise show that their contribution to total measurement uncertainties is negligible such that noise levels are dominated by background photons from the atmosphere.

Measurements of the HAWC+ optical system in the laboratory are consistent with optical models, *and flight data have confirmed that the observations are diffraction limited at all wavelengths.*

Table 8-1 shows the Full Width Half Maximum (FWHM) of each bandpass as measured using Gaussian profiles, the finite size of the HAWC+ detectors, and a convolution across the measured filter bandpasses. The Instrumental Polarization (IP) of HAWC+ at each band is shown in terms of the normalized Stokes parameters, q and u , which were estimated using the observations of planets during several observing runs on November 2016 and May 2017. The IP is mainly derived from the tertiary mirror of SOFIA with the position angle of polarization perpendicular to the tertiary mirror direction. The filter transmission curves (text tables) are available as a [zip file](#) or individually from [Table 8-1](#).

For polarimetry observations, the current configuration of HAWC+ lacks a second T polarization state array; as such, the field of view is reduced to approximately half in the largest side of the array, providing a 32x40 pixel size rather than 64x40 pixels (the first element of the Field of View in [Table 8-1](#)). Total intensity observations are unaffected and can use the whole field of view via the R polarization state.

Table 8-1: Instrument Characteristics**Important: Sensitivity values were updated on June 15, 2018 to reflect final commissioning analysis based on Cycle 5 & Cycle 6 observations.**

Instrument Characteristics

Parameter	Units	Band A	Band C	Band D	Band E
Mean Wavelength (λ_0)	μm	53	89	154	214
Bandwidth ($\Delta\lambda$)	-	9.01	16.91	33.88	42.8
Beam Size (FWHM)	arcsec	4.85	7.8	13.6	18.2
Pixel Size ^a	arcsec	2.55	4.02	6.90	9.37
Total Intensity FOV	arcmin	2.8x1.7	4.2x2.7	7.4x4.6	10.0x6.3
Polarimetry FOV	arcmin	1.4x1.7	2.1x2.7	3.7x4.6	5.0x6.3
NESB ^b (photo)	$\text{MJy sr}^{-1} \text{h}^{1/2}$	18.8	6.3	1.6	0.8
MDCF ^c	mJy	250	300	154	214
Mapping Speed ^d	See footnote ^d	0.0027	0.029	1.1	7
MDCPF ^e	% Jy	40	20	21	24
IP ^f	q	-0.0154	-0.0151	0.0028	-0.0129
	u	-0.0030	0.0090	0.0191	0.0111
MIFP ^g	$\text{MJy sr}^{-1} \text{h}^{1/2}$	28,000	6,000	2,000	1,300
Response Curve		png file	png file	png file	png file
		txt file	txt file	txt file	txt file

^a The center-to-center spacing of the pixels; pixel sizes (the space taken up by the photon sensitive area) are smaller by 0.21 arcsec at 53 μm and 0.75 arcsec at 215 μm .

^b Noise Equivalent Surface Brightness for $S/N = 1$ into a single HAWC+ beam (FWHM given here).

^c Minimum Detectable Continuum Flux for a point source with $S/N = 4$ in a 900 second integration.

^d Real scan rate required to achieve a given an NESB. Units: $\text{arcmin}^2 \text{h}^{-1} (\text{MJy sr}^{-1})^{-2}$

^e Minimum Detectable Continuum Polarized Flux for a point source with a $S/N = 4$ in a

900 second integration.

^fInstrumental Polarization estimated using the observations of planets during several observing runs. The uncertainty of the instrumental polarization is smaller than 0.003 in both Stokes q and u .

^gMinimum total Intensity required to measure Polarization (MI_{fP}) to an uncertainty level $\sigma_p \leq 0.3\%$. All chop/nod and polarization overhead values have been applied to this value.

HAWC+ point source sensitivities were updated on June 2, 2017 and the values given here are based on the in-flight performance of the instrument. Note that values used in previous SOFIA observing cycles (Cycles 4 & 5) were estimates that contained an error (approximately a factor of two) in the expected point source sensitivity, so proposals should be updated accordingly for Cycle 6 before submission.

All photometric sensitivity estimates assume 100% observing efficiency without chopping and nodding. These values are pre-flight estimates and subject to change after the HAWC+ instrument has been commissioned. The USPOT time calculator will estimate the correct overhead values for NMC.

Additionally, analysis of data obtained on flights suggest the sensitivity may be lower than expected. The MDCF values will be correspondingly higher than the predicted pre-flight ones shown in [Table 8-1](#) and used in [Figure 8-4](#). The SOFIA webpages should be checked for the most current information.

Entries in blue represent predicted values; Band B is currently unavailable due to saturation in the band but may be offered as shared risk in future cycles.

[Return to Table of Contents](#)

8.1.2.1 Filters

HAWC+ can produce images using continuum bandpasses in either Total Intensity Imaging or Polarimetry Imaging configurations. In Polarimetry Imaging, the dual-beam nature of HAWC+ allows for the simultaneous measurement of both orthogonal lineal polarization components and obtain the Stokes parameters I , Q , and U . In Total Intensity Imaging, the sum of the R and T arrays provides the total intensity, Stokes I . As the HWP are used in Polarimetry Imaging, there is a slight loss of sensitivity as the HWP transmission is $< 100\%$ and additional overhead is required to account for rotating the HWP.

Both observing modes can utilize any one of five filters (however, to reiterate, Band B is not currently available). [Figure 8-3](#) shows transmission profiles including all filters for all bandpasses. The effective wavelengths and bandwidths averaged over the total filter transmission are given in [Table 8-1](#).

Figure 8-3.

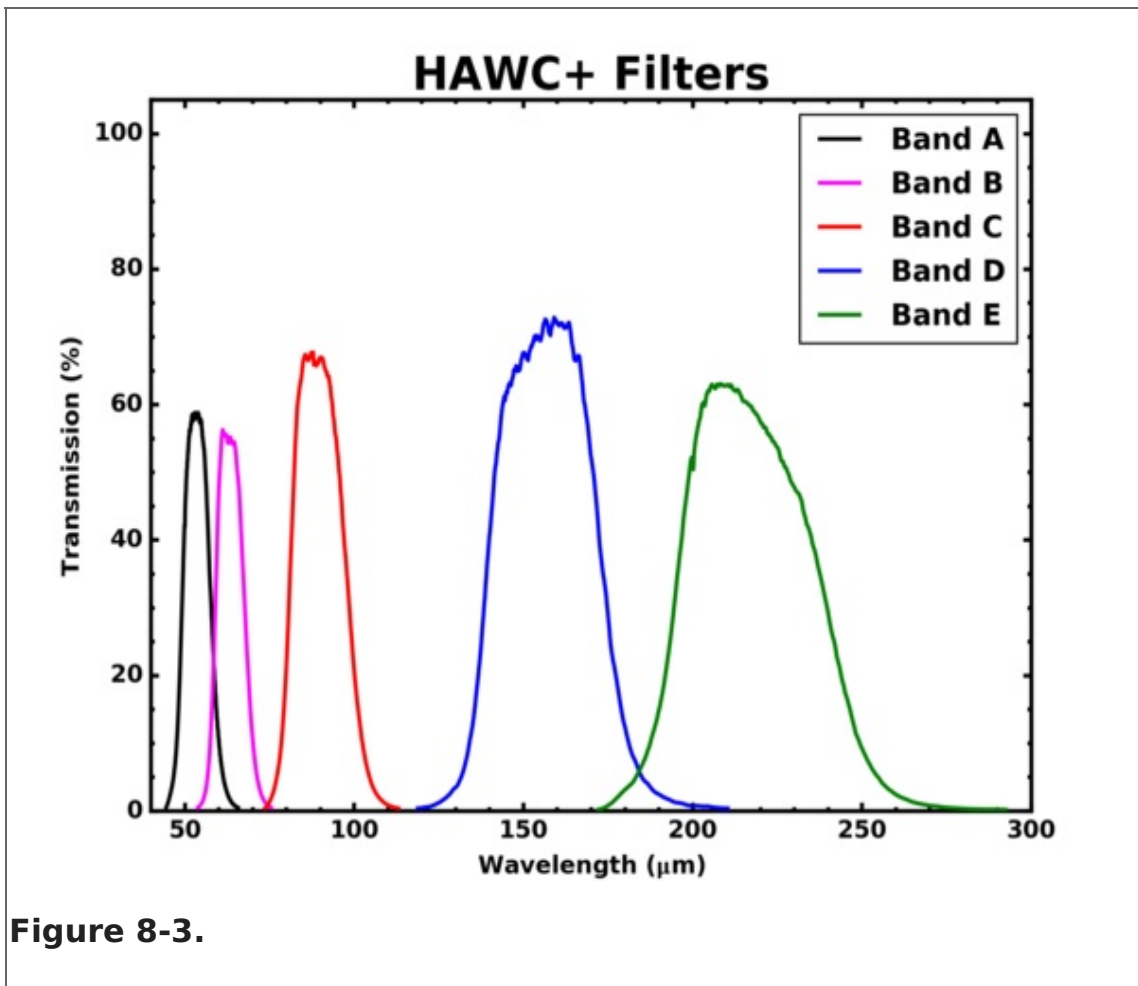


Figure 8-3.

[Return to Table of Contents](#)

8.1.2.2 Total Intensity Imaging Sensitivities

Observations with HAWC+ for measurements of Total Intensity can be performed using either on-the-fly scanning (OTFMAP, where the telescope moves continuously at rates of ~ 10 – 200 arcsec/second without chopping of the secondary mirror) or using rapid modulation (chopping ~ 5 – 10 Hz) of the secondary accompanied by slow nodding of the telescope. The chopping option consists of a two-position chop, parallel to the nod direction where the chop amplitude matches the nod amplitude (NMC).

[Figure 8-4](#) and [Table 8-1](#) present HAWC+ imaging sensitivities for point sources, surface brightness, and mapping speed through each bandpass. Surface brightness is measured in units of MJy/sr and is the intensity required for a $S/N = 1$ observation in a one-hour integration time averaged over a single HAWC+ beam. The Minimum Detectable Continuum Flux into a HAWC+ beam is that needed to obtain a $S/N = 4$ in 900 seconds of on-source integration time. [Figure 8-4](#) plots the MDCF for both observing modes OTFMAP and NMC where the latter follows from the former based on overheads related to chopping and nodding the telescope. NMC and OTFMAP are covered extensively in [Section 8.2](#).

Figure 8-4.

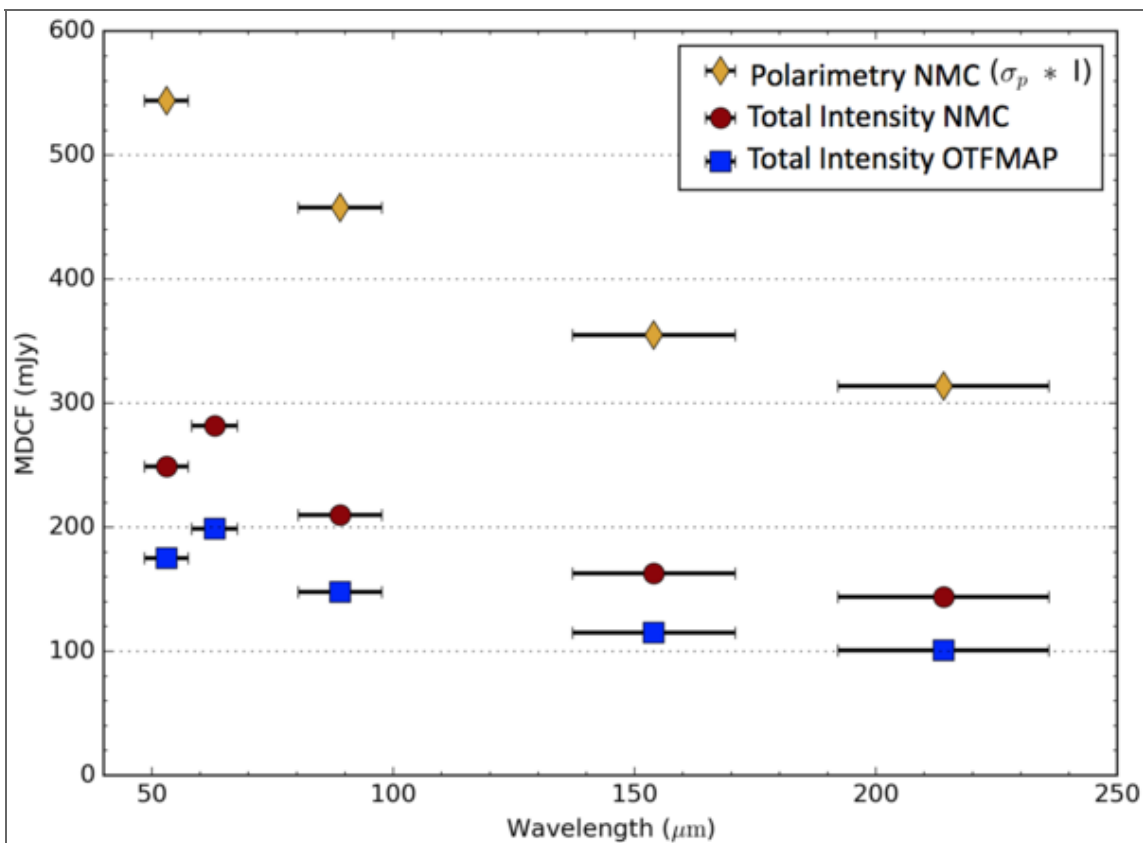


Figure 8-4. HAWC+ Sensitivity estimates in units of the Minimum Detectable Continuum Flux (MDCF) into a single HAWC+ beam. (Recall that the beam area changes with bandpass). Values plotted here take into account all expected overheads. For example, [Table 8-1](#) gives an MDCF of 57 mJy at 53 μm in OTFMAP, but is plotted here as 66 mJy to account for a 75% array detector yield. For Polarimetry, the plotted data show the polarized intensity $p \times I$, where p is the fractional polarization (not percent). Note: analysis of data obtained on flights suggest the sensitivity may be lower than expected. The MDCF values will be correspondingly higher than the predicted pre-flight ones shown in [Table 8-1](#) and used in Figure 8-3.

HAWC+ time estimates should be made using the on-line exposure time calculator, SITE. Note that integration times scale as shown in [Equation 8-1](#) and [Equation 8-2](#) from the values in [Table 8-1](#):

(Eq. 8-1)

$$t = \left(\frac{\text{NESB}}{\sigma} \right)^2$$

(Eq. 8-2)

$$t = \left(900 \text{ s} \right) \left(\frac{\text{NESB}}{\sigma} \right)^2$$

where t is the integration time and σ is the desired sensitivity for $S/N = 1$, each in the appropriate units. For OTFMAP, a useful sensitivity value is the mapping speed given in

Equation 8-3:

(Eq. 8-3)

$$M = \frac{d\Omega}{dt} = \frac{\gamma\Omega_{\text{array}}}{s^2}$$

where γ is related to the filling factor, Ω_{array} is the solid angle of the HAWC+ detector array, and s is some measure of the instrument sensitivity (e.g., MDCF or NESB). The values in [Table 8-1](#) are given for $S/N = 1$ in a one-hour integration time assuming $\gamma = 1$, while SITE and [Figure 8-3](#) use a more realistic value $\gamma = 0.75$. The time to map an area Ω ($\geq \Omega_{\text{array}}$) to a sensitivity level σ is given by [Equation 8-4](#):

(Eq. 8-4)

$$t = \frac{\Omega}{M\sigma^2}$$

Note that this scaling only applies to map areas larger than the array field of view.

Atmospheric transmission will affect sensitivity, depending on water vapor overburden as will telescope zenith angle and telescope emissivity. For the estimates in [Table 8-1](#) and [Figure 8-3](#) we use a precipitable water vapor of $7.3 \mu\text{m}$, a 50° zenith angle, and a telescope emissivity of 15%.

[Return to Table of Contents](#)

8.1.2.3 Polarimetry Imaging Sensitivities

HAWC+ contains four monochromatic HWPs. For Bands C, D, and E, the HWP thicknesses are matched to the bandpass filters. The thickness of the Band A HWP is matched to a wavelength between those of Bands A ($53 \mu\text{m}$) and B ($63 \mu\text{m}$), approximately $58 \mu\text{m}$. However, this slight mismatch should not introduce significant systematics into the system. For the pre-flight HAWC+ sensitivity estimate here, the total system polarization efficiency (HWP + polarizing grid + all other optics) is assumed to be 90% for all five passbands.

The polarization sensitivity σ_p follows from the imaging sensitivity σ_I so that [Equation 8-5](#) is true:

(Eq. 8-5)

$$\sigma_P = \frac{\sigma_I\sqrt{2}}{\eta_p I}$$

where I is the source intensity, η_p is the system polarization efficiency, and σ_p is measured in units of percent (%). The Minimum Detectable Continuum Polarized Flux (MDCPF) reported in [Table 8-1](#) is the value $\sigma_p \times I$ above, and follows from the total intensity MDCF. USPOT will add overhead values appropriate to NMC mode for polarimetry.

For Polarimetry Imaging, another useful quantity is the Minimum total Intensity required

in order to measure polarization (MIfP) to a given depth in a given time interval. Choosing $\sigma_p = 0.3\%$ allows a polarization $S/N = 3$ for a source polarization of 1%, a value not atypical of bright Galactic clouds and a likely lower limit for HAWC+ systematic uncertainties. [Table 8-1](#) lists these values for a one-hour integration time in units of surface brightness for an extended source where, unlike other values in [Table 8-1](#), all appropriate overhead values have been added.

HAWC+ time estimates should be made using the on-line exposure time calculator, SITE. Note that integration times scale as shown in [Equation 8-6](#) and [Equation 8-7](#) from the values in [Table 8-1](#):

(Eq. 8-6)

$$t = (1 \text{ h}) \left(\frac{\text{MIfP}}{I} \right)^2 \left(\frac{0.3\%}{\sigma_p} \right)^2$$

(Eq. 8-7)

$$t = (900 \text{ s}) \left(\frac{\text{MDCPF}}{4\sigma_p I} \right)^2$$

where t is the integration time and σ_p is the desired sensitivity for $S/N = 1$, each in the appropriate units.

A simple estimate for the polarization angle uncertainty is given by [Equation 8-8](#):

(Eq. 8-8)

$$\sigma_\varphi = \frac{180}{\pi} \frac{\sigma_p}{2p} [\text{degrees}]$$

Current best estimates for systematic uncertainties are 0.8% in percent polarization and 10° in polarization position angle.

[Return to Table of Contents](#)

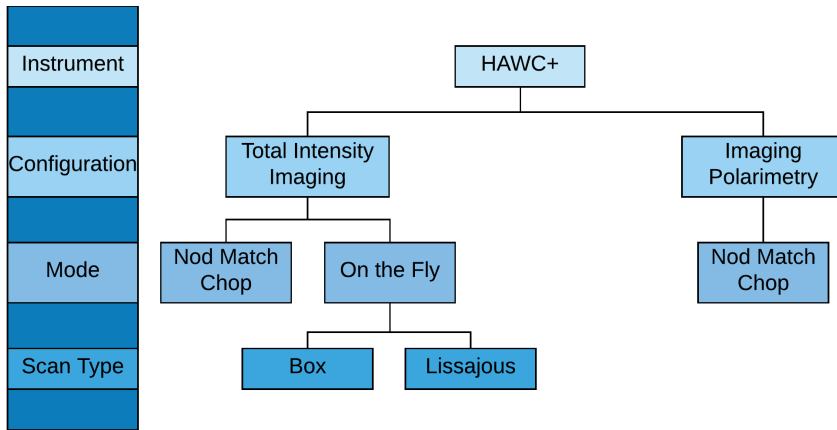
8.2 Planning Observations

Table of Contents

- [8.2 Planning Observations](#)
 - [8.2.1 Total Intensity Observations](#)
 - [8.2.1.1 On the Fly Mapping](#)
 - [8.2.1.1a Lissajous](#)
 - [8.2.1.1b Box](#)
 - [8.2.1.2 Nod Match Chop](#)
 - [8.2.2 Polarimetry Observations](#)
 - [8.2.2.1 Nod Match Chop](#)

Return to the Table of Contents for this section at any time by selecting [Return to Table of Contents](#). Users may also navigate through the entire Observer's Handbook by using the complete Table of Contents menu to the right.

8.2 Planning Observations

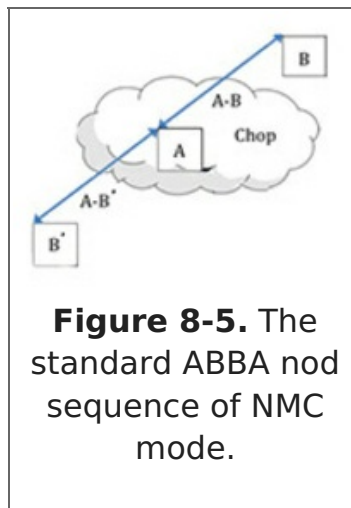


The HAWC instrument has two main observing configurations: Total Intensity Imaging and Polarization Imaging. The instrument also has two standard observing modes for imaging: the Nod Match Chop (NMC) mode combines traditional chopping with nodding and On the Fly Mapping (OTFMAP) mode keeps the secondary mirror fixed as the telescope primary is scanned across the source. The NMC observing mode is used for polarization observations; this mode includes chopping and nodding cycles in multiple half wave plate (HWP) positions.

The standard NMC mode is a subset of the standard two-position chopping with nodding mode (C2N). NMC consists of several steps, listed below and illustrated in [Figure 8-5](#).

1. *Chop*, where the secondary mirror of the telescope is moved at some frequency and angle.
2. *Nod*, where the telescope nods back and forth, each chopper beam being placed on the desired source.
3. *Dither*, which is a set of Nods at small offsets on the sky (nominally four positions), with each position having a Chop/Nod observation taken.

Figure 8-5.



Total Intensity observations with OTFMAP mode produce a continuous telescope motion with a two choices of pattern shape, the sizes of which are selected by the proposer. The first pattern (Box) is a series of linear scans used to map some rectangular region on the sky. The second pattern (Lissajous) is a curvilinear shape meant to cover a small region whose size is less than the array field of view.

[Return to Table of Contents](#)

8.2.1 Total Intensity Observations

8.2.1.1 On the Fly Mapping

In OTF mode, the secondary mirror remains stationary on the optical axis of the telescope while the telescope assembly itself slowly moves with respect to the sky. This scan motion modulates the celestial source with respect to the atmosphere in a manner similar to chopping the secondary mirror. Scan rates must reach (~ 2 Hz) \times (HAWC+ beam width) in order to remove the source from the atmospheric background. This implies rates ~ 10 – 80 arcseconds per second depending on the bandpass.

In order to ensure absolute flux calibration in this mode, observers must carefully plan observations so that some of the mapped region contains no extended emission from the science target. Otherwise, one can only measure a differential flux with respect to the lowest measured intensity level. Further removal of residual atmospheric signal is performed by removing common-mode noise observed in all HAWC+ detectors. This averaging amounts to a spatial filter with size equal to the HAWC+ FOV. Therefore, while large maps may be necessary to reach a true zero-intensity level, users should be aware that one cannot also recover all spatial scales in a given region.

HAWC+ offers two scan types for OTFMAP scan patterns: Lissajous and Box. Lissajous scans are recommended for sources smaller than the HAWC+ field of view (FOV) at a given bandpass, while Box scans (analogous to traditional raster scanning methods) are more efficient at mapping large areas several times the FOV. The patterns in [Figure 8-6](#) show the two-dimensional location of the array center during the progression of a scan, with Lissajous scans depicted in the two top images and Box scans shown in the two bottom images. Two-dimensional scans are necessary in order to reconstruct all spatial scales in a map. The Lissajous scans are two-dimensional by definition, however Box scans require multiple scans, even in the case where a source fits completely in the HAWC+ FOV. The secondary (or cross) scan direction of a Box scan should be rotated with respect to the initial scan (orthogonal scans are best,

although not absolutely necessary).

Figure 8-6.

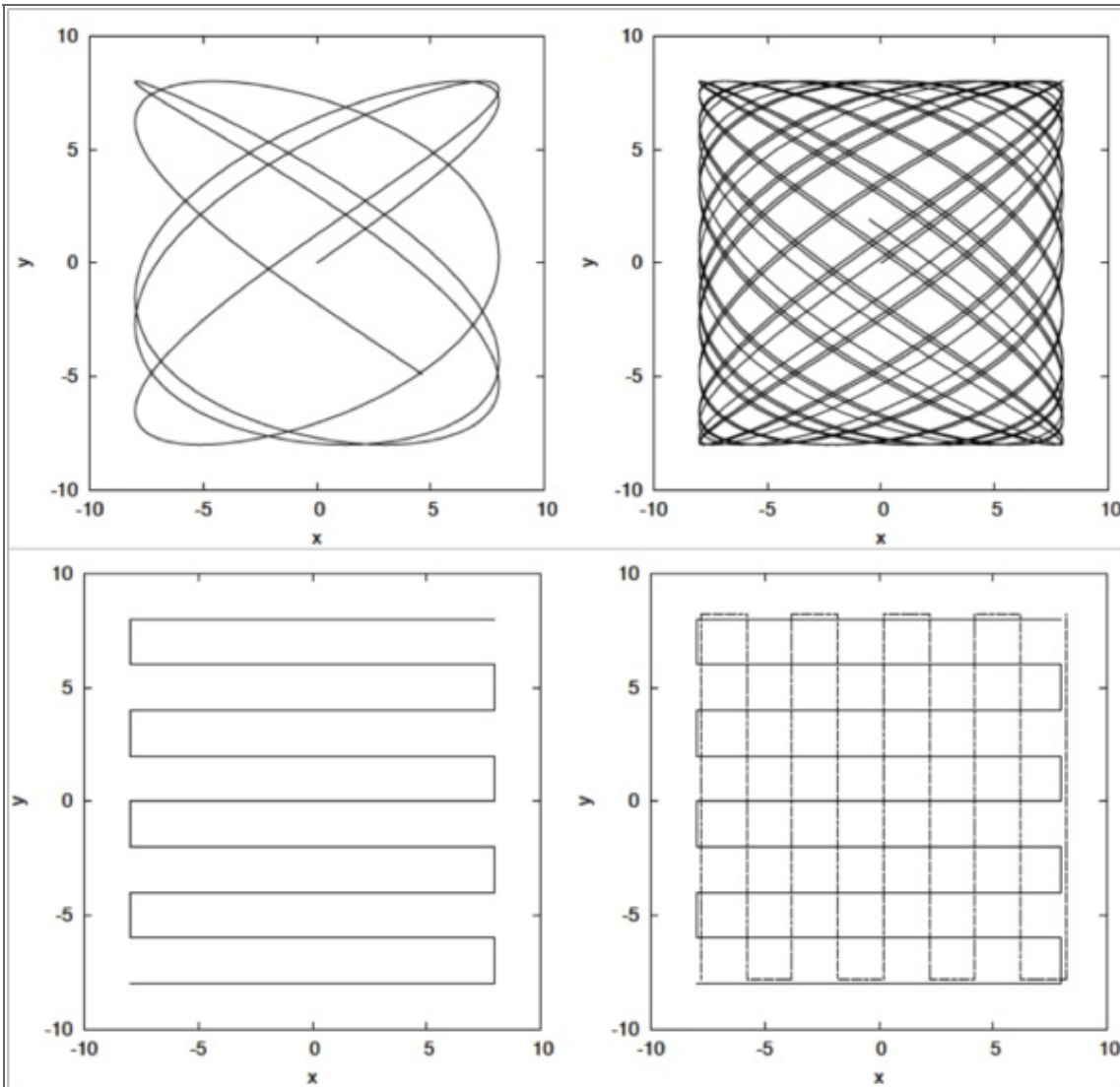


Figure 8-6. Example scan patterns for HAWC+ OTFMAP mode. These patterns show the location of the central array pixel, which moves along the paths at a user-defined rate. The upper panels are Lissajous patterns. The top-left panel is shortly after starting an integration, while the top-right panel is after a longer time period. The lower-left panel shows a series of linear scans used to cover a larger region. The lower-right panel also shows the required cross-scan in the case of linearly scanned areas. Plots taken from Kovács (2008).

While proposers must request an area for scan mapping, they do not need to specify any specific pattern in Phase I proposals. Successful proposers will work with a SOFIA Support Scientist to choose an optimal scan pattern and strategy for their observations. For the purposes of the proposal, scan map time estimates should be made using the sensitivity estimates in [Table 8-1](#). For sources smaller than the HAWC+ FOV, use the MDCF or NESB. For larger maps one may use the Mapping Speed.

Scan durations shorter than 10 min are recommended to ensure the stability of continuous OTFMAP observations for large periods of time. If a given map area and sensitivity cannot be achieved in that time, then multiple pointing positions should be

used.

[Return to Table of Contents](#)

8.2.1.1a Lissajous

In Lissajous observations, the telescope is driven to follow a parametric curve at a non-repeating period; as the scan progresses longer in time, more and more of the area defined by a scan amplitude will be covered. *As commissioning of HAWC+ progresses, this sequence will be refined and may include additional calibration observations during the sequence described.*

Figure 8-7 demonstrates the actual scan modes used in flight. The white box shows the Total Intensity FOV, the orange line shows the actual path as taken by the telescope, and the background images are the resulting image after the scan data is reduced.

Figure 8-7.

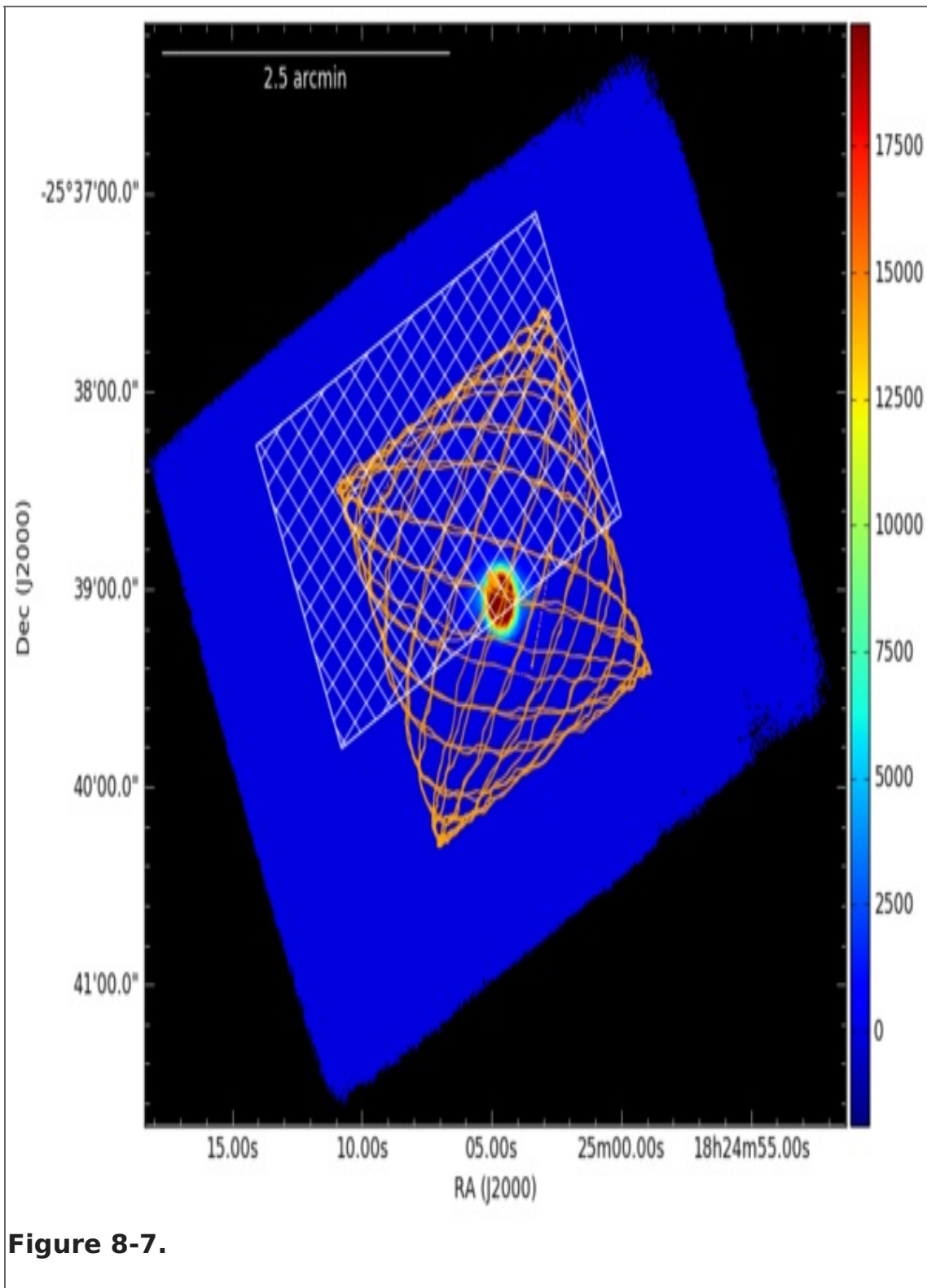


Figure 8-7.

[Return to Table of Contents](#)

8.2.1.1b Box

In Box scans, the telescope is driven in a linear fashion at the specified rate in one direction for the given length and then moved perpendicularly before scanning in the reverse direction—similar to how one would mow a very large lawn. This is continued until the desired area is covered, after which the process repeats in the perpendicular direction to cross the same areas in the perpendicular direction. For optimal reduction and coverage, three scans are performed, each at a slightly different starting angle to improve coverage and provide reduction robustness against systematic effects. *As commissioning of HAWC+ progresses, this sequence will be refined and may include*

additional calibration observations during the sequence described.

Figures 8-8, 8-9, and 8-10 demonstrate the actual scan modes used in flight. The white box shows the Total Intensity field of view, the orange line shows the actual path as taken by the telescope, and the background images are the resulting image after the scan data is reduced.

Figure 8-8.

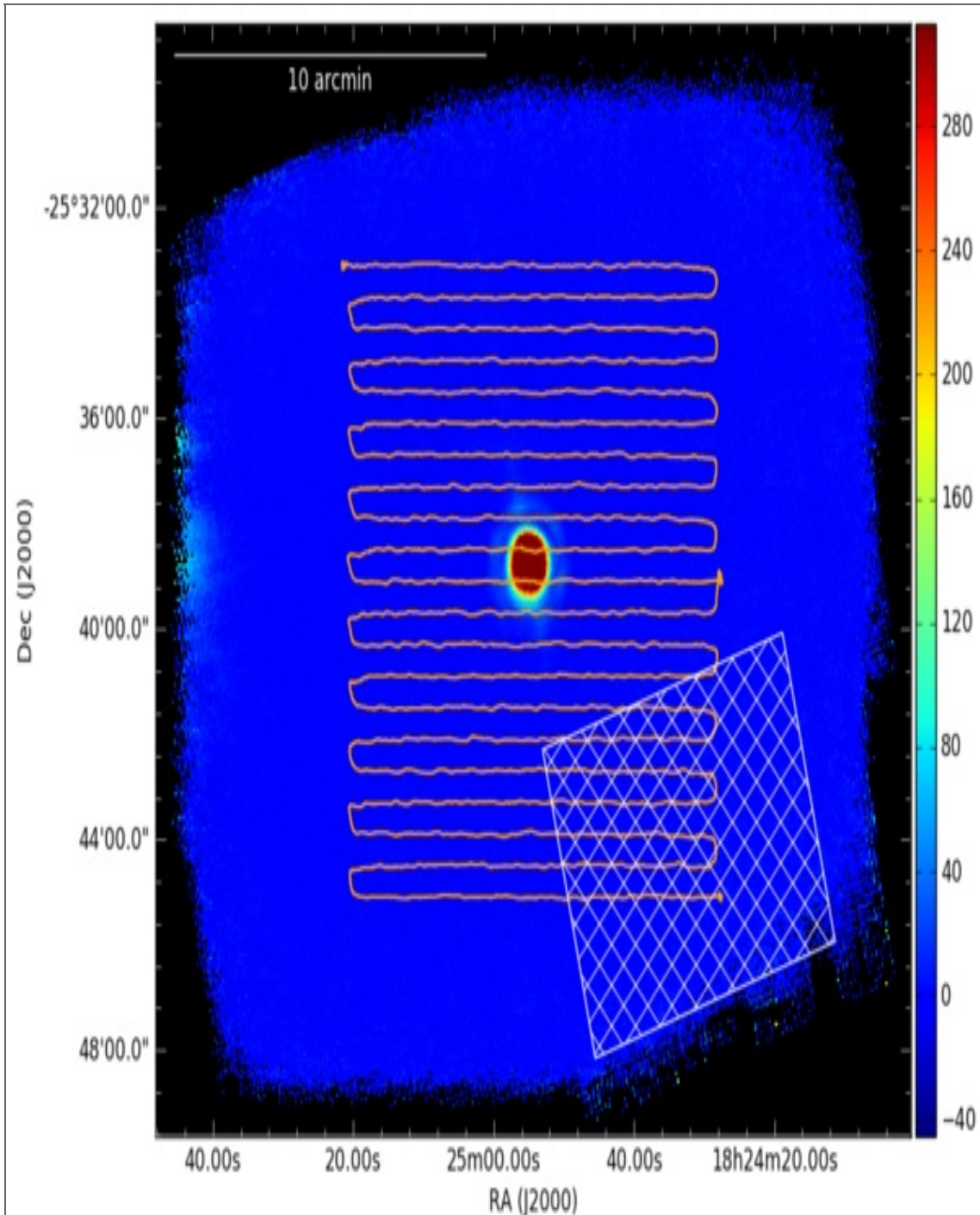


Figure 8-8. The scan starts at the bottom right, pauses midway through to obtain an estimate of tracking performance (the orange dot on the middle right) and then proceeds until the end.

Figure 8-9.

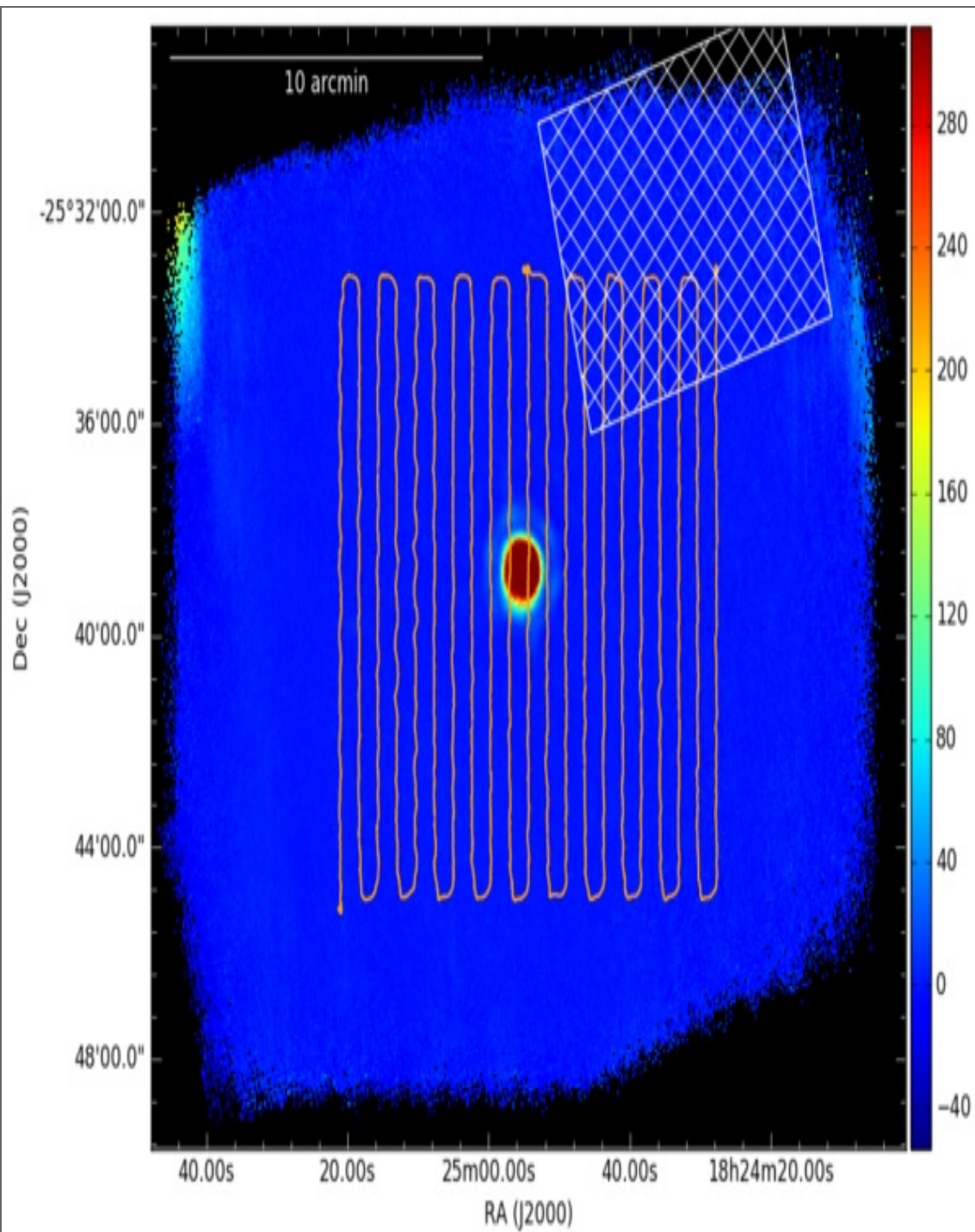


Figure 8-9. The scan starts at the upper right, pauses midway through to obtain an estimate of tracking performance (the orange dot on the middle of the top) and then proceeds until the end. The two directions are then combined to obtain the image below.

Figure 8-10.

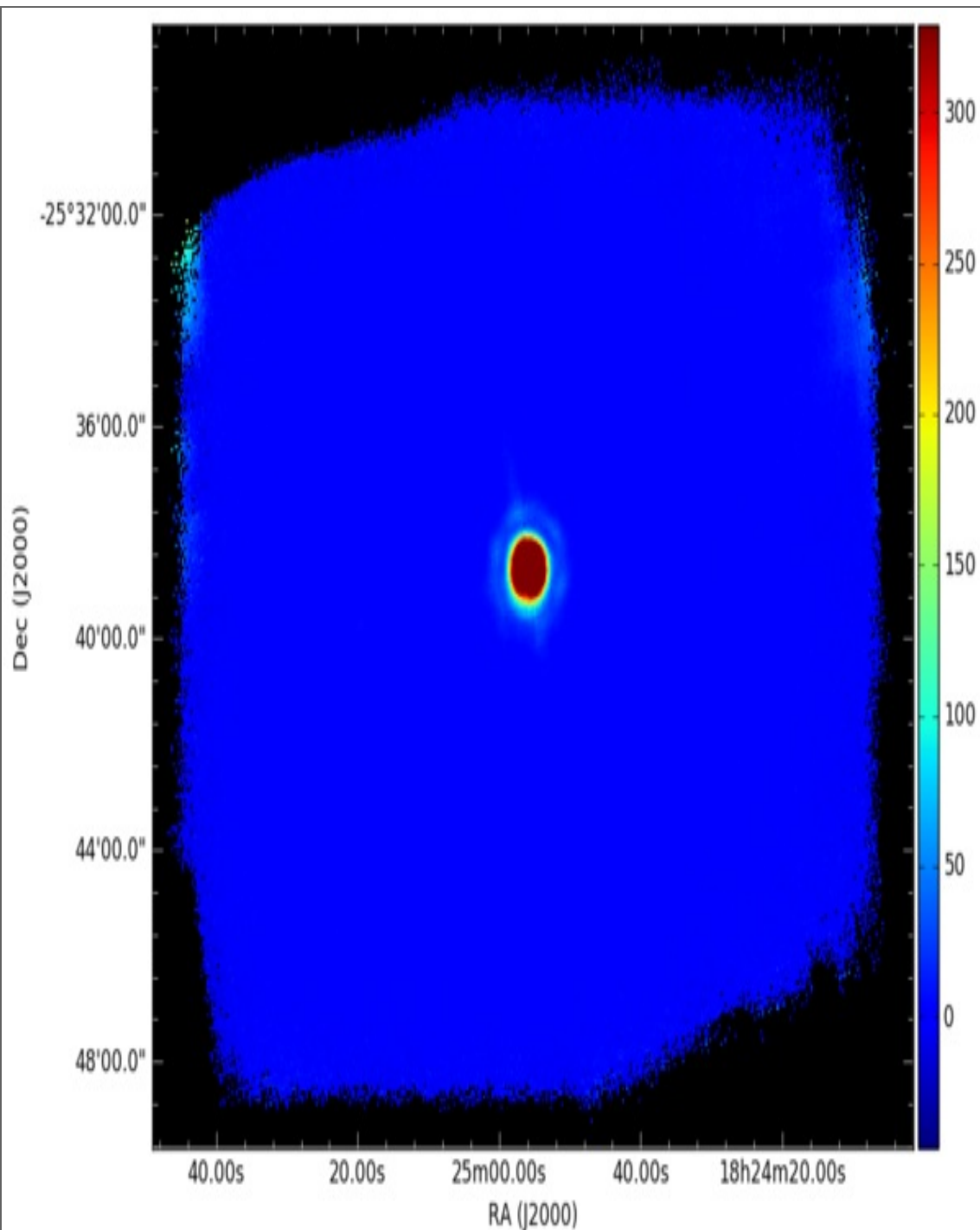


Figure 8-10. The two directions from Fig.8-7 are then combined to obtain this image.

[Return to Table of Contents](#)

8.2.1.2 Nod Match Chop

In NMC mode, four dither points are created symmetrically about the central object coordinates; an example is given in [Figure 8-11](#). At each dither position, chopping is started at the given throw and angle and the telescope is noded between two symmetrically located points 180 degrees separated from each other (positions A and B). *As commissioning of HAWC+ progresses, this sequence will be refined and may include additional calibration observations during the sequence described.*

NMC mode observations, are very time intensive and are subject to large observational overheads waiting for the telescope and/or secondary mirror assembly to complete

chop/nod/dither movements. Estimated overheads before first flights were purposefully large (factors of 10!) and these large overhead factors remain in USPOT. As such, it is recommended that observers consider utilizing OTFMAP mode for Total Intensity observations, which provides better sensitivity and smaller overheads.

If the source has an angular extent larger than the HAWC+ FOV in NMC mode, or larger than can be accommodated in a 10 minute OTFMAP, the central position of each HAWC+ field must be specified, with due consideration of the desired overlap of the individual frames. For mosaic observations, proposers should ensure that they request the total integration time required for all fields.

Figure 8-11.

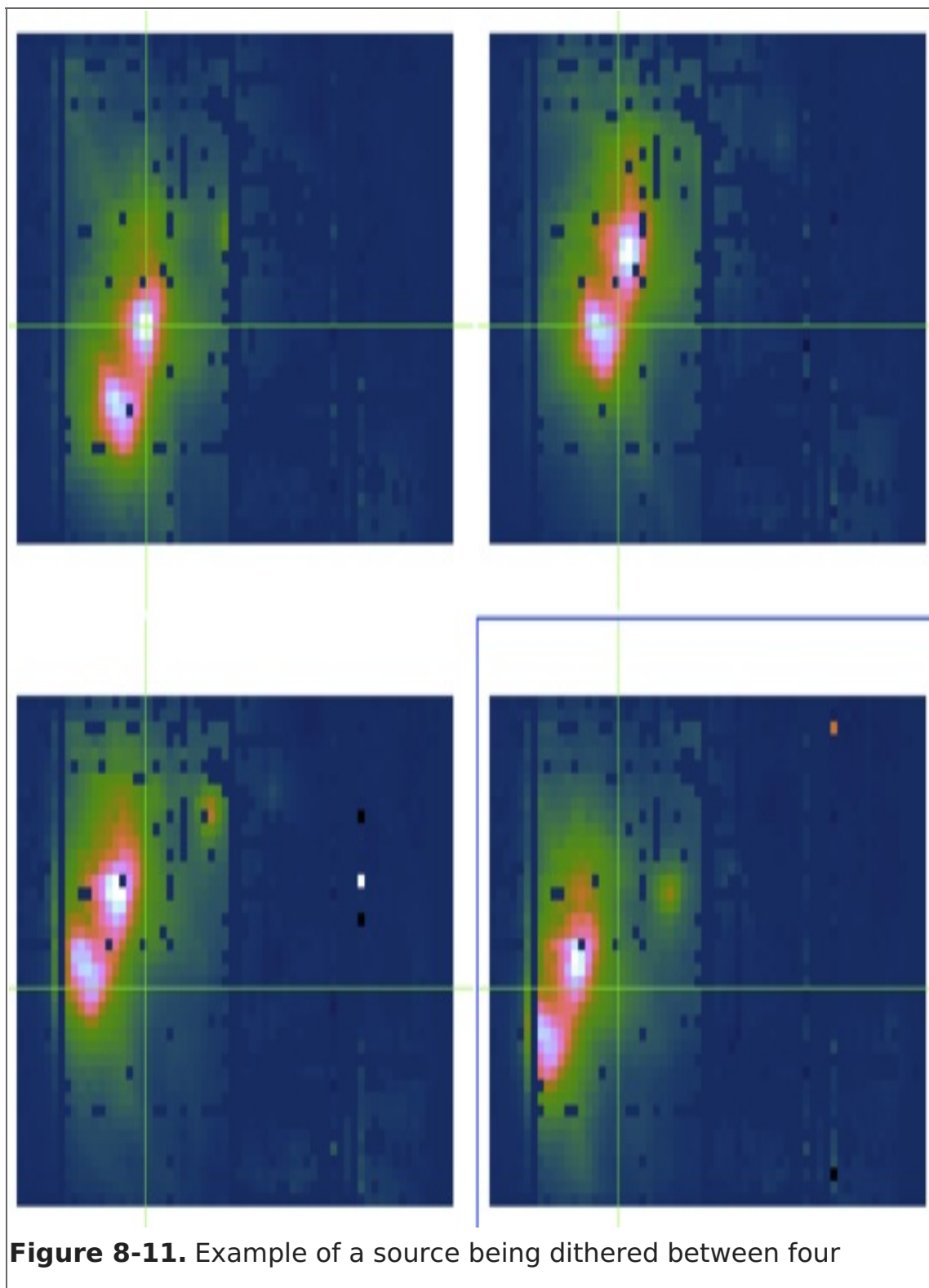


Figure 8-11. Example of a source being dithered between four

positions. The green crosshairs give the position of one of the sources and is at the same physical location for each image, showing the image movement.

[Return to Table of Contents](#)

8.2.2 Polarimetry Observations

For Cycle 6, HAWC+ polarization observations may only be performed using the NMC observing mode. In this mode, four standard NMC observations are performed, one at each of four angles of the HWP (relative angles 0, 22.5, 45, and 67.5 degrees). This is followed by dithering, where the HWP cycle is repeated again for a total of four dither positions. We currently estimate an additional overhead of 90% efficiency associated with moving the HWP between positions. This has been incorporated into polarization sensitivities in [Figure 8-3](#). The minimum time for a single polarization NMC observation with dithering is ~20 min.

As in the case of Total Intensity NMC, chopping into regions of bright, extended flux must be carefully avoided. Additionally, the polarization state of that reference flux must be considered in both percent polarization and angle. Typically, neither of these values will be known for HAWC+ observations (although proposers may want to consult the latest Planck data release). This polarized reference beam will produce additional systematic uncertainties in the data. In the case where the source and reference beam have the same polarization level, the systematic polarization uncertainty is linearly proportional to the reference-to-source intensity ratio. For further discussion, see Schleuning et al. (1997) and Novak et al. (1997).

If the source has an angular extent larger than the HAWC+ FOV in NMC mode, the central position of each HAWC+ field must be specified, with due consideration of the desired overlap of the individual frames. For mosaic observations, proposers should ensure that they request the total integration time required for all fields.

[Return to Table of Contents](#)

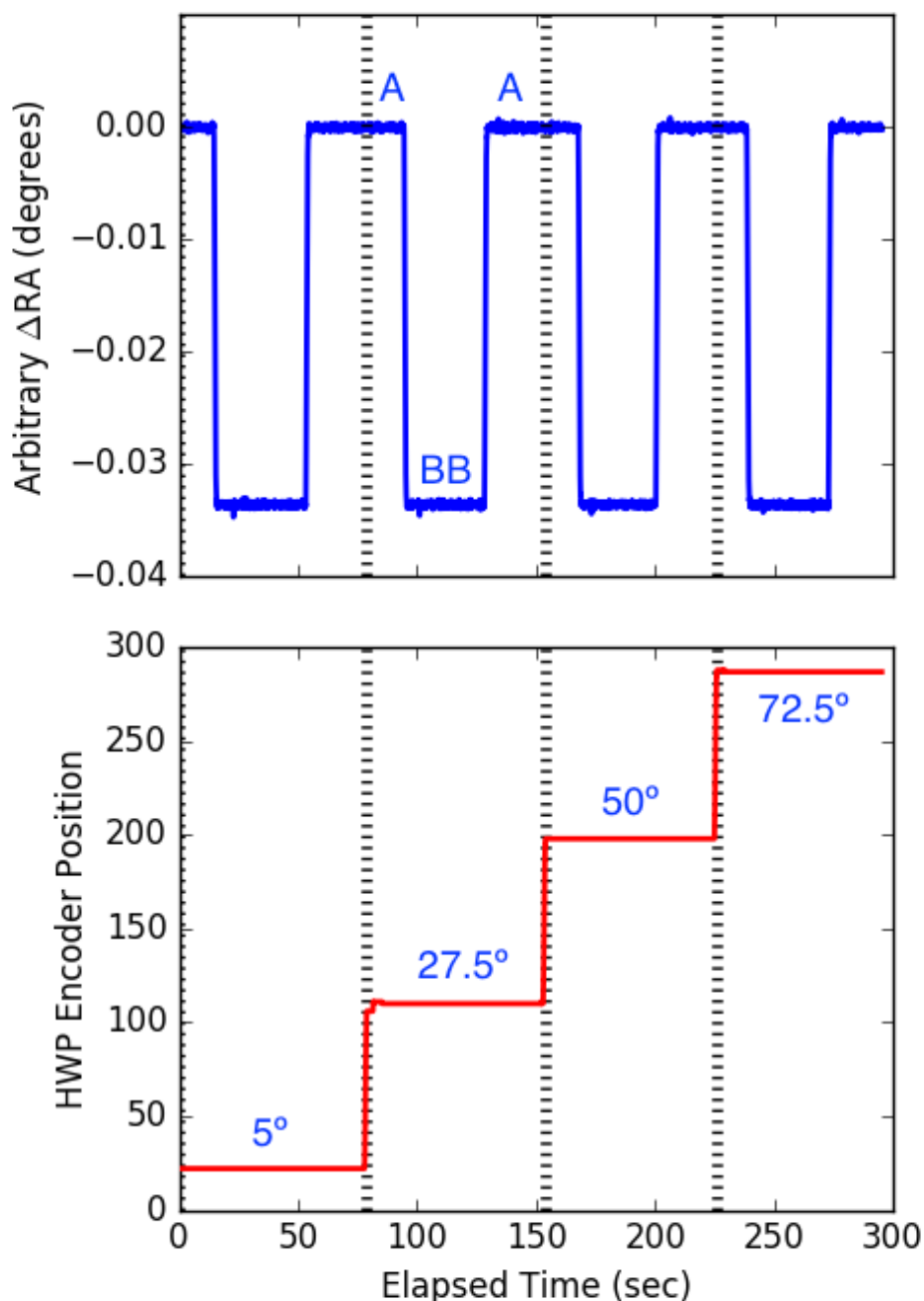
8.2.2.1 Nod Match Chop

In NMC mode, four dither points are created symmetrically about the central object coordinates. At each dither position, chopping is started at the given throw and angle and the telescope is noddied between two symmetrically located points 180 degrees separated from each other (positions A and B). Observations are performed in sequence at position A, then B, then B again, and back to position A. After one of these ABBA nod sequences, the HWP is rotated to the next angle; this continues until the HWP has gone through four angles, after which the telescope moves to the next dither position and repeats. *As commissioning of HAWC+ progresses, this sequence will be refined and may include additional calibration observations during the sequence described.*

[Figure 8-12](#) below shows both the change in source RA (illustrating the noddied of the source) and the half-wave plate angle for a single dither position of a polarization sequence. The dashed lines denote the completion of a half-wave plate observing sequence. This same sequence (four half-wave plate angles) is repeated for each dither

position to move the source appreciably and assist in the correction of bad/missing pixels. The source is being chopped during this entire sequence (and accounts for the thickness of the blue source RA line) but is not specifically highlighted here. The standard ABBA nod sequence and the half-wave-plate angles are highlighted.

Figure 8-12.



NMC mode observations, are very time intensive and are subject to large observational overheads waiting for the telescope and/or secondary mirror assembly to complete chop/nod/dither movements. Estimated overheads before first flights were purposefully large (factors of 10!) and these large overhead factors remain in USPOT.

[Return to Table of Contents](#)

9. HIPO

- 9. HIPO
 - 9.1 [Specifications](#)

- 9.1.1 Instrument Overview
 - 9.1.1.1 Design
 - 9.1.1.2 Angular Resolution
 - 9.1.1.3 Filter Suites
- 9.1.2 Performance
 - 9.1.2.1 Imaging Sensitivities
 - 9.1.2.2 Sensitivity Spreadsheet
- 9.2 Planning Observations

9.1 Specifications

Table of Contents

- 9.1 Specifications
 - 9.1.1 Instrument Overview
 - 9.1.1.1 Design
 - 9.1.1.2 Angular Resolution
 - 9.1.1.3 Filter Suite
 - 9.1.2 Performance
 - 9.1.2.1 Imaging Sensitivities
 - 9.1.2.2 Sensitivity Spreadsheet

Return to the Table of Contents for this section at any time by selecting [Return to Table of Contents](#). Users may also navigate through the entire Observer's Handbook by using the complete Table of Contents menu to the right.

9.1. Specifications

9.1.1 Instrument Overview

IMPORTANT: *The High-Speed Imaging Photometer for Occultation (HIPO) is not offered for Cycle 6. As stated in the Cycle 6 Call for Proposals, "The High-speed Imaging Photometer for Occultation (HIPO) is not offered through this call, either stand-alone or in combination with FLITECAM. The instrument is potentially available through use of the remaining Guaranteed Time Observations assignment of the PI. High-speed visual photometry is still possible on SOFIA using the Focal Plane Imager Plus (FPI+)." The information presented in this chapter should be used for reference only.*

The **H**igh **S**peed **I**maging **P**hotometer for **O**ccultations (HIPO) is a special-purpose science instrument for SOFIA that is designed to provide simultaneous high-speed time resolved imaging photometry at two optical wavelengths. It is possible to mount HIPO and FLITECAM on the SOFIA telescope simultaneously, called the FLIPO configuration, to allow data acquisition at two optical wavelengths and one near-IR wavelength. HIPO has a flexible optical system and numerous readout modes, allowing many specialized observations to be made. The instrument characteristics required for our proposed scientific pursuits are closely aligned to those needed for critical tests of the completed SOFIA Observatory, and HIPO has been used heavily for these tests. The general design and performance goals of the instrument are described in Dunham et al. (2004, SPIE, 5492, 592). Additional references are available on the [HIPO web page](#).

The primary scientific use of HIPO is for observing stellar occultations. In a stellar occultation, a star serves as a small probe of the atmospheric structure of a solar system

object or the surface density structure of a planetary ring or comet. Such observations provide information at high spatial resolution that would otherwise require a space mission to obtain. This work makes use of SOFIA's mobility, freedom from clouds, and near-absence of scintillation noise to provide the best possible occultation data.

The low atmospheric scintillation in airborne photometry gives HIPO the potential to detect P-mode stellar oscillations in sunlike stars and will provide excellent photometry of stellar transits by extrasolar planets. HIPO will be available for observers use on a collaborative basis, and potential observers should [contact](#) the PI prior to proposing to ensure that the proposed observations are feasible, that they make the best use of HIPO's capabilities, and that the proposal is as strong as possible.

[Return to Table of Contents](#)

9.1.1.1 Design

The HIPO optical system is reconfigurable to meet its varied requirements. It incorporates two dichroic beamsplitters, one to divert the infrared beam to FLITECAM (if mounted) and one to split the red and blue sides of the HIPO optical paths. Either or both of these may be removed if desired. It is also possible to move either CCD so it is placed directly at the optimal SOFIA focal plane for highest spatial resolution and throughput. The optical design is described in detail in Dunham (2003, SPIE, 4857 62).

The 8-position filter wheels are located near the pupil image formed by the collimator optics. Two positions in the red CCD's filter wheel are normally used for Shack-Hartmann lenslet arrays, but these may be replaced if necessary for a particular observation. We have contemplated adding grism capability to HIPO but have not yet carried this out.

The region between the mounting flange and the gate valve on the telescope can be evacuated to reduce image degradation due to density fluctuations in this region of the optical path. When this is done a window is installed at the location of the gate valve.

HIPO provides a number of CCD readout modes as described in Dunham et al. (2008, SPIE, 7014, 70144Z). The most commonly used are the single frame mode and a frame transfer time series (basic occultation) mode with readout frequency up to 50 Hz. A variety of readout rates are available allowing the observer to optimize the subframe size, speed, noise, full well, and linearity tradeoff for a particular event. This is also discussed together with HIPO data format details in the HIPO Data Cycle System Software Interface document.

[Return to Table of Contents](#)

9.1.1.2 Angular Resolution

The primary HIPO detectors are e2v CCD47-20 1024x1024 pixel frame transfer CCDs with plate scales of 0.33x0.33 arcsec pixels at low resolution and 0.05x0.05 arcsec pixels at high resolution. The HIPO field of view (FOV) is a 5.6 arcmin², the 8 arcmin diagonal of which corresponds to the 8 arcmin diameter SOFIA FOV. Pixels will normally be binned to best match the seeing blur size and to reduce the effect of read noise. The high resolution mode includes no re-imaging optics. It is possible to replace one or both of the CCD47's with CCD67's having half the field of view, twice the pixel size, and much faster imaging operation.

The HIPO image quality is dominated by seeing and image motion effects. The red curve in Figure 9-1 is the nominal image quality expected at first light for SOFIA, based on the expected shear layer seeing, the as-built optical performance, and 2 arcsec rms image motion. The blue curve represents the ultimate combined optical quality and image motion requirement (80% encircled energy in a 1.6 arcsec diameter circle) convolved with the expected shear layer seeing. Also plotted are representative photometry aperture diameters likely to be used for processing occultation frames under both conditions described above. The image motion assumed is larger than will be experienced when observing at high frame rates. Occultation photometry will be extracted from data frames using effective aperture sizes comparable to the 80% enclosed light diameter plotted here.

Figure 9-1.

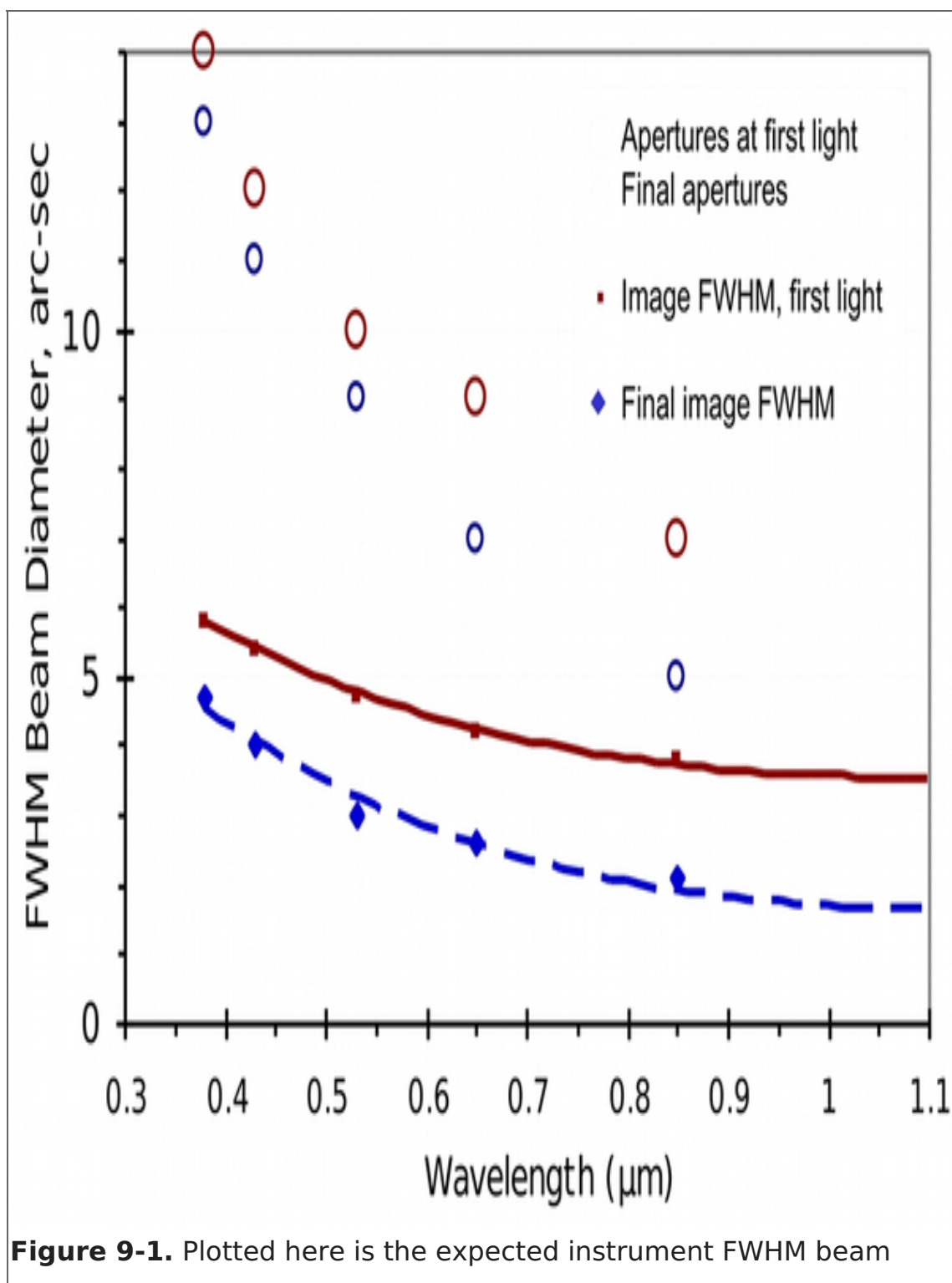


Figure 9-1. Plotted here is the expected instrument FWHM beam

diameter as a function of wavelength.

[Return to Table of Contents](#)

9.1.1.3 Filter Suite

Wavelength range: 0.3–1.1 μm . HIPO currently includes standard Johnson UBVRI and Sloan Digital Sky Survey u' g' r' i' z' filters. Occultation observations will normally be unfiltered for events involving faint stars or will use specialized filters such as the narrow-band methane filter ($\lambda_c \sim 0.89 \mu\text{m}$) for events with bright stars. Additional custom filters will be added as needed for specific events.

HIPO uses a dichroic reflector to separate its blue and red channels. Two dichroics are currently available with transition wavelengths of 0.575 and 0.675 μm respectively. Other dichroics will be added as necessary for specific events. The 0.575 μm dichroic transition wavelength is close to the boundary between the Sloan g' and r' filters and the 0.675 μm transition is close to the boundary between the Sloan r' and i' filters.

HIPO has been upgraded recently with the addition of deep depletion CCDs having a multi-layer antireflection coating. This provides higher quantum efficiency across the board with much higher quantum efficiency at longer wavelengths. It also nearly eliminates fringing at longer wavelengths. The figures below reflect this improvement.

Below are two plots (Figures 9-2 and 9-3) of the HIPO total system throughput including atmospheric extinction, SOFIA telescope throughput, and instrument throughput for each of the available bandpasses. The first figure shows the total system throughput for the Johnson and methane filters with the 0.575 μm dichroic. The second figure shows the Sloan filters with the 0.675 μm dichroic. These figures assume that the FLITECAM dichroic beamsplitter is not installed. The very low total system throughput for HIPO is due to the dichroic tertiary mirror in the telescope. The long-planned aluminized tertiary will increase our throughput by a factor of nearly 3, on average, when it becomes available. The corresponding throughputs are presented in Figures 9-4 and 9-5.

Figure 9-2.

Figure 9-2.

A rectangular box with a thin black border, intended for the content of Figure 9-2. The box is currently empty.

Figure 9-3.

Figure 9-3.

A rectangular box with a thin black border, intended for the content of Figure 9-3. The box is currently empty.

Figure 9-4.

Figure 9-4.

Figure 9-5.

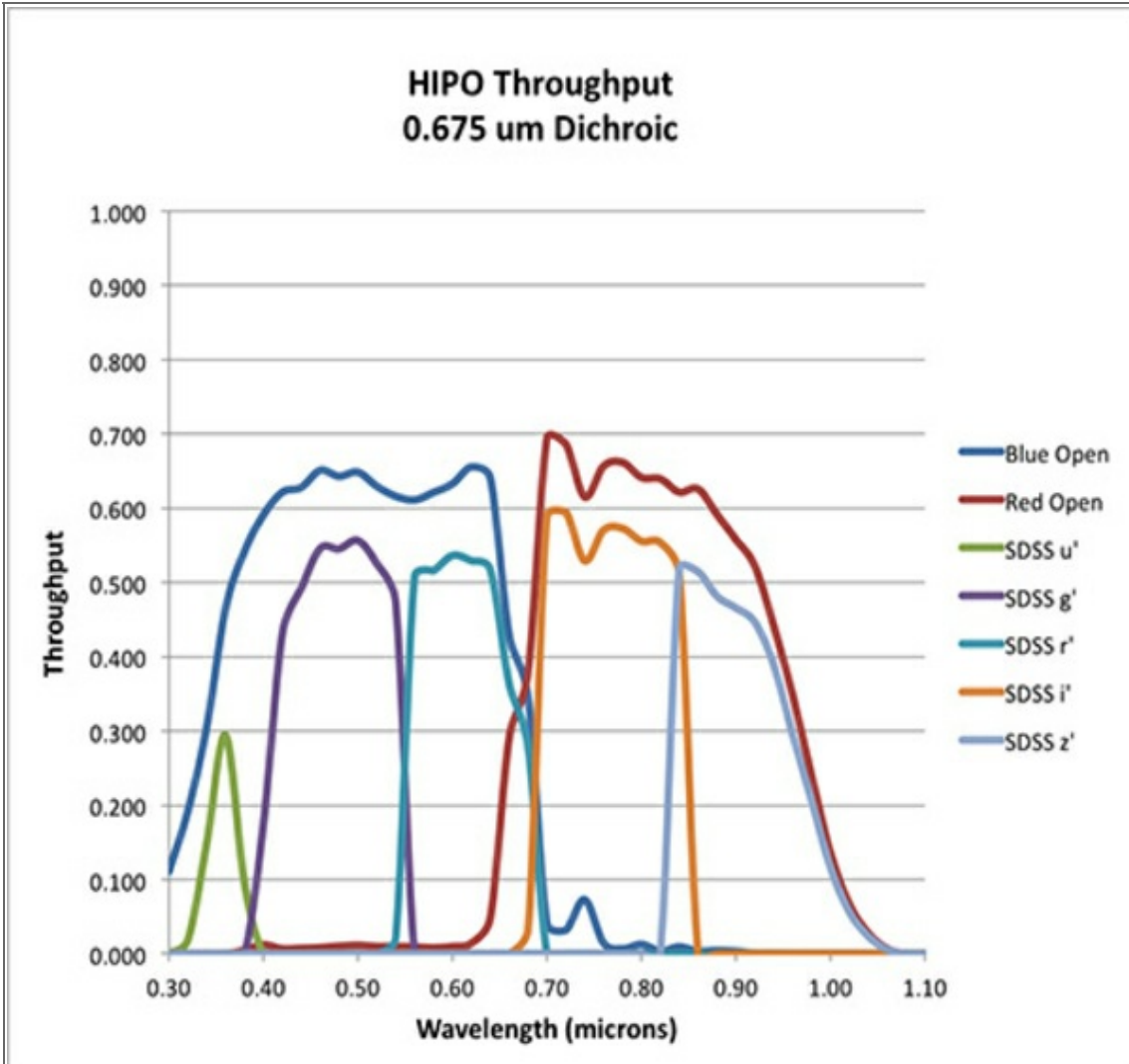


Figure 9-5.

[Return to Table of Contents](#)

9.1.2 Performance

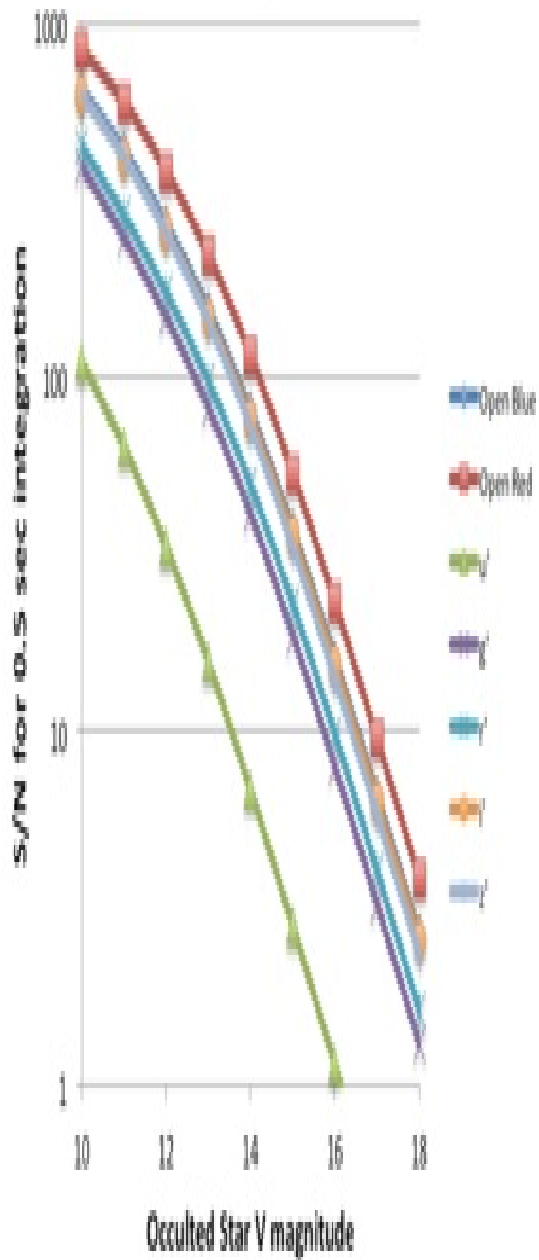
9.1.2.1 Imaging Sensitivities

Plotted in Figure 9-6 below are HIPO first-light sensitivities for several representative cases. These figures assume that the FLITECAM dichroic beamsplitter is not installed. The upper figures correspond to occultations by Pluto or Triton while the lower two are for the case of a very faint occulting object. The left and right figures are for 0.5 sec and 50 ms integrations, respectively. Each figure shows S/N for no filter (dichroic only) and for the 0.675 μm dichroic plus standard Sloan filters. The dichroic transition is assumed to occur from 0.57 and 0.67 μm.

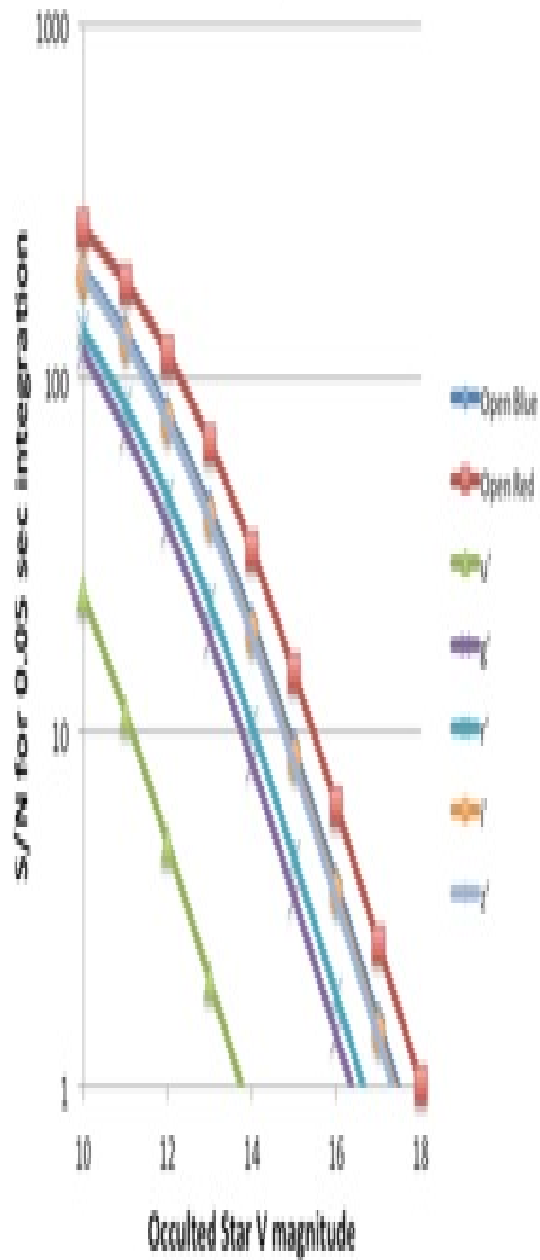
Figure 9-6.



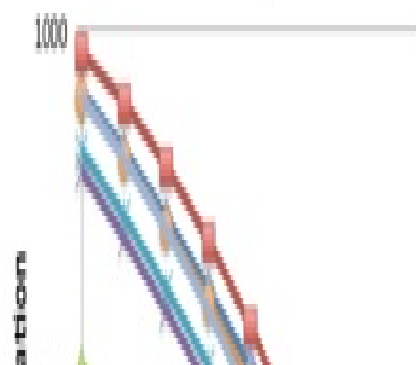
Pluto or Triton Occultation
0.5 sec Integration Time



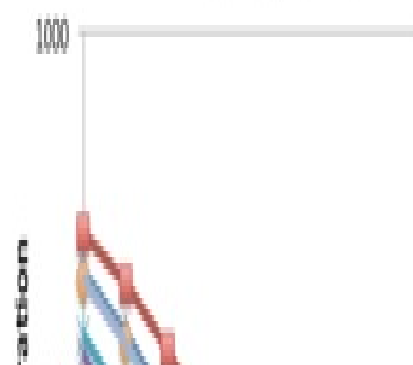
Pluto or Triton Occultation
0.05 sec Integration Time



S/N Ratio
Kuiper Belt Object Occultation
0.5 sec Integration Time



S/N Ratio
Kuiper Belt Object Occultation
0.05 sec Integration Time



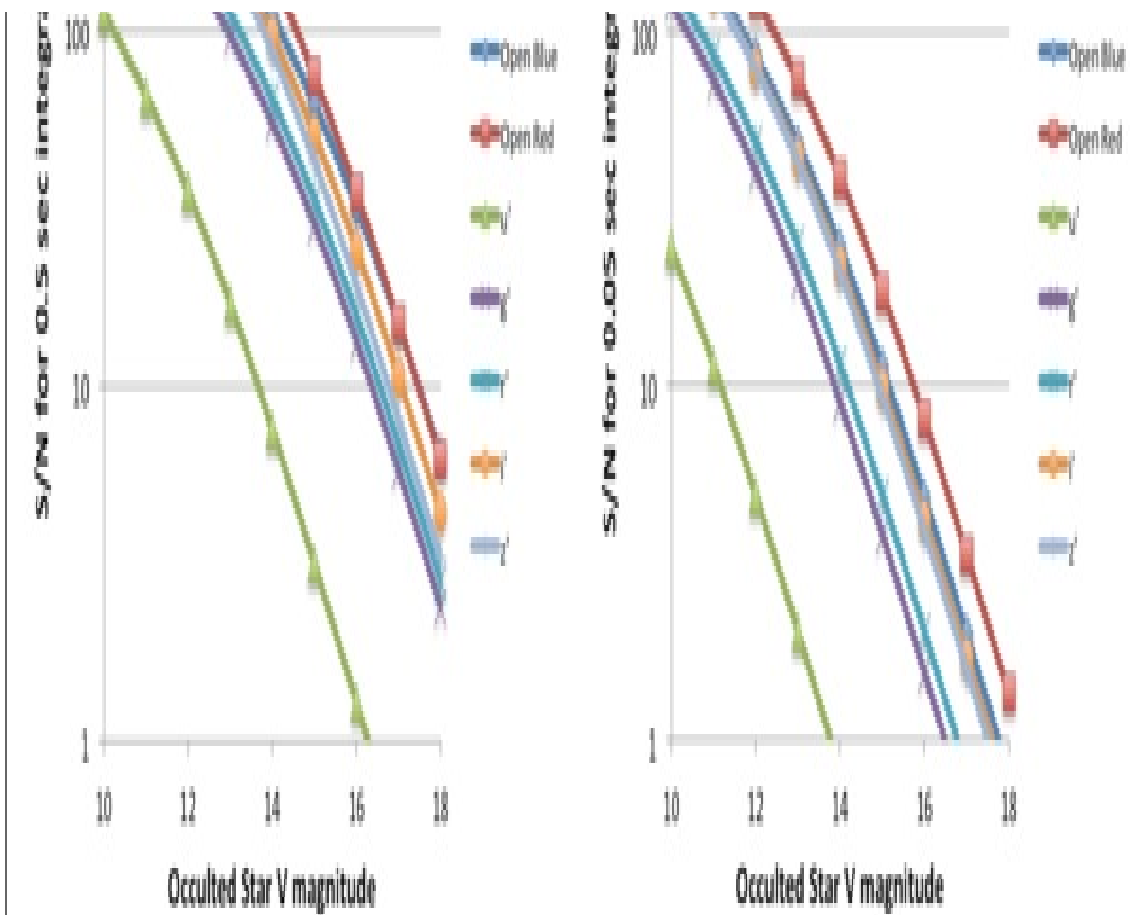


Figure 9-6. Plotted here are the anticipated sensitivities for HIPO for several representative occultation scenarios.

The deviation of S/N from a square root dependence is mostly due to shot noise on the occulting object in the upper left figure, about equally shot noise on the occulting object and read noise in the upper right figure, about equally shot noise on the sky and read noise in the lower left figure, and read noise in the lower right figure. Once the aluminized tertiary mirror is available read noise will only be significant in the lower right figure. The improved final SOFIA pointing stability will increase sensitivity for sky-limited events and improve discrimination from nearby bright objects (e.g. Neptune for a Triton occultation).

[Return to Table of Contents](#)

9.1.2.2 Sensitivity Spreadsheet

A spreadsheet exposure time and SNR estimator for HIPO is available [here](#). This spreadsheet accounts for transmission of all optical components from the atmosphere through the telescope, and inside HIPO, ending with the quantum efficiency of the detectors. It accounts for shot noise on the target, a possible background object (important for occultation work), and sky brightness as well as read noise. The wavelength dependence of the stellar flux is simply modeled as blackbody radiation, with the effect that there are systematic errors in the predictions that vary with wavelength and spectral type. The spreadsheet has been checked against a number of spectrophotometric standard stars with calibrations traceable through Vega to blackbody sources. Observed signals of these standards with the deep depletion CCDs is typically ~10% higher than predicted but in the Johnson I and Sloan i' bands the observed signals

are ~30% higher than predicted.

The spreadsheet SNR estimation does not account for systematics that dominate at high SNR values (~500 or higher) on timescales of ~10 minutes or longer. This remains a research area, [contact](#) the PI if you have any questions along these lines.

The spreadsheet is operated from its first tab, the Control Sheet. The next four tabs deal with optics that are common to both sides of HIPO (e.g. the atmosphere and telescope optics), optics peculiar to the blue or red sides, and the special case of the bare CCD. The last two tabs deal with blackbody and sky fluxes and the final combination of all the previous calculations that eventually appear back on the Control Sheet.

The spreadsheet is operated by filling in the yellow (most commonly used) and orange (less commonly used) cells to account for the star brightness and effective temperature, observing circumstances, CCD operations (integration time, binning, photometric aperture diameter), optics selections, and CCD choices. Results are returned in the light green cells. The main results are the signal levels from target, sky, and background object and the various noise contributions modeled by the spreadsheet. Scintillation noise is very difficult to measure and its value is not well determined yet. Finally the overall S/N ratio and fractional error are given. An estimate of the peak pixel signal in a star image is given in cells G34-H36. This is highly dependent on focus state and image jitter, and somewhat dependent on altitude so should be only used as a guide. The peak signal for the target star is also given in units of full well (assumed to be 100,000 electrons) in cells G35-H35. Note that full well is not affected by binning in a CCD47-20 since this CCD has no summing well. It is sometimes convenient to know the flux-weighted effective wavelength of a given filter/star combination. These are returned near the top center of the Control Sheet for the blue and red sides. For convenience the names of the beamsplitters, filters, and windows, or an indication if they have been removed, is given in the green cell above the selection cell for each optical element. The same applies to the CCD selection cells.

The optical elements modeled, in order, follow:

- Atmosphere: Atmospheric extinction is a combination of ozone (assumed to be 300 Dobson units) and Rayleigh scattering appropriate for 41,000 foot altitude. This matches observations quite closely. The usual $\sec(Z)$ airmass correction is applied.
- Telescope: The condition of the aluminum coatings on the telescope optics can be changed using cells J43-L43. At present the only tertiary mirror available is the dichroic tertiary and cell L43 has no effect. Cell B26 allows selection of either the dichroic tertiary or the not-yet-available aluminized one. If the aluminized tertiary is selected the aluminum coating condition in L43 does have an effect. The SOFIA coatings are maintained in excellent condition so cases 0 and 1 are the only reasonable ones to use.
- Fore optics: If the tub is to be evacuated the gate valve window must be installed. Whether this window is installed or not is modeled by selecting 1 or 0 in cell C26. The dichroic reflector used in the FLIPO configuration is controlled by cell D26. It can be left out (0), be the new Reynard dichroic (1), or the old Lick dichroic (2). The Reynard dichroic has about half the emissivity of the Lick one and similar optical performance so is likely to be preferred in most cases.
- The dichroic beamsplitter internal to HIPO is controlled by cell E26 and can be left out

(0) or be one of the two presently available ones (1 or 2). If it is left out no light reaches the blue side CCD.

- Filters for the blue, red, and bare CCD cases are controlled by cells F26-H26. There is a short explanation of what the various codes mean to the right of the cells used to select the various optics. New filters are certain to be added from time to time.
- CCD selection is made using cells F30-H30 with 0 being the original standard silicon CCDs and 1 being the newer deep depletion CCDs. The deep depletion CCDs have substantially higher QE and will be preferred in most cases in spite of their greater cosmic ray sensitivity. For UV work the thin blue CCD has better sensitivity than the deep depletion CCD.

A helpful figure showing the total signal per micron of bandwidth as a function of wavelength is shown in the upper right of the Control Sheet. It gives a graphical representation of the total signal accounting for everything from the star and sky through the CCD. The vertical axis on this graph autoscales.

An informational box related to the systematic error introduced by the blackbody approximation for stellar fluxes is given in the lower right of the control sheet. Errors at the ends of the wavelength range for very red stars can be ~50% but are 30% or less for most cases.

Another informational box at bottom center provides a crude estimate of effective temperature given either spectral class or B-V for a target object.

Finally the revision list is given at bottom left. This spreadsheet will be updated from time to time as optics or detector selections change, or as additional information becomes available. The sky brightness estimate is currently a weak area and may be changed relatively soon.

[Return to Table of Contents](#)

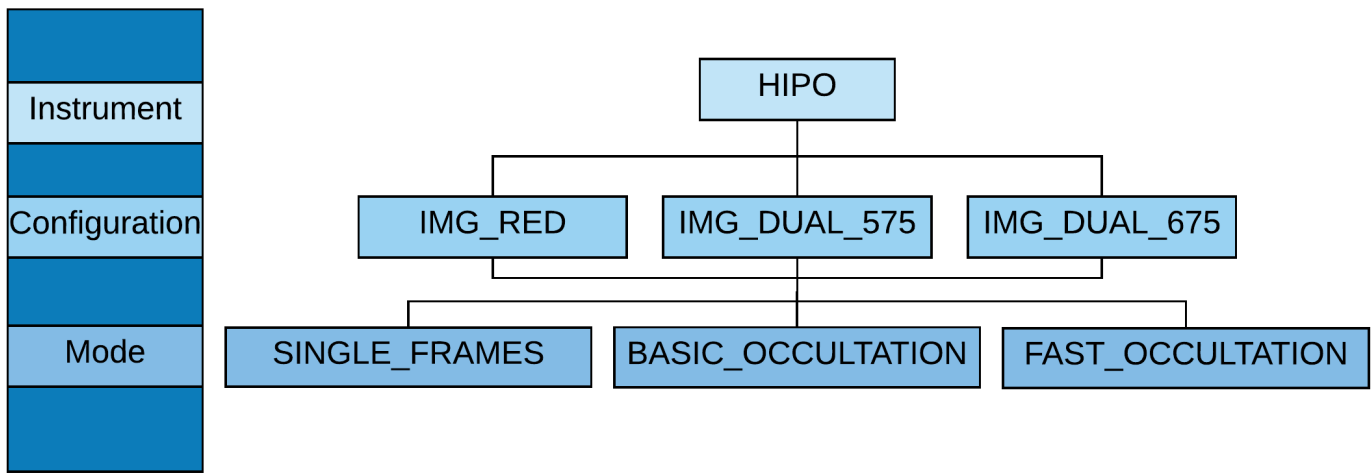
9.2 Planning Observations

Table of Contents

- [9.2 Planning Observations](#)

Return to the Table of Contents for this section at any time by selecting [Return to Table of Contents](#). Users may also navigate through the entire Observer's Handbook by using the complete Table of Contents menu to the right.

9.2 Planning Observations



HIPO is a special purpose instrument, and the material included here is suitable for getting an initial idea of its capabilities. In order to propose to use HIPO, or the combination of HIPO and FLITECAM it is necessary to consult with the instrument Principal Investigator (PI). It is expected that the details of observation planning will be a central part of the discussions. HIPO (and HIPO+FLITECAM) proposals require the endorsement of the PI.

[Return to Table of Contents](#)

10. The Data Cycle System

Table of Contents

- 10. The Data Cycle System
 - 10.1 Data Rights and Availability

Return to the Table of Contents for this section at any time by selecting [Return to Table of Contents](#). Users may also navigate through the entire Observer's Handbook by using the complete Table of Contents menu to the right.

10. The Data Cycle System

SOFIA proposals and observation data are managed by the [SOFIA Data Cycle System \(DCS\)](#). The DCS is designed primarily to support Science and Mission Operations activities associated with proposal programs for the observatory. Observatory data flow is cyclic in nature (see [Figure 10-1](#)). First a proposal must be developed and submitted to the SOFIA Science Mission Operations (SMO). Once approved, the proposal becomes an observing plan that the proposer uses to create and update astronomical observation requests (AORs) that are used in both flight planning and on-aircraft execution. After execution of the observations in-flight, the resulting data are archived and, for Facility Science Instruments (FSIs), automatically processed (pipelined) to produce the final data products, which are then served back to the original proposer via a simple user-interface -- thus completing the cycle begun by the original proposal and perhaps driving new proposals. The data products are made available to the astronomical community for archival research purposes after an appropriate proprietary period.

Figure 10-1.

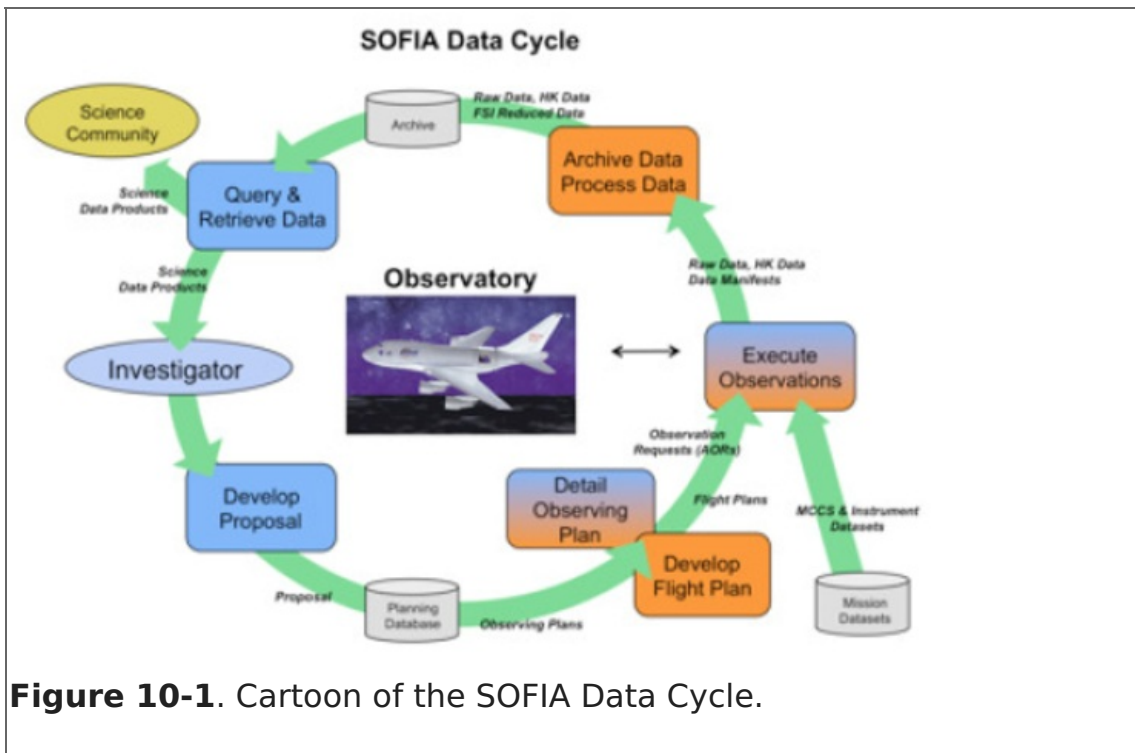


Figure 10-1. Cartoon of the SOFIA Data Cycle.

The goal of the SOFIA DCS is to maximize the scientific productivity and efficiency of the observatory by providing a suite of easy-to-use tools and infrastructure that are integrated with each other as well as other applications (e.g. Flight Management Infrastructure) at each step in the data cycle.

The DCS Archive is the permanent repository for all raw scientific and housekeeping data accumulated during SOFIA flights and any pipeline products produced thereafter (for example, pipeline reduced data for FSIs). Access to the SOFIA Data Archive is via the DCS web pages. Data can be retrieved from the archive during the proprietary period using an assigned DCS login username and password. The proprietary period for Cycle 6 will be 1-year from the date of ingestion into the DCS Archive. Once the proprietary period expires, the data becomes public and can be accessed by anyone in the general community.

In order to make use of most of the features of the DCS website, users must register by clicking on the [Register with DCS](#) link on the DCS home page. After the registration form has been submitted, the user will be notified by e-mail when the account has been created. (Users should verify that mail from "sofia.usra.edu" is not blocked by any spam filters.) After logging in, a registered user can change his/her profile and password at any time using the View Profile link displayed next to the login name at the top of the DCS pages.

The DCS includes a suite of software tools to archive data and to assist in the preparation and submission of proposals:

SOFIA Proposal Tool (USPOT)

SOFIA proposals are created and modified using USPOT, a stand-alone application available for a wide variety of platforms. The [Download USPOT](#) page includes links to download the application and installation instructions for all supported platforms. Complete help files are included with the application distribution and can be accessed via the Help menu options within USPOT.

Time Estimators

In order to assist in the creation of SOFIA observing proposals, the DCS web site provides an online [SOFIA Instrument Time Estimator](#) that calculates the total observation time required or signal-to-noise achieved for FLITECAM and FORCAST imaging modes. The DCS also maintains the on-line [FLITECAM Grism Exposure Time Calculator](#) and the online [FORCAST Grism Exposure Time Calculator](#). Exposure time calculators for GREAT and EXES are also available, and links may be found on the [SITE](#) page.

Atmospheric Transmission Estimator (ATRAN)

To allow proposers to estimate the effects of atmospheric transmission on potential observations and exposure times with SOFIA instruments, the DCS provides access to a [web-based version](#) of the ATRAN program written by Steve Lord. For a specified observing altitude and wavelength range, the web page will run ATRAN and generate an output file and plot of the atmospheric transmission as a function of wavelength. Both the output file and plot can be downloaded to the user's desktop. A brief description of the input parameters and how to run ATRAN is given at the top of the web page.

Visibility Tool (VT)

The Target Visibility Tool provides the capability to estimate what date, time, and aircraft heading are required to observe an astronomical target. The tool is a Java applet that is accessible on the [Visibility Tool page](#). Details of which operating systems and browsers are compatible with VT are provided on the [Visibility Tool page](#). A stand-alone version of VT is available for download.

To find the visibility of a given target, the user enters its co-ordinates (J2000 RA and DEC), the estimated latitude and longitude of the observation (which defaults to the SOFIA take-off location of Palmdale, CA), the start date and time, and the duration of interest. The application plots the target elevation for the period of interest. A target is visible to SOFIA if the elevation is in the range 20° to 60°.

Proposers may use VT to check the periods of visibility for their targets. For flights that take off from and return to Palmdale, the southernmost allowed declination is -36°. Southern targets will be scheduled for observation during the Southern Hemisphere Deployment that will take place during the southern winter of 2018.

Instructions on how to use VT and help on specific topics are available as part of the tool, using either the **Help** pull-down menu or the **?** button, both at the top, left of the applet window.

In addition, the DCS provides users with a variety of search options for proposals, data, and observing plans.

Proposal Search

All proposals submitted via USPOT are stored in the DCS observation planning database and can be accessed from the DCS web pages. Users can retrieve summary data for available proposals by using the [Proposal Search page](#) and entering the relevant search criteria for the proposal(s) of interest. Summary

information will be displayed for each proposal (appropriate to the permissions of the user).

Archive Search

Summary information is available for all public data in the DCS archive. From the [Science Archive Search page](#), [MCS Archive Search page](#), or the [Ancillary Files Search page](#), users can specify search criteria to identify data of interest. Summary info for resulting matches is shown in a table with appropriate links based upon user permissions. Data that are still proprietary are available only to those on the associated observing plan. Hence, *users must log in using a DCS username to view any proprietary data*. Proprietary data can only be seen by those associated with the program and selected SMO staff members. From the Summary Information table for science data, users can click through to a list of all data products associated with a particular observation (e.g., raw or pipelined data), or identify data to be downloaded.

Observing Plans Search

Once a proposal is approved, it becomes an observing plan, which can be accessed and modified as needed to support science and mission requirements by the proposer and selected SMO staff members. Observing plans can be accessed from the planning database using the [Search Observing Plans](#) link on the DCS web page. Summary information will be displayed for each observing plan along with links to the Observing Plan Details page. The Observing Plan Details page provides all the information available for a plan and corresponding links to the editor functions to make changes (for users with appropriate permissions).

Data Retrieval

Data can be retrieved by identifying desired data in the summary table and then clicking the **Retrieve Data** button. In order to retrieve any data, the user must be logged in. Only those with appropriate permissions and SMO staff are able to retrieve data that is still within the proprietary period. Once designated for retrieval, the files are staged to a public FTP server and a direct link is e-mailed to the user. All science data products are available in their original format (e.g., FITS). The same retrieval process is used for the MCCS and Ancillary data files.

[Return to Table of Contents.](#)

10.1 Data Rights and Availability

All scientific data from SOFIA observations will be distributed via the [SOFIA Data Cycle System's Science Archive](#). All data will be archived as Level 1 data (raw). Where appropriate, Level 2 (corrected for instrumental and atmospheric effects) and Level 3 (flux calibrated) will also be archived. These data will be accessible to the general community after a proprietary period of twelve months, starting at the ingestion of the calibrated data into the archive.

In order to query the archive and retrieve data, it is necessary to register with the DCS. This can be done by following the appropriate link ([Register with DCS](#)) on the main [DCS page](#). Registration is not required for using the proposal preparation and submission tools.

[Return to Table of Contents.](#)



Hina Kazmi, NASA
SOFIA Program
Manager
NASA Ames

Margaret Meixner,
USRA
Science Mission
Operations Director
NASA Ames